KAUNAS UNIVERSITY OF TECHNOLOGY

MANTAS JUCEVIČIUS

DEVELOPMENT AND INVESTIGATION OF A METHOD FOR DIRECT AND CONTINUOUS MONITORING OF JAW MOTION

Doctoral dissertation
Technological Sciences, Measurement Engineering (T 010)

Kaunas, 2023

This doctoral dissertation was prepared at Kaunas University of Technology, Biomedical Engineering Institute during the period of 2018–2022. The studies were partly supported by the Lithuanian Agency for Science, Innovation and Technology (MITA) (Grant No. 31V-184).

Scientific Supervisors

Assoc. Prof. Dr. Darius JEGELEVIČIUS (Kaunas University of Technology, Technological Sciences, Electrical and Electronics Engineering, T 001) 2019–2022.

Prof. Dr. Vaidotas MAROZAS (Kaunas University of Technology, Technological Sciences, Electrical and Electronics Engineering, T 001) 2018–2019.

Edited by: English language editor Brigita Brasienė (Publishing House *Technologija*), Lithuanian language editor Rozita Znamenskaitė (Publishing House *Technologija*).

Dissertation Defence Board of Measurement Engineering Science Field:

Dr. Vytautas PETKUS (Kaunas University of Technology, Technological Sciences, Measurement Engineering, T 010) – **chairperson**;
Prof. Dr. Julius GRIŠKEVIČIUS (Vilnius Gediminas Technical University, Technological Sciences, Mechanical Engineering, T 009);
Prof. Dr. Aleksejs KATAŠEVS (Riga Technical University, Latvia, Technological Sciences, Mechanical Engineering, T 009);
Prof. Dr. Liudas MAŽEIKA (Kaunas University of Technology, Technological Sciences, Measurement Engineering, T 010);
Prof. Dr. Dangirutis NAVIKAS (Kaunas University of Technology, Technological Sciences, Measurement Engineering, T 010).

The official defence of the dissertation will be held at 10 a.m. on 17 March, 2023 at the public meeting of Dissertation Defence Board of Measurement Engineering Science Field in the Meeting room A228 at Santaka Valley of Kaunas University of Technology.

Address: K. Baršausko 59-A228, Kaunas, LT-51423, Lithuania.
Tel. no. (+370) 608 28 527; e-mail doktorantura@ktu.lt

Doctoral dissertation was sent on 17 February, 2023.
The doctoral dissertation is available on the internet http://ktu.edu and at the library of Kaunas University of Technology (K. Donelaičio 20, Kaunas, LT-44239, Lithuania).

KAUNO TECHNOLOGIJOS UNIVERSITETAS

MANTAS JUCEVIČIUS

ŽANDIKAULIO JUDESIŲ TIESIOGINIO IR NUOLATINIO STEBĖSENOS METODO VYSTYMAS IR TYRIMAS

Daktaro disertacija
Technologijos mokslai, matavimų inžinerija (T 010)

Kaunas, 2023

Disertacija rengta 2018–2022 metais Kauno technologijos universiteto Biomedicininės inžinerijos institute. Mokslinius tyrimus dalinai rėmė Mokslo, inovacijų ir technologijų agentūra (MITA) (Dotacijos Nr. 31V-184).

Moksliniai vadovai
Doc. dr. Darius JEGELEVIČIUS (Kauno technologijos universitetas, technologijos mokslai, elektros ir elektronikos inžinerija, T 001) 2019 – 2022 m.

Prof. dr. Vaidotas MAROZAS (Kauno technologijos universitetas, technologijos mokslai, elektros ir elektronikos inžinerija, T 001) 2018 – 2019 m.

Redagavo: anglų kalbos redaktorė Brigita Brasienė (leidykla „Technologija“), lietuvių kalbos redaktorė Rozita Znamenskaitė (leidykla „Technologija“).

Matavimų inžinerijos mokslo krypties disertacijos gynimo taryba:
dr. Vytautas PETKUS (Kauno technologijos universitetas, technologijos mokslai, matavimų inžinerija, T 010) – **pirmininkas**;
prof. dr. Julius GRIŠKEVIČIUS (Vilniaus Gedinimo technikos universitetas, technologijos mokslai, mechanikos inžinerija, T 009);
prof. dr. Aleksejs KATAŠEVS (Rygos technikos universitetas, Latvija, technologijos mokslai, mechanikos inžinerija, T 009);
prof. dr. Liudas MAŽEIKA (Kauno technologijos universitetas, technologijos mokslai, matavimų inžinerija, T 010);
prof. dr. Dangirutis NAVIKAS (Kauno technologijos universitetas, technologijos mokslai, matavimų inžinerija, T 010).

Disertacija bus ginama viešame Matavimų inžinerijos mokslo krypties disertacijos gynimo tarybos posėdyje 2023 m. kovo 17 d. 10 val. Kauno technologijos universiteto „Santakos“ slėnyje, Posėdžių kambaryje A228.

Adresas: K. Baršausko g. 59-A228, Kaunas, LT-51423, Lietuva.
Tel. (+370) 608 28 527; el. paštas doktorantura@ktu.lt.

Disertacija išsiųsta 2023 m. vasario 17 d.
Su disertacija galima susipažinti interneto svetainėje http://ktu.edu ir Kauno technologijos universiteto bibliotekoje (K. Donelaičio g. 20, LT-44239, Kaunas).

CONTENTS

LIST OF TERMS AND ABBREVIATIONS

2D – Two-dimensional
3D – Three-dimensional
ANN – Artificial neural network
AV – Audio-video
BEI – Bruxism episode index
BMF – Background magnetic field
CBCT – Cone beam computed tomography
ECG – Electrocardiography
ED – Euclidian distance
EEG – Electroencephalography
EMG – Electromyography
FEM – Finite element model
IMU – Inertial measurement unit
LS – Least squares
MEMS – Micro-electromechanical system
PCB – Printed circuit board
PLA – Polylactide
PPG – Photoplethysmography
PSG – Polysomnography
PSO – Particle swarm optimization
RMSE – Root mean square error
RSS – Root sum of squares
TMJ – Temporomandibular joint

INTRODUCTION

Relevance of the research

Bruxism is the most common and dangerous jaw parafunction. Its damage to natural and restored teeth is often severe and irreversible. The real percentage of the population suffering from this disorder falls between 8% and 31.4% [1], which could be considered an epidemic. Bruxism is difficult to diagnose before seeing the damage, and current diagnostic methods have many limitations. This reveals a large gap between large, precise appliances for clinical jaw kinematics evaluation, and significantly more primitive, wearable electromyography (EMG) or occlusal splint based bruxism detectors. A method offering a direct and continuous jaw movement recording with high patient mobility is yet to be created, let alone the one that offers sub-millimetric precision. An ergonomic wearable device aimed at recording continuous jaw position in relation to the skull would bring a significant improvement to bruxism diagnostics. Moreover, it could provide hours of extensive datasets to evaluate and study all jaw parafunctions. It might be utilized for the experiments on dental wear, the development of prosthetics, the evaluation of masticatory efficiency as well as research of dysphagia and apnea. Currently, several various clinical machines based on different physical phenomena are available for estimating jaw position and recording its motion trajectories. Such devices are accurate and effective in jaw kinematics evaluation needed for treating temporomandibular disorders, involving jaw muscles, temporomandibular joint (TMJ), or both [2]. These appliances are great for developing and fitting prostheses and can be utilized in orthognathic surgery for pre-operative and post-operative evaluation. Nevertheless, for all available clinical jaw trackers, bulky external accessories must be mounted directly on the head or the jaw and the patient's movement is very limited, making continuous, nightlong examinations impossible. Moreover, such accuracy is not necessary in the behavior assessment, where only the shape and topology of movement trajectories carry the diagnostic information, such as the prominent type of bruxism, the duration of occlusal contact, and the amount of teeth impacts as well as the frequency and intensity of the parafunctional episodes. In such cases, long-term, ergonomic monitoring is the priority, allowing patients to continue their daily routine with minimal intervention. The ability to perform basic oral functions (including parafunctions) with minimal discomfort and awareness is very important.

As far as minimally restricting, continuous jaw motion monitoring is concerned, the research field of bruxism diagnostics has made the most advances. The golden standard for bruxism diagnostics is a multi-sensor sleep study polysomnography (PSG). Even without any direct data of jaw mechanics, PSG enhanced with Audio-video (AV) recordings is considered the most reliable, exhaustive, and comprehensive method for diagnosing sleep bruxism [3]. However, the cost and duration of overnight hospitalization make the method unfit for the widespread use. The devices based on masseter and temporalis muscle EMG are as

well indirect and do not provide spatial data, but are ergonomic, affordable, and quite popular for initial diagnosis. Nevertheless, this method is susceptible to noise and movement artifacts due to the low signal amplitudes and variations in skin resistance [4].

Sensor-enhanced intra-oral occlusal splints is another widely researched solution. Nevertheless, only “Bruxane” (Bruxane, Marburg, Germany) has reached commercial production stage. It registers bite events and generates vibrational biofeedback. In oral splints, the main source of discomfort is the thickness of the device on the occlusal surface [5]. Besides, it has an effect on the bruxism episode frequency and intensity [6]. It is a useful quality that is utilized in anti-bruxism bite splints, but the one that could discard the measurement of diagnostic splints.

In recent years, a demand for a novel, wearable solution for continuous mandibular activity monitoring has increased, but no innovative and atypical approaches have been proposed yet. In order to outperform the existing solutions, the device should be resistant to motion artifacts, waterproof, unobtrusive for the patient, and the occlusal surface should remain uncovered. A hypothesis was raised that such requirements could be met by a permanent magnet tracking system that could detect the impacts of teeth by acceleration measurements. The concept of jaw motion tracking by measuring the field of the attached permanent magnet dates back to 1977 [7]. However, the limited technical specifications of magnetic sensors during that time allowed for the method to be utilized for low accuracy, single-axis motion detection only. Low-powered inertial measurement unit (IMU), micro-electromechanical systems (MEMS) currently have integrated tri-axial magnetometers, accelerometers, and gyroscopes in a single 2–3 mm package. An appliance based on the modern IMU could be implemented intra-orally.

No electrical contact between the mandible and maxilla is required when the permanent magnet is used. It as well allows to determine the relative position of the mandible by using magnetic field equations. The position could be solved by nonlinear optimization methods. It could be utilized to record the movement of the jaw and dynamic closure over a long period of time, identify the pathological behavior, and show the prevailing trajectories, indicating the type and sub-type of jaw parafunction. This patient-specific information could be very useful for the diagnosis and dental rehabilitation. While precise clinical jaw kinematics evaluation is necessary for full temporomandibular disorder diagnostics and treatment, in some cases, continuous monitoring of patient behavior and masticatory trajectories could be instrumental for following the progress of treatment.

Scientific-technological problem and working hypothesis

Bruxism results in a lot of irreversible teeth damage for a large part of the population, and there are obvious limitations of current methods for jaw parafunction diagnostics. It calls for more sophisticated approaches to be explored in order to create a better diagnostic method, covering the actual practical requirements of the physicians.

The scientific-technological problem of this work is how to assess and quantify the jaw parafunctions in continuous, direct, the least obtrusive way. The working hypothesis is that a small permanent magnet and two adjacent 3-axial magnetometers fastened to the teeth can provide enough data to estimate complete jaw movement that could be used for the parafunction assessment.

Research object

The research is based on the development and investigation of a method for direct and continuous jaw motion registration and an experimental device development based on the proposed method. Such technology could serve as a tool for jaw parafunction diagnostics and generation of extensive datasets for new jaw parafunction research.

The aim of the research

The research aims to develop and investigate a direct, least obtrusive method for continuous jaw movement registration for jaw parafunction monitoring and assessment.

The objectives of the research

1. To investigate possibilities of a permanent magnet tracking setup for direct and continuous jaw position registration by using mathematical model.
2. To propose a method to track jaw motion with minimal number of magnetometers, resistant to ambient conditions.
3. To develop a prototype of jaw motion tracking system and evaluate it in realistic conditions.

Scientific novelty

In this dissertation, the first method for direct and continuous intraoral jaw position registration is proposed. Current methods that aim to evaluate jaw kinematics are unfit for continuous use, while wearable continuous jaw activity detectors are unable to provide data for spatial position estimation. The method described in this work uses only two adjacent tri-axial magnetometers for ambient field resistant magnetic localization, which was not reported to be done before. The predictable orientations of the sensor and the permanent magnet when attached to the jaw allowed using the localization method of only 3 degrees of freedom (DOF). The 5-DOF localization was achieved by utilizing the kinematic limitations of the human masticatory system and deriving a system of trigonometric equations to relate the linear translation of the selected point of the jaw to its rotation in two degrees of freedom. A method suitable for the use in a wearable device was created that with the calibration, can achieve similar accuracy to the clinical precision appliances.

Practical significance

The proposed method allows designing a wearable sensor, which can continuously track jaw motion during normal life activities. In fact, 24-hour jaw position data could allow physicians to properly diagnose jaw parafunctions, including the sub-type of parafunction, jaw movement trajectories, episode frequency and intensity, number of teeth impacts, and other needed statistics. The recorded data can be visualized in a software environment by using three-dimensional (3D) models of scanned teeth, allowing the physician to review the patient's temporomandibular activity. Such patient-specific diagnostic information puts this research in the field of precision medicine. It could allow selecting appropriate treatment for people with natural teeth and choosing suitable materials and manufacturing techniques for the dental restorations. This would guarantee the longevity of both natural teeth and prostheses. The physicians treating TMJ and jaw muscle disorders could use the method as well to continuously monitor the behavior of the patient or follow the course of treatment.

Approval of the results

The results of this doctoral dissertation have been published in two publications in scientific journal referred in the Master List of Thomson Reuters Web of Science with an impact factor (Q2). The results were presented in 2 international scientific conferences held in Slovenia (Portoroz) and Lithuania (Vilnius) as well as one national scientific conference (Kaunas).

Hexapod-based jaw motion simulator that had been created and used in this research was granted "EIT Health" prize at the Young Scientists Exhibition "Technorama 2020" (Kaunas University of Technology).

Statements presented for defense

1. 3-DOF spatial position of a 2 x 2 mm cylindrical magnet in small (15 mm) range can be estimated with sub-millimeter trueness by measuring its magnetic field and employing condition-restricted non-linear optimization algorithm.
2. The location of said magnet can be estimated with total resistance to natural, homogenous ambient magnetic field by using two adjacent tri-axial magnetometers that are in a fixed position to each other.
3. The proposed magnetic system can be employed to estimate 5-DOF jaw movement by mounting the magnet to the maxilla and two-magnetometer sensor board to the mandible, while jaw rotations are accounted for linking the jaw translation to its rotation by custom trigonometrical equations and jaw dimension measurements.
4. The proposed method fills the gap between the precision jaw kinematics evaluation machines and primitive EMG or occlusal splint based jaw activity registrators by offering sub-millimetric precision combined with high mobility and prolonged measurements.

Structure and contents of the dissertation

The dissertation consists of an introduction, four chapters, conclusions, future scope of research, a list of references, and a list of the author's publications.

1. In the first chapter, the problematics of bruxism and other jaw parafunctions are explained, and there is an introduction to the anatomy and biomechanics of the jaw. Moreover, the current methods for assessing jaw function and parafunction are overviewed.
2. In the second chapter, there is a literature overview of methods for tracking the permanent magnet in the biomedical applications. The working principle of magnetic localization and possible algorithms for estimating the magnet position from magnetic field measurements are reviewed as well as layouts and quantities of magnetometers that have been used.
3. In the third chapter, the methodology for this dissertation is described. It consists of a thorough description of the proposed method for magnetic jaw localization and the methodology for conducted tests, evaluations, and experiments, both theoretical and experimental.
4. In the fourth chapter, the results of theoretical estimations and theoretical experiments using a finite element model (FEM) are presented as well as the results of practical experiments, some of which replicate previous theoretical simulation experiments in practice. The results of the experiments are reviewed and assessed, and the limitations of the study and method are stated.
5. The conclusions are presented in the fifth chapter.
6. Future scope of the research is presented in the final chapter.

Parts of section 3 have been quoted verbatim from [8] and [9] publications of the same author. The overall volume of the dissertation is 105 pages, including 66 figures, 4 tables, and 85 bibliographic references. The volume of the summary is 57 pages.

1. CLINICAL SIGNIFICANCE OF JAW MOVEMENT TRACKING

1.1. Physiological and medical background

1.1.1. Introduction to bruxism and other jaw parafunctions

Oral parafunction can be described as any involuntary oral motion or habit that is not associated with eating or speech and include bruxism, clenching, lip or cheek biting, nail chewing, and thumb sucking. Usually, such parafunctions are intermittent, not intensive, and do not require treatment. Oral parafunctions can be categorized as psycho-physiological disorders [10, 11]. They are thought to be caused by the psychological factors, such as anxiety, stress, and fatigue, and are provoked by alcohol, nicotine, and stimulant drugs [11]. Even though all jaw parafunctions may negatively affect the quality of life and require treatment, most of them are easy to self-diagnose and do not cause permanent damage. Bruxism is the most dangerous and the most common of the parafunctional jaw activities in the general population [10, 12]. The prevalence of this oral habit is increasing, mainly due to the rising pace of life and a growing number of people under stress. Bruxism may be characterized as an involuntary, rhythmic, or spasmodic temporomandibular motion that includes grinding, gnashing, or clenching of teeth. The prevalence of bruxism disorder in the general population may be from 8% to 31.4% [1]. This percentage heavily depends on the evaluation criteria of the research and the threshold for the frequency of the episodes, based on which a person is considered to have bruxism. It should be noted that there are no universal, standard parameters to define bruxism. It may be because there are no direct clinical methods or equipment for diagnosing masticatory function disorders, not to mention continuously recording jaw movements. According to the literature, there is no significant difference in the manifestation of this disorder based on the race and sex; however, its presence tends to be less common in older age [11]. Bruxism may be categorized into awake bruxism and sleep bruxism. Sleep bruxism is the most dangerous [13] because of the sleeping person's inability to notice and control the involuntary muscle motion. The human jaw may generate forces of up to 200 N in women and 400 N in men [14], which in cases of involuntary misuse, may lead to trauma. The most damaging motion for both natural teeth and restorations is side-lateral grinding, which as well occurs while sleeping. Considering these facts, it is only natural that the majority of research and commercial devices are aimed at mitigating and recording sleep bruxism specifically. As for the consequences of bruxism, such drastic wear can cause significant loss of vertical dimension of the natural teeth, chipping and abfraction as well as gum recession (Fig. 1.1).

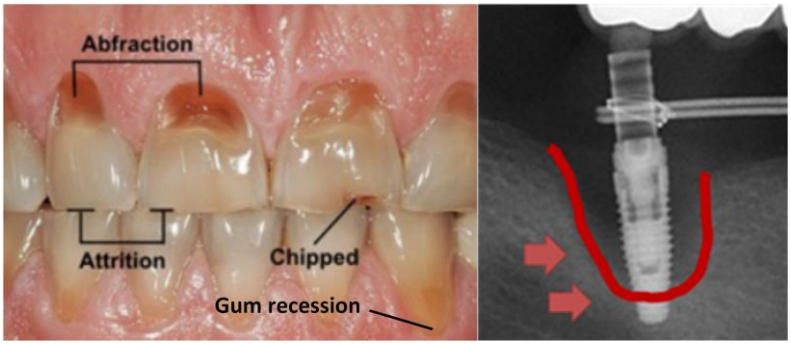

Fig. 1.1. Consequences of bruxism on natural teeth (left) and implant-supported rehabilitations (right); based on [15] and an original photograph with copyright permission

Other symptoms include: loss of masticatory efficiency, pulpitis, and sensitivity to temperature. Intense clenching of teeth causes masticatory muscle hypertrophy and myalgia as well as degenerative lesions in temporomandibular joint (TMJ) and articular disc displacement [5]. Implant-supported restorations may experience excessive load leading to bone loss around the implants, implant fracture, and subsequent failure of the implants [16].

Non-instrumental diagnosis of bruxism can be made from signs of dental wear and damage, which are often too late, self-evaluation of the patient, and most commonly, grinding noises during sleep that are heard by the family members. In some cases, other clinical signs might be present, such as headache, muscle tension, and stiffness of the jaw in the morning. However, the absence of these signs does not necessarily indicate the absence of bruxism [17]. In fact, in 80% of cases, there might be no grinding noises or muscle discomfort and hypertrophy [5].

The only quantitative metric found in literature is a bruxism episode index (BEI), which is the direct number of episodes per hour of sleep. The index of 0–2 represents irrelevant, 2–4 mild to moderate, and >4 severe sleep bruxism [18].

Different people experience different grinding patterns. The knowledge of patient's grinding pattern allows the physician to know which teeth experience the largest forces as well as directions of those forces. It can be useful when manufacturing prosthesis and assessing the effectiveness of prescribed treatment. The classification of grinding patterns is canine-dominance grinding without mediotrusion grinding (Fig. 1.2 a), canine-dominance grinding with mediotrusion grinding (Fig. 1.2 b), group grinding without mediotrusion grinding (Fig. 1.2 c), and group grinding with mediotrusion grinding (Fig. 1.2 d) [19].

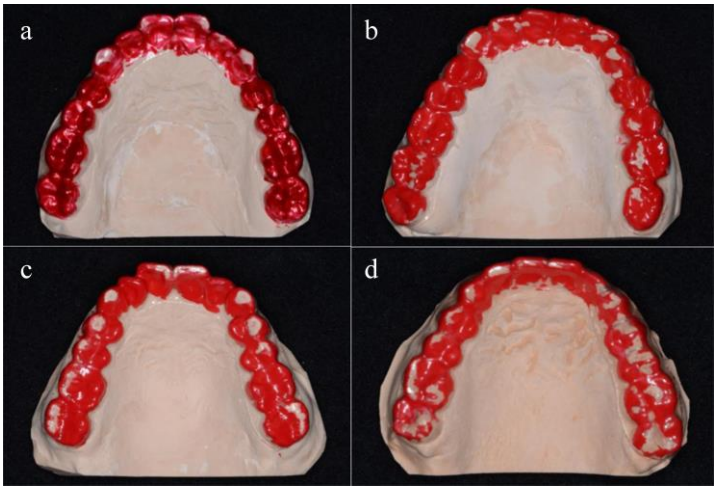

Fig. 1.2. Grinding patterns on BruxChecker (Scheu-dental, Iserlohn, Germany) splint: (a) canine-dominance grinding without mediotrusion grinding, (b) canine-dominance grinding with mediotrusion grinding, (c) group grinding without mediotrusion grinding, (d) group grinding with mediotrusion grinding [19]

1.1.2. Anatomy of the human jaw

The lower jaw, the main moving component of the human masticatory system, is called mandible. It may be characterized by a horseshoe shape and is the largest and strongest bone of the human face. At the posterior of the mandible, there are two heads of joints on the sides. Those are called condylar heads. They are blunt and convex in all directions, allowing them to slide and rotate simultaneously. The sockets in which the condylar heads are placed are called glenoid fossa or glenoid cavities and are located right under the ears. Between the condylar head and the glenoid surface, there is an articular disk (Fig. 1.4), which is held in place and moved by a ligament connected to the lateral pterygoid muscle. It serves as an intermediate component separating the two bone structures. Anterior to the glenoid cavity, there is an articular tubercle, or articular eminence. Together with glenoid cavity, it forms an area on which the condylar head can move around, separated by the articular disk. This area, which is covered with hyaline cartilage and has virtually no friction, defines the condylar path. Together with several others, these are the key components that form a TMJ, a drawing of which is presented in Figure 1.3 [20].

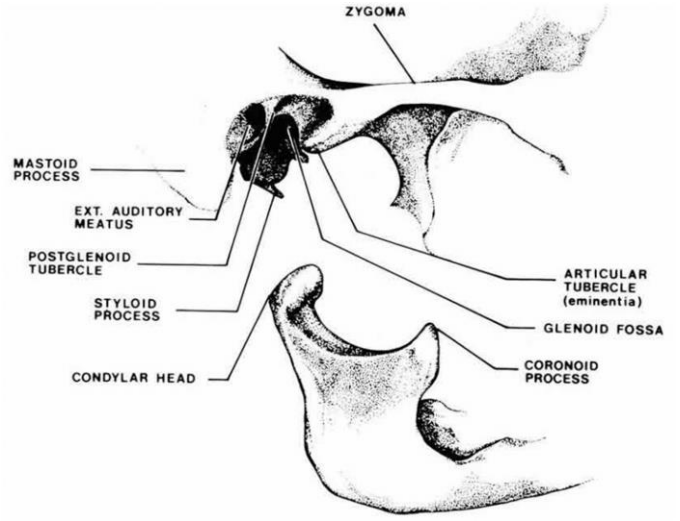

Fig. 1.3. Components of TMJ [20]

The fact that form and curvature of the articular eminence vary among different individuals makes the condylar path an important specification in the dentistry. This means that the characteristics of individual jaw motion will depend on the inclination, curvature, and general shape of the condylar path. Even though it can be approximated and generalized, it should be taken into account that this might be the source of some uncertainties and errors when predicting the jaw position or modeling jaw motion.

There are seven pairs of muscles dedicated to opening (depression) and closing (elevation) of the jaw, which are presented in Figure 1.4.

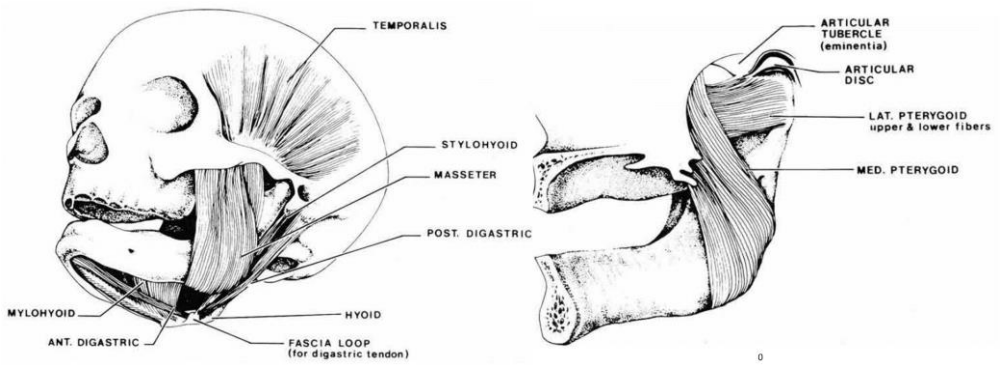

Fig. 1.4. A drawing depicting the muscles dedicated to opening (depression) and closing (elevation) of the jaw [20]

The main muscles for opening the jaw (depression) are lateral pterygoids. When facing increasing resistance, digastric, geniohyoid, and mylohyoid muscles are activated accordingly [20]. Platysma muscle contributes to opening the jaw as well, but its main function is making facial expressions [21]. Temporalis, masseter, and medial pterygoid are the main muscles that work together in closing the jaw, while lateral pterygoids are activated to oppose the resistance [20].

The arthrokinematics of the human jaw goes in the following way: when the jaw begins to vertically open (first rotational degree of freedom), the primary motion is rotational. Both joints stay in the glenoid cavity ant rotate until it reaches the static rotation limit, which is usually between 15° and 25°, but may vary significantly in some individuals. Then follows the translational motion called gliding when the condylar head with the articular disc slides onto the articular eminence slope. The trajectory of the gliding, i.e., the condylar path, is characterized by the shape of the articular eminence. However, in case of further opening of the jaw, the rotation does not stop during the glide, and a fully open jaw has to have fully glided in anterior direction and rotated to the maximum. The lateral motion to the side combines two types of motion that have been described above. For example, in the case of the right lateral motion, the right condyle remains inside the glenoid cavity and rotates, while the left condyle glides along the articular eminence both rotating and translating. This allows the jaw to rotate around the vertical axis (second rotational degree of freedom). In the case of protrusive motion, both condyles glide forward and slightly downward, following the articular eminence slope with minimal rotation, while during retrusive motion, it simply returns following the same path [20]. Rotation in the third rotational degree of freedom occurs only during lateral rotation, when one condyle slightly translates vertically, while sliding along the articular eminence. However, the rotation in the third degree of freedom is not visible, and in comparison to the first two rotational degrees of freedom, it is virtually non-existent. In addition to three-translational degrees of freedom, any movement of the jaw can be sufficiently described in 5 degrees of freedom.

1.1.3. Normal masticatory function

The biting force of a healthy individual during chewing is merely 20–40 N, which is ~10 times less than 200–400 N force that is generated during sleep bruxism [14]. In normal conditions, the jaw is usually relaxed and slightly open, and the teeth are not in contact. The consensus is that normally, the teeth are in contact for no more than 20 minutes in 24 hours, and it happens only while chewing, swallowing, and speaking. Anything more, might be considered a parafunction [22].

1.2. Current methods for jaw function assessment

In this chapter, the currently available methods for jaw activity assessment are reviewed. The focus is on the solutions providing information about the jaw activity. The parallel functions of the reviewed devices, e.g., biofeedback or therapeutic features, while might be mentioned, are outside of this work scope of interest. It

should be noted that some technical details, parameters, and especially measurement methods of commercial devices are often undisclosed or otherwise unavailable.

1.2.1. Oral splints

The use of oral (occlusal) splints is the leading solution for people suffering from bruxism both in diagnostics and therapy. Medical protective occlusal splints distribute the forces experienced by teeth and reduce the tension in masticatory muscles. According to the occlusal splint therapy literature review [23], occlusal splints can be used to provide diagnostic information, protect the teeth of patients with bruxism, stabilize unstable occlusion, and relax the jaw muscle in cases of stress-related muscle pain and headache. The splints can be generally divided into two categories, i.e., permissive splints that are aimed to protect the teeth and control the muscle forces and directive splints that are aimed to shift the joint away from the starting position, used in the treatment of TMJ joint pain treatment.

Mechanical diagnostic splints are attrition-based color-coated disposable instruments that allow to visually [19] or semi-automatically [24] inspect bruxism-related damage post-wear, which are presented in Figure 1.2 and Figure 1.5 a.

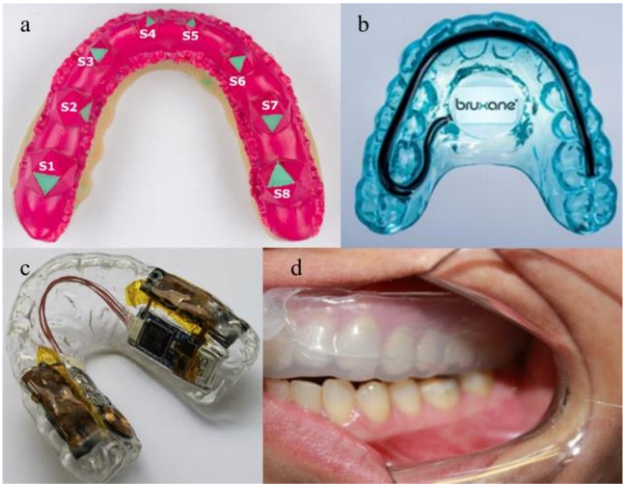

Fig. 1.5. Splints for bruxism diagnostics: (a) attrition-based splints for semi-automatic inspection by 3D scanning [24], (b) Bruxane splint with integrated pressure sensors [25], (c) splint with integrated piezoresistive pressure sensors [5], (d) splint with optical fiber sensors [26]

As for electronic devices, there have been several attempts to integrate various pressure sensors on the occlusal surface of the oral splint in order to register the bite force and its variation in time. The only one that reached commercialization is “Bruxane“ (Bruxane, Marburg, Germany) [25], which is shown in Figure 1.5 b. It provides vibrational biofeedback and registers masticatory events. In publication by Bergmann et al. [27], it has been validated as able to reduce the number and

intensity of bruxism episodes, but no details are provided regarding the sensor, data analysis, and decision-making [1].

Claude et al. has proposed splints with piezoresistive pressure sensors [5] placed on the occlusal surface, which is presented in Figure 1.5 c. The authors are stating 2 mm thickness of the splint, and the electronic control units are placed in the palate area. The experiments show successful registration of intentional masticatory events as well as a full 7-hour night recording. However, the authors do not provide a reference diagnostic method or annotation; hence, there is no way to quantitatively assess the recorded data on the effectiveness of the splint.

An interesting approach of using optical fiber pressure sensing was implemented in the oral splint by Nascimento et al. [26], which is presented in Figure 1.5 d. Fiber Bragg grating optical sensors refractive properties change with applied mechanical pressure; hence, it changes the wavelength of the light travelling through it. Due to the very low thickness of the optic wire, this method allows for thinner splints.

Sensor embedded dental restorations [28] for oral activity recognition could be a solution that overcomes many drawbacks of occlusal splints. The authors suggest that as artificial teeth are removed for nightly cleaning, it can be recharged. However, the dental implant based restorations are not daily removable, and this specific group of patients faces most risks from bruxism-related damage.

In addition to the mechanical protection of the teeth, the use of oral splints has an influence on the patient's behavior, reducing the frequency and intensity of bruxism episodes [29], especially for the several first nights it is worn [6]. It is an excellent feature for harm prevention. However, this feature has an inherent drawback in cases of sensor-enhanced splints: by directly affecting the patient's behavior, it effectively discredits its own measurement. One of the most reported causes of patient discomfort is the thickness of the oral splint [5]. Lundqvist stated that for natural teeth, occlusal perception begins at barely 20 μm [30].

1.2.2. Electromyography-based devices

Electromyography (EMG) is the measurement of potential differences that occur during muscle activation, which allows recording the electric activity of the muscle. Depending on the observed muscle, the measured potentials may fall anywhere in the range of several μV to tens of mV. In the case of masticatory muscle activity, most sense is in the recording temporalis and masseter muscle EMG due to their relatively large size. According to the scoping review of the existing methods for EMG use in bruxism diagnostics [31], the masseter muscle was the preferred choice for EMG registration in 58% of the reviewed studies. Wearable masticatory muscle EMG devices can detect the presence of bruxism and record data about the intensity and frequency of parafunctional episodes with relatively low patient discomfort and for prolonged periods of time. There are several commercially available EMG based bruxism detectors. In literature review by Yamaguchi et al. [32], nine wearable EMG devices were assessed, and it was

concluded that it is a suitable method for the detection of sleep bruxism episodes. A stated drawback was that cut-off criteria are required for awake bruxism assessment. However, it is a problem with most jaw function detectors, because of the talking, chewing, and other daytime activities. The systems that were the most mentioned and validated in the scientific literature are described in this subsection.

"BiteStrip" (Scientific Laboratory Products, Ltd., Tel Aviv, Israel) [33] is a discontinued, masseter muscle EMG-based disposable device aimed to serve as a home test for bruxism, displaying the test result on a chemical indicator. It provides its own bruxism severity index (0–3) after the measurement. The device has been fairly widely used both by the patients and academics researching the disorder of bruxism. It has been assessed to be a moderate method for sleep bruxism screening and confirmation. However, it was deemed as lacking accuracy in estimating the intensity of the episodes, mainly due to the inability to differentiate between rhythmic masticatory muscle activity and unrelated orofacial motor activities [34].

"Bruxoff" (Spes Medica, Genoa, Italy) [35] is a more expensive, usually clinically used device that records the masseter EMG and the patient's electrocardiogram (ECG) overnight. The decisions are made by an artificial neural network that has been taught on annotated signals. The main novelty of this device is the ECG incorporation into bruxism detection. The reasoning behind it relies on the statements that bruxism episodes are triggered by brainstem arousal, which as well leads to the increase in heart rate [36]. According to a paper by Castroflorio et al. [37], ECG and EMG usage in Bruxoff device data resulted in 1% misclassification error from bruxers and non-bruxers, while ECG data elimination from the ANN inputs resulted in substantially higher error.

EMG based biofeedback devices should be mentioned as well. Although they do not provide diagnostic information, they are useful in behavior modification and harm prevention. It as well gathers and displays a number of episodes in a smart phone application. For example, a pilot study of temporalis muscle EMG based device Grindcare (Medotech, Copenhagen, Denmark), which delivers a mild electric shock prompting the patient to stop harmful behavior, reported symptomatic improvement based on the patient self-report [38].

In conclusion, EMG method is ergonomic and effective in initial diagnostics of bruxism. Its most commonly stated drawbacks are that it is susceptible to movement artifacts, electrical noise, skin resistance variation, and has low signal amplitudes [14]. However, in the light of this research, the main drawback of EMG based systems is that it provides too little information for the analysis of the bruxism disorder, especially in cases of single-muscle systems. It is indirect and lacks information about the motion of the jaw, its movement direction or trajectory, and consequently, grinding patterns and intensity of the episodes.

1.2.3. Polysomnography with audio-video recordings

The golden standard for instrumental bruxism diagnostics is polysomnography (PSG) with audio-video (AV) recordings [3], which is essentially a sensor-enhanced

manual monitoring of a patient. The technique requires overnight hospitalization. In addition to the physician or technician reviewing of AV recordings, it may use many additional sensors, including, but not limited to, EMG, electroencephalography (EEG), ECG, and photoplethysmography (PPG). PSG provides the most reliable sleep bruxism research diagnostic criteria to this day. Nevertheless, it should be noted that this technique is time-consuming and cost-intensive both financially and personnel-wise, which hinders its wide-spread routine use.

1.2.4. Jaw position registrators

Currently, several various methods are available for estimating the jaw position and recording its motion trajectories that offer the state of the art performance and precision. In this chapter, the most significant devices on the market are mentioned. Optical KaVo Arcus Digma 3 (KaVo Kerr, Brea, CA, USA) [39] stating 0.05 mm positional accuracy in the occlusal area with 60 Hz imagery rate, optical ModJaw (ModJaw, Lyon, France) [40] has 90 to 150 µm accuracy stated by a distributor and 120 Hz imagery rate, magnetic JT-3D (BioResearch Associates Inc., Milwaukee, WI, USA) [41] states 1.5 µm accuracy in small movement measurements that are ±10 mm from the zero position and states to have the best linearity in the industry with ±5% of the full scale, and magnetic K7x (Myotronics, Kent, WA, USA) [42] that states the maximum error of 0.5 mm in vertical and 0.7 mm in lateral direction in 10 x 10 x 8 mm clinical space. In a higher tier, there is an optical marker enhanced cone beam computed tomography (CBCT) based clinical scanner “Planmeca 4D Jaw Motion” (Planmeca, Helsinki, Finland) [43]. These clinical devices are great for developing and fitting prostheses and can be used in orthognathic pre-operative and post-operative evaluation. However, large external appliances need to be mounted, and steadiness is required from the patient, making 24 h monitoring nearly impossible. These are large clinical machines aimed at short term measurements. Moreover, clinical environment is not a natural environment, while large accessories mounted on the patient’s head and teeth do not make the situation particularly comfortable. A homely mental state of the patient is essential in diagnosing psycho-physiological disorders. Therefore, even if overnight hospitalization is arranged, it would most likely affect the measurement.

1.3. Conclusions of the chapter

In conclusion, there are many ways to continuously detect parafunctions by using wearable devices as well as ways for direct, precision jaw kinematics evaluation and masticatory trajectory recording in a clinical environment. Both fields individually attract a lot of interest both in scientific and commercial sectors, and the demand for a more capable wearable jaw activity registrator is only growing along with the increasing numbers of bruxism patients. However, there are no solutions for assessing the jaw motion directly and continuously. Moreover, according to one of the leading scientists in the field Daniele Manfredini, none of the current portable instrumental diagnostic methods can be employed as a stand-alone

method to replace PSG in bruxism diagnostics [44]. After reviewing the existing solutions and their technical limitations, it was concluded that in order to overcome current technologies and serve as a stand-alone method, the following conditions should be met:

- the device should be able to work continuously,
- the occlusal surface should not be covered,
- the system should be suitable for a wearable application, allowing the patient to perform basic oral functions, including parafunctions,
- the device should be resistant to moisture and movement artifacts.

It is safe to conclude that the currently available methods do not cover the above-mentioned criteria, and an entirely different approach should be taken. Although it is outside the scope of this dissertation, in the early stages of this research, various options for a new approach were explored both in theory and experiments. The possibilities to use ultrasound, inertial measurements, and permanent magnet tracking were inspected. Ultrasonic methods were unable to provide any spatial information, except for the detection of teeth contact. Inertial methods require direct mounting of sensors to the bone (to the teeth) as well as with magnetic sensors. Since there are multiple devices with integrated inertial and magnetic sensing capabilities, both methods can be utilized simultaneously in one system. It resulted in an informed hypothesis that magnetometer-based permanent magnet localization system could be utilized to match the criteria listed above, and it could be supplemented by the inertial measurements. Magnetic approach is the only method with the prospect of providing spatial information of jaw motion that does not require electrical contact between the mandible and maxilla.

2. OVERVIEW OF PERMANENT MAGNET TRACKING METHODS USED IN MEDICAL APPLICATIONS

2.1. Principles of permanent magnet localization

The magnetic field around the magnetic dipole is described in three axial components: x, y, and z. It consists of the magnetic field of the magnet and an ambient magnetic field, which will be called the background magnetic field (BMF) throughout this work. Magnetic localization can be described in two main steps. First one is measuring the magnetic field in the point of interest. In biomedical applications, it is usually done by the micro-electromechanical systems (MEMS) containing 3-axial magnetometers or magnetoresistors, although large high-range magnetic measuring systems may be used in larger scale applications. The second step is processing the acquired data to estimate the position of the magnetic object in relation to the sensor. The magnetic field can be calculated by using a set of nonlinear equations, when relative positions and orientations of the sensor and the magnet are known. However, the equations are too complicated to simply express the inverse problem and solve the coordinates due to the nonlinear nature of the problem and many interconnected variables.

A solution for a permanent magnet position, from magnetic field equations, can be linear [45], nonlinear [46, 47], or combined, feeding less precise but more robust solution as the initial guess for the precision algorithm. For example, linear solution can be used as an initial guess for the Least squares (LS) optimization method [48]. Moreover, particle swarm optimization (PSO) algorithm can guarantee better chances to find global convergence than the LS method, which requires an initial guess. Therefore, the methods can be combined as well by using PSE result as the initial guess for LS [49]. Sensor position could as well be estimated by using neural networks that are taught using realistic data, simulated by the finite element model (FEM); however, it is unclear with what accuracy, especially with BMF contaminated data.

The quality of localization is usually estimated in localization error. It is usually a point-to point distance from the original position to the estimated one. Since the spatial position has three components, the distance is found by calculating the root sum squares between the original and estimated positions. When a test includes many measurements, such as the test trajectory experiment, the average error of all measured points can be calculated. In dynamic experiments, when the measurement is not synchronized and it is unknown which point of the reference matches the measurement, Euclidian distance can be calculated, which represents the minimal point-to-curve distance.

2.2. Approaches realized in the medical applications

Magnetic tracking has been used to solve medical and industrial positioning problems for years. However, with the rise of precise, small scale, Hall sensor based tri-axial magnetometers, the possibilities for magnetic field based position

estimation significantly increased. With growing MEMS magnetometer capabilities, the body of work, regarding magnetic tracking in general and biomedical engineering fields, is growing as well.

2.2.1. Medical instrument tracking in body

Application with probably the largest body of research in permanent magnet position estimation is for tracking the medical instruments inside the body with an integrated permanent magnet. Capsule endoscope is a way to examine the gastrointestinal system by swallowing a camera in a pill, avoiding unpleasant and painful experience of inserting the classic cable endoscope. Moreover, it allows to examine the whole intestine, while cable endoscope is limited to the length of the cable, which makes 4 to 6 meters of small intestine unreachable [50]. With the capsule endoscope, it is important to know the location and orientation of the device in order to relate the recorded footage with the actual location in body [51]. This application usually consists of a large structure of magnetic sensor arrays to cover the whole torso of a patient. The method by a team in Shenzen, China, presented in Figure 2.1, for estimating the position from the magnetic values uses a combination of linear and non-linear algorithm. The team has rejected Powell and Downhill methods for their lack of accuracy, while DIRECT and multilevel coordinate search (MCS) proved to be accurate but too slow. The paper states that Levenberg–Marquardt optimization algorithm was the best choice for the permanent magnet localization. Their latest average localization error is about 1.8 mm [49, 51, 52].

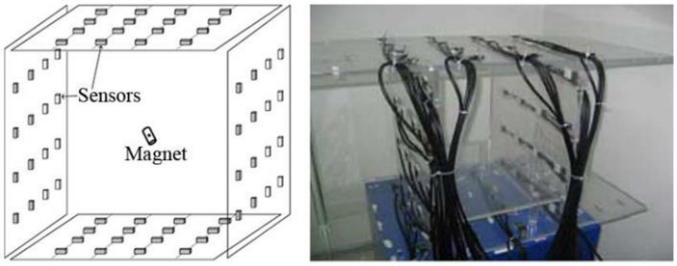

Fig. 2.1. Cubic magnetic sensor array, (a) cubic magnetic sensor array scheme, (b) real cubic magnetic sensor array [52]

Another team in a proof-of-concept publication for a point tracking system for surgical instrument guidance reached the average localization error of 2.65 mm [53]. Their system requires a minimum of 3 sensors and uses triangulation for the position estimation.

For more information, an informative and thorough review of magnetic systems for endoscopic capsule localization is given in [54]. It states that the working range is the main problem with permanent magnet based endoscopic capsule localization methods due to the magnetic field having an inverse third power

relationship with distance. Moreover, assessing the orientation of the magnet is essential for proper determination of pathological issues. However, it should be duly noted that it is not entirely reasonable to compare the average localization errors for methods that have different sized working spaces and use different numbers of sensors.

2.2.2. Eye tracking

A recent and strong set of papers describing a multi-sensor system for eye tracking was published by Biancalana et al. [55, 56, 57]. The system consists of a contact lens with an integrated permanent magnet and a one-sided frame around the eye, similar to the glasses for shortsightedness (Fig. 2.2).

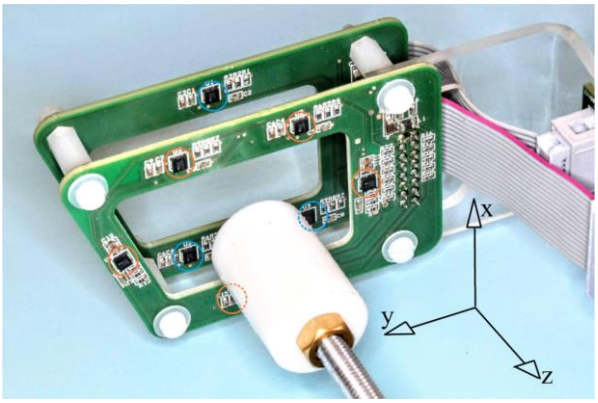

Fig. 2.2. A system for magnetic eye tracking with a magnetic contact lens [55]

The introduced system consists of 8 magnetoresistors distributed around the eye throughout two parallel planes and uses the Levenberg–Marquardt optimization algorithm to get the localization estimate with an emphasis on the initial guess to get the correct local minimum. The precision reached by the team is unclear due to the lack of reference method, but the authors stated sub-millimetric eye-tracking as well as demonstrated test trajectory records of excellent resolution and 100 Hz real time data acquisition and processing rate.

2.2.3. Finger tracking

The methods for tracking movements of the human hand are as well being developed. A finger tracking method was introduced in [58], in a form of a wearable finger accessory with a permanent magnet and 3–4 magnetometers fastened to the back side of the hand. Its objective is to serve as a pointing input for interfacing with electronic devices. It has been only confirmed in simulation and has not been implemented due to the hardware challenges and limitations. The algorithm described in the paper uses a particle filter with 500 particles and a kinematic chain for position estimation. The kinematic chain provides information where and in what orientation the tip of the finger can move, effectively limiting the number of

solutions and decreasing the possibility for error. The simulation resulted in 95% of the points' error (Euclidian distance to the true position) below 4.8 mm. A similar layout was used in another system for tracking a magnet mounted on a finger for handwriting input device [59]. It solves a two-dimensional (2D) problem and uses bi-axial magnetometers. The system used the steepest descent algorithm for the position estimation from B values. The authors report success, and the practical experiment results appear promising; however, no quantitative measure of error was stated in the publication. More recently, there have been a few attempts to create similar finger tracking systems based on the electromagnetism. Finexus system [60] with active electromagnets allows tracking three fingers simultaneously, and in comparison to the reference, the optical tracker demonstrated error of 1.33 mm. Of course, active electromagnet requires wire connection to the control board mounted to the back side of the hand. This drawback is absent in AuraRing [61] system that used a battery-powered coil as a ring on a finger with the measurement electronics implemented in a form of a wristwatch. They experiment with two position assessment algorithms, i.e., LS nonlinear optimization Levenberg–Marquardt algorithm and a closed-form neural network. The authors state that Levenberg–Marquardt algorithm resulted in mean Euclidian error of 4.4 mm and mean 4.65° orientation error, in comparison to the reference optical tracker.

2.2.4. Jaw tracking

There are not many magnetic jaw tracking publications, moreover, recent ones. In 2002, a Japanese research group introduced a jaw tracking system that consists of two permanent magnets attached to the maxilla and mandible, and a fixed array of 32 two-axial flux-gate magnetometers. The localization error within 2 mm was achieved. Moreover, a Russian patent was submitted in 2015, describing an electronic device with an unspecified sensor for collecting data of the lower jaw movements in relation to the upper jaw [62].

2.3. Methods of localization from measured magnetic field values

In this subsection, the algorithms that are potentially suitable or have been mentioned in literature as suitable for magnetic position estimation are described and reviewed. Only the principle of operation and performance specifications of the algorithms are explained, and the amount of calculus is kept to the minimum.

2.3.1. Linear solution

Hu et al. [45] has presented a linear algorithm specifically for solving a nonlinear model of a dipole's magnetic field (2.1) for a 6-DOF localization of a permanent magnet by using a matrix of a minimum of five tri-axial magnetometers (l = 1,2,…,N). For a better understanding of this chapter, the methodology of this dissertation in subsection 3.1.2 explains the model of magnetic dipole and the definitions of variables in detail. The variables used in this subchapter are matching the variables used throughout this dissertation. The schematic visualizing the

variables that describe a magnetic dipole in a coordinate system is presented in Figure 2.3.

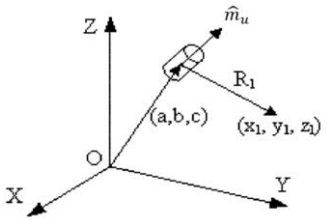

Fig. 2.3. Variables describing a magnetic dipole in a coordinate system [45]

Derivation of Hu's linear model begins by making a cross product of B field value equation (2.1) on its both sides with $\overrightarrow{X_l}$, resulting in the equation (2.2), since $\overrightarrow{X_l} \times \overrightarrow{X_l} = 0$.

$$\overrightarrow{B_l} = B_T \left(\frac{3(\hat{m}_u \cdot \overrightarrow{X_l})\overrightarrow{X_l}}{R_l^5} - \frac{\hat{m}_u}{R_l^3} \right), \tag{2.1}$$

$$\overrightarrow{B_l} \times \overrightarrow{X_l} = -B_T \frac{\overrightarrow{\hat{m}_u} \times \overrightarrow{X_l}}{R_l^3}; \tag{2.2}$$

where $\overrightarrow{B_l}$ is the B field value of a cylindrical magnet at point $\overrightarrow{X_l}$, $\hat{m}_u = (m, n, p)$ is a normalized vector of the dipole magnetic moment, representing the orientation of the magnetism of magnet, (m, n, p) being the vector's projections to the (x, y, z) axes, respectively. B_T is a constant calculated by the formula (3.2). The authors state that since the $\hat{m}_u \times \vec{X}$ is orthogonal to $\hat{m}_u$, the dot product of $\hat{m}_u$on both sides of the equation (2.2) is as follows:

$$(\overrightarrow{B_l} \times \overrightarrow{X_l}) \cdot \hat{m}_u = 0, \tag{2.3}$$

which can be expanded to:

$$\begin{pmatrix} B_{lx} \\ B_{ly} \\ B_{lz} \end{pmatrix} \times \begin{pmatrix} x_l - a \\ y_l - b \\ z_l - c \end{pmatrix} \cdot \begin{pmatrix} m \\ n \\ p \end{pmatrix} = 0. \tag{2.4}$$

Moreover, further expanding (2.4), it results in the following equation:

$$\begin{aligned} &B_{lx}bp - B_{lx}y_l p + B_{lx}z_l n - B_{lx}cn + \\ &+B_{ly}cm - B_{ly}z_l m + B_{ly}x_l p - B_{ly}ap + \\ &+B_{lz}an - B_{lz}x_l n + B_{lz}y_l m - B_{lz}bm = 0. \end{aligned} \tag{2.5}$$

Equation (2.5) can be simplified to:

$$\overrightarrow{F_l}\vec{R} = u_l; \tag{2.6}$$

where

$$\overrightarrow{F_l} = [f_{l1}, f_{l2}, f_{l3}, f_{l4}, f_{l5}] = \left[B_{lx}, B_{ly}, B_{lz}, \left(B_{lz}y_l - B_{ly}z_l\right), (B_{lx}z_l - B_{lz}x_l)\right], \quad (2.7)$$

$$\overrightarrow{R_l} = [r_1, r_2, r_3, r_4, r_5] = [(b - cn'), (cm' - a), (an' - bm'), m', n']^T, \quad (2.8)$$

$$u_l = B_{lx}y_l - B_{ly}x_l; \quad (2.9)$$

with $m' = m/p$ and $n' = n/p$. In equation (2.6), $\overrightarrow{F_l}$ and u_l are the functions of magnetic components (B_{lx}, B_{ly}, B_{lz}) at the (x_l, y_l, z_l) location, which are independent of the six permanent magnet parameters (a, b, c, m, n, p) that were being searched for, while $\vec{R}$ is on the contrary, its only components are the six parameters that are being searched for. That allows solving the equation for $\vec{R}$ using:

$$\vec{R} = \vec{M}^{-1}\vec{U}, \quad (2.10)$$

with the matrix of five tri-axial magnetic sensors $\vec{M} = [F_1, F_2, F_3, F_4, F_5]^T$ and a vector $\vec{U} = [u_1, u_2, u_3, u, u_5]^T$. Hu et al. has tested the method with simulations and stated that in cases when $\vec{M}$ is a non-singular matrix, they were able to find a solution. In cases where the $\vec{M}$ is singular, the authors propose to increase the number of magnetometers and use slightly altered equations that can be found in [45] as well as the final details of extracting each member of the matrix from R, which will not be described in this paper. The resulting average localization error for this method with 16 tri-axial magnetometers in 200 x 300 mm area was 5.6 mm, while the orientation error was 2.9%. The authors state that nonlinear optimization showed similar results but with much longer processing duration.

2.3.2. Algorithms for nonlinear optimization

In their essence, the optimization algorithms are used for solving nonlinear equations or their systems by searching for minima in their error functions. They take an initial guess of the variables that need to be solved, inputs it into the equations (objective function), solves it, and compares the result with the known variables (algorithm inputs). Then, it changes the guess in the direction of the smaller error and iteratively solves the equations until the error is minimal. The selection of the next guess is done by going against the direction of the gradient. The minimization of a multivariate function requires finding a point where the gradient is equal to zero. The points where the gradient is equal to zero are the extremums that are called the local minima and the local maxima. In the case of a convex function, where is only one lowest point, the local minimum is the global one. Several local minima problem is the reason behind the importance of proper and well-informed selection of the initial guess. Incorrect initial guess may converge to the wrong minimum. It as well suggests that the problem with a lot of local minima that may require a different approach.

The gradient represents the rate in which the function is changing. It is calculated by a partial derivative. It is a tangent line to the function at the point of interest, which results in a vector pointing in the direction of the greatest increase of

the function. The point at which the gradient is equal to zero (2.11) is the location of the local minimum, where there is no direction for the gradient to point. The steeper is the slope of the error function, the greater is the gradient.

$$\frac{dF}{dx} = 0 \tag{2.11}$$

Gauss–Newton's method [63] should be mentioned as well, which is very fast. It can be described as iterative approximation of the roots of the error function. When the point of interest x_k is near the minimum x* of the function, it has quadratic speed of convergence. Nevertheless, it does not converge to the minimum of the function when the function has negative curvature. Negative curvature means that the approximation B_k of the Hessian matrix H_k (a square matrix of the second-order partial derivatives of a scalar-valued function) that used by the algorithm is negative. One possible way to mitigate this problem is the steepest descent algorithm, which uses an identity matrix as an approximation of the real Hessian function, which is very inaccurate, but always positive. However, this algorithm has linear speed of convergence, which is very slow [64].

Gradient descent, or Steepest descent algorithm follows the direction of the negative gradient and optimizes the step size, which is taken in the direction of the gradient based on the steepness of the gradient. If it is steep, the likelihood of running into the local minimum is low; hence, the steps can be larger. The gradient approaching zero is a sign that the local minimum is near; thus, the steps should be very small, and the algorithm should ultimately converge to the right solution.

In cases when a function has multiple variables, there will be multiple derivatives, and in turn, multiple gradients, i.e., one for each variable. LS method minimizes the sum of squared errors, hence reducing the number of gradients to one. The two LS optimization methods available in Matlab Optimization Toolbox are Trust Region Reflective and Levenberg–Marquardt.

Trust Region methods select a region around the locally best point and try to approximate it by using some model, usually quadratic. Then, based on that model, the algorithm makes a step towards the best location of the model. If a significant gradient decrease is observed, the algorithm believes that the model will be a good representation of the real function. The size of the Trust region in the next iteration depends on the previously made improvement: the better is the improvement, the more the algorithm trusts to find notable gradient decrease in that direction and expands the region. In a negative curvature case, Trust Region methods simply perform a large step in search of a more interesting region [65].

Levenberg–Marquardt method adaptively changes the way of updating the parameters. It acts more like the Gradient descent method when the parameters are far from the minimum and becomes more similar to the Gauss–Newton method when approaching the optimal values of the parameters [66]. In a negative curvature case, Levenberg–Marquardt algorithm is slower than Trust Region methods.

2.3.3. Particle swarm optimization

Particle swarm optimization (PSO) is an interesting approach based on the collective behavior of large groups of animals. Although the swarming theory was researched by observing fish schooling and bird flocking and was attempted to be simulated mathematically before [67], the concept of using particle swarm methodology for the optimization of nonlinear functions was introduced in 1995 by Kennedy and Eberhart [68]. What is unique about this algorithm is that it does not depend on the gradient of the objective function, which allows solving the optimization problems that are not differentiable. However, PSO does not guarantee that an optimal solution will ever be found. It relies on a few simple equations and basic mathematical operations and uses only a few parameters. The group of the particles is called the swarm, while the members of the population imitating the group of animals are the particles. The algorithm begins by creating a group of random particles, where each of them is a possible solution to the objective function. In order to assess whether the position of the particle is good or bad, a fitness function is solved, which is the same as an objective function in LS algorithms. Each particle remembers its and its neighbors best previous positions. Each particle as well knows its own position and velocity, and in each iteration, these values are updated. The particles can update their position by equation (2.12) based on the direction and magnitude of the velocity vector, and their velocity vector is found by equation (2.13), based on the previous velocity, position of personal best value (cognitive component), and position of global best value (social component).

$$\vec{x}_i(t+1) = \vec{x}_i^t + \vec{v}_i(t+1), \tag{2.12}$$

$$\vec{v}_i(t+1) = w\vec{v}_i(t) + c_1 r_1\left(\vec{p}_i(t) - \vec{x}_i(t)\right) + c_2 r_2\left(g(t) - \vec{x}_i(t)\right); \tag{2.13}$$

where x_i stands for the i-th particle of the swarm, v_i is the i-th particle velocity defining the size and direction of the particle step, t is the discrete time step showing the iteration number of the algorithm, w is an inertia coefficient, c_1 and c_2 are the coefficients representing acceleration, r_1 and r_2 are randomly generated values uniformly distributed in the range from 0 to 1, $p_i(t)$ and g(t) are personal best and group (global) best values, respectively. The random numbers are needed to introduce some chaos into the system, in order for it to become dynamic, explorative, and not to converge too quickly, thus missing the best solution. The acceleration coefficients are needed to control the amount of chaos, effectively controlling the speed of the whole process.

2.3.4. Neural networks

Artificial neural networks (ANN) is a method for computing inspired by the biological neural networks found in the brain. It is trained to recognize patterns in the provided data by developing neural pathways in a network of software-simulated neural cells and is able to categorize or otherwise process the unseen data of the same type. The first mention of such idea in the scientific literature was in 1943 by

McCulloch and Pitts [69]. Be that as it may, the invention of this world-changing technology cannot be credited to one person, because the development of this method was gradual and slow. Backpropagation algorithm [70] and the introduction of unsupervised learning [71] may be considered among the key contributions. Nevertheless, the technology started to boom at the beginning of the 21st century due to the rapidly increasing computational capabilities of computers and an increasing number of advances in the field.

ANN consists of many interconnected nodes that represent biological neurons and are called artificial neurons. There can be a countless number of possible configurations of the ANN; however, some general rules and terms apply to most of them. In order to describe the general principle of ANN, a basic multilayer perceptron can be used, and its operation goes as follows. The links connecting the artificial neurons are called the edges. Each of them has a numerical multiplication coefficient called the weight that represents the significance of the input. The layers are the groups of artificial neurons. The input layer requires as many neurons as there are input variables, because it takes in the outside data. There can be from 1 to any number of hidden layers that are used to perform the operations on data. At the neurons of hidden layers, the data is being multiplied by weights and added along with the bias value of those particular neurons, resulting in their activation functions. Forward propagation is when the data travels forward through the layers and the activation functions determine whether the neuron will forward the data to the next layer and with what weight it will do that. Backpropagation is when the network is fed data with known outputs, which propagates backward through the network and iteratively calibrates the weights that the inputs match the provided output. It is done by computing the gradient across all network layers to minimize the loss function. The loss function or the error function is yet another name for an objective function when the minimum is searched, while the objective function is where the maximum is searched and is called the reward function or fitness function. However, it does not make a lot of sense to search for the maximum error. The output layer consists of as many neurons as there are possible categories or solutions, and the neuron with the highest value shows that it is the most likely that the data belongs to the category assigned to it.

The possibility to use ANN for magnetic localization has been investigated and described in [72] for the case of indoor localization. The main advantage of using ANN for solving inverse problems is a much higher speed. The training data is constructed by direct calculation of magnetic field values for most cases of possible magnetic source position. The training data consists of all magnetic field components for each sensor and the corresponding location of the magnetic source. In order to increase the quality of predictor functions, it is suggested to pre-process the training data by logarithmical transformation of the magnetic field values due to the high attenuation of the magnetic field. However, the authors do not state the configuration of used ANN. The resulting localization error of the described study was 44 mm in a 2 x 2 x 2 m cubic space.

2.3.5. Particle filter

A particle filter is otherwise known as a sequential Monte Carlo method. In turn, Monte Carlo method is a probabilistic method used for solving problems that are deterministic in their nature. It is useful when an objective function is nonlinear, multi-componential, or otherwise complicated, but it is possible to measure some parameters regarding the problem, and something is known about the relation between the measurements and the problem. The idea of the particle filter is to generate a lot of possible solutions, called particles, throughout the map of possible solutions to the problem. Based on the known relationship of the position and the measurements, for example, an objective function, it can be determined how likely it is that the guessed particle position is correct. Based on this likelihood of how well the particle position explains the measurement, each guessed particle is assigned a numerical coefficient called the weight. In the next step, all unlikely particles are discarded, and a new set of particles is newly generated in close proximity to the more likely particles with all the weight values cleared. The third step is propagating the particles in time by using preliminarily estimated model of possible velocities of the object. After this, the steps are repeated iteratively. This allows the filter to discard singular matches and follow the change in topography of the objective function, instead of singular measurement of one point. This feature makes the method attractive for tracking moving objects, and it has been popular in complicated and noisy live localization problems.

2.4. Conclusions of the chapter

It should be mentioned that throughout the reviewed research, in all described methods and solutions, the minimal number of used magnetometers was three; however, there were significantly more in most cases. The extra sensors are necessary in order to estimate nine variables, i.e., three components, each for position, orientation, and ambient field, and in the mentioned applications, this feature is necessary. However, in a more restricted and predictable mechanical system, such as the human jaw, dropping the orientation estimation could add a lot of robustness to the method, while the orientation could be assessed otherwise. Another feature that is common to all the described methods is the range of the measurement, which ranges from several to tens of centimeters. This requires larger, stronger magnets and larger magnetometer matrixes. It makes sense, since there is almost no reason for implementing passive, electrically disconnected component tracking in such close range. However, in the case of human jaw application, it might be just right: the human masseter, in relation to the skull, has known and limited movement directions and inherent range limitations. Utilizing the limited and predetermined movement characteristics of the finger as a mechanical system in the use of kinematic chain for aiding finger detection is an interesting idea. The mechanical system of the human jaw has even less joints, and the predictability of its limited motion will be utilized in this work.

Based on the literature and review of the non-linear optimization algorithms, LS methods seem to be most suitable for solving magnetic field equations. Both Trust-Region and Levenberg–Marquardt methods are fit to handle the task; however, Trust-Region method is faster, especially in cases when the curvature of the optimization function is negative. Linear solution is complex, but might be useful if an uninformed initial guess is not sufficient for the standard LS algorithms. PSO algorithm and neural networks as well appear to have potential and should be practically assessed, especially due to being computationally inexpensive and fast. The data processing methods and implemented algorithms are very important in magnetic localization, and it may not be possible to definitely determine the best approach for a certain situation from the literature. Among the reviewed publications, there was no comparative study of magnetic localization algorithms using the same dataset; therefore, such test was performed in this work on two most promising methods (LS and PSO) based on the literature.

3. METHODS AND EXPERIMENT METHODOLOGY

3.1. Proof of concept for single-magnetometer based magnet localization and accelerometric teeth impact detection

3.1.1. Finite element model of a permanent magnet

In order to better understand and verify the mathematical model of the magnetic field around the magnetic dipole that is used in this work, to test the method, evaluate localization algorithms, find optimal layout and optimal configuration of the sensor, a FEM of the used permanent magnet was created by "Comsol Multiphysics 5.1" (COMSOL Corporation, Stockholm, Sweden) software. The FEM magnet with the vectors representing the modeled magnetic field is shown in Figure 3.1.

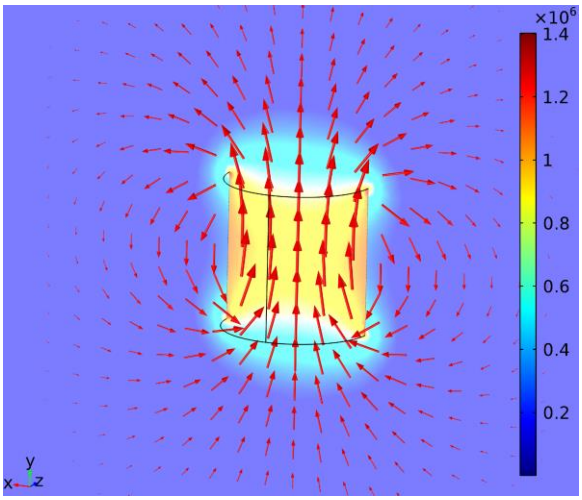

Fig. 3.1. FEM of a cylindrical dipole magnetic field; color: magnetic density norm (μT); arrow (logarithmic): flux density

Physics controlled, extremely fine, free tetrahedral mesh was used with the maximum element size of 0.401 mm and minimum element size of 0.00401 mm, the maximum element growth rate of 1.3, curvature factor of 0.2, and the resolution of narrow regions of 1. The complete mesh consisted of 2168866 domain elements, 36288 boundary elements, and 704 edge elements. In the whole FEM space that surrounds the permanent magnet (200 × 200 × 200 mm), at each spatial point with a 0.1 mm step, the values of the magnetic field have been found. When it was needed to imitate the ambient field, a BMF = [0 65 0] μT magnetic field vector was added to the FEM data.

3.1.2. Proof of concept for single-magnetometer based 3-DOF localization

Method. The conception for the permanent magnet based jaw position estimation relies on the physical properties of the magnetic field around the dipole; its strength and direction can be precisely calculated at any spatial point, and every point in one hemisphere of the dipole has a unique, non-recurring B field vector value [74]. It can be found by knowing the orientation of the permanent magnet, the orientation of the point of interest (sensor position), and its spatial position, relative to the magnet. This implies that B field measurement can be used for an inverse problem of estimating the relative sensor position. A very suitable feature for this particular application is the absence of electrical connection between the mandible and the maxilla. The magnet could be attached to the upper molars (maxilla) and the electronics, including a tri-axial magnetometer, could be mounted on the lower molars (mandible). The illustration of the concept is presented in Figure 3.2 [8].

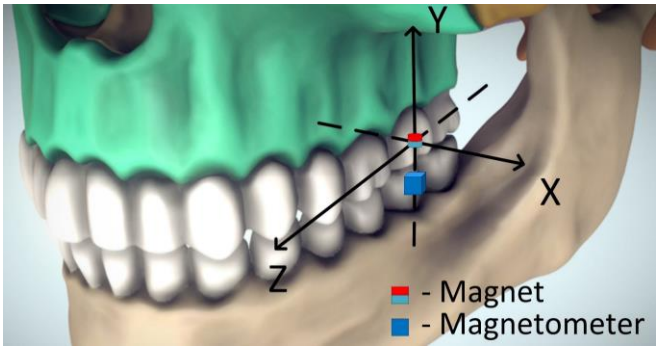

Fig. 3.2. Basic jaw tracking concept with one magnetometer based on [75]

Throughout all experiments in this research, the same kind of a permanent magnet was used. It was decided to use a cylindrical magnet; thus, in one direction, the magnetic field would be radially symmetric, and the closest to that of an ideal dipole. The smallest and strongest permanent magnet available in retail was chosen. It was a neodymium (NdFeB) magnet that had a residual magnetism of 1.4 T, resulting in a uniform magnetization magnitude of M_0 = 1,114,084 A/m, directed along the rotational axis, length of 2 mm, and a radius of 1 mm.

Formula (3.1) is a model describing B field value of a cylindrical magnet at point X [45].

$$\vec{B} = B_T \left(\frac{3(\hat{m}_u \cdot \vec{X})\vec{X}}{R^5} - \frac{\hat{m}_u}{R^3} \right), \tag{3.1}$$

$$B_T = \frac{\mu_r \mu_0 \pi r^2 L M_0}{4\pi}, \tag{3.2}$$

$$\vec{X} = \big((x-a),(y-b),(z-c)\big), \tag{3.3}$$

$$R = \sqrt{((x-a)^2 + (y-b)^2 + (z-c)^2)}; \tag{3.4}$$

where $\widehat{m}_u = (m, n, p)$ is a normalized vector of the dipole's magnetic moment, representing the orientation of the magnet's magnetism, (m, n, p) being the vector's projections to the (x, y, z) axes, respectively. B_T is a constant calculated by the formula (3.2), where μ_r is the relative permeability of the medium (air), $\mu_0 = 4\pi \times 10^{-7}$ (T·m/A) is the magnetic constant, L – the length of the magnet (m), r – the radius of the magnet (m), and M_0 is the magnetization of the magnet (A/m). X is the location of a magnetometer calculated by (3.3), in relation to the permanent magnet location, which is (a, b, c) = (0, 0, 0) and represents the main frame of reference. R is the magnitude of the X vector calculated by the formula (3.4) [45]. It should be mentioned that (3.1)–(3.4) expressions describe the first-order dipole approximation, which is applicable (with the maximum error that is less than 1%) to the points that are no closer than $1.5 \times \sqrt{R^2 + \left(\frac{L}{2}\right)^2}$ to the magnet center [76]. In the case of a 2 × 2 mm cylindrical magnet used in this work, it would be 2.14 mm.

The model can be expanded into three separate equations for each axial constituent of magnetic field:

$$B_x = B_T \left(\frac{3[m(x-a)+n(y-b)+p(z-c)](x-a)}{R^5} - \frac{m}{R^3} \right), \quad (3.5)$$

$$B_y = B_T \left(\frac{3[m(x-a)+n(y-b)+p(z-c)](y-b)}{R^5} - \frac{n}{R^3} \right), \quad (3.6)$$

$$B_z = B_T \left(\frac{3[m(x-a)+n(y-b)+p(z-c)](z-c)}{R^5} - \frac{p}{R^3} \right). \quad (3.7)$$

Electromagnetic theory states that magnetic field values of a magnetic dipole can be found, if coordinates and orientations of the magnet and the observer (sensor) are known. However, an opposite expression is not derived that easily. The equations contain too many interconnected components, and there is no way of directly expressing the dipole location from the measured B values. A nonlinear LS optimization method was chosen to solve the equations in the proof of concept stage, and Trust Region Reflective algorithm was selected to be used for LS error optimization. It iteratively solves the provided optimization function (the used equation system) and gradiently changes the solution value until the error is minimized. The solution value initially starts as a guess, until the sum of squared errors between the possible solution and the provided function input reaches the predetermined minimum.

The code for localization from B value measurements was written in Matlab (Mathworks Inc., Natick, MA, USA). The validity of the algorithm was verified by using a FEM of the permanent magnet ant its surrounding space, described in subchapter 3.1.1.

The boundaries of the working range of the measurement were manually set for the algorithm. For estimating the position during the first measurement, the initial guess was pointed at the position closest to the magnet, where the magnetic field is the highest; therefore, the error gradient is very steep and clear. In order to

avoid single erroneous measurements throwing off the whole trajectory, the average of several positions is used. In order to estimate the following positions, previous positions are used as the next initial guess. This approach, in the case of following a trajectory, pointed the algorithm very close to the solution and reduced the computation time. In [55], there is a compelling discussion by Biancalana et al. on the nuances of proper initial guess selection and its significance in optimization algorithms. The physiology of the jaw determines that all possible position solutions will be located in the same hemisphere of the magnetic dipole. Therefore, when the sensor orientation is known, there are no duplicate values anywhere in the working range, and the optimization is much easier with a single local minimum.

Experiment. In order to prove the concept of the magnetic position estimation method in practice, a single-magnetometer test was executed. The same test was performed both on the theoretical data from FEM and in practice. The magnetic field was measured with MPU-9250 (TDK InvenSense, San Jose, CA, USA) 9 degrees-of-freedom (DOF) inertial measurement units (IMU), containing 3-axial digital magnetometers with a dynamic range of ±4912 μT. The IMU chip dimensions were 3 x 3 x 1 mm. The sensors were controlled by using an nRF52832 microcontroller development kit (Nordic Semiconductor, Oslo, Norway). The BMF was measured with a reference magnetometer mounted away from the main sensor and was subtracted from the recorded data. Both magnetometers were calibrated pre-test. In order to simulate the masticatory function, a natural masticatory trajectory was needed. Therefore, it was sampled from a paper describing a method for video-based jaw tracking [77], where the authors have recorded their own jaw motion. The sensor was moved along the test masticatory trajectory using Elinta EMS-301 (Elintos Matavimo Sistemos, Kaunas, Lithuania) 3D positioning system, which has positioning resolution of 0.1 mm. The data acquisition from the sensor as well as the control of the positioning system was implemented by using Matlab software. The magnet was attached in a static position as the positioning system controlled the sensor position. The experimental setup and the photograph of the system are presented in Figure 3.3.

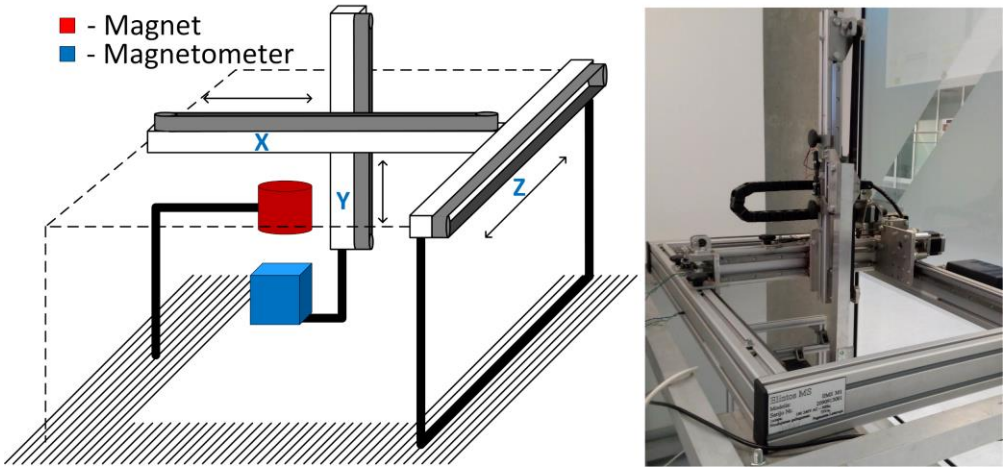

Fig. 3.3. Experimental setup (left) and 3D positioning system “EMS 301” (right)

Localization error expression. Localization errors are usually expressed in Root mean square error (RMSE) for point-to-point position estimation or in the Euclidian distance (ED) for point-to curve position estimation. When more than one measurement is performed, the localization error estimates are averaged, and a standard deviation is calculated for the set of measurements in order to describe the dispersion of the resulting error throughout different measurement iterations. For all cases of practical experiments in this dissertation, each experimental measurement was performed for 10 iterations. Such number of iteration was chosen due to the working time limitations in robotics laboratory.

Part of this subsection has been quoted verbatim from the source [8].

3.1.3. The use of accelerometry for teeth impact detection

Method. The method for detecting the impacts of teeth from the changes in the sensor acceleration is not complicated. In realistic conditions, especially in grinding, the impacts of teeth may be vertical as well as lateral or protrusive. Considering that, the first step is calculating the magnitude of the vector of acceleration. It is done by finding a root sum of squares (RSS) of x, y, and z components of the said vector. Further signal processing, such as filtering, squaring, or differentiation, may be required to emphasize the real impacts, while suppressing other artifacts. However, in laboratory conditions, it was unnecessary, because even soft teeth impacts showed significant changes in the acceleration. However, during the experiments, the vibration of the articulator motors and uneven motion were noticeable in the data, which should not be a problem in the clinical application.

Experiment. A custom, servo motor driven single-hinge articulator was built to simulate vertical jaw motion with teeth impacts. An MPU9250 (TDK InvenSense, San Jose, CA, USA), 9-DOF IMU evaluation board was attached to the moving part

of the articulator. The board contained a tri-axial accelerometer that was used for impact detection and a 3-axial gyroscope that was utilized as a reference for illustrating the motions of the articulator. The articulator and the setup of the experiment are presented in Figure 3.4.

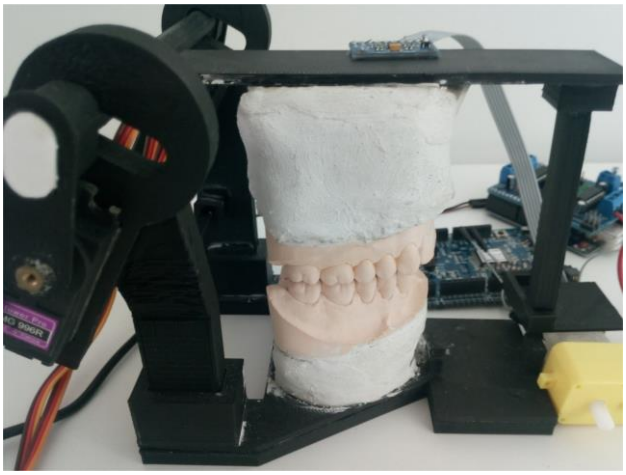

Fig. 3.4. Single-hinge vertical motion articulator with attached IMU

In order to form a firm mechanical connection that would transfer the vibrations to the sensor well and prevent sensor movement, cyanoacrylate glue was used. The sensor was placed on a flat surface of the moving part of the articulator to increase the contact surface.

The aim of the experiment was to assess whether it is possible to recognize teeth impacts from the changes in acceleration, well enough to differentiate between the similar motions with and without the impact. Therefore, during the experiment, a gypsum model of teeth was brought to occlusion with a mild impact in half of the motion cycles, while the other half was nearly identical motions but without the impact. The type of motion was alternated every three cycles.

3.1.4. Dynamic 3-DOF localization test with teeth impact detection

Experiment. A robotic jaw motion articulator was built for proving the concept of magnetic position estimation with simultaneous accelerometric teeth impact detection. It was designed to imitate chewing. A custom made 6-DOF Stewart platform, as well known as a hexapod, was used as a basis for the device. It was driven by 6 servo motors. The device was able to execute masticatory motion with a model of teeth that was 3D printed from polylactide (PLA). Due to the nature of the economy-class custom device and its components, it was not possible to achieve good repeatability and accurate replication of the given coordinates. Therefore, a state-of-the-art electromagnetic localization system “3D Guidance TrakStar” (Ascension Technology Corporation, Shelburne, VT, USA) was utilized

as a reference method for recording the actual trajectory, in which the articulator was moving. The TrakStar system has a heavy transmitter and a small, wired receiver. It works by alternating low radio-frequency electromagnetic fields; therefore, it neither affects the readings of the proposed magnetic localization system, nor is it affected by it. The data was processed after the experiment. The experimental measurement was synchronized to the reference measurement by using time-stamps in the recorded data and operator-induced artificial synchronization artifacts at the beginning of the experiment. A 2 x 2 x 2 mm cylindrical neodymium magnet was mounted on the maxilla using cyanoacrylate glue. The sensors were mounted on the mandible using hot glue. The articulator and the experimental setup are presented in Figure 3.5.

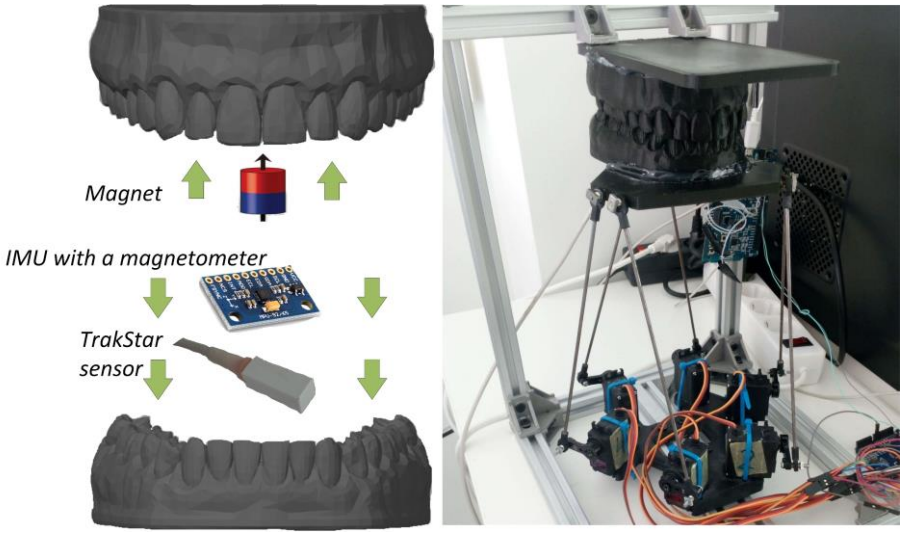

Fig. 3.5. Experimental setup for the general system test using a custom Stewart platform

During this experiment, the sensor was in motion. For dynamic measurements, the data collection rate was 100 Hz. Moreover, a N = 19 window size moving average filter was used for data smoothing and random noise cancellation. The optimal size of the filter window was determined experimentally by visual inspection and evaluation of the form and quality of the recorded trajectory line. For the best results, a compromise had to be made between the preservation of the real shape of the trajectory and the smoothing of magnetometer output fluctuations. The threshold of processed acceleration data was determined experimentally that it would suit this particular experimental setup. The materials and forces are different in the real patients, and the parameters would have to be adapted for clinical application.

3.2. Background magnetic field

3.2.1. Effects of background magnetic field

In the beginning of any work, including magnetic measurements, the BMF effects must be accounted for. Every magnetic measurement has components of the magnetic field of the Earth, which varies around 25–65 μT [78], depending on the location and elevation (height above the sea level). Based on this, throughout this work, the value of 65 μT was used in BMF simulation and assessment. It should be noted that the principle of superposition applies to the magnetic field; thus, the BMF components can be removed by basic subtraction, if they are known.

Experiment. While changing the magnet-sensor distance throughout the 15 mm working range, the errors were estimated that would result from the BMF acting in three different directions. During the experiment, both FEM and experimental data were used. The sensor was moved in one axis, while other axes positions were constant and equal to 0. The schematic illustrating the experiment is presented in Figure 3.6.

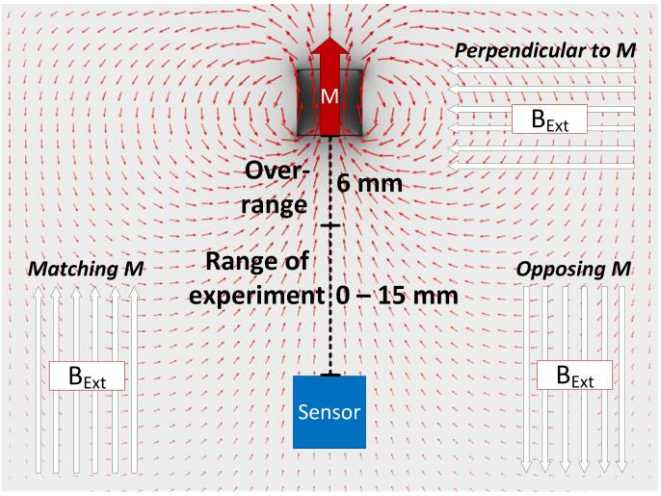

Fig. 3.6. Principle of evaluating the influence of BMF vector B_{EXT} acting in various directions

3.2.2. Methods for mitigating background magnetic field

In some cases, there is an option to use magnetic shielding for the BMF mitigation. In other words, it is a physical coverage of the whole measurement environment. Such approach is not suitable for the biomedical applications, unless the whole room is being shielded. Shielding can be passive when the volume in which the measurement is made is covered by a high permeability ferromagnetic material. There are materials for passive shielding, for example, a material commercially marketed as MuMetal (Magnetic Shield Corporation, Bensenville, IL,

USA) [79]. It is an iron and nickel alloy that has been specifically designed to attenuate magnetic field. Another way of shielding is active shielding [80]. It is usually used on a passively shielded area to actively compensate for the magnetic field that was not completely blocked. This is possible due to the principle of superposition that applies to the magnetic field. Magnetic shielding is not an option for a wearable intra-oral device, because a stationary shielded room is expensive and beats the purpose of a wearable device for continuous measurements.

Subtractive compensation requires at least 35 mm distance from the main sensor and significantly increases the size of the device, which is as well undesirable in the intraoral device. There has been several approaches described in literature [53, 56] of multiple magnetometer systems being used for both localization and BMF compensation by solving the optimization task with all recorded data. Therefore, a hypothesis was raised that two magnetometers might be able to be used for utilizing BMF estimation and magnet localization simultaneously. In such case, with only two magnetometers, the position of the reference magnetometer (in relation to the main magnetometer) must be known and constant. Nevertheless, both sensors could be used inside of the magnetic field of the permanent magnet, which would significantly reduce the size of the system.

Experiments. Due to its short dynamic range, it might be possible to use the subtractive BMF compensation for the proposed method. According to [81] study, the average length of the human dental arch is 33.60 ± 2.94 mm, and the average width is 51.27 ± 2.68 mm. Needless to say, the size of the skull depends on the individual's sex, ethnicity, and genetics in general. Small reach of the magnet field should allow placing the reference sensor on the opposing sides of the dental arch. In order to prove this theory, the dependency of the magnetic flux density magnitude to the magnet-sensor lateral distance (x) was drawn. The vertical distance was kept at a constant of 6 mm (start of the dynamic range).

The experiments for proving the concept of BMF compensation by using a LS optimization algorithm are the same as for proving the concept of the two-magnetometer 3-DOF localization method, because two adjacent magnetometer localization with BMF compensation is a single method for solving two problems, hence, one does not work without the other. Therefore, the methods of proof of concept experiments of the BMF compensation by optimization algorithm are referred in subchapter 3.3.1.

3.3. Two-magnetometer approach

3.3.1. Two-magnetometer 3-DOF localization with BMF compensation

Method. In order to use two adjacent magnetometers for both position and BMF calculation, the position of the reference magnetometer (in relation to the main magnetometer) must be known and constant. In this way, both magnetometers take part in the position determination as well as in the BMF evaluation and compensation. Such solution can significantly reduce the size of the system, since it eliminates the need to place the reference magnetometer outside of the field of the

permanent magnet. The aim of this subsection is to validate the possibility of simultaneously solving BMF values and the magnet position by utilizing two adjacent, tri-axial magnetometers with a fixed (22 mm) distance to each other. An illustration of the two-magnetometer based 3-DOF permanent magnet localization method is presented in Figure 3.7.

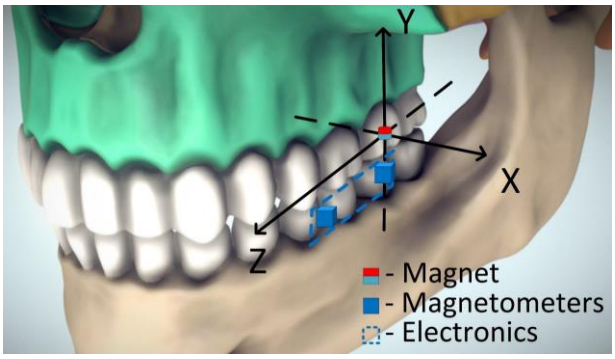

Fig. 3.7. Illustration of the concept of the method based on [75]

By adding 3 extra measured values (B_{refx}, B_{refy}, B_{refz}) with 3 extra equations describing them, 3 more unknown variables could be solved. In the case of the proposed method, in addition to x, y, and z position determination, such an algorithm could solve 3 constituents of the BMF (BMF_x, BMF_y, BMF_z), while simultaneously compensating for them. The system of equations for the improved model is presented below, where B values for the main magnetometer are in (3.8)–(3.10), and B_{ref} values for the reference magnetometer are in (3.11)–(3.14). The connection between the main and the reference equations is described in equations (3.15)–(3.17).

$$B_x = B_T\left(\frac{3[m(x-a)+n(y-b)+p(z-c)](x-a)}{R^5} - \frac{m}{R^3}\right) + BMF_x, \tag{3.8}$$

$$B_y = B_T\left(\frac{3[m(x_l-a)+n(y_l-b)+p(z_l-c)](y_l-b)}{R^5} - \frac{n}{R^3}\right) + BMF_y, \tag{3.9}$$

$$B_z = B_T\left(\frac{3[m(x_l-a)+n(y_l-b)+p(z_l-c)](z_l-c)}{R^5} - \frac{p}{R^3}\right) + BMF_z, \tag{3.10}$$

$$x_{ref} = x, \tag{3.11}$$

$$y_{ref} = y, \tag{3.12}$$

$$z_{ref} = z + \Delta z, \tag{3.13}$$

$$R_{ref} = \sqrt{(x_{ref} - a)^2 + (y_{ref} - b)^2 + (z_{ref} - c)^2}, \tag{3.14}$$

$$B_{refx} = B_T\left(\frac{3[m(x_{ref}-a)+n(y_{ref}-b)+p(z_{ref}-c)](x_{ref}-a)}{R_{ref}^5} - \frac{m}{R_{ref}^3}\right) + BMF_x, \tag{3.15}$$

$$B_{refy} = B_T \left(\frac{3[m(x_{ref}-a)+n(y_{ref}-b)+p(z_{ref}-c)](y_{ref}-b)}{R_{ref}^5} - \frac{n}{R_{ref}^3} \right) + BMF_y, \quad (3.16)$$

$$B_{refz} = B_T \left(\frac{3[m(x_{ref}-a)+n(y_{ref}-b)+p(z_{ref}-c)](z_{ref}-c)}{R_{ref}^5} - \frac{p}{R_{ref}^3} \right) + BMF_z; \quad (3.17)$$

where Δz is the distance between the magnetometers on the printed circuit board (PCB) of the sensor in the z axis. On the other axes, the main-to-reference magnetometer distances Δx and Δy are equal to 0, but could be added as well if needed.

In order to keep the optimization method that has been selected to solve the above-mentioned equations on track, the limitations on the maximum magnitude of the BMF should be set. The magnitudes of the possible solutions of the three BMF components should be recalculated at every point of optimization and adaptively limited to not exceed the 65 μT maximum magnetic field of the Earth.

Experiment. The experiments for one-magnetometer proof-of-concept described in subchapter 3.1.2 were repeated with the two-magnetometer 3-DOF localization method with BMF compensation. These experiments were as well performed on the FEM data with simulated BMF = [0 65 0] μT and the experimental data from Elinta 3D positioning system.

Part of this subsection has been quoted verbatim from [9].

3.3.2. Estimation of jaw rotation angles

In the method described above, the position estimation is possible if the orientations of the magnetometer and the magnet are known. This would suggest that by using two tri-axial magnetometers, it is only possible to evaluate the relative 3D position of two objects that are unable to rotate in any axis, resulting in 3-DOF position estimation. However, if the rotation correlates with translation in a rational way, it should be possible to assess probable sensor angle values from the sensor-based 3-DOF position estimate. Therefore, a hypothesis was raised that if the rotation of the human jaw correlates with translation, it should be possible to implement an algorithm, estimating the 5-DOF position from 3-DOF data. It can be done by simplifying the motions of the jaw to a 5-DOF mechanical system and utilizing the measurable dimensions of the jaw and trigonometry. As it is described in detail in subchapter 1.1.2, the TMJ can both rotate and slide forward. The forward sliding trajectory (condylar path) is dependent on the size of the articular tubercle, otherwise called the articular eminence. Some people have almost a straight horizontal condylar path, while others jaws slide forward and slightly downward onto the articular tubercle [20].

Vertical rotation around the x axis (opening): after the jaw opens at first 10–20°, it only rotates. When opening further, it starts sliding forward with both joints following the condylar path. It as well continues rotating. In chewing, talking, or bruxing, the jaw usually does not reach such an angle.

Horizontal, (side) rotation around the y axis: when the jaw turns to the side, it rotates around the joint of that side to which it is turning, while the joint of the other side slides forward, following the condylar path.

The only rotation around the z axis is the slight tilting during the side (y) rotation, while one joint is fixed translation-wise and the other side slides onto the articular tubercle. Otherwise, the jaw is not able to rotate around the z axis, meaning it is not possible to open only one side of the jaw while the other remains in contact. Moreover, predicting jaw rotation around the z axis is not possible: its rotation cannot be linked to any translation, as the jaw is free to translate (slide) along the z axis, while following the condylar paths of each joint. Considering the mentioned reasons, the z rotation has not been accounted for in the proposed method. Thankfully, the slight z axis tilting during the side (y axis) turn has a trivial effect on the position evaluation, compared to the significant advantages of predicting the other two DOFs of rotation (x and y axes).

Method. Vertical rotation (around the x axis) angle α_V can be linked to the vertical translation Y_V via (3.18)–(3.20) with an explanatory drawing presented in Figure 3.8. The L (length) and H (height) TMJ-to-sensor dimensions must be measured, while Y_V is calculated from the sensor output.

$$TS_V = \sqrt{L^2 + H^2}, \tag{3.18}$$

$$\beta_V = \arccos\left(\frac{L}{TS_V}\right), \tag{3.19}$$

$$\alpha_V = \arcsin\left(\frac{H+Y_V}{TS_V}\right) - \beta_V. \tag{3.20}$$

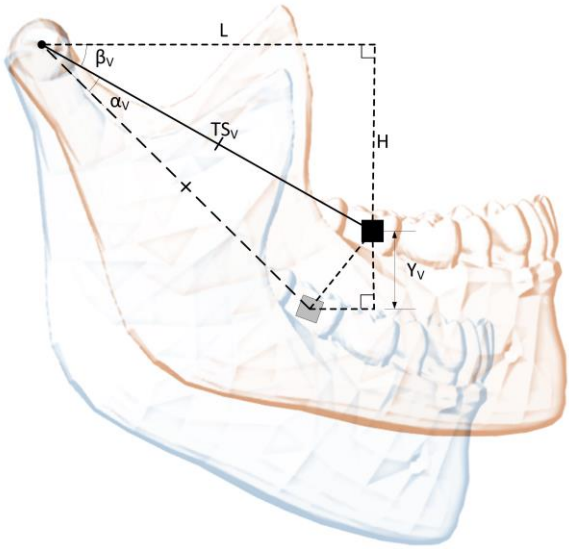

Fig. 3.8. Vertical rotation angle relation to vertical linear displacement, based on [82]

Linking horizontal rotation (around y axis) angle α_H to the horizontal (side) translation X_H is slightly more complicated. Since the sensor is placed on one side of the jaw, the dimensions are different for each side, although the same equations (3.21)–(3.24) are applicable in both cases. An explanatory drawing for horizontal rotations is presented in Figure 3.9. The L (length) and W_H (width) TMJ-to-sensor dimensions must be measured, while X_H is calculated from the sensor output.

$$TS_H = \sqrt{L^2 + W_H^2}, \tag{3.21}$$

$$Y_H = W_H - X_H, \tag{3.22}$$

$$\beta_H = \arccos\left(\frac{L}{TS_H}\right), \tag{3.23}$$

$$\alpha_H = \arcsin\left(\frac{Y_H}{TS_H}\right) - \beta_H. \tag{3.24}$$

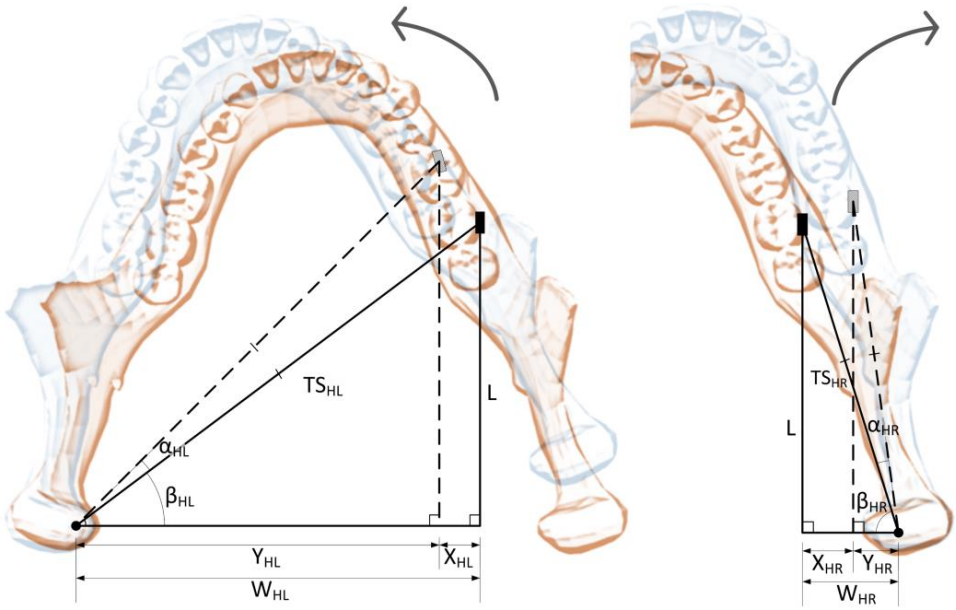

Fig. 3.9. Horizontal rotation angle relation to left and right horizontal linear displacements, based on [82]

The rotation of the sensor coordinate system that is centered on the main magnetometer calls to re-evaluate the change of the reference magnetometer position. If the sensor did not rotate, there would be a constant 22 mm displacement at the z axis (as placed on the PCB) and 0 mm at x and y axes. However, when rotations are involved, the projection on the z axis shortens, and the projections on

the x and y axes increase. The rotation in two axes results in translation in all three axes. This is described in equations (3.25)–(3.28), taking into account that the limits of the jaw rotation are far less than 90°:

$$y_{ref} = y + (\Delta z \cdot \sin(\alpha_V)), \tag{3.25}$$

$$\Delta z_y = \Delta z \cdot \cos(\alpha_V), \tag{3.26}$$

$$x_{ref} = x + (\Delta z_y \cdot \sin(\alpha_H)), \tag{3.27}$$

$$z_{ref} = \Delta z_y \cdot \cos(\alpha_H); \tag{3.28}$$

where y_{ref} is the final position of the reference magnetometer on y axis, Δz is the true distance between the magnetometers, α_V and α_H are vertical and horizontal rotation angles, respectively, Δz_y is Δz projection on z axis after the vertical rotation (y translation), x_{ref} and z_{ref} are the final positions of the reference magnetometer on x and z axes, respectively. It should be noted that based on the orientation of the skull coordinate system specified in Figure 3.7, the only possible translation in the y (vertical) axis is negative. Negative translations in other axes are matched by the negative rotation angles as well. In practice, 5-DOF (extra 2 DOFs) evaluation was implemented by adding trigonometric translation-to-rotation dependency equations to the optimization algorithm. During each iteration of the optimization algorithm, the calculated B values were rotated by using a rotation matrix, by the angles acquired from the translation-to-rotation dependency equations. Only then, the result was compared to the measured B values.

Experiment. In order to confirm whether the proposed equations for jaw translation-to-rotation dependency are valid, a state of the art TrakStar 3D electromagnetic position tracking system was used. A volunteer had a sensor attached to the jaw and moved the jaw aiming to cover all possible locations. The head was stable and firmly fastened to the examination table. The investigation resulted in a cloud of random, various 6-DOF jaw positions that are shown in Figure 3.10. It represents translation-to-rotation relationship throughout the whole amplitude of jaw motion in any direction.

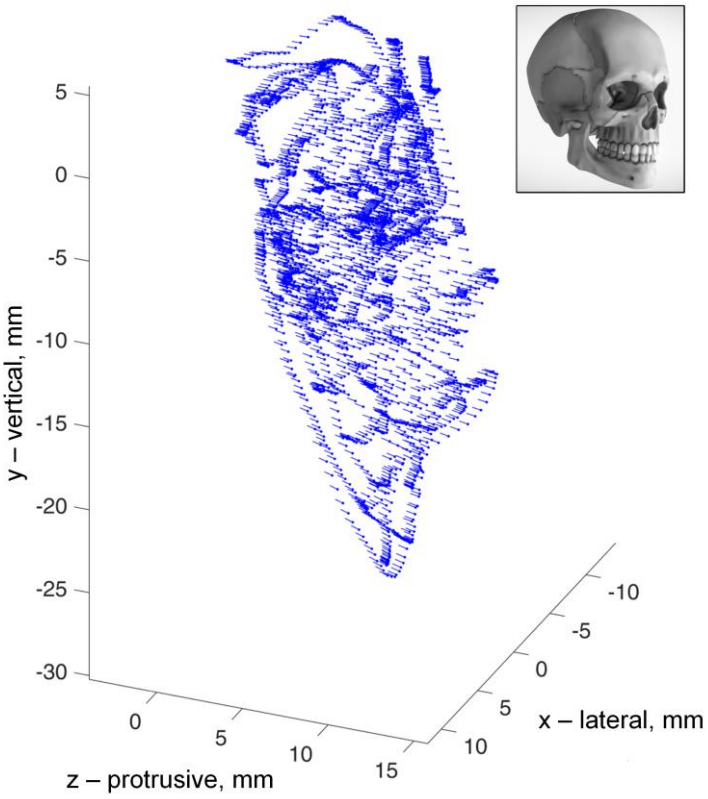

Fig. 3.10. Cloud of recorded 6–DOF reference jaw positions with rotational angles, depicted as vector arrows; the skull image [11] is provided as orientation reference

In order to create the translation-to-rotation dependencies from a randomly recorded cloud of 6-DOF data points, a 2D graph based on 2 out of 6 parameters had to be drawn. The points that are representing mentioned dependencies were plotted from each recorded position and compared to the dependencies calculated for the same individual by using the proposed equations. The inputs for equations are the linear displacement (translation) of the jaw and the physical dimensions of the jaw.

A part of this subsection has been quoted verbatim from [9].

3.4. Two-magnetometer sensor prototype

3.4.1. Wired sensor prototype

A prototype of a small size (26.3 × 5.5 × 2) mm, low power sensor was created for the experimental validation of the proposed method, and it is presented in Figure 3.11.

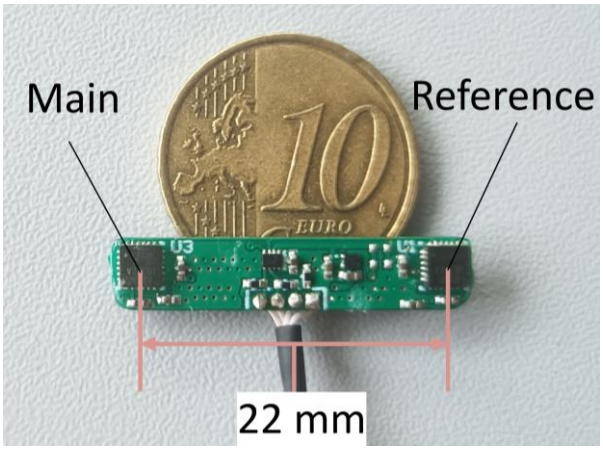

Fig. 3.11. Prototype sensor board with two magnetometers

The main components, two ICM-20948 (TDK InvenSense, San Jose, CA, USA) IMUs were placed in 22 mm (center-to-center) distance to one another. These devices contain tri-axial magnetometers, accelerometers, and gyroscopes. For teeth impact detection, the accelerometers of the same IMU are used. Other components include LDLN025 (STMicroelectronics, Geneva, Switzerland) ultra-low noise low-dropout voltage regulator, LSF0102 (Texas Instruments, Dallas, TX, USA) bidirectional voltage level translator, and passive supporting components.

I2c protocol was used for the sensor communication with the nRF52832 microcontroller development board. The maximum data acquisition rate of the sensor is 100 Hz. Most of the localization error evaluation experiments that have been described in this dissertation were performed using this version of the sensor.

3.4.2. Wireless sensor prototype

The final version of the two-magnetometer sensor prototype was based on 2 x 2 x 1 mm LSM303AGR (STMicroelectronics, Geneva, Switzerland) 6-DOF IMUs containing tri-axial magnetometers. The dimensions of the prototype were 26 x 6.5 x 2 mm. Wireless operation was enabled by 8.5 x 3.25 x 0.85 mm EYSHSN (Tayo Yuden, Tokyo, Japan) control and communications module, containing a nRF52832 microcontroller and a Bluetooth antenna. A photograph of the final prototype is presented in Figure 3.12.

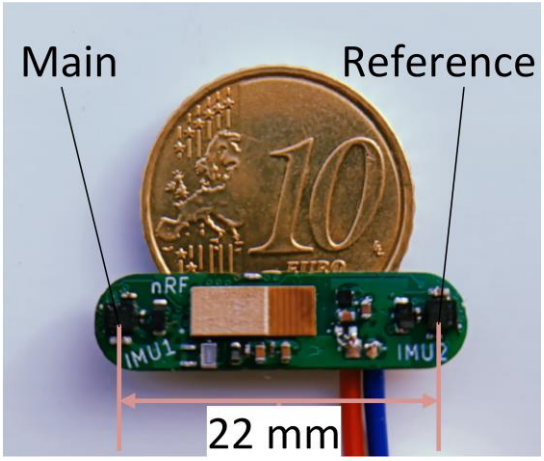

Fig. 3.12. The prototype of the wireless two-magnetometer sensor

A 3.1 V, 64 mAh battery pack was manufactured from four 1.55 V, 16 mAh silver oxide batteries (Renata SA, 379 SR521SW, Itingen, Switzerland). It was of similar size to the sensor prototype. With 15 mAh average consumption of the sensor, such battery pack can power sensor from 4 to 5 h. The battery pack is presented in Figure 3.13.

Fig. 3.13. Custom 3.1 V, 64 mAh battery pack

3.4.3. Sensor mounting solution

The key condition for mounting the sensor, battery, and permanent magnet was to leave the occlusal surface uncovered. The two options were either using Panavia™V5 (Kuraray Noritake Dental Inc., Okayama, Japan) dental cement to attach the components directly to the teeth or using custom dental splints that do not cover the occlusal surface. Custom dental splints were created and manufactured in a private laboratory (Dental 3D, Vilnius, Lithuania) for both mandible and maxilla by the order of a partnering company in this research (Investigo, Kaunas, Lithuania).

Several materials were evaluated for the manufacturing of custom splints, such as CopraPeek (Whitepeaks Dental Solutions, GmbH & Co. Essen, Germany), mono shaded PMMA (Aidite Technology Co., Ltd., Qinhuangdao, China), Zirlux Acetal (Henry Schein Inc., Melville, NY, USA). Coritec 350i Pro (imes-icore GmbH., Eiterfeld Hessen, Germany) milling machine was used for splint manufacturing. The splints of various thicknesses and forms were tested, evaluating the resulting rigidity, strength, resistance to breaking and cracks, functionality, and the ability of the milling machine to manufacture complex designs. The splints from acetal material were chosen with component encapsulation cases that have been manufactured as separate units.

The case holding the permanent magnet was attached to the maxilla splint (Fig. 3.14 a), and the cases encapsulating the sensor and the battery were attached to the mandible splint (Fig. 3.14 b).

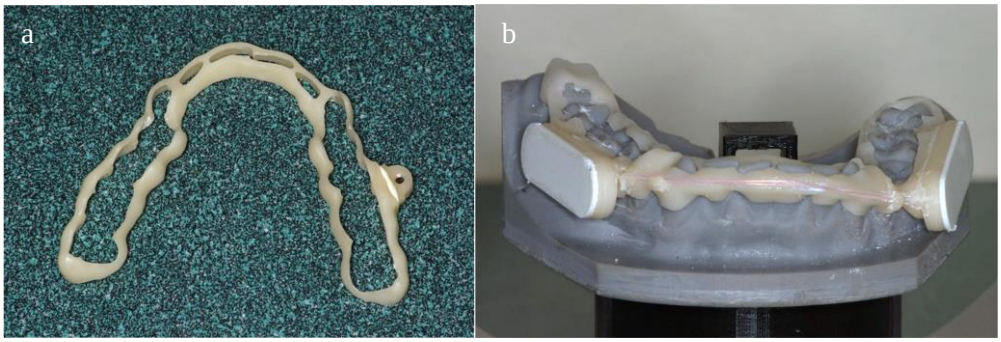

Fig. 3.14. Dental splints for mounting the permanent magnet on maxilla (a) and the sensor with a battery on the mandible (b)

It was concluded that in the volunteer's case, it was not possible to achieve occlusion with two dental splints on; however, it was possible to do it with one. Therefore, it has been decided to use a combined solution of direct attachment by dental cement for the permanent magnet and dental splints for the sensor and the battery. The system implemented intraorally is presented in a subchapter 3.5.4., Figure 3.22.

3.4.4. Sensor calibration

Sensor offset calibration has to be done either before or after the experiment, since the offset change is a problem in hall sensors at such level of precision and even more in cases with a strong external magnetic field.

During the experiments, the sensor offset was calibrated by rotating the sensor around in various directions to create a sphere of BMF values for each magnetometer. Since the two magnetometers are soldered on the same inflexible board, they experience the BMF nearly equally. Both spheres are then aligned to the coordinate system by adding or subtracting offset calibration values that are needed

for the spheres to center around the origin. The BMF spheres pre and post calibration are presented in Figure 3.15.

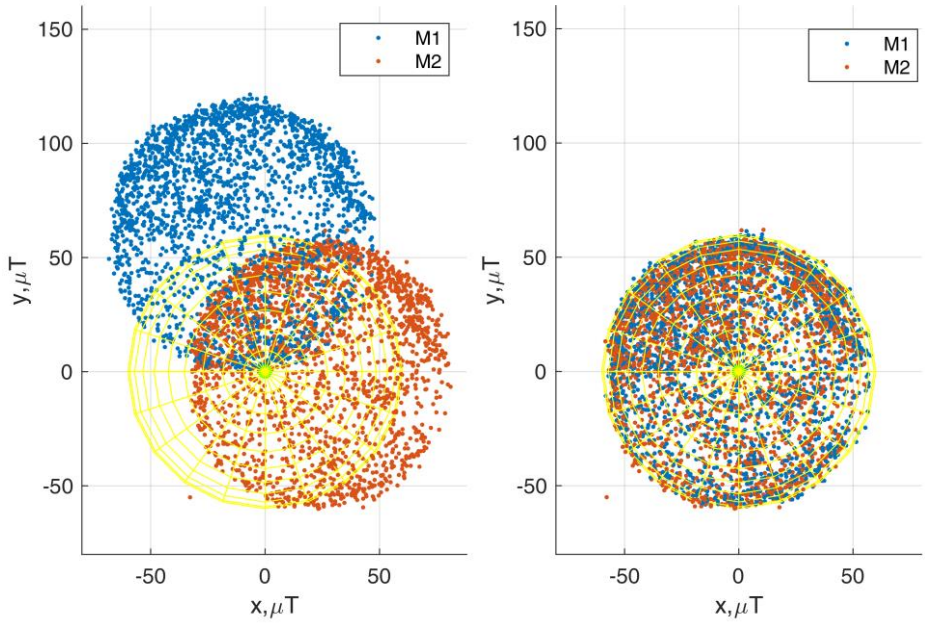

Fig. 3.15. BMF value spheres pre-calibration (left) and post-calibration (right)

3.4.5. Methods for noise mitigation

In order to mitigate random noise, a moving average filter can be used. However, even though it smooths the curve and is very effective in reducing signal spikes, it does pose a risk to smooth-out some true characteristic points in cases of very fast position change. If the noise can be characterized by a certain range of frequency, a bandstop filter can be used. Since the random noise of used magnetometer does not exceed 2 μT (see Figure 4.16), it has almost no effect on the localization accuracy.

3.5. Final system test

In order to move the sensor prototype with precision, the IRB120-3/0.6 (ABB, Zurich, Switzerland) robotic arm was used. The robot can be seen in Figure 3.16.

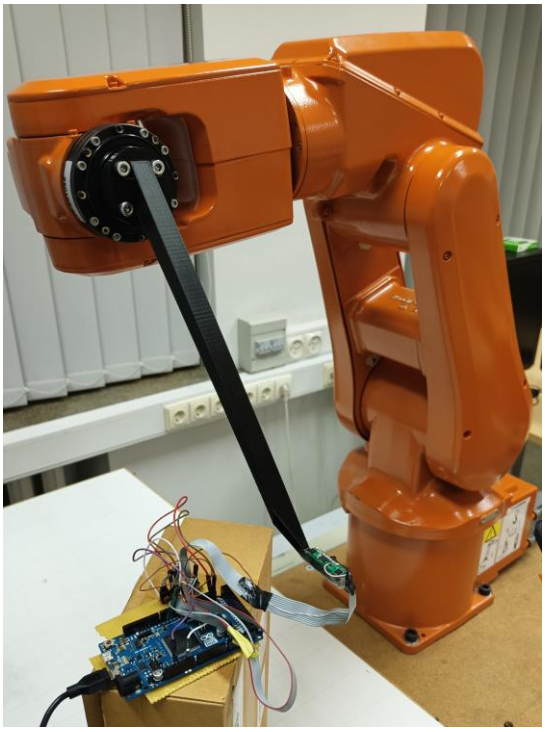

Fig. 3.16. Robotic arm with a sensor fastened to the custom mounting tool

It was programmed using RobotStudio (ABB, Zurich, Switzerland) software. The specifications of the robotic system state 0.01 mm linear and 0.01° angular repeatability. However, the robotic arm has motors that contain both permanent magnets and electromagnets. Fortunately, the proposed BMF compensation method is able to compensate for any BMFs that affect both magnetometers equally. Therefore, it does not matter if it is the natural magnetic field of the Earth or the one generated by an industrial robot, as long as it is homogenous in the volume of the sensor. Therefore, a custom sensor-mounting tool was 3D printed to fasten the sensor further from the robot that its magnetic field would be weaker and more homogenous in the volume of the sensor. The trajectory was first run without a permanent magnet in the vicinity to assess the homogeneity of the ambient field (in the volume of the sensor) by comparing the data of the magnetometers. The average differences were (ΔBx, ΔBy, ΔBz) = (0.99, 3.27, 0.59) μT. These differences could be described as offsets, because they remained constant during the robot motion and B value changes. In such a manner, the sensor was moved away from the flange of the robot by 18 cm in the Y (vertical) and 16 cm in the Z (perpendicular) axes. While effectively mitigating the effects of the magnetic field of the robot, such tool certainly increased the positioning uncertainty by slightly bending and vibrating while in motion.

The final 5-DOF experiment is divided into three stages:

- A full working range test performed both on the theoretical data and experimentally on a robotic platform in realistic conditions.
- Static 5-DOF localization test was done discretely with full stops by recording the average of 20 measurements at each point of the path. Thus, 10 iterations of a test masticatory trajectory were replicated.
- Dynamic 5-DOF localization test was done by continuously recording data at the rate of 100 Hz, while the robotic arm replicated the masticatory trajectory at its maximum speed.

  A part of this subsection has been quoted verbatim from the source [9].

3.5.1. Full working range test

Experiment. The precision of the sensor is strongly dependent on the distance from the magnet. Since the magnetic field of the permanent magnet attenuates in an inverse cube law, the percentage of the BMF component in the measurement rapidly increases as the sensor recedes from the magnet. Therefore, it would be unbefitting to evaluate the errors of the sensor without any relation to the distance from the magnet. In order to assess the mentioned dependency as well as whether the method is effective all throughout the working range, the experiments covering the whole working range of the sensor were executed with the theoretical (FEM) and experimental data. The proposed range is limited by the radius from the magnet: R ranging from 6 mm to 20 mm (15 mm in total). The range is as well limited by a horizontal plane starting at zero-point, 6 mm below the magnet, because the jaw cannot move upward from a closed position. In Figure 3.17, all test points used in the experiment are represented. Figure 3.18 is an illustration on how the working range of the sensor was divided into spheres at different radiuses from the magnet, including the test masticatory trajectory used in the other experiments for scale.

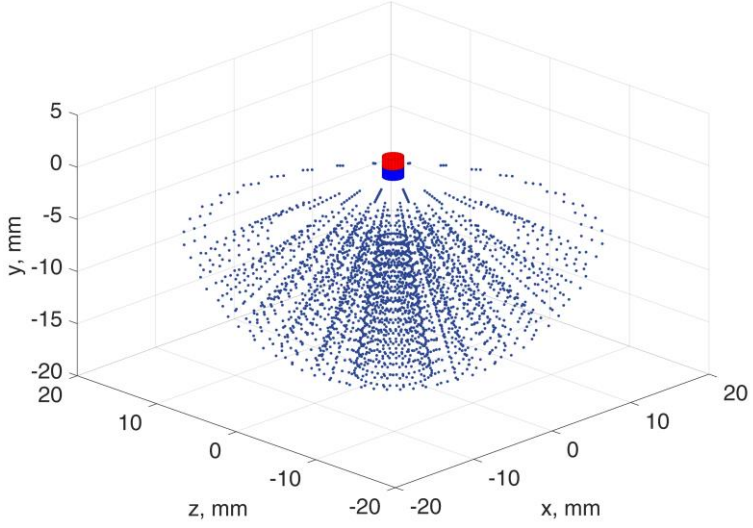

Fig. 3.17. Every measured point in the full working range test

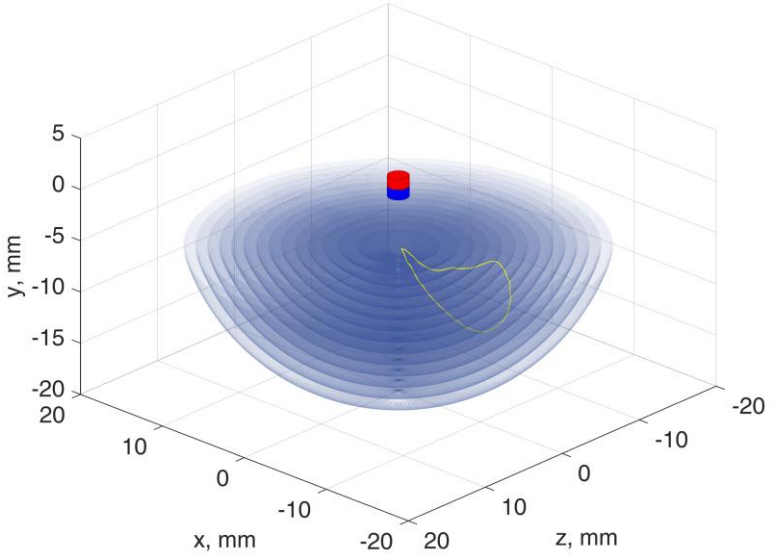

Fig. 3.18. Working range divided into spheres at different radiuses from the magnet, from 6 to 20 mm; 6 mm is the minimal magnet-to-sensor distance; the previously used test masticatory curve is included for scale

The data was contaminated by 65 μT BMF, and it was compensated during the position estimation. The experiment showed the localization error in root-mean-squared error (RMSE) at different radiuses of the working range.

3.5.2. 5-DOF localization test

Experiment. The 3-DOF test trajectory was expanded to 5-DOF, using previously described jaw angle-to-linear displacement equations (18)–(24). LS True Region-Reflective algorithm was used for magnet localization to perform static, dynamic, and full range experiments on a robotic platform. Sensor-estimated test masticatory trajectories were compared to the defined trajectory by calculating point-to-point root-mean-squared error (RMSE) and Euclidian distance (ED) from each recorded point to the defined trajectory. ED was chosen for comparing static (discrete) and dynamic (continuous) measurements because RMSE calculation is not possible for the latter. The 5-DOF test masticatory trajectory programmed in RobotStudio software can be seen in Figure 3.19.

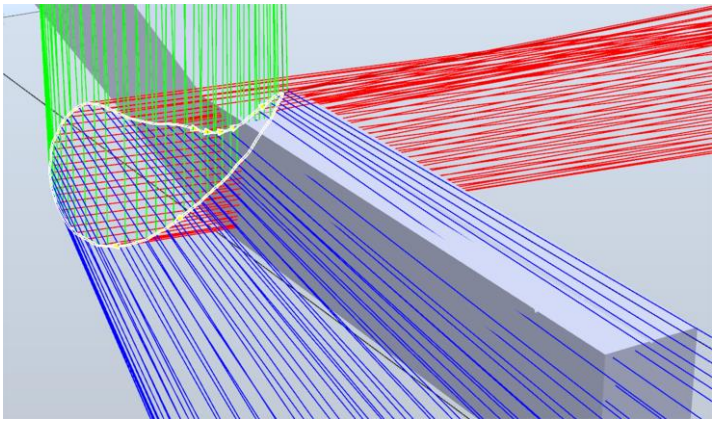

Fig. 3.19. Programmed masticatory trajectory path in the RobotStudio software

The test masticatory trajectory is represented in yellow. Red, green, and blue lines show the orientation of each point, representing the x, y, and z axes, respectively. For the laboratory experiments, the trajectory representing natural masticatory motion was sampled from [77]. This particular trajectory was chosen for consistency with the purpose of comparing the results with the previous experiments. The data was recorded at 100 Hz rate. The robotic arm stopped at each point of the trajectory for static position testing, while the average value of 20 measurements was recorded. The aim of this test was to evaluate the ability of the algorithm, hence stopping and averaging to obtain precise B values and overcome the limitations of the magnetometer noise and data collection frequency. The masticatory trajectory was recreated with the maximum speed of the robot for dynamic testing, taking 2 s to complete one cycle. In order to smooth the estimated trajectory, a moving average filter was used with a window size of N = 4. The aim of this test was to evaluate the method in motion.

A part of this subsection has been quoted verbatim from [9].

3.5.3. Automatic articulator test

A custom platform was created for precise replication of the natural motion of the human jaw, based on a high-end dental articulator KaVo PROTAR evo 7 (KaVo Kerr, Brea, CA, USA) controlled by a Dobot Magician (Shenzhen Yuejiang Technology Co., Ltd, Shenzen, China) robotic arm. The platform is presented in Figures 3.20 and 3.21.

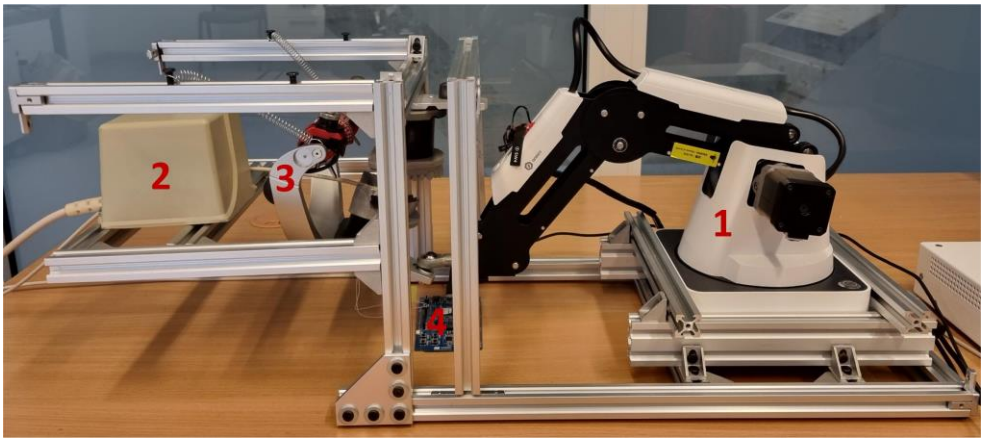

Fig. 3.20. Robot-controlled articulator platform

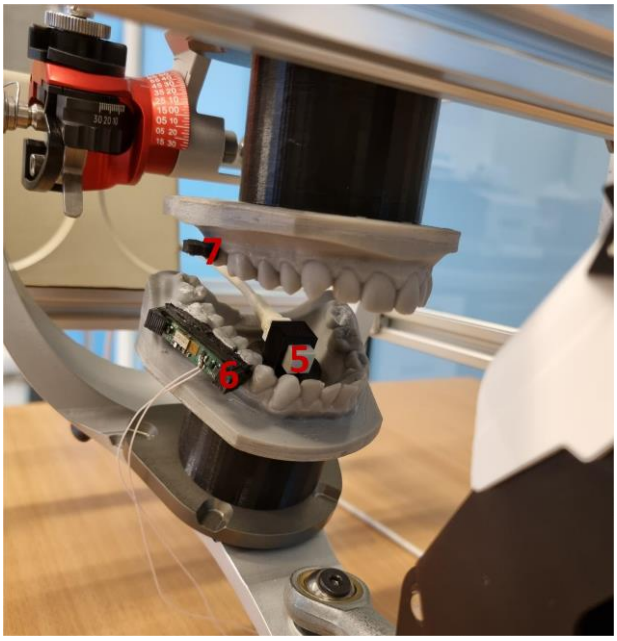

Fig. 3.21. Robot-controlled articulator platform

The platform was comprised of the following elements:

1. “Dobot Magician” robotic arm,
2. Transmitter of a reference electromagnetic localization system “TrakStar”,
3. High-end dental articulator KaVo PROTAR evo 7,
4. nRF52832 microcontroller evaluation board,
5. Sensor of a reference electromagnetic localization system “TrakStar”,
6. Prototype of the two-magnetometer jaw localization sensor,
7. Permanent magnet.

The robot controlled the articulator, which allowed the dental model to be moved only in realistic trajectory and angles. The sensor was powered from the nRF52832 evaluation board, which as well collected the data transmitted from the sensor via Bluetooth. TrakStar system was used as a reference localization method. The masticatory trajectory was repeated for 10 iterations during the experiment.

3.5.4. Intraoral test

In the final experiment, the system was tested intra-orally. The permanent magnet was fastened to the maxilla by using temporary dental cement, while the sensor and the battery were encapsulated in the cases attached to the custom dental splint that does not cover the occlusal surface. The illustration of the intraoral experiment is presented in Figure 3.22.

Fig. 3.22. The system implemented intraorally; the encapsulated sensor and battery are attached to the splints that do not cover the occlusal surface, and the magnet is attached directly to the teeth using temporary dental cement

The impacts of the teeth were detected by thresholding a sum of differentiated acceleration signals and discarding false positives based on the proximity to the occlusion, which was estimated by the magnetic localization.

3.6. Conclusions of the chapter

In this chapter, the methods of operation for the proposed system are presented in detail. The proof of concept of a single-magnetometer system has shown low errors in ideal conditions, but the existence of ambient magnetic field hampers the applicability of this approach. Two-magnetometer localization was proposed as an approach that can compensate the ambient field by nonlinear optimization while keeping the sensor relatively small. The use of subtractive compensation with a reference magnetometer increases the dimensions of the system and defeats the purpose of the single magnetometer approach. The possibility to use accelerometry for teeth impact detection was proposed and verified as well. Since the proposed method has only 3-DOF, the rotations of the jaw had to be assessed otherwise. Therefore, a system of trigonometric equations linking rotation of the jaw to its

translation was proposed. This step was essential for the applicability of proposed magnetic localization method for jaw motion estimation. Qualitative properties of each approach are presented in Table 1.

Table 1. Qualitative properties of developed magnetic localization methods described in this chapter

	One-magnetometer method	**Two-magnetometer method**	**Two-magnetometer method with trigonometric jaw angle assessment**
3-DOF localization	✓	✓	✓
Ambient field compensation	×	✓	✓
5-DOF jaw localization	×	×	✓

Three iterations of the two-magnetometer sensor were created. The latest version is capable of transmitting the recorded data via Bluetooth. A method for encapsulating and attaching the sensor to the patient's teeth was developed, based on the dental splint that does not cover the occlusal surface. A battery suitable for 4–5 h of operation (with the current level of software optimization) was manufactured. This proved the possibility of the system to be utilized in practice.

Static and dynamic localization experiments were performed at each stage of development, using various automated positioning platforms. The experiments allowed precise quantitative evaluation of the proposed system. The final experiments were aimed at demonstrating and estimating the performance of the system in practical, realistic conditions. The motion of the jaw was replicated by a custom robot controlled dental articulator platform, and an intraoral experiment was performed on a volunteer.

4. RESULTS

4.1. Proof of concept for single-magnetometer based magnet localization and accelerometric teeth impact detection

4.1.1. Proof of concept for single-magnetometer based 3-DOF localization

Single-magnetometer 3-DOF localization for the cubic test trajectory was first performed on the simulated data with resulting localization error RMSE = 0.231 mm.

"Elinta EMS 301" tri-axial positioning system that is shown in Figure 3.3 was used for the execution of single magnetometer, a proof of concept localization experiments. Easily assessable cubic and natural masticatory trajectories were used. The position of one point was estimated from the average of 10 subsequently measured magnetic field values.

The static 3-DOF localization for the cubic test trajectory was repeated for 10 iterations in separate measurements. It resulted in the average RMSE and standard deviation of RMSE = 0.328 ± 0.005 mm. The values measured by the reference magnetometer were used for subtractive BMF compensation. In Figure 4.1, the numbers from 0 to 90 represent all measured points, while transparent markers show sensor-based estimate of 10 iterations of each point. In order to demonstrate the error for each point measurement and reproducibility of 10 iterations, mean RMSE and standard deviation of each point are presented in Figure 4.2.

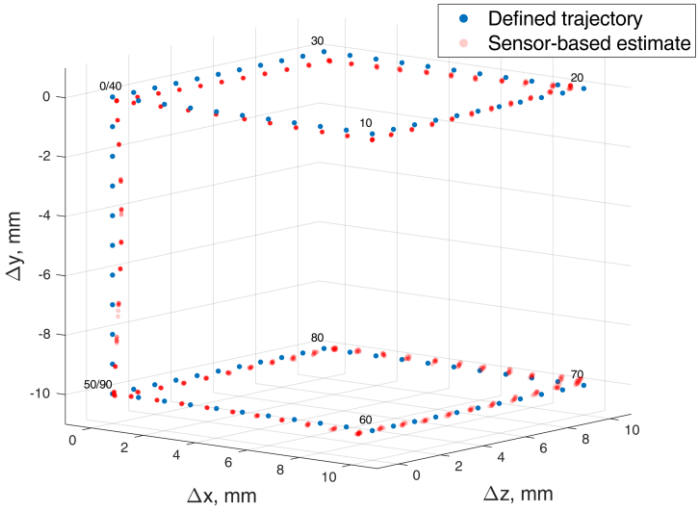

Fig. 4.1. Cubic test trajectory drawn with a 3D positioning system (blue) and determined from the magnetic field values (red); the numbers from 0 to 90 represent all measured points, while transparent markers show sensor-based estimate of 10 iterations of each point

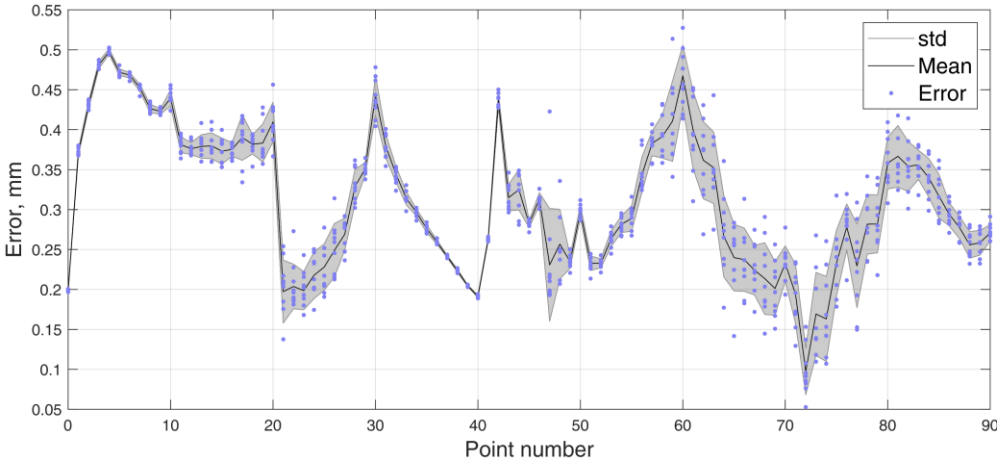

Fig. 4.2. RMSE of every measured point in 10 iterations of cubic test trajectory with mean and standard deviation

The experiment proved that the magnetic localization method in practice with cubic test trajectory allows to comprehend and assess the performance of a method better.

Single-magnetometer 3-DOF localization for the test masticatory trajectory was first performed on the simulated data, resulting in localization error of RMSE = 0.099 mm.

The static 3-DOF localization for the test masticatory trajectory was repeated for 10 iterations in separate measurements, resulting in an average RMSE and standard deviation of RMSE = 0.260 ± 0.004 mm. The values that have been measured by the reference magnetometer were used for subtractive BMF compensation. In Figure 4.3, the numbers from 0 to 90 represent all measured points, while transparent markers show sensor-based estimate of 10 iterations of each point. In order to demonstrate the error of measurement of each point and 10 iterations reproducibility, the mean and standard deviation of each point is presented in Figure 4.4.

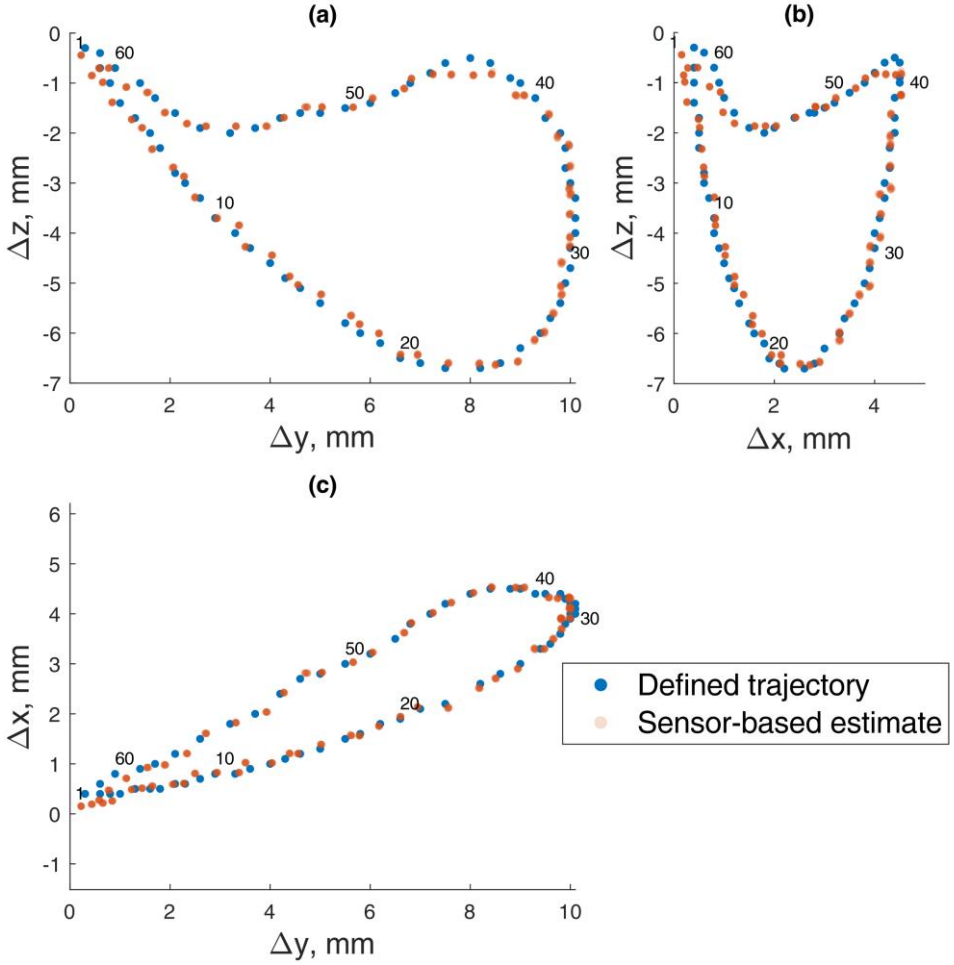

Fig. 4.3. Test masticatory trajectory drawn with a 3D positioning system (blue) and determined from the magnetic field values (red); the numbers from 0 to 62 represent all measured points while transparent markers show sensor-based estimate of 10 iterations of each point: (a) lateral–vertical view (y–z), (b) protrusive–vertical view (x–z), (c) lateral–protrusive view (y–x)

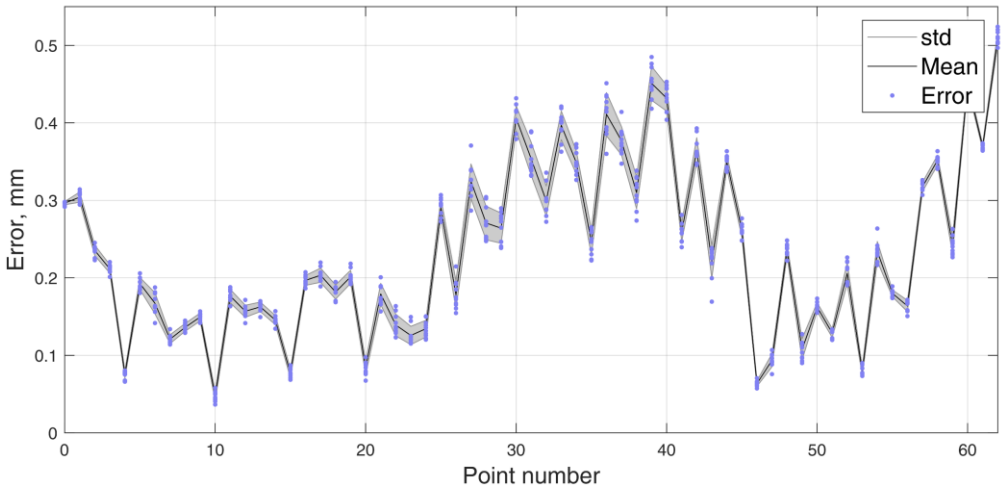

Fig. 4.4. RMSE of every measured point in 10 iterations of the masticatory test trajectory with mean and standard deviation

The natural masticatory trajectory experiment has shown that the concept of magnetic localization is suitable for the jaw activity assessment and is worth further development.

4.1.2. The use of accelerometry for teeth impact detection

The aim of this experiment was to validate the possibility for teeth impact detection by using acceleration of a sensor attached to the teeth. The vertical jaw motion for this experiment was imitated by a custom articulator for the vertical jaw movement simulation (Fig. 3.4). During the experiment, the acceleration and angular speed of gypsum teeth attached to the articulator were recorded. A processed acceleration signal with detected impacts of teeth marked in red is presented in Figure 4.5. The experimentally chosen detection threshold on the magnitude of acceleration was 5 m/s^2. The angular speed recorded using a gyroscope of the same IMU was used as a reference of the motion of the articulator. It visualizes that all motions were of similar rate and velocity, despite whether they ended up with an impact or without it. Moreover, the motion cycles that end in teeth impacts are annotated in red stems on the same graph.

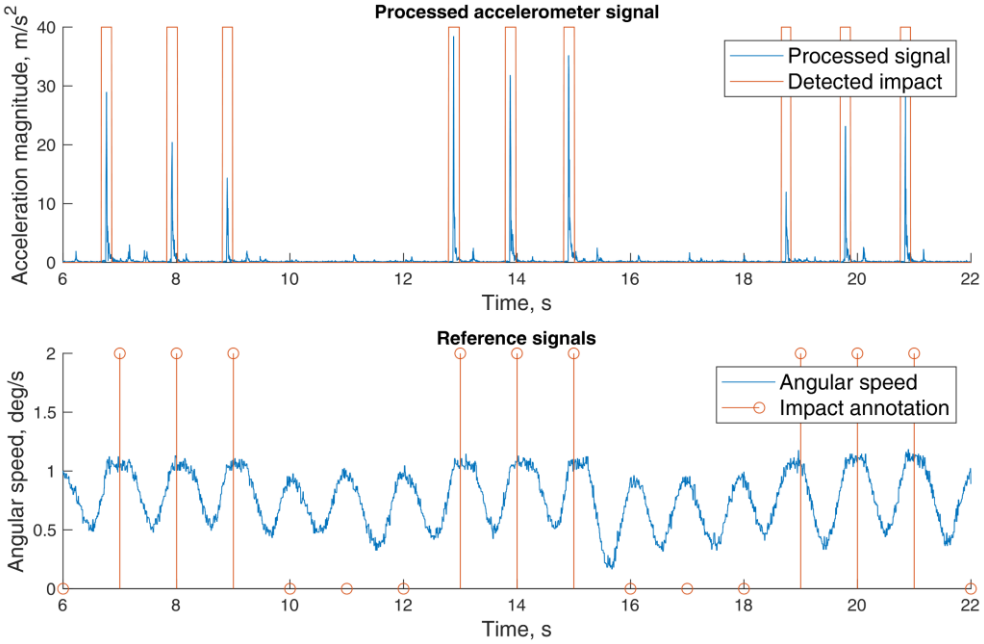

Fig. 4.5. Impact detection in vertical movement: (a) acceleration magnitude signal and (b) a reference signal of angular velocity with impact annotation

The experiment demonstrated that the teeth impact detection using a MEMS accelerometer is possible.

4.1.3. Dynamic 3-DOF localization test with teeth impact detection

In order to test the 3-DOF dynamic localization with impact detection, a custom hexapod (Stewart platform) was used to simulate simplified mandibular movements (Figure 3.5). The magnitude of the vector of acceleration was used for the impact detection (Figure 4.6 a). The 5 m/s^2 detection threshold for the magnitude of the vector of acceleration was determined experimentally. It could be seen that the signal reached the peak twice in one masticatory cycle. The first is caused by a slight grind during the untouching of the model teeth, which happened due to the lack of stability of the platform and should not be seen on a real patient. The second one, at the end of the masticatory motion, is caused by the actual impacts of teeth. In Figures 14 b–d, the coordinate of each recognized impact is highlighted (green) on the jaw motion trajectory that was estimated using the permanent magnet tracking method (red). The simulated motion was as well recorded with a reference localization method (blue). The marked coordinates clearly match the occlusive section of the masticatory cycle. At this point, the model teeth came into contact while grinding in a laterally-protrusive motion.

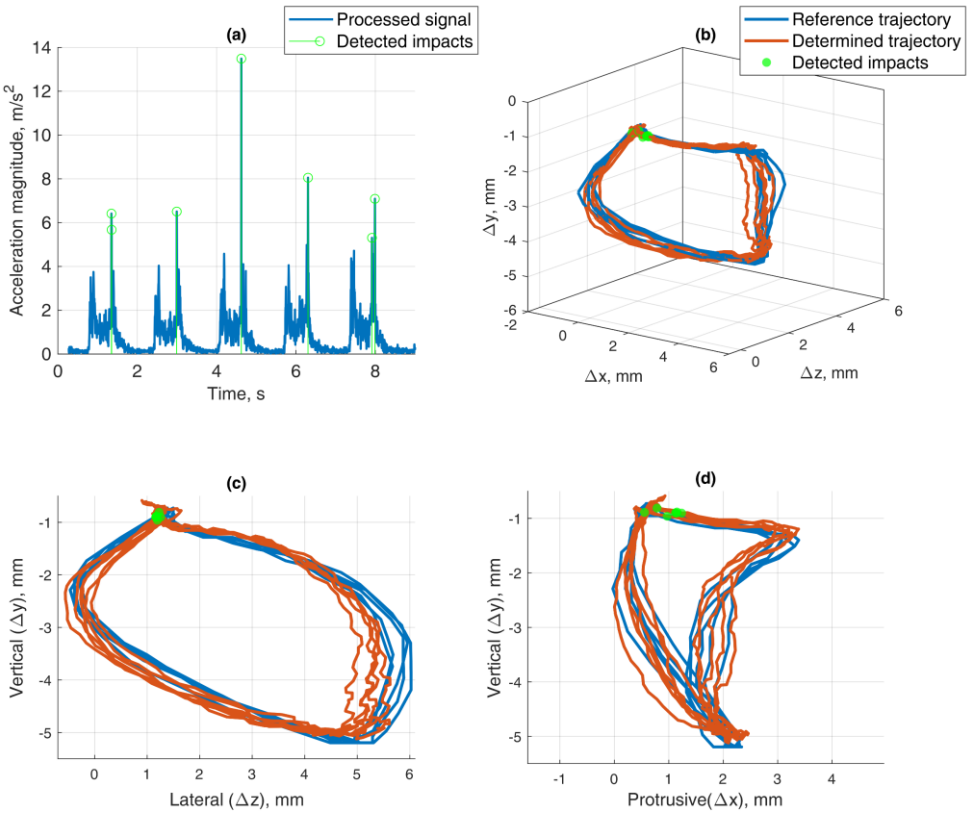

Fig. 4.6. (a) Teeth impacts detected by an experimentally selected threshold of 5 m/s^2, set on acceleration the vector magnitude value (RSS of X, Y, and Z components); (b) masticatory trajectory determined by the magnetic position tracking and reference methods while detected teeth impacts are marked at the points of detection, 3D view; (c) lateral–vertical view (z–y); (d) protrusive–vertical view (x–y)

The experiment demonstrated that it is reasonable to expect that if solid magnetic jaw motion tracking solution was developed, it could be enhanced by the accelerometric teeth impact detection. Therefore, for magnetic measurements, MEMS containing accelerometers should be considered when designing a prototype device.

4.2. Background magnetic field

4.2.1. Effects of background magnetic field

The errors resulting from 65 μT BMF are presented in Figure 4.7. The effects of BMF were assessed by introducing 65 μT field to theoretical (FEM) and compensated experimental data in various directions.

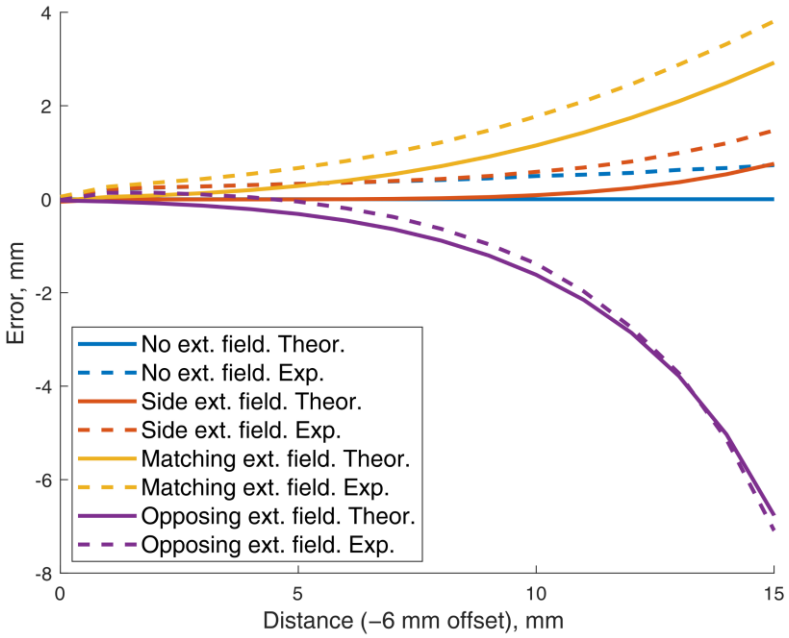

Fig. 4.7. Errors induced by artificial, maximal B field of the Earth (65 μT), acting in various directions, both on theoretical and experimental data

Based on the graph, it could be concluded that the errors were minimal at the beginning of the working range. However, due to the magnetic field attenuation following the inverse cube law, the relative size of the BMF component in the measured magnetic field rapidly increased with distance. At 10 mm distance, a localization error was approaching 2 mm. From a practical perspective, an ideal precision at 10 mm from the occlusion is not as necessary as at the start of the working range, since there is no chance of teeth contact and subsequent bruxism activity. However, the effective working range is decreased by the errors of such magnitude, and it cannot be ignored. Therefore, it can be concluded that BMF compensation must be implemented.

4.2.2. Methods for mitigating background magnetic field

A theory was raised that the small reach of the magnet field should allow placing the reference sensor on the opposing sides of the dental arch. According to [81] study, the average length of the human dental arch is 33.60 ± 2.94 mm, and the average width is 51.27 ± 2.68 mm. In order to prove this theory, the dependency of the magnetic flux density magnitude to the magnet-sensor lateral distance (x) was drawn. The vertical distance was kept at a constant of 6 mm (start of the dynamic range). In Figure 4.8, the estimation results are presented, based on the simulation of the used cylinder-shaped 2 x 2 mm permanent magnet with 1.4 T residual magnetism. It can be seen that the rate of change for the magnetic flux density

magnitude slows down at the lateral distance of 30 to 40 mm. At such distance, the magnetic flux density magnitude was around 7.9–18.6 µT. It is only 20% of the maximum magnetic field of 65 µT at the Earth's surface, and 3 times lower than the average of 35 µT [78]. This indicates that a subtractive BMF compensation could be an option for an intra-oral system.

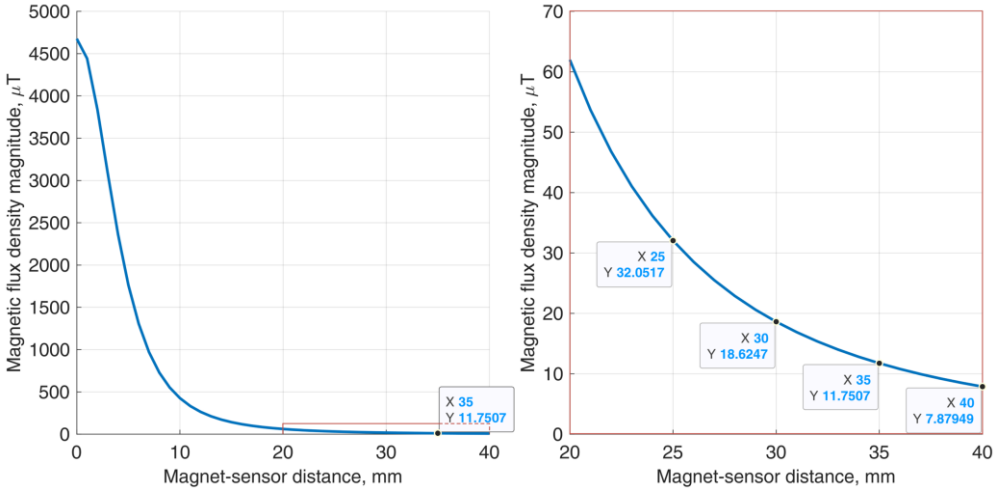

Fig. 4.8. Dependency of the magnetic flux density magnitude to the magnet-sensor lateral distance (x) at constant 6 mm vertical distance (y) (start of the dynamic range), marked area zoomed on the right

Based on the information provided above, 35 mm distance would be the closest sensible location for the reference magnetometer. However, for the ideal compensation by subtraction, the reference magnetometer has to be fully removed from the permanent magnet field. Moreover, the main and reference sensor orientations in relation to each other should be precisely known.

The subchapter 4.3.2 should be reviewed for the BMF compensation by optimization algorithm proof of concept experiment results.

4.3. Two-magnetometer approach

4.3.1. Comparison of localization algorithms

Least. Squares optimization. The trust region algorithm for LS optimization was tested on FEM data, simulating two-magnetometer sensor. It showed promising results with data uncontaminated with BMF at the limit of the sensor working range, the position estimation error was RMSE = 0.445 mm. Strangely, when the ambient magnetic field was introduced and had to be compensated, the position estimation error significantly decreased to RMSE = 0.083 mm. It was not entirely clear why the error was larger without the BMF compensation in the case of clean uncontaminated data. It might have been that the BMF compensation corrected the discrepancies of

the used mathematical model of the magnetic field by transferring it to the BMF value estimation.

The estimated positions of points located at the limit of the sensor working range, at R = 20 mm radial distance from the permanent magnet, are shown in Figure 4.9. For comparison, the presented cases include: a) data without BMF contamination and compensation, b) data with BMF contamination but without compensation, c) data with BMF contamination and compensation.

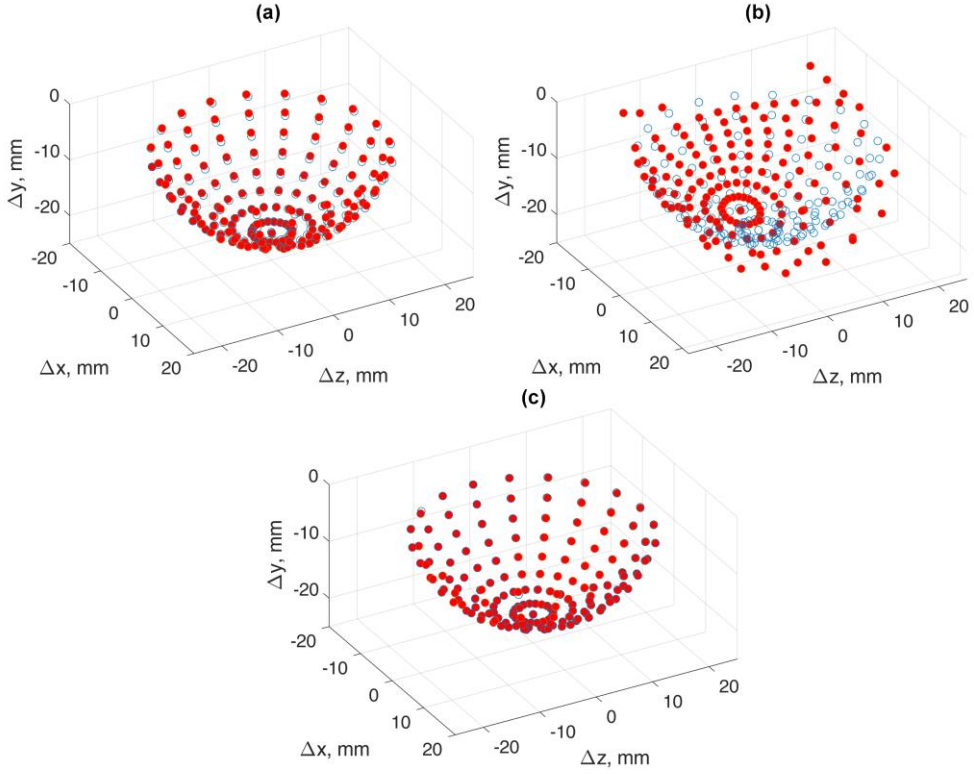

Fig. 4.9. LS Trust Region algorithm test on the FEM data; the visualization of the estimated positions of points located at the limit of the sensor working range, at R = 20 mm radial distance from the permanent magnet: a) position estimation without BMF compensation from the data uncontaminated with ambient field, b) position estimation without BMF compensation from the data contaminated with ambient field, c) position estimation with BMF compensation from the data contaminated with ambient field

Particle swarm optimization (PSO) algorithm was tested on the FEM data, simulating two-magnetometer sensor. It showed promising results with data uncontaminated with BMF: at the limit of the sensor working range, the position estimation error was RMSE = 0.46 mm. However, when the ambient magnetic field was introduced and had to be compensated, the position estimation error increased significantly to RMSE = 4.17 mm.

The estimated positions of the points are located at the limit of the sensor working range, at R = 20 mm radial distance from the permanent magnet, are shown in Figure 4.10. For comparison, the presented cases include: a) data without BMF contamination and compensation, b) data with BMF contamination but without compensation, c) data with BMF contamination and compensation.

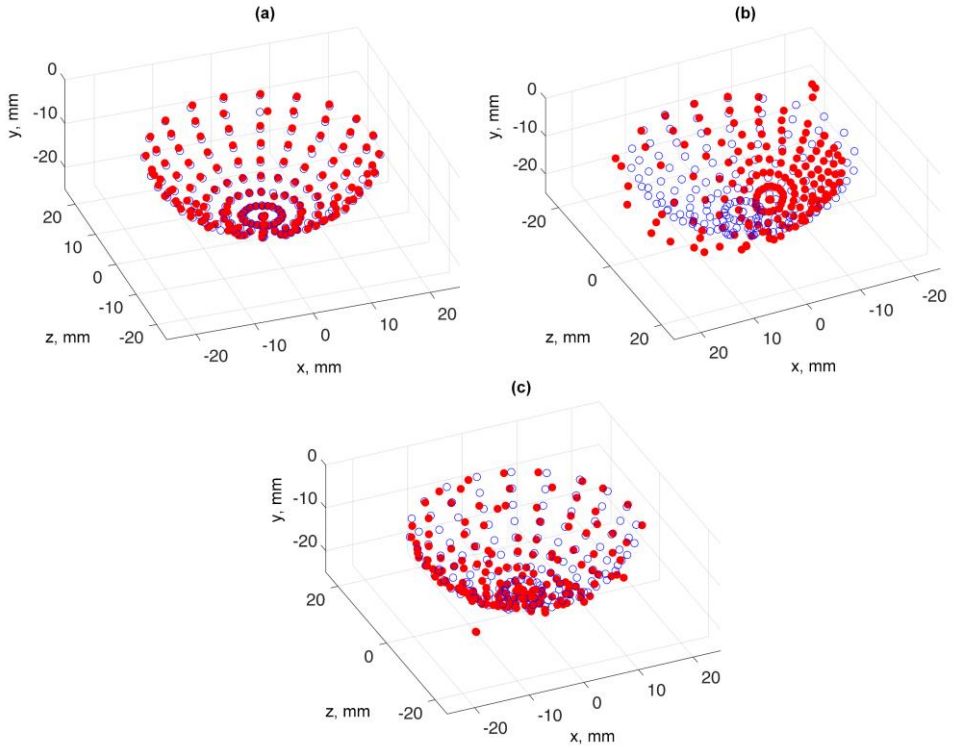

Fig. 4.10. PSO algorithm test on FEM data; the visualization of estimated positions of points located at the limit of the sensor working range, at R = 20 mm radial distance from the permanent magnet: a) position estimation without the BMF compensation from the data uncontaminated with ambient field, b) position estimation without the BMF compensation from the data contaminated with ambient field; c) position estimation with the BMF compensation from the data contaminated with ambient field

Comparison. Throughout the full working range of the sensor, RMSE and ED were calculated for LS and PSO methods and presented in Figure 4.11. The data was contaminated by a 65 µT BMF, and it was compensated during the position estimation.

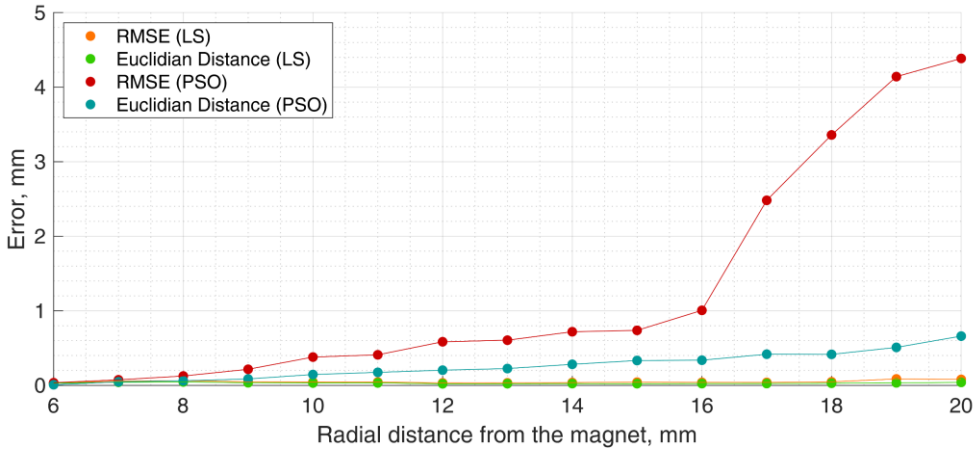

Fig. 4.11. Position estimation results from the FEM model data using PSO and LS algorithms; RMSE and Euclidian distance (ED) to original trajectory at different radiuses from the magnet

It is safe to conclude that the LS optimization method has shown significantly better performance than PSO and should be selected to use as the basis for the magnetic localization algorithm.

4.3.2. Two-magnetometer 3-DOF localization with background magnetic field compensation

The test masticatory trajectory is presented in Figure 4.12 together with the position estimations using magnetic localization on the theoretical FEM and experimentally recorded data.

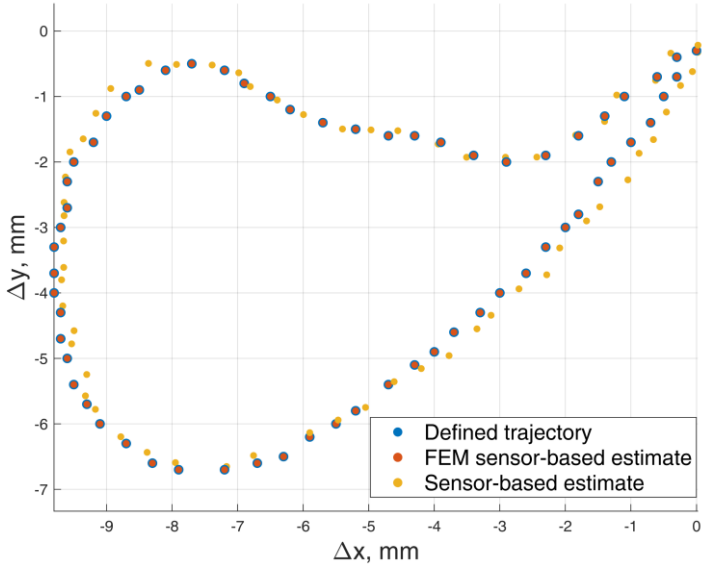

Fig. 4.12. Original input trajectory and estimated trajectory while using BMF compensation from FEM simulation data, RMSE = 0.05 mm (red), and the prototype sensor, based data with natural BMF, RMSE = 0.28 mm (yellow)

The 3-DOF trajectory estimated from the FEM data resulted in an RMSE = 0.05 mm, and it is shown in red. The BMF that was introduced in FEM data as an additional 65 μT magnetic field vector was estimated as BMF = [−0.13 57.89 −0.05] μT. Based on the localization error, it outperforms the single-magnetometer method, which showed RMSE = 0.1 mm on the same FEM data without any BMF contamination. An analogous experiment was replicated in a laboratory with a sensor prototype, a real permanent magnet, and natural BMF of the Earth, and the sensor-based trajectory estimate is presented in Figure 4.12 with yellow markers. The sensor was moved along the defined trajectory by an EMS 301 (Elintos Matavimo Sistemos, Kaunas, Lithuania) 3D positioning system, which had a positioning resolution (step) of 0.1 mm. The resulting test masticatory trajectory localization error was RMSE = 0.28 mm. The natural Earth's BMF was estimated as BMF = [−8.95 57.19 −12.24] μT. It showed similar performance as the single-magnetometer method, which showed RMSE = 0.26 mm on the same positioning system with BMF removed by subtractive compensation [8].

4.3.3. Validation of equations for jaw angle estimation

This experiment demonstrates the validity of trigonometric equations for jaw translation-to-rotation dependency. It is done by comparing the output of equations to data extracted from the precision 6-DOF jaw position measurement of the same individual. The volunteer's jaw dimensions were taken manually and were as

follows: L = 45 mm, H = 33 mm, W_L = 64 mm, and W_R = 16 mm. The dependencies are compared in Figures 4.13 and 4.14.

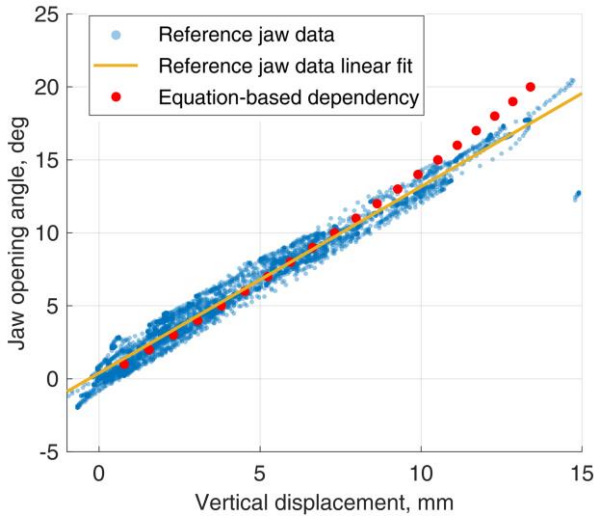

Fig. 4.13. Vertical translation to jaw opening rotation dependency; the correlation coefficient between reference and equation-based dependency lines is 0.9989

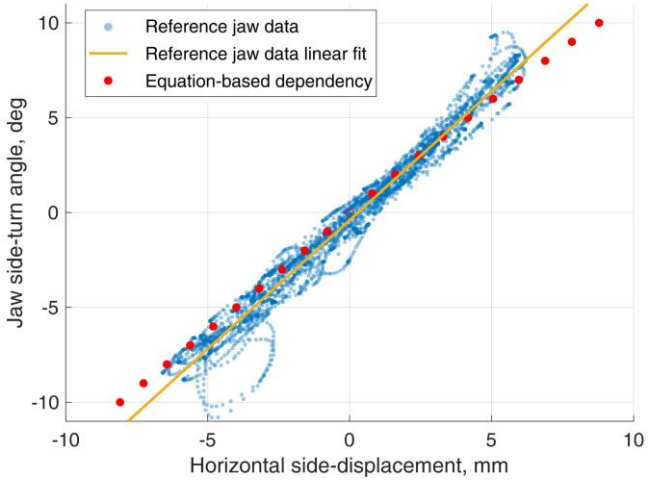

Fig. 4.14. Horizontal (lateral) translation to jaw side rotation dependency; the correlation coefficient between reference and equation-based dependency lines is 0.9996

The rotation-to-translation dependencies for both vertical and lateral motion appear to be linear. The correlation coefficient for two lines is a cosine of the angle between them. It was calculated to quantitatively estimate how much the proposed angle estimation method matches the experimental reference data. Therefore, the

resulting correlation coefficient between reference and equation-based dependency lines for the vertical motion is 0.9989, while for the lateral motion, it is 0.9996. It can be seen that the linearity slightly decreases with higher motion amplitudes. The average maximum angle of the jaw rotation is stated in [83] and is equal to 31.6° for women and 35.8° for men [83], which happens during vertical opening. Moreover, the jaw is rarely fully open, and from a medical-parafunctional perspective, the precise position in such case is trivial.

4.4. Two-magnetometer sensor prototype

4.4.1. Main-to-reference magnetometer distance

The data simulated in a FEM was as well used to find a suitable location of the reference magnetometer. Using two-magnetometer localization by the LS optimization methodology described in subchapter 3.1.3, the optimal distance between the two sensor magnetometers was estimated. Inside the modeled field of the magnet, the two-magnetometer device was imitated by measuring B values at two mutually fixed points, simultaneously moving along the same trajectory. The test was repeated with 21 different main-to-reference magnetometer distances, ranging from 10 mm to 30 mm with a step of 1 mm. The test masticatory trajectory position estimates with different sensor layouts were compared to the test masticatory curve, and RMSE were calculated.

In Figure 4.15 a, RMSE-to-distance dependency shows the theoretical localization error with various main-to-reference magnetometer distances. The optimal distance between the magnetometers can be seen as the lowest point in a curve created by multiplying the localization error with corresponding magnetometer distance (Fig. 4.15 b).

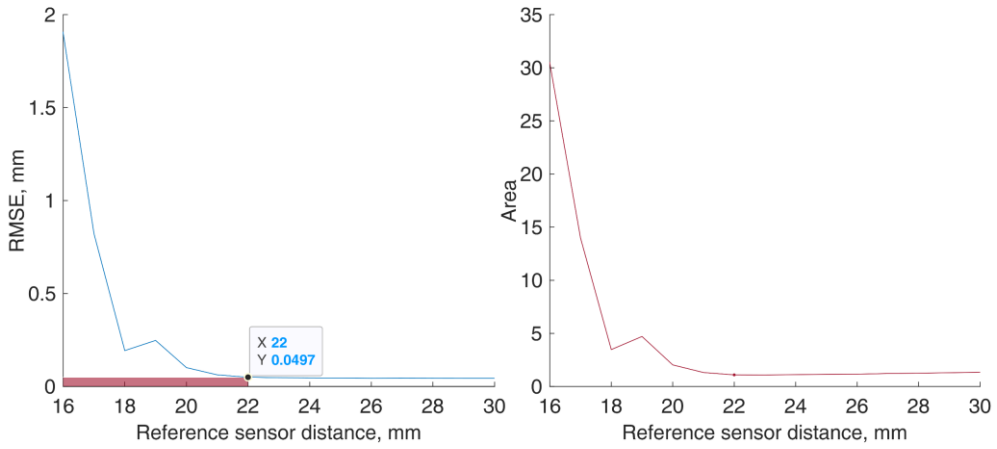

Fig. 4.15. (a) Dependency between localization RMSE and reference sensor distance to the main sensor, FEM data, (b) curve created by multiplying the localization error with corresponding magnetometer distance with the lowest point marked

In the resulting curve, RMSE is large with small main-to-reference magnetometer distance, but the curve clearly drops and flattens with increased distance. The selected position was at the smallest distance where the error stops rapidly decreasing. Based on this graph, a 22 mm center-to-center main-to-reference magnetometer distance was chosen in further experiments as well as in manufacturing an experimental sensor prototype.

4.4.2. Magnetometer selection

The key parameters for a tri-axial magnetometer to be suitable for a particular purpose of this work are range (±5000 μT), accuracy, and insusceptibility to noise. Two commercially available devices that fit the requirements are 3 x 3 x 1 mm ICM-20948 9-DOF IMU and 2 x 2 x 1 mm LSM303AGR 6-DOF IMU. The latter does not contain a gyroscope, which is not utilized in this work anyway. It should be noted that the LSM303AGR system on a chip was acquired late in this research, and most measurements were executed using ICM20948 system on chip. Nevertheless, it was important to compare the two available options and determine the most suitable one for further research and final prototype manufacturing, not to mention that the LSM303AGR chip is significantly smaller. Moreover, the ICM20948 required very frequent calibration due to zero offset change, which was greatly increased by the permanent magnet being in proximity of the sensor. Therefore, finding a more advanced sensor that would be more robust in terms of keeping calibrated is very important for further implementation of this method. The key specifications stated by the manufacturers of the two magnetometers are presented in Table 2.

Table 2. Specifications of the ICM20948 and LSM303AGR magnetometers as stated by the manufacturers

	ICM20948	**LSM303AGR**	**Units**
Range (all axes)	±4912	±4912	μT
Resolution	0.15	0.15	μT
Zero offset change	300	6*	μT
Magnetic noise	n/a	0.3	μT
Output data rate	100	100	Hz

*stated value with "with offset cancellation" enabled, excluding change from magnetic shock.

It should be noted that most influence on the measurement is generated by the zero offset change from the magnetic shock by the permanent magnet in proximity with the main magnetometer nearly reaching the limits of its working range every time the teeth are in occlusion. The two tests that were run on magnetometers in the mentioned systems-on-chip were as follows.

A measurement of random noise amplitude in static conditions, where both sensors were run for 15 seconds, and their readings were offset to zero by

subtracting the average of the signal. The boxplots of noise-induced 15 s signal variations for each axis of both sensors are presented in Figure 4.16.

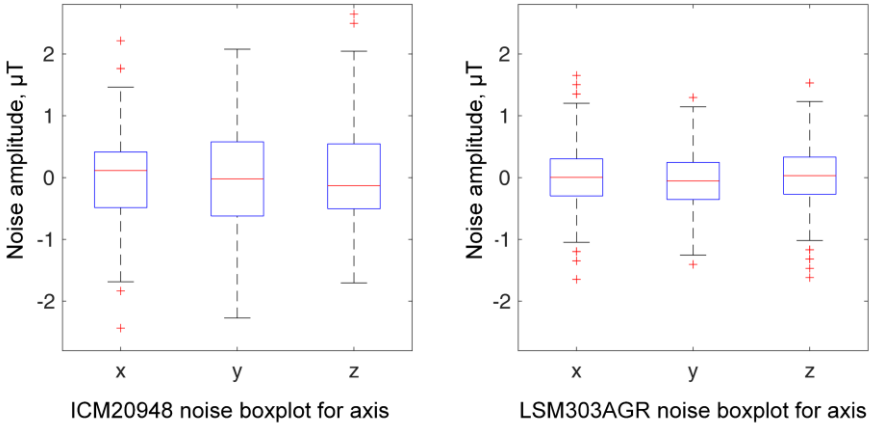

Fig. 4.16. Comparison of ICM20948 and LSM303AGR noise amplitude dispersions during the static data read

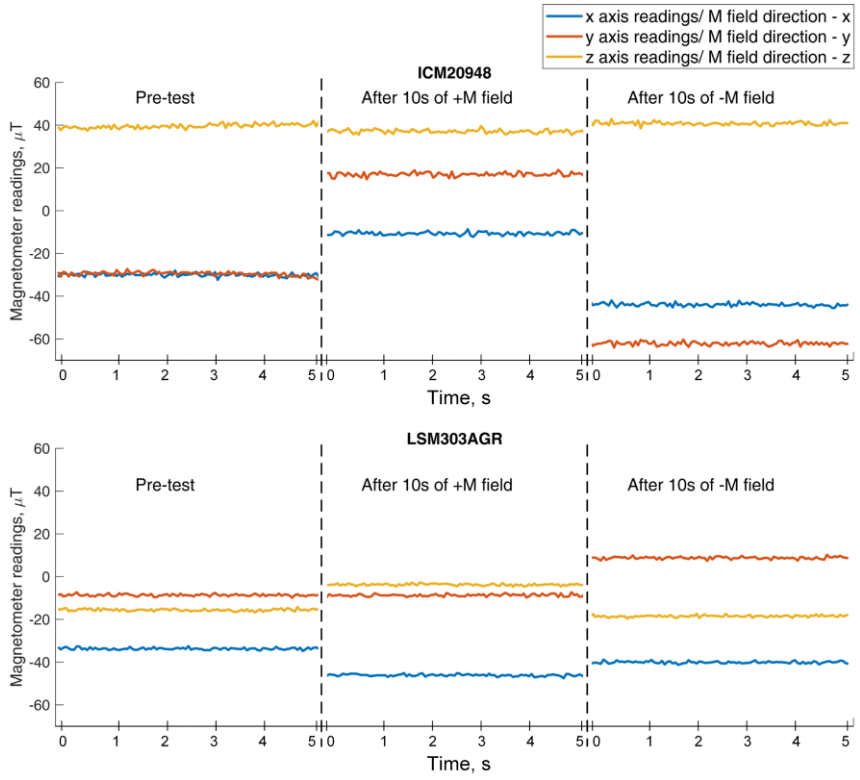

Fig. 4.17. Comparison of ICM20948 and LSM303AGR, zero-offsets affected by the external magnetic field

Zero offset change after a 1.4 T NdFeB permanent magnet was introduced in proximity (6 mm) of both devices, approaching the limit of the sensor working range. Magnetization field direction was either matching (+M) or opposing (-M) the axis being recorded at the time. The results of this experiment for both sensors are presented in Figure 4.17.

An experiment was run to assess and compare if and how zero offset change of both sensors is affected by the mechanical shock; the resulting signals are presented in Figure 4.18.

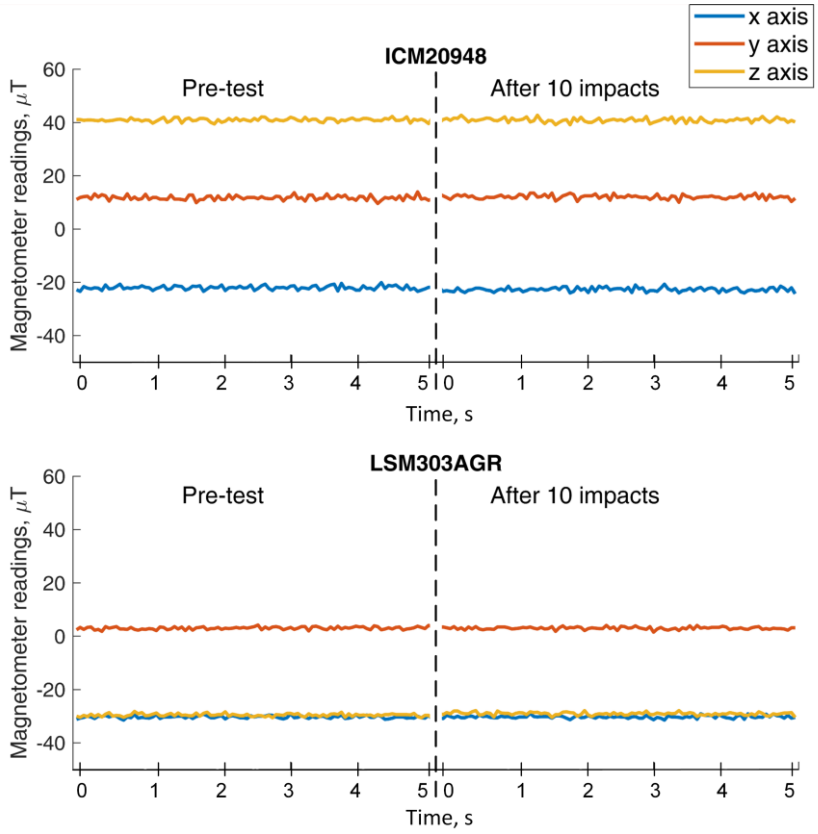

Fig. 4.18. Comparison of ICM20948 and LSM303AGR; zero-offsets not affected by the mechanical shock

To sum up, the results show slightly better performance of LSM303AGR system on a chip in the executed tests. None of the sensors are sensitive to the physical shock; however, the noise and zero-offset change was a little lower on the LSM303AGR chip. Another interesting finding was that ICM20948 chip was more susceptible to zero-offset change in y axis than in the other axes. Therefore, LSM303AGR should be considered to be used in further research and development, although most measurements in this work were done using ICM20948 system on the

chip. Nevertheless, the difference between the magnetometers is minimal, and the replication of all previous measurements with only slightly better sensor would have no benefits.

In addition, this experiment clearly illustrates the bottleneck of this technology, i.e., the zero-offset change. Up to 80 µT shift in the static data readings in between the presence of two opposite external magnetic fields suggests a need for frequent calibration of the sensor and subsequent problems in the practical application. The best solution to this drawback would be a more advanced, robust magnetometer, which was not available at the time of this research. However, the quantitative assessment must be made regarding this problem, including the comparison of how differently the zero-offset of the main and the reference magnetometers affect the position estimation. It is presented in Figure 4.19, as the magnitude of the error caused by various zero-offset changes at different magnet-to-sensor distances throughout the proposed working range of the system.

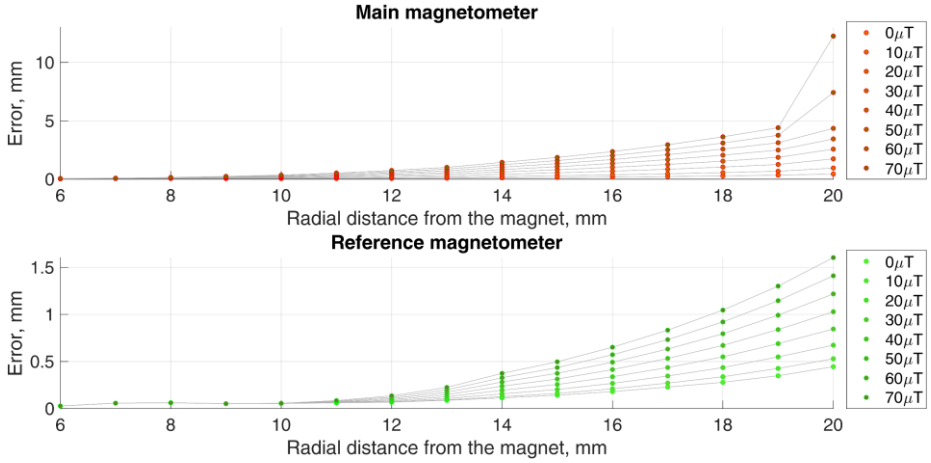

Fig. 4.19. The magnitude of error expressed in RMSE, caused by various main and reference magnetometer zero-offset changes at different magnet-to-sensor radiuses throughout the proposed working range of the system

4.4.3. Modeling magnetometers' alignment influence

When estimating possible sources of error in magnetic measurements, an imperfect sensor placement has to be considered. The magnetometer can be displaced in two stages, i.e., during the stage of IMU chip manufacturing and soldering of the sensor PCB [84]. Firstly, a tri-axial magnetometer consists of three separate hall sensors, none of which are placed in the same spot. Even though the distances are in the order of microns that makes the system not an ideal dot system; however, in case of this work, it would be highly excessive to take this into account, as there are much larger sources of error. Nevertheless, the magnetometer placement during the assembly of the sensor PCB may introduce a noticeable change in the measured data, particularly in a case of manual soldering. In relation to the main

magnetometer, the reference magnetometer could be misplaced translation-wise and rotation-wise. It should be numerically evaluated how much such misalignment increases the total error of the measurement. As a means of comparison, a test masticatory trajectory position was estimated in a FEM with various chip misplacement cases, and the resulting RMSE was calculated. The chosen range of misplacement was ±0.5 mm for translation and ±5° rotation over-cautious choices for a 2 mm wide chip with a pin pitch of 0.4 mm. However, such values were chosen to exceed the worst case scenario of both chips being oppositely misplaced. The drawing that is illustrating the possibilities of misalignment is presented in Figure 4.20 with arrow colors matching the colors of corresponding RMSE errors in the following graphs.

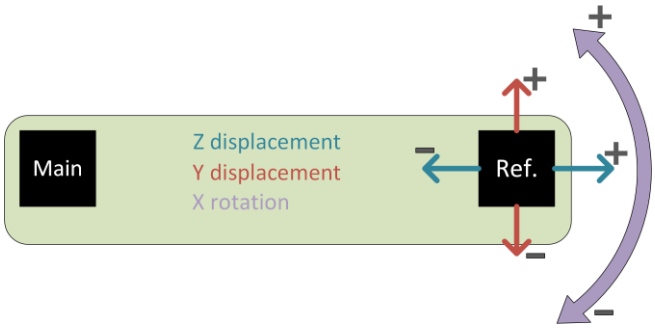

Fig. 4.20. Possible cases of magnetometer misalignment

In Figure 4.21, the RMSE errors induced by the linear displacement (translation) are presented while the RMSE errors induced by rotation are presented in Figure 4.22.

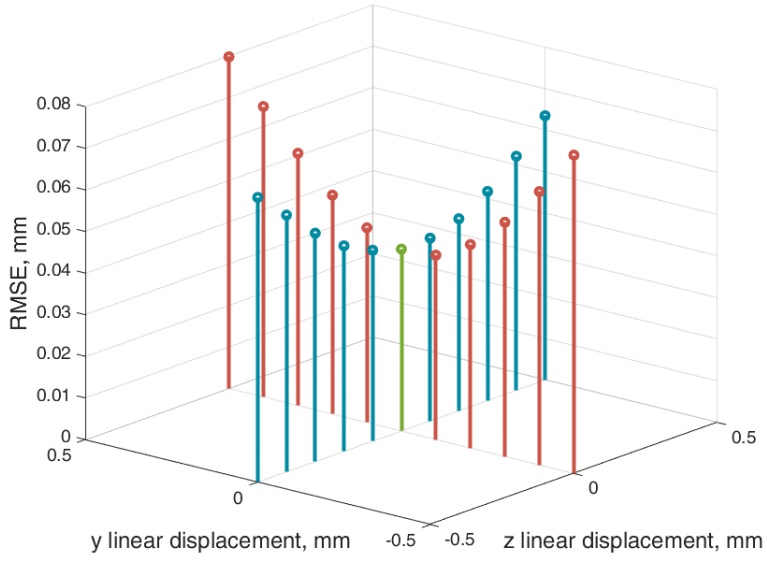

Fig. 4.21. RMSE increase induced by the linear misalignment of magnetometers

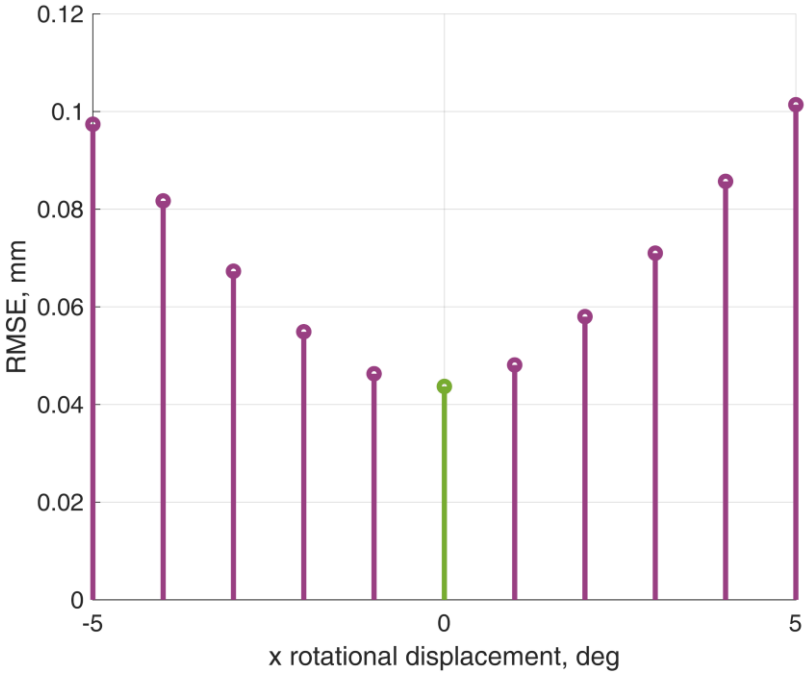

Fig. 4.22. RMSE increase induced by the rotational misalignment of magnetometers

4.4.4. Modeling the influence of magnet factory parameters

Based on the specifications of used 2 x 2 mm cylindrical NdFeB permanent magnet, each manufactured piece could slightly differ in dimensions and magnetization. The dimensions and tolerance margins that are stated in the datasheet are 2 ± 0.1 mm for height and 2 ± 0.1 mm for diameter, while the magnetization value can fall in the range of 1.37–1.42 T. A test masticatory trajectory position was estimated in a FEM with various magnet magnetization values, and the resulting RMSE was calculated. The results of the assessment are presented in Figure 4.23.

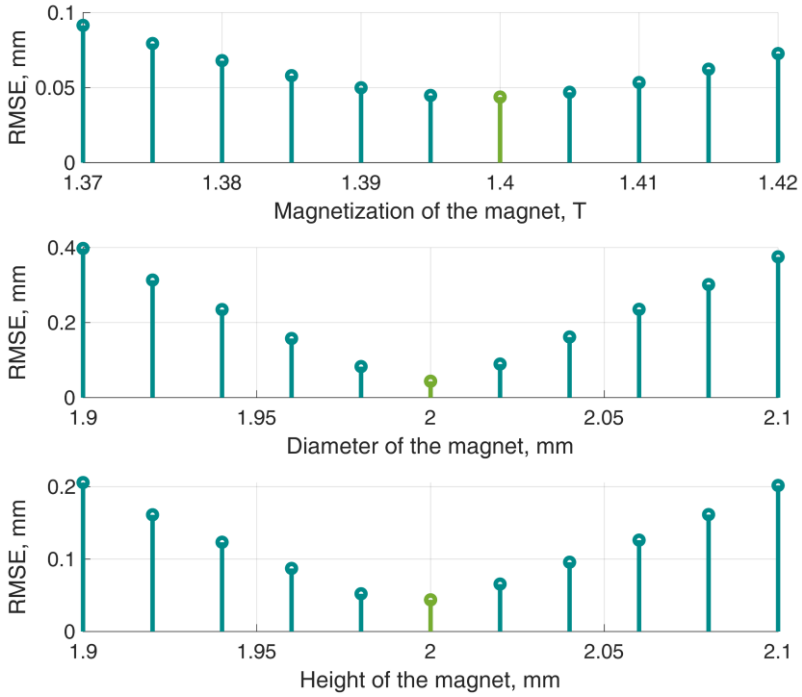

Fig. 4.23. RMSE increase induced by the factory deviation from the objective values of the permanent magnet magnetization, diameter, and height

To summarize, the errors induced by the magnetometer placement during the PCB assembly as well as the errors caused by the factory tolerances during the permanent magnet and magnetometer manufacturing will not hinder the operation of the method. While it may increase the localization error, these errors will be systematic and can be mitigated by the software tuning.

4.5. Final system test

4.5.1. Full working range test

During this experiment, both theoretical and experimental 3-DOF localization errors were estimated using two-magnetometer approach with BMF compensation. LS optimization was used. FEM-simulated data was contaminated with a 65 μT BMF, and in experimentally measured data, natural BMF was present. Since the trueness and robustness of the method depend mostly on the distance from the magnet, the RMSE was calculated at various radiuses from the magnet. The sensor was moved (translated in 3-DOF) to cover the space at various radial distances (from R = 6 to R = 20 mm) from the magnet, while keeping below the y = -6 mm minimal distance at vertical (y) axis. The R was changed in steps of 1 mm. For demonstration, the results of the experiment for the theoretical case at the limit of the sensor working range (R = 20 mm) are presented in Figure 4.24. The trajectories

of both main and reference magnetometers are visualized. The resulting localization error for this theoretical case resulted in RMSE = 0.088 mm.

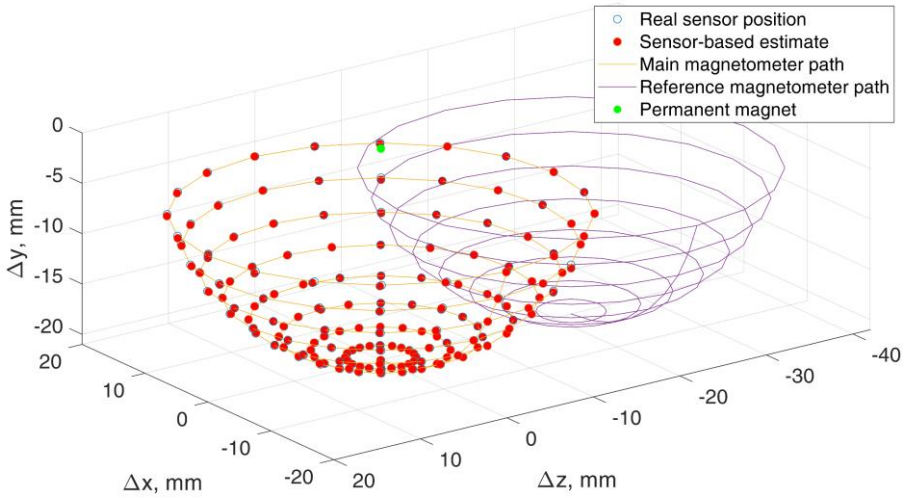

Fig. 4.24. Two-magnetometer 3-DOF localization with BMF compensation on the theoretical FEM data for the case of the maximum radial distance of R = 20 mm

Theoretical. For theoretical model, RMSE and ED at all radiuses of the full working range were calculated and presented in Figure 4.25.

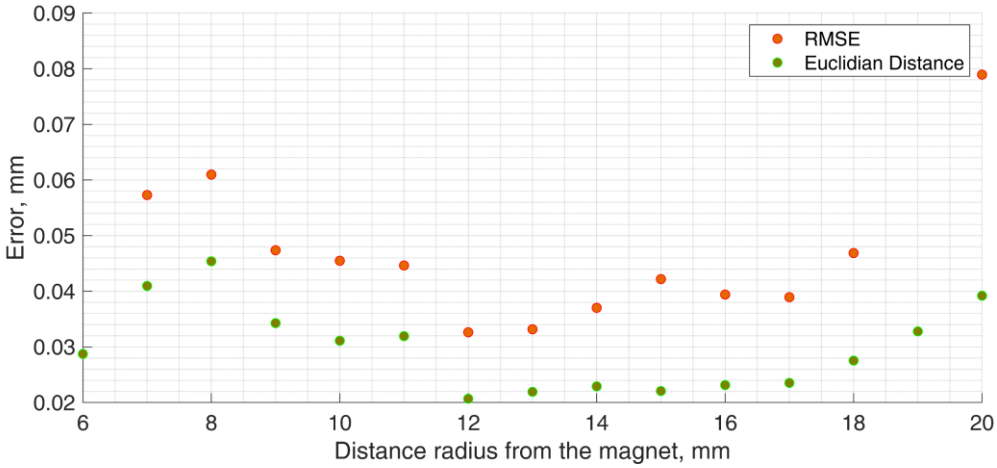

Fig. 4.25. Two-magnetometer localization approach with BMF compensation results from the FEM data; RMSE and average ED to the real sensor trajectory at different radiuses from the magnet

Experimental. The same full working range test was replicated in practice on an ABB robotic platform. Every performed measurement was repeated for 10 iterations. The experimentally measured error-to-distance dependencies are presented in Figure 4.26 and Figure 4.27 for RMSE and ED, respectively.

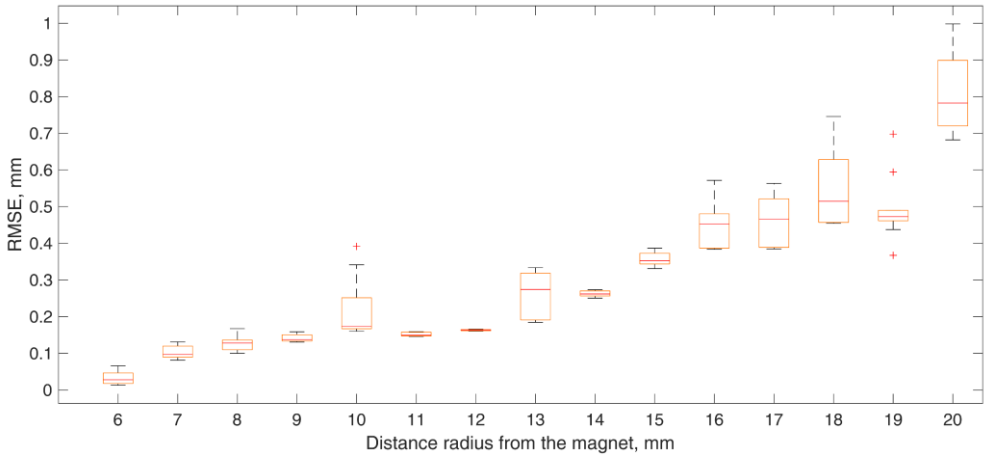

Fig. 4.26. 10 measurement RMSE median and standard deviation for the experimental measurements at different radiuses from the magnet

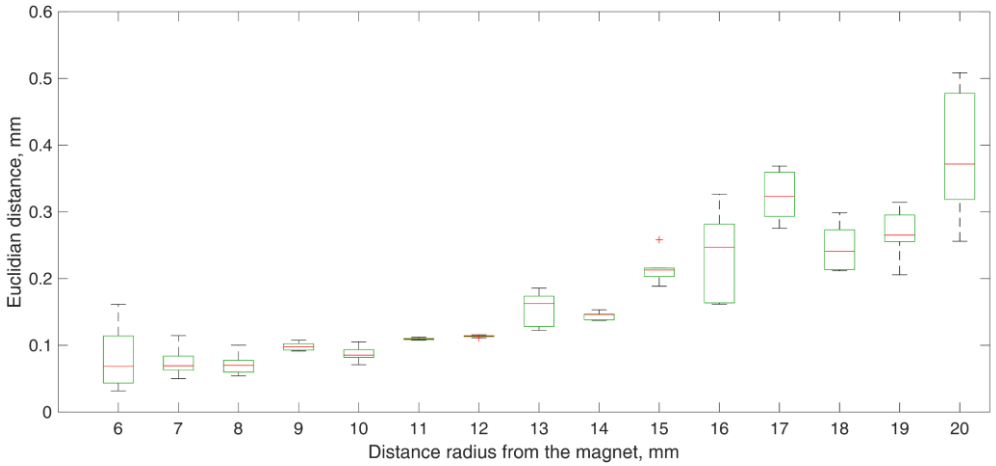

Fig. 4.27. 10 measurement ED median and standard deviation for the experimental measurements at different radiuses from the magnet

It has been observed that the method is the most prone to error in the area between the main and reference magnetometer. However, due to the jaw mechanics and the proposed locations for the magnet and sensor placement, the magnet will only move away from the reference magnetometer. The data shows that the localization error does not exceed RMSE of 0.1 mm at the occlusal area and RMSE

of 1 mm at the far end of the 15 mm working range. Such results exceed the expectations, since it does not fall far from the expensive clinical jaw kinematics evaluation devices. Such performance is sufficient for bruxism diagnostics and patient behavior monitoring with room to spare for the localization error increase from the decalibration.

4.5.2. Static 5-DOF jaw localization test

During the static 5-DOF jaw localization experiment, the ABB robotic arm moved the sensor along the defined masticatory trajectory.

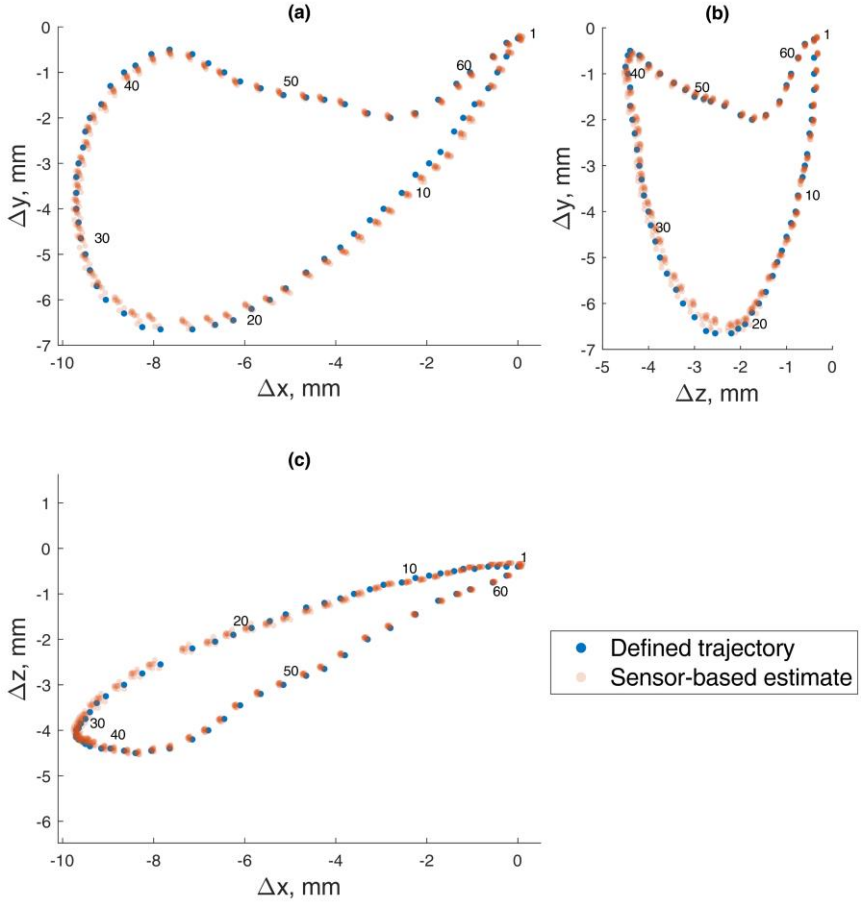

Fig. 4.28. The 5–DOF masticatory test trajectory estimated with BMF compensation and angle compensation; magnetic values at each point recorded with the sensor in the static state, mean localization error, and standard deviation RMSE = 0.165 ± 0.020 mm (ED = 0.098 ± 0.014 mm); the measured points are numbered from 0 to 62, and all 10 iterations are represented in transparent markers: (a) lateral–vertical view (x–y), (b) protrusive–vertical view (z–y), (c) lateral–protrusive view (x–z)

The measurements were discrete, stopping for measurement at each point of the trajectory. The test was repeated for 10 iterations. In Figure 4.28, the defined and sensor-estimated trajectories are presented, which resulted in the mean RMSE and standard deviation of 0.165 ± 0.020 mm. In Figure 4.29, the mean RMSE and error distribution of each point are shown. It should be noted that in dynamic experiments, discrete measurements are not possible. Therefore, in order to be able to compare this static experiment with dynamic experiments presented further in this work, the ED was calculated as well. It resulted in mean ED and standard deviation of 0.098 ± 0.014 mm that are shown in Figure 4.30.

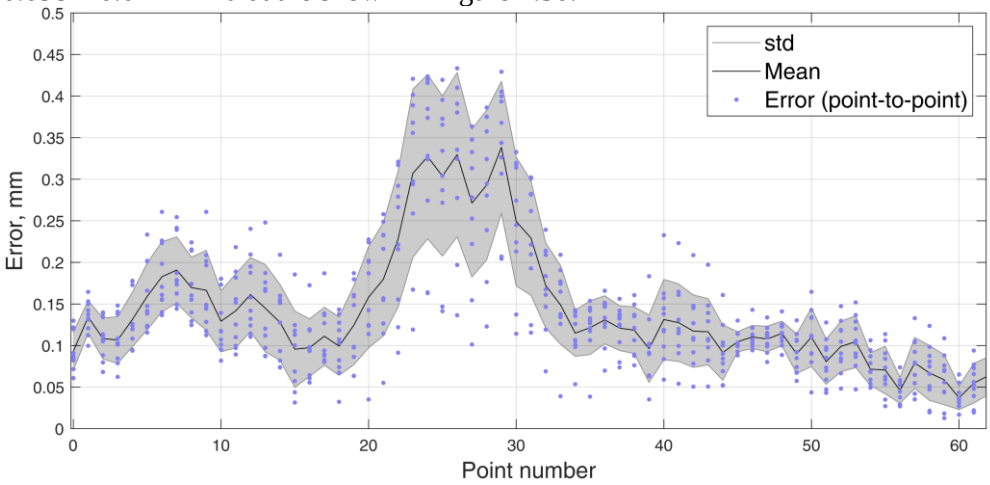

Fig. 4.29. Static 5-DOF experiment; localization (point-to-point) error RMSE of every point measurement in 10 trajectory iterations with the mean and standard deviation

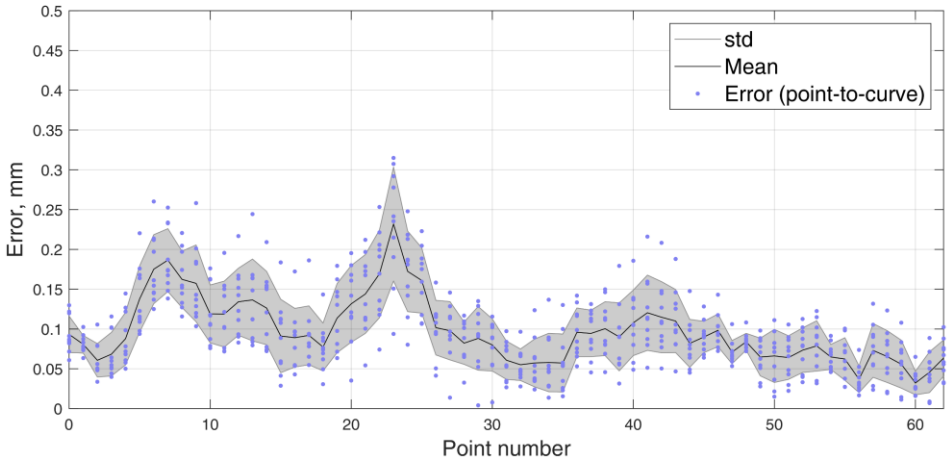

Fig. 4.30. Static 5-DOF experiment; localization (point-to-curve) ED error for every point measurement during 10 trajectory iterations with the mean and standard deviation

Although static conditions are not realistic in clinical application, this experiment shows the true method performance with minimum influence of the mechanical vibrations and magnetometer technical limitations. It is clear that the method is capable of accurately estimating realistic masticatory activity.

4.5.3. Dynamic 5-DOF jaw localization test

During the dynamic 5-DOF jaw localization experiment, the ABB robotic arm moved the sensor along the defined masticatory trajectory with its maximum speed. The duration of one cycle was 2 s. Both robot motion and measurements were continuous. The test was repeated for 10 iterations. The localization error was significantly reduced by utilizing the moving average filter. A window size of N = 4 was chosen experimentally, based on visually inspecting the shape of the trajectory. The window size was small due to 100 Hz data collection rate, which allowed only ~200 recorded samples per trajectory. In Figure 4.31, the defined and sensor-estimated trajectories are presented, which resulted in mean ED and standard deviation of 0.175 ± 0.003 mm. In Figure 4.32, the mean ED and error distribution of each point are shown.

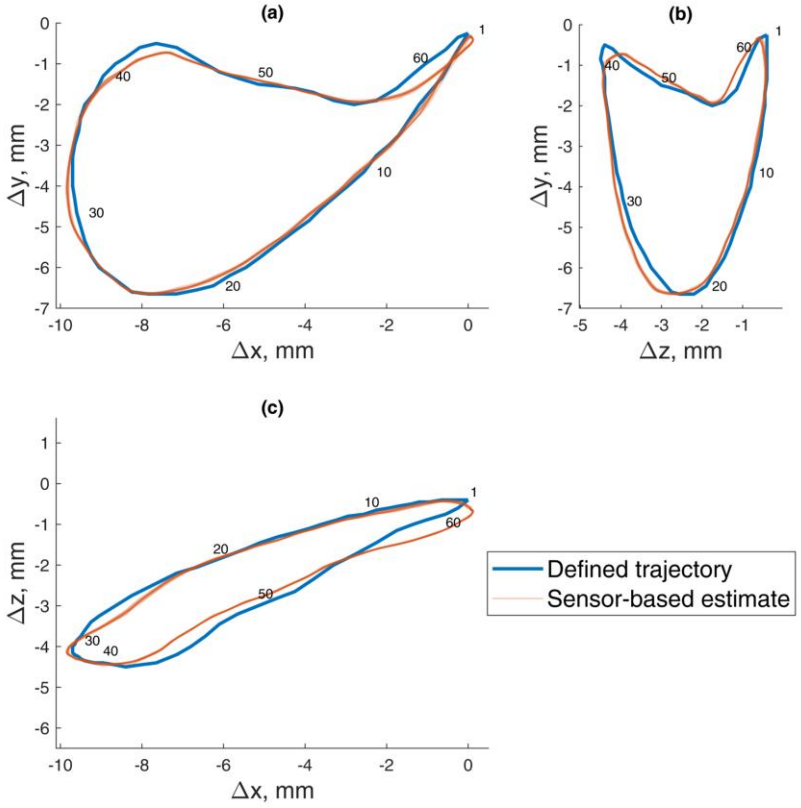

Fig. 4.31. 5-DOF masticatory test trajectory estimated with BMF compensation and angle compensation; magnetic values recorded with the sensor in motion, 2 s per

cycle; mean localization error with standard deviation ED = 0.175 ± 0.003 mm; the measured points are numbered from 0 to 62, and all 10 iterations are represented in transparent markers: (a) lateral–vertical view (x–y), (b) protrusive–vertical view (z–y), (c) lateral–protrusive view (x–z)

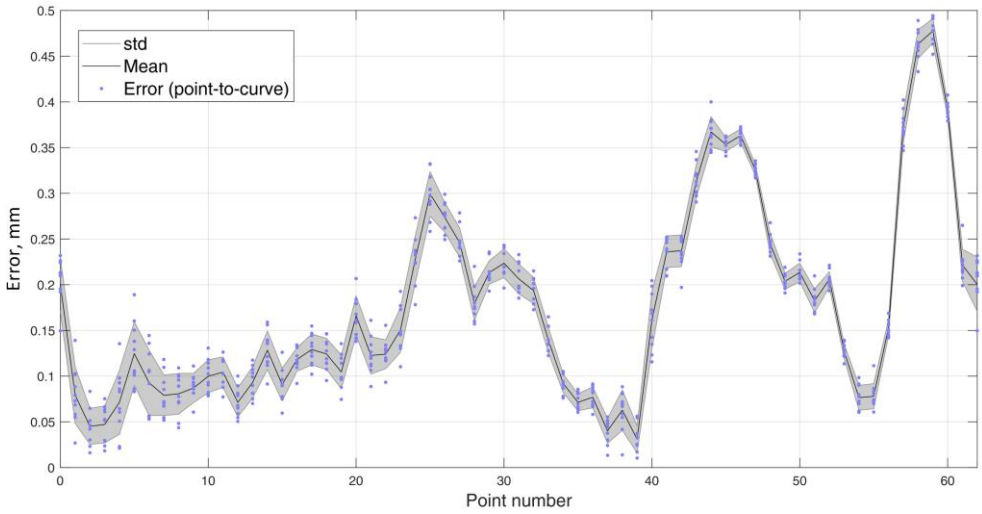

Fig. 4.32. Error (point-to-curve) from the reference masticatory trajectory to the estimated trajectory of the dynamic test, expressed in Euclidian distance (ED) with the mean and standard deviation of ED in 10 measurement iterations

The dynamic experiment has shown that with current technical limitations, the method is still able to estimate the natural masticatory activity in realistic conditions. Despite low localization error, some systematic shape discrepancies between the defined and sensor-estimated trajectories are visible. It is likely that it was caused by the mechanical and elastic properties of the protracted plastic tool for mounting the sensor. The tool was necessary to increase the distance from the motors of the robot, but with its ~28 cm length, some elasticity and springiness were inevitable. It resulted in some amortization and delay during sudden changes of movement direction. The fact that the sensor movement along the defined trajectory is not achieved with precision is a limitation of the study, which might indicate that even lower error could be recorded by increasing the quality of the study.

4.5.4. Automatic articulator test

The magnetic sensor-based estimate of a masticatory trajectory simulated by a robot-controlled articulator is presented in Figure 4.33 along with a reference trajectory registered using TrakStar system. The masticatory motion was repeated 10 times.

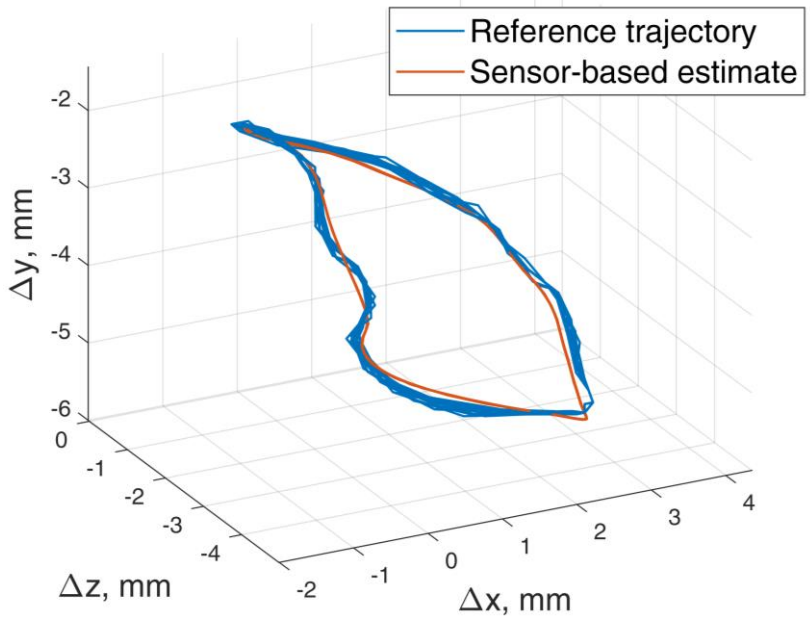

Fig. 4.33. Magnetic sensor-based estimate recorded in robot-controlled articulator test; reference trajectory recorded using TrakStar system

The resulting localization error for robot-controlled articulator test was ED = 0.240 mm. The sensor based-estimate showed high repeatability with the recorded trajectory, nearly identical for each of 10 iterations of the masticatory motion, contrary to the reference method. Therefore, in future research, a more accurate reference method with higher repeatability might be considered.

4.5.5. Intraoral test

Intraoral performance of the system was demonstrated by recording vertical chattering and masticatory motion of the volunteer, and the recorded trajectories are presented in Figures 4.34 and 4.35, respectively.

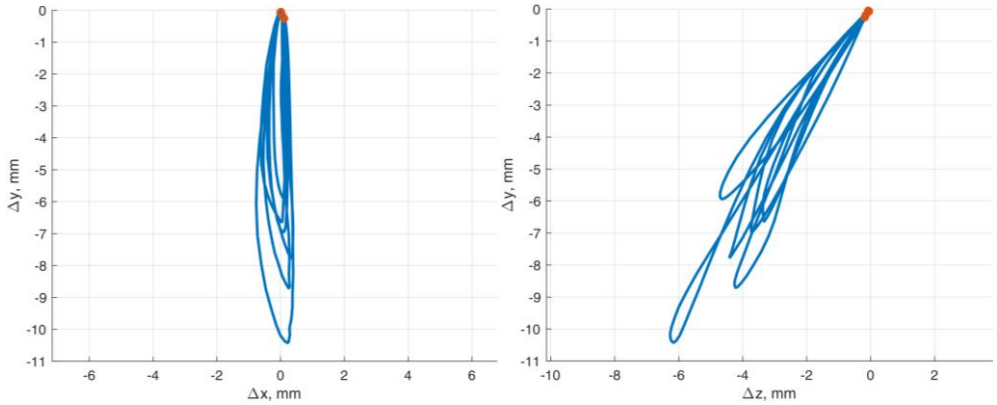

Fig. 4.34. Sensor-based estimate of a vertical chattering motion recorded intraorally with detected teeth impacts marked in red; front and side projections

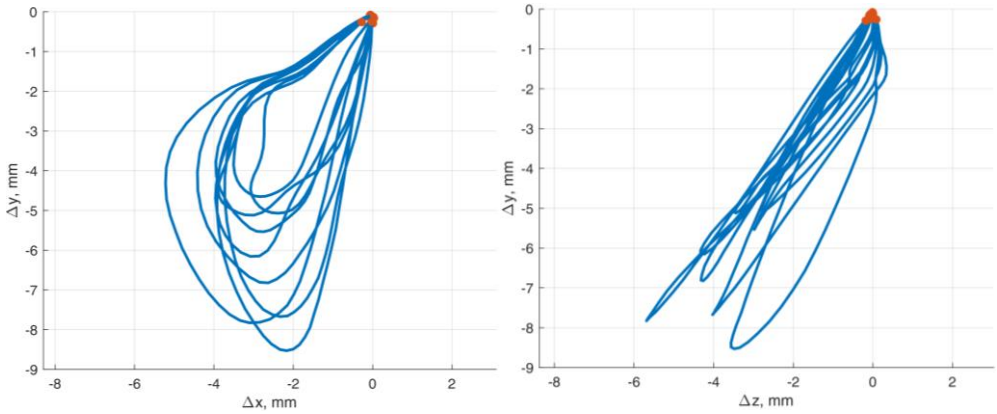

Fig. 4.35. Sensor-based estimate of a masticatory motion recorded intraorally with detected teeth impacts marked in red; front and side projections

Practical intraoral experiment helped to understand both the strengths and the weaknesses of the method better. The magnetic localization showed robustness and practicality. The method was capable of recording comprehensive motion of the jaw even without calibration. However, detecting the impacts of teeth with accelerometry appeared to be more challenging and required a combined analysis of both magnetic sensor localization and acceleration.

4.6. Conclusions of the chapter and discussion

Limitations of the study. Elinta 3D positioning system had a minimal 0.1 mm step. Even though it is a precision instrument from high quality components, its repeatability and its motion precision were not stated by the manufacturer. Moreover, it was custom-built a decade ago, and its performance may have degraded

with time. However, there were no signs of reduced performance. The ABB robotic arm had a minimal translation step of 0.01 mm and minimal rotation step of 0.01°. The limitations of the "Elinta" 3D positioning system could be considered as a reason for similar localization errors in one and two-magnetometer experiments (RMSE = 0.26 mm and RMSE = 0.28 mm, respectively). In a subsequent 5-DOF experiment performed on a more advanced robotic platform (ABB), the localization error was 37% lower, despite additional two degrees of freedom.

All electromechanical positioning systems contained electric motors that emit magnetic fields. This was very noticeable with the ABB robotic arm. This type of contamination was accounted for, reduced by increasing sensor-to-robot distance by a long mounting tool, and compensated together with the natural BMF. However, such sources of electromagnetic radiation will not be present in the clinical conditions.

The motion speed of the custom articulators and positioning systems used in dynamic localization testing was too slow in comparison with the swift natural motion of the human jaw. Therefore, the dynamic test results that were described in this work may slightly differ from the realistic conditions, and the clinical tests should be arranged in the future.

Inevitably, a long sensor mounting tool for ABB robot experiments was slightly springy and elastic. It resulted in a systematically altered reproduction of the defined trajectory, which certainly increased the resulting errors in the dynamic 5-DOF localization experiment.

The "TrakStar" system in the robotic articulator experiment showed worse repeatability than the proposed magnetic method. It suggests that the reference method might be lacking quality for this research.

Limitations of the method. The two-magnetometer method can compensate the BMF that is homogenous throughout the 22 mm distance between the magnetometers. In cases of metal or magnetic objects in proximity, as well as natural inhomogeneities in the ambient field, the method would not be able to compensate. However, 22 mm distance is very small, and the effects of this limitation are minimal.

As it was discussed in the methodology chapter, the magnetometer placement error might introduce some error in position estimation. It includes the unknown precise placement location of the three hall sensors during the tri-axial magnetometer manufacturing as well as component placement error during soldering. However, possible errors induced by component misplacement were estimated to be in the order of 0.1 mm. Moreover, these errors are systematic, and they can be mitigated by the software tuning.

According to the datasheet of the permanent magnet used in this research, there are tolerances of manufacturing for the magnet mechanical dimensions and magnetization. The possible errors induced by such changes of diameter and magnetization of the magnet were estimated to be below 0.4 mm. The difference in

the magnet magnetization may be fully compensated by the software calibration, and this error can be avoided; however, it does need to be considered.

The proposed system is difficult to scale due to the properties of the magnetic phenomena itself: the magnetic field has an inverse cube with distance. Therefore, in order to increase the resistance to the ambient field and the system working range by a few millimeters, the magnetization of the magnet and the working range of the magnetometer should be increased at least 10 times.

The localization is the most unstable when the magnet is located in the area between the magnetometers. However, in the proposed magnet and sensor placement layout on the jaw, the jaw mechanics does not allow the magnet to move towards the reference magnetometer.

The error to distance dependency should be mentioned, meaning that the localization error is not even throughout the system working range. However, the good thing is that it is low where it matters, i.e., in the beginning of the working range, around the occlusal zone.

The most serious drawback of the proposed approach is the magnetometer zero offset change. Moreover, it is especially affected by the strong magnetic fields. As it was estimated during the experiments, the offset on the zero value of the measured magnetic field may change in the range of ±40 μT. Therefore, in this method, where a magnet reaching the full working range of the magnetometer is used, the magnetometer is bound to have zero offset change. If not compensated, depending on which magnetometer experienced the offset change and the distance to the magnet, it may introduce up to 4 mm of error at the limit of the working range (open mouth). However, in positions approaching occlusion, a change of 40 μT is insignificant. This indicates that the method has potential to be useful, despite this drawback. Nevertheless, the magnetometer offset must be calibrated before the measurement.

Summary of the results. In this work, a two-magnetometer, 5-DOF jaw motion tracking concept was created and examined. The method was verified with the FEM data. A sensor prototype was created to verify the method in practice. The method is proposed along with solutions for two of the largest sources of error for such jaw tracking approach, i.e., the ambient magnetic field and the rotation of the jaw. In order to illustrate the effects of these solutions, the test masticatory trajectory localization was performed with and without the BMF compensation and jaw angle estimation. The resulting trajectories along with the defined masticatory trajectory were visualized in Figure 4.36.

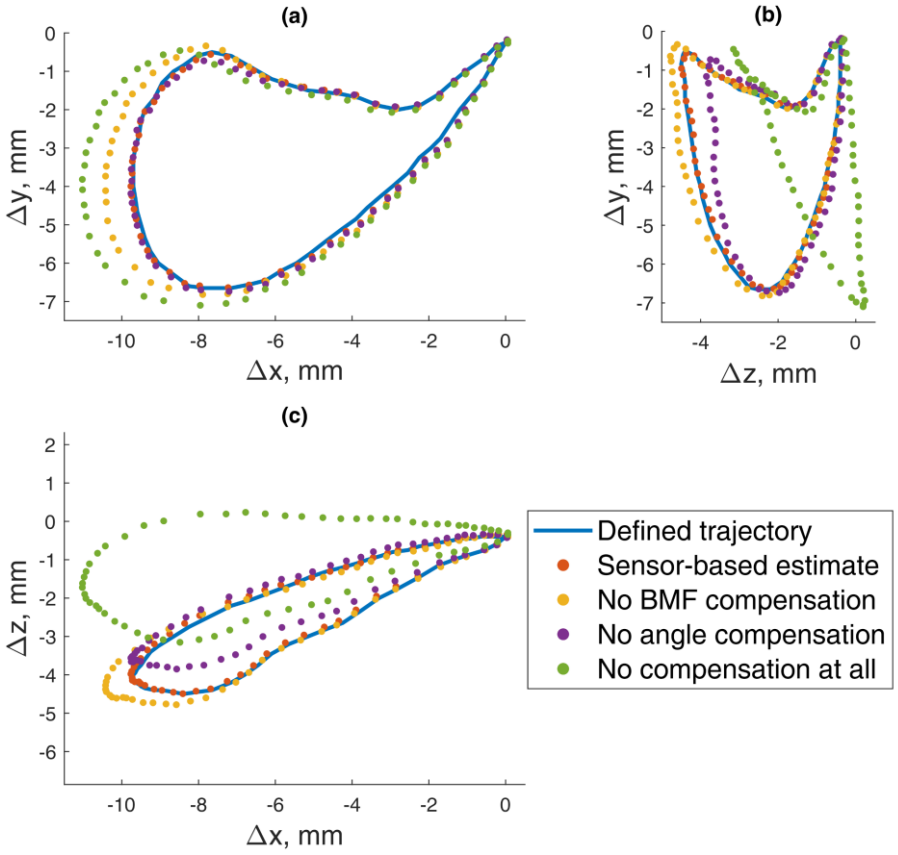

Fig. 4.36. The 5–DOF masticatory test trajectory estimated with and without the BMF compensation and jaw angle estimation algorithms; magnetic field values at each point recorded with a sensor in the static state: (a) lateral–vertical view (x–y), (b) protrusive–vertical view (z–y), (c) lateral–protrusive view (x–z)

Trigonometric equations representing rotation-to-translation relationship of the jaw increase the number of the method DOF from 3 to 5. This allows to estimate the angles of vertical and lateral jaw rotation, thus enabling the method to be practically implemented in realistic conditions. Otherwise, large localization errors would be caused by the unaccounted rotations of the jaw. The equations were successfully verified by the comparison to 6-DOF reference data that have been collected from a volunteer. It is known and acknowledged that the complex dynamics of the jaw were simplified in this approach. For instance, the influence of the articular tubercle curvature was ignored by supposing that z axis rotation is equal to 0 and excluding it from the estimation. It was done this way because it is not possible to link z axis rotation of the jaw to any linear translation. Despite this, the proposed approach does predict two main angles of the jaw rotation moderately well.

The approach of using two adjacent magnetometers is effective in compensating homogenous BMFs. Based on the FEM theoretical experiments, it should make the method more accurate as well, since twice as much data is used for the localization. However, in practical experiments, one and two-magnetometer approaches showed similar localization errors of RMSE = 0.26 and RMSE = 0.28 mm, respectively. In theoretical FEM case, the localization errors were RMSE = 0.1 mm and RMSE = 0.05 mm, respectively. Secondly, it should be considered that a similar error with two-magnetometer approach was achieved with BMF contaminated data, as opposed to the BMF-free data for the single-magnetometer case. In realistic conditions, the single-magnetometer approach requires the second magnetometer anyway that must be placed outside the magnetic field of the magnet. Therefore, two-magnetometer approach reduces the sensor dimensions, which makes it a better option for the intra-oral use. All things considered, the superiority of the two-magnetometer approach is evident.

The static 5-DOF test of the method resulted in the mean localization error with a standard deviation of RMSE = 0.165 ± 0.020 mm (ED = 0.098 ± 0.014 mm). In the dynamic 5-DOF experiment, the resulting mean localization error with standard deviation was ED = 0.175 ± 0.003 mm. As it was mentioned in the limitations of the study, the experiment was slightly negatively affected by a low rate of data acquisition and flexibility of the protruded plastic sensor-mounting tool. In Tables 3 and 4, the results of the practical one and two magnetometer, 3-DOF and 5-DOF static and dynamic experiments with test masticatory trajectory, are presented to be compared in RMSE and ED.

Table 3. One and two-magnetometer 3-DOF approaches in the static experiments and two-magnetometer 5-DOF approach in the static and dynamic experiments compared; 10 measurement mean and standard deviation of the localization error expressed in Root mean square error (RMSE); its projections on different axes are presented as well

Approach, test	**RMSE, mm**	**RMSE, x proj., mm**	**RMSE, y proj., mm**	**RMSE, z proj., mm**
1 mag. 3-DOF, static	0.260 ± 0.004	0.174 ± 0.003	0.107 ± 0.001	0.064 ± 0.001
2 mag. 3-DOF, static, BMF comp.	0.280 ± 0.006	0.167 ± 0.002	0.123 ± 0.004	0.097 ± 0.005
2 mag., 5-DOF, static, BMF comp.	0.165 ± 0.011	0.114 ± 0.008	0.043 ± 0.009	0.036 ± 0.005
2 mag., 5-DOF, dynamic, BMF comp.	-	-	-	-

Table 4. One and two-magnetometer 3-DOF approaches in static experiments and two-magnetometer 5-DOF approach in static and dynamic experiments compared; 10 measurement mean and standard deviation of the localization error expressed in Euclidean distance (ED); its projections on different axes are presented as well

Approach, test	ED, mm	ED, x proj., mm	ED, y proj., mm	ED, z proj., mm
1 mag., 3-DOF., static,	0.127 ± 0.002	0.071 ± 0.001	0.059 ± 0.002	0.060 ± 0.001
2 mag. 3-DOF, static	0.189 ± 0.006	0.113 ± 0.002	0.080 ± 0.004	0.062 ± 0.005
2 mag., 5-DOF, static	0.098 ± 0.014	0.049 ± 0.014	0.056 ± 0.010	0.042 ± 0.009
2 mag., 5-DOF, dynamic	0.175 ± 0.003	0.080 ± 0.001	0.103 ± 0.002	0.076 ± 0.001

A robot-controlled articulator was used to simulate realistic jaw motion, resulting in ED = 0.240 mm localization error, in comparison to the reference method. The operation of the system was demonstrated intraorally using a wireless sensor prototype.

In comparison to the clinical jaw kinematics evaluation systems, the working range of the method (R = 15 mm) is perfectly sufficient, since most precision jaw kinematics machines state similar (most effective) working range as well. This means that the method does not fall behind the expensive clinical appliances in the working range while as well offering sub-millimeter accuracy. This does not mean that the method is comparable to the clinical approaches: the need for frequent calibration and zero-offset change problem put the method in a lower tier than the clinical precision instruments. Moreover, temporomandibular kinematics cannot be properly evaluated without assessing the positions of the condyles in relation to the skull [85]. The method, as it was designed, is more suitable for the patient's behavior analysis than jaw kinematics and condylar movement evaluation. To summarize, precision 5-DOF experiments validated the proposed jaw position estimation method with simultaneous BMF compensation and jaw angle estimation, proving the method's eligibility for further development. In future research, the size of the prototype should be reduced as much as possible; software optimization to lower power consumption must be done, and a better powering solution should be found. New technical advancements in the field of magnetic sensors should be followed as the method is limited by the performance characteristics of current MEMS magnetometers.

5. CONCLUSIONS

1. A method for dynamic jaw position estimation with jaw rotation assessment and ambient field compensation was developed. The method was theoretically assessed by using a finite element modeled magnetic field map of a permanent magnet. For test masticatory trajectory in theoretical case, the error was RMSE = 0.05 mm. The one-magnetometer proof-of-concept without the BMF compensation ability was confirmed experimentally with mean localization error with a standard deviation of RMSE = 0.260 ± 0.004 mm. The two-magnetometer proof-of-concept with the BMF compensation ability was confirmed experimentally with the error of RMSE = 0.28 mm. The possibility to enhance the method with the accelerometric teeth impact detection was confirmed as well.
2. A comparative evaluation of the methods for two-magnetometer jaw position estimation from the magnetic field values was done on the simulated data. LS method showed substantially better performance and was chosen over the particle swarm optimization. The customized LS optimization method with BMF compensation, jaw angle estimation, and adaptive BMF limits was successfully tested on both simulated and experimental data. Throughout the working range, the theoretical localization errors at various radial distances (from R = 6 mm to R = 20 mm) did not exceed the average RMSE of 0.1 mm.
3. A two-magnetometer sensor prototype was developed and tested using a robotic arm, simulating 5-DOF jaw motion in static and dynamic experiments. The optimal sensor layout was determined by utilizing a FEM. The concept of the method with two magnetometers that has BMF compensation and jaw angle estimation in static experiment resulted in mean localization error and standard deviation of RMSE = 0.165 ± 0.020 mm (ED = 0.098 ± 0.014 mm), and in dynamic experiment, it resulted in mean localization error and standard deviation of ED = 0.175 ± 0.003 mm. It has been shown that the error significantly depends on the magnet-to-sensor distance, as localization errors were estimated throughout the whole working space of the sensor. Throughout the R = 6 mm to R = 20 mm (radial distance from the magnet) working range, the average errors of experimentally recorded trajectories ranged from RMSE < 0.1 mm at the beginning of the working range to RMSE < 1 mm at the end of the working range. A robot-controlled articulator was used to simulate realistic jaw motion, resulting in ED = 0.240 mm localization error, in comparison to the reference method. A wireless sensor prototype was created as well as powering and mounting solutions for intraoral use, and the operation of the system was demonstrated intraorally.

6. FUTURE SCOPE OF THE RESEARCH

The proposed method is a powerful tool to gather diagnostically significant data. However, the methods for recognizing parafunctions in jaw trajectory data have not been proposed yet. Moreover, the prototype device can be improved regarding both performance and ergonomics. Therefore, the following tasks are in the future scope of the research:

1. Development of a method for the jaw parafunction recognition from motion trajectories,
2. Clinical trials on bruxism patients with a control group,
3. Improving ergonomics for users and convenience of use for the physicians,
4. Further minimization of the sensor and improvement of the powering solution,
5. Algorithm optimization for the data processing speed or search for superior, faster algorithm for magnetic field data processing.

SANTRAUKA

ĮVADAS

Tyrimo aktualumas

Esama atotrūkio tarp tikslių klinikinių žandikaulio judesių registratorių ir gerokai primityvesnių, elektromiograma (EMG) arba okliuzinėmis kapomis paremtų dėvimų bruksizmo detektorių. Dar nėra sukurta metodo, galinčio pasiūlyti laisvą paciento judėjimą tęstinės žandikaulio lokalizacijos metu, juolab su milimetro neviršijančiomis paklaidomis. Ergonomiškas dėvimas prietaisas, registruojantis žandikaulio poziciją kaukolės atžvilgiu, pakeltų bruksizmo diagnostikos kokybę. Jis galėtų sukurti beprecedentį kiekį duomenų žandikaulio parafunkcijų vertinimui ir tyrimams; taip pat galėtų būti taikomas dantų dėvėjimosi eksperimentams, protezų tobulinimui, kramtymo efektyvumo vertinimui ar miego apnėjos bei disfalgijos tyrimams. Šiuo metu rinkoje yra nemažai įvairiais fizikiniais reiškiniais paremtų klinikinių aparatų, skirtų nustatyti žandikaulio pozicijai ir registruoti jo judėjimo trajektorijoms. Tokie prietaisai tikslūs ir efektyvūs vertinant žandikaulio kinematiką. Jie gali būti naudojami projektuojant protezus ir ortognatinėje chirurgijoje atliekant priešoperacinį bei pooperacinį vertinimą. Nepaisant to, visiems esamiems metodams reikalingi ganėtinai stambūs ir nepatogūs išoriniai įtaisai, tvirtinami tiesiogiai ant paciento žandikaulio ir galvos. Tai pastebimai apriboja jo judesius ir padaro tęstinius (t. y. visos nakties) tyrimus neįmanomais. Juoba kad toks tikslumas nėra esminis vertinant elgseną, kai vien judesio trajektorijos forma ir topologija atskleidžia tokią diagnostinę informaciją kaip vyraujantis bruksizmo tipas, okliuzinio kontakto trukmė ir dantų kontaktų skaičius, taip pat parafunkcinių epizodų pasikartojimo dažnumas ir intensyvumas. Tokiu atveju prioritetas yra tęstinė, ergonomiška stebėsena, leidžianti pacientams tęsti savo įprastą rutiną su kiek įmanoma mažiau intervencijos. Galimybė atlikti bazines oralines funkcijas (įskaitant parafunkcijas) su minimaliu diskomfortu ir kitų dėmesio atkreipimu yra labai svarbi. Daugiausia tęstinių ir minimaliai ribojančių kramtomosios veiklos sekimo metodų pasiūlyta bruksizmo diagnostikos srityje. Auksinis standartas – multisensorinis miego tyrimas – polisomnografija (PSG). Net be jokių tiesioginių žandikaulio kinematikos duomenų PSG, papildyta garso ir vaizdo (AV) įrašais, yra patikimiausias ir išsamiausias miego bruksizmo diagnostikos metodas [3]. Deja, visą naktį trunkančios hospitalizacijos kaina ir trukmė daro šį metodą netinkamą plačiam ir dažnam taikymui. Prietaisai, paremti kramtomojo ir smilkininio raumenų EMG, taip pat yra netiesioginiai, bet jie ergonomiški, nebrangūs ir ganėtinai populiarūs įrankiai pirminei diagnostikai. Visgi šis metodas neatsparus triukšmams ir judesio artefaktams dėl nedidelės signalo amplitudės ir odos varžos skirtumų [4]. Kitas, ganėtinai plačiai tyrinėjamas, sprendimas yra okliuzinės kapos su integruotais slėgio jutikliais, iš kurių vienintelis komerciškai išplėtotas yra „Bruxane“ (*Bruxane*, Marburgas, Vokietija). Jis registruoja bruksizmo epizodus ir skleidžia vibracinį bioatsaką, kai yra sukandamas. Okliuzinės kapos storis – viena pagrindinių pacientų

diskomforto priežasčių [5]. Jis taip pat tiesiogiai veikia paciento elgseną, šitaip sumažinamas bruksizmo epizodų pasireiškimo dažnis ir intensyvumas [6]; tai puiki savybė žalos prevencijai, antra vertus, diskredituoja patį matavimą.

Naujo dėvimo prietaiso tęstiniam stomatognatinės funkcijos vertinimui poreikis pastaraisiais metais auga, bet nebuvo pasiūlyta jokių inovatyvių problemos sprendimo būdų. Siekiant viršyti esamų sprendimų galimybes, okliuzinis paviršius turėtų likti neuždengtas, prietaisas turėtų būti mažai pastebimas pacientui ir atsparus drėgmei bei judesiams. Buvo iškelta hipotezė, kad nuolatinio magneto pozicijos sekimo sistema galėtų atitikti šiuos kriterijus. Taip pat ji galėtų būti papildyta akcelerometriniu dantų kontakto momento atpažinimu. Moderniose mažos galios inercinių matavimų sistemų (IMS) jutiklių mikroelektromechaninėse sistemose (MEMS), viename mažame korpuse, būna integruoti triašiai magnetometrai, akcelerometrai ir giroskopai. Mažų gabaritų IMS leistų pritaikyti metodą intraoraliai dėvimuose prietaisuose. Nuolatinio magneto naudojimui nereikalingas elektrinis kontaktas tarp viršutinių ir apatinių dantų. Magnetinio lauko lygtys galėtų būti pritaikytos nustatyti tiksliai jutiklio pozicijai magneto atžvilgiu. Tokia sistema leistų tęstinai registruoti žandikaulio poziciją bei dinaminę okliuziją, atpažinti patologinę elgseną ir pamatyti, kokie yra vyraujantys bruksizmo judesiai. Tokia specifinė paciento informacija būtų itin naudinga diagnostikai ir dantų atkūrimui. Taip pat, nors klinikinis žandikaulio kinematikos vertinimas ir būtinas išsamiai temporomandibuliarinių sutrikimų diagnostikai bei gydymui, tam tikrais atvejais tęstinė paciento elgesio stebėsena galėtų būti išnaudota sekant gydymo eigą ir pažangą.

Mokslinė technologinė problema

Bruksizmas sukelia negrįžtamų pažeidimų nemažos populiacijos dalies dantims, ir esami žandikaulio parafunkcijų diagnostikos metodai turi akivaizdžių techninių ribotumų.

Mokslinė technologinė šio darbo problema yra: kaip tiesioginiu, tęstiniu ir neįkyriu būdu kiekybiškai įvertinti žandikaulio parafunkcijas? Darbinė hipotezė – jog prie dantų pritvirtinti du triašiai magnetometrai ir mažas nuolatinis magnetas gali suteikti pakankamai duomenų išsamiam žandikaulio judesių nustatymui, kuris reikalingas vertinant parafunkcijas.

Tyrimo objektas

Tyrimai paremti tiesioginio ir tęstinio žandikaulio judesių registravimo metodo kūrimu ir tyrinėjimu, taip pat eksperimentinio prietaiso siūlomam metodui kūrimu. Tokia technologija galėtų būti įrankis žandikaulio parafunkcijoms diagnozuoti ir išsamiems duomenų rinkiniams, kurie būtų skirti naujiems žandikaulio parafunkcijų tyrimams, sudaryti.

Tyrimo tikslas

Šio tyrimo tikslas – sukurti ir ištirti minimaliai pacientui trukdantį tęstinio žandikaulio judesių registravimo metodą, skirtą žandikaulio parafunkcijų stebėsenai ir vertinimui.

Tyrimo uždaviniai

1. Sumodeliuoti ir ištirti nuolatinio magneto sekimo konceptą panaudojant magnetometrus, tinkamus dinaminiam intraoraliniam žandikaulio pozicijos stebėjimui.
2. Išplėtoti duomenų apdorojimo algoritmus žandikaulio pozicijos įvertinimui remiantis magnetometrų duomenimis.
3. Sukurti, išbandyti ir įvertinti jutiklį ant laboratorinio žandikaulio modelio ir realiomis sąlygomis.

Mokslinis naujumas

Šioje disertacijoje pasiūlytas pirmasis metodas tiesioginiam, tęstiniam, intraoraliniam žandikaulio pozicijos registravimui. Esami žandikaulio kinematikos vertinimo metodai netinka tęstiniams tyrimams, o dėvimi žandikaulio veiklos registratoriai negali pateikti duomenų erdvinei žandikaulio pozicijai nustatyti. Šiame darbe aprašytu metodu foniniam magnetiniam laukui (FML) atspariai magnetinei lokalizacijai naudojami tik du, greta vienas kito esantys, triašiai magnetometrai. Tai anksčiau nebuvo daryta. Nuspėjami žandikaulio pasisukimo kampai leido atlikti 5 laisvės laipsnių (LL) žandikaulio pozicijos nustatymą taikant 3 LL magnetinės lokalizacijos metodą. Tai atlikta pritaikant kinematinius žmogaus kramtymo sistemos ribotumus ir išvedus trigonometrinių lygčių sistemą, susiejančią žandikaulio linijinius poslinkius su pasisukimo kampais. Sukurtas metodas tinka dėvimam intraoraliniam prietaisui, kurio tikslumas artimas precizinių klinikinių įrenginių tikslumui.

Praktinė reikšmė

24 valandų žandikaulio pozicijos įrašai gydytojams leistų aiškiai diagnozuoti žandikaulio parafunkcijas, įskaitant vyraujantį parafunkcijos tipą, žandikaulio judėjimo trajektorijas, epizodų pasireiškimo dažnį bei intensyvumą, taip pat išgauti kitą reikalingą statistiką. Tokia išsami diagnostinė informacija leistų paskirti tinkamą gydymo planą žmonėms su natūraliais dantimis, taip pat pasirinkti tinkamas medžiagas ir gamybos metodiką dantų atkūrimui, kuris užtikrintų natūralių ir restauruotų dantų ilgaamžiškumą. Įrašyti duomenys naudotojo sąsajoje galėtų būti vizualizuojami panaudojant trimačius (3D) skanuotų paciento dantų modelius, o tai leistų gydytojui peržiūrėti tikslius dominančių epizodų atkartojimus. Specialistai, gydantys temporomandibuliarinio sąnario (TMS) ir žandikaulio raumenų sutrikimus,

galėtų pritaikyti metodą tęstinei paciento elgsenos ir gydymo eigos bei pažangos stebėsenai.

Tyrimo rezultatų aprobavimas

Šios daktaro disertacijos rezultatai publikuoti dviejuose straipsniuose moksliniuose žurnaluose, esančiuose „Master List of Thomson Reuters Web of Science“ sąraše su cituojamumo indeksu (Q2). Rezultatai taip pat pristatyti dviejose tarptautinėse konferencijose, kurios vyko Slovėnijoje (Portorožėje) ir Lietuvoje (Vilniuje).

Stiuarto platforma paremtas žandikaulio judesių simuliatorius, sukurtas ir panaudotas šiame darbe aprašytiems tyrimams, buvo apdovanotas „EIT Health“ prizu jaunųjų mokslininkų parodoje „Technorama 2020“ (Kauno technologijos universitete).

Gynimui teikiami teiginiai

1. 2 mm × 2 mm cilindro formos magneto 3 LL erdvinė pozicija siaurame darbiniame diapazone (15 mm) gali būti įvertinta su mažesne nei 1 mm lokalizacijos paklaida, matuojant jo magnetinį lauką ir pritaikant apribotą netiesinės optimizacijos algoritmą.
2. Magneto lokacija gali būti įvertinta su atsparumu natūraliam, homogeniškam foniniam magnetiniam laukui, panaudojant du triašius magnetometrus su fiksuotu nedideliu tarpusavio atstumu.
3. Siūloma sistema gali būti panaudota įvertinti 5 LL žandikaulio judesiams pritvirtinus magnetą prie viršutinio žandikaulio, dviejų magnetometrų jutiklį prie apatinio žandikaulio ir žandikaulio pasisukimo kampus įvertinant trigonometrinėmis lygtimis iš žandikaulio linijinio poslinkio matavimų.
4. Pasiūlytas metodas užpildo spragą tarp precizinių žandikaulio kinematikos vertinimo sistemų ir primityvesnių EMG arba okliuzinėmis kapomis paremtų žandikaulio veiklos registratorių. Pasiektas submilimetrinis tikslumas išlaikant paciento mobilumą ir tęstinių matavimų galimybę.

Disertacijos struktūra

Disertaciją sudaro įžanga, keturi dėstymo skyriai, išvados, ateities tyrimų kryptys ir šaltinių bei autoriaus publikacijų sąrašai.

1. Pirmajame skyriuje paaiškinama bruksizmo ir kitų žandikaulio parafunkcijų problematika, pateikiamas trumpas žandikaulio anatomijos ir biomechanikos aprašymas, taip pat apžvelgiami esami žandikaulio funkcijų ir parafunkcijų stebėsenos metodai.
2. Antrajame skyriuje pateikiama biomedicininiams taikymams skirtų nuolatinio magneto pozicijos sekimo metodų literatūros apžvalga.

Apžvelgtas magnetinės lokalizacijos veikimo principas, galimi algoritmai magneto pozicijos įvertinimui, magnetinio lauko matavimų ir naudotų magnetometrų skaičius bei išdėstymai.

3. Trečiajame skyriuje aprašyta disertacijos metodologija. Ji susideda iš išsamaus pasiūlyto magnetinės žandikaulio lokalizacijos metodo ir atliktų tyrimų, įvertinimų bei eksperimentų metodologijų aprašymo.
4. Ketvirtajame skyriuje pristatomi teorinių įvertinimų bei teorinių eksperimentų rezultatai ir praktinių eksperimentų rezultatai, kurių dalis buvo prieš tai atliktų teorinių eksperimentų atkartojimas praktiškai. Pateikiamas atliktų tyrimų vertinimas ir diskusija, taip pat metodo ir tyrimų ribotumai.
5. Penktajame skyriuje pristatomos išvados.
6. Paskutiniame skyriuje nurodomos ateities tyrimų kryptys.

Kai kurios 3 skyriaus dalys cituotos pažodžiui iš [8] ir [9] disertacijos autoriaus publikacijų. Bendra disertacijos apimtis yra 105 puslapiai, įskaitant 66 iliustracijas, 4 lenteles ir 85 bibliografinius šaltinius. Santraukos apimtis – 57 puslapiai.

1. KLINIKINĖ ŽANDIKAULIO JUDESIŲ REGISTRAVIMO SVARBA

1.1. Fiziologiniai ir medicininiai pagrindai

Oralinės parafunkcijos yra apibrėžiamos kaip nevalingas oralinis judesys ar įprotis, nesusijęs su valgymu ar kalba. Joms priskiriamas bruksizmas (t. y. griežimas dantimis), dantų spaudimas, lūpos ar skruosto kramtymas, nagų kramtymas ir nykščio čiulpimas. Daugeliui pacientų šie sutrikimai pasireiškia švelnia forma ir jiems nereikia jokio gydymo. Oralinės parafunkcijos yra kategorizuojamos kaip psichofiziologiniai sutrikimai [10], [11]. Manoma, jog jas sukelia tokie psichologiniai faktoriai kaip nerimas, stresas bei nuovargis, ir gali išprovokuoti alkoholis, nikotinas bei stimuliantai [11]. Nors visos oralinės parafunkcijos gali neigiamai paveikti gyvenimo kokybę, daugelis jų yra lengvai diagnozuojamos ir nesukelia negrįžtamos žalos. Bruksizmas yra pavojingiausia ir labiausiai paplitusi parafunkcija. Šis sutrikimas nuolat plinta daugiausia dėl kylančio gyvenimo tempo ir didėjančio skaičiaus žmonių, kurie patiria intensyvų stresą. Esant skirtingiems vertinimo metodams ir sutrikimo sunkumui, suaugusiųjų populiacijoje bruksizmą gali turėti tarp 8 % ir 31,4 % žmonių [1]. Bruksizmo pasekmės (1.1 pav.) natūraliems dantims gali būti ne tik skilimai, lūžinėjimai, nudilimas ir dantenų retrakcija, bet ir padidėjęs jautrumas, pulpitas ir kramtymo efektyvumo praradimas. Stiprus dantų sukandimas sukelia galvos skausmą, kramtomųjų raumenų hipertrofiją ir mialgiją, bei žandikaulio sąnario disko išnirimą ir temporomandibuliarinio sąnario (TMS) degeneraciją [5]. Taip pat bruksizmas sukelia dideles apkrovas ant implantų stovinčioms dantų restauracijoms, kas gali lemti implantų lūžius, kaulo tirpimą aplink implantą bei tai sekantį implantų atmetimą. Deja, dažnai bruksizmas diagnozuojamas tik iš pasekmių.

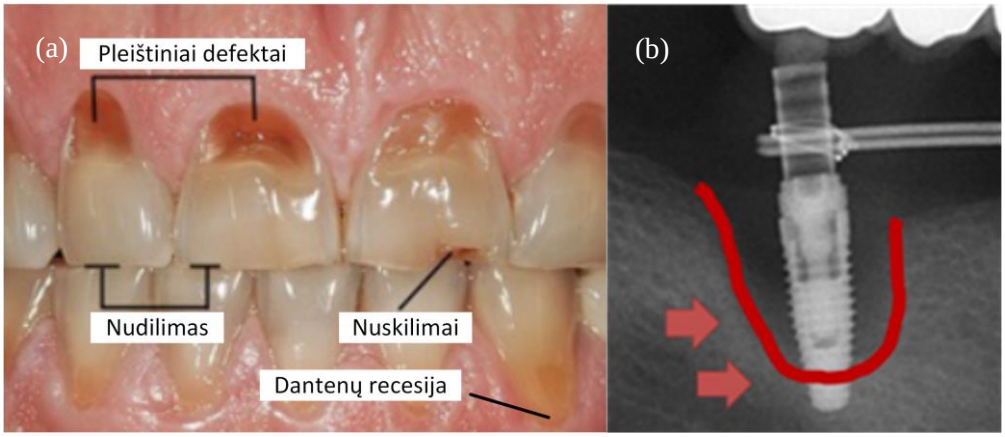

1.1 pav. Bruksizmo pasekmės natūraliems dantims (a) ir implantais paremtoms restauracijoms (b) [15] šaltinio ir originalios nuotraukos (su autoriaus leidimu) pagrindu

1.2. Metodai žandikaulio funkcijai vertinti

Populiariausias sprendimas kenčiantiems nuo bruksizmo yra okliuzinių kapų naudojimas – tiek diagnostikai, tiek žalos prevencijai. Medicininės apsauginės kapos plačiau paskirsto dantų patiriamą apkrovą bei atpalaiduoja kramtomuosius raumenis [23]. Diagnostinės kapos (1.2 pav.) gali būti skirstomos į nutrinamąsias kapas [19] [24] ir kapas su integruotais slėgio jutikliais, kurios registruoja sukandimų skaičių, jų stiprumą ir pasireiškimo dažnumą. Kai kuriais atvejais, generuoja vibracinį ar garsinį bioatsaką jas sukandus. Vienintelis tokio tipo komerciškai prieinamas prietaisas yra Bruxane (Bruxane, Marburgas, Vokietija) [25]. Taip pat, literatūroje galima rasti tyrimų aprašančių kapas su integruotais pjezorezistyviniais [5] bei optiniais [26] slėgio jutikliais.

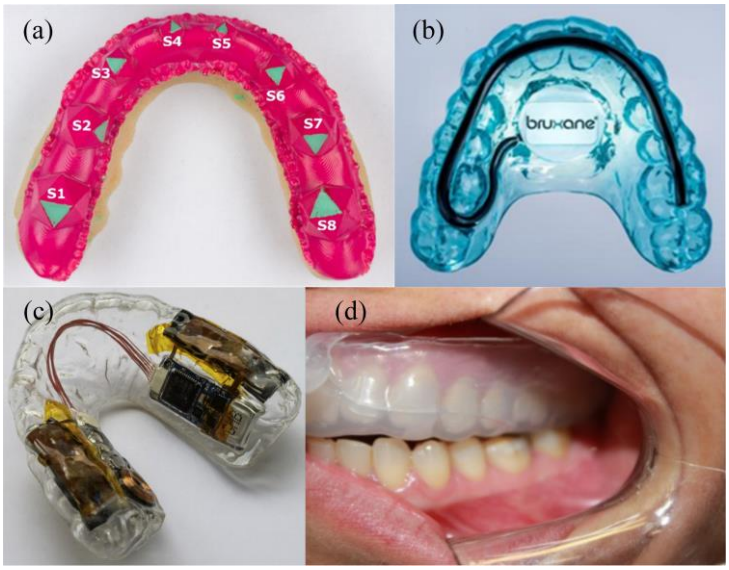

1.2 pav. Okliuzinės kapos bruksizmo diagnostikai: (a) nusitrinančios kapos pusiau automatiniam vertinimui skanuojant [24]; (b) „Bruxane“ kapos su integruotais slėgio jutikliais [25]; (c) kapa su integruotais pjezorezistiniais slėgio jutikliais [5]; (d) kapa su optinio pluošto slėgio jutikliais [26]

Okliuzinės kapos veikia ir paciento elgseną – jos sumažina parafunkcinių epizodų pasireiškimo dažnį ir intensyvumą. Tai naudingas bruožas žalos prevencijai, tačiau kartu diskredituoja jomis atliekamus matavimus [29], [6]. Dar svarbu paminėti, jog esminė pacientų diskomforto priežastis dėvint kapas yra jų storis [5]. Žmogus su natūraliais dantimis svetimkūnį okliuzinėje zonoje pradeda justi nuo 20 µm storio [30].

Kramtomojo arba smilkininio raumens EMG leidžia atpažinti žandikaulio veiklos aktyvumą išoriškai. Nors netiesioginis, šis bruksizmo diagnostikos metodas yra itin populiarus dėl nedidelės kainos ir ergonomiškumo. Esama nemažai šio

metodo interpretacijų [32], ir šiame skyriuje apžvelgiamos daugiausiai mokslinėje literatūroje minėtos bei validuotos sistemos. Vienkartinio naudojimo ant kramtomojo raumens klijuojamas bruksizmo testas „BiteStrip“ (*Scientific Laboratory Products, Ltd.*, Tel Avivas, Izraelis) [33] cheminiu indikatoriumi parodo bruksizmo sutrikimo lygį 0–3 skalėje. „Bruxoff“ (*Spes Medica*, Genuja, Italija) [35] yra brangesnis ir sudėtingesnis prietaisas; jame naudojama ne tik EMG, bet ir elektrokardiografija (EKG). Prietaisas paremtas teorija, jog bruksizmą sąlygoja smegenų kamieno sužadinimas, kuris taip pat padidina širdies ritmą [36]. Sprendimai priimami dirbtiniame neuroniniame tinkle (DNT). Šaltinyje [37] teigiama, jog prietaiso validavimo metu buvo pasiekta 1 % klasifikavimo paklaida, skirstant tiriamuosius tarp sveikų žmonių ir nuo bruksizmo kenčiančių pacientų. Svarbu paminėti EMG paremtų prietaisų galimybę bioatsaku daryti įtaką paciento elgsenai ir mažinti tiesioginę bruksizmo žalą. „Grindcare“ (*Medotech*, Kopenhaga, Danija) yra ant smilkininio raumens klijuojamas EMG prietaisas, kuris silpno elektrinio šoko bioatsaku skatina pacientą nutraukti žalingus veiksmus. Šio prietaiso bandomojoje studijoje [38] teigiama, jog fiksuoti palengvėję tiriamųjų simptomai. Apibendrinant, EMG metodai yra tinkami bruksizmo faktui užfiksuoti; tačiau jie netiesioginiai ir nefiksuoja informacijos, gydytojams reikalingos išsamesnei ir tikslesnei sutrikimo diagnostikai, taip pat gydymo ar restauracijų pritaikymo paciento būklei koreguoti. Šių prietaisų pagrindiniai trūkumai yra jautrumas triukšmams ir judesio artefaktams, kylantys iš mažos signalo amplitudės ir odos varžos variacijų [14].

Auksinis standartas bruksizmo diagnostikoje yra polisomnografija (PSG) su garso ir vaizdo (AV) įrašais [3]. Tai yra multisensorinis metodas, taikomas miego tyrimams; jo metu dažniausiai registruojama elektroencefalograma (EEG), EMG, EKG ir fotopletizmograma (FPG). Nors PSG taip pat nesuteikia tiesioginės informacijos apie žandikaulio judėjimą, iki šiol tai yra pats patikimiausias ir išsamiausias metodas bruksizmo diagnostikai. Tiriant tokiu būdu reikalinga vienos nakties hospitalizacija, todėl laiko ir kitų išteklių sąnaudos riboja platų ir dažną jo taikymą.

Klinikiniai žandikaulio judesių registratoriai yra visai kitos rūšies technologijos nei minėtosios. Jie gali užregistruoti žandikaulio judesio trajektorijas įvairių veiksmų metu, padeda gydytojams atpažinti patologinius žandikaulio funkcijos atvejus, gali būti naudojami dantų restauracijų gamyboje bei ortognatinėje chirurgijoje prieš ir po operacijos. Šie prietaisai yra brangūs, tikslūs ir dažniausiai kokybiški. Optinis „KaVo Arcus Digma“ (*KaVo Kerr, Brea*, Kalifornijos valstija, JAV) [39] skelbia 0,05 mm pozicijos nustatymo tikslumą okliuzinėje zonoje. Optinis „ModJaw“ (*ModJaw*, Lionas, Prancūzija) platintojų puslapyje skelbia 150 µm tikslumą. Magnetinis „JT-3D“ (*BioResearch Associates Inc.*, Milvokis, Viskonsino valstija, JAV) [41] skelbia 1,5 µm tikslumą diapazone, neviršijančiame ±10 mm spindulio nuo okliuzijos. Magnetinis „K7x“ (*Myotronics*, Kentas, Vašingtono valstija, JAV) [42] skelbia 0,5 mm tikslumą vertikaliąja ir 0,7 mm šonine kryptimis, 0 mm × 10 mm × 8 mm darbinėje erdvėje. Aukščiausioje lentynoje yra kūginio

spindulio kompiuterinės tomografijos mašina „Planmeca 4D Jaw Motion“ (*Planmeca*, Helsinkis, Suomija) [43], gebanti įrašyti kaulinio audinio judesius ir išmatuoti jų parametrus prie dantų tvirtinamų optinių žymiklių dėka. Kaip ir minėta, šie įrenginiai labai tikslūs ir efektyvūs vertinant žandikaulio kinematiką ir sąnario judesius. Vis dėlto tai yra griežtai klinikiniai metodai. Dideli įtaisai turi būti tvirtinami ant paciento galvos ir žandikaulio; o tai kelia diskomfortą, riboja judesius ir leidžia tik mažos trukmės tyrimus.

Reziumuojant, yra pakankamai būdų aptikti bruksizmui tęstinio tyrimo metu, taip pat pakankamai būdų žandikaulio judesiams bei jų ypatumams preciziškai registruoti klinikinėje aplinkoje. Visgi nėra tarpinio sprendimo, leidžiančio, nors ir prastesniu tikslumu, tačiau tęstinai sekti žandikaulio judesio trajektorijas. Tai ganėtinai keista, nes abi sferos sulaukia pakankamai mokslininkų susidomėjimo bei finansavimo, ir minėto sprendimo poreikis didėja dėl augančio bruksizmo problemą turinčių pacientų skaičiaus. Vieno iš žymiausių bruksizmo parafunkcijos tyrėjų D. Manfredini teigimu, kol kas nė vienas iš esamų metodų negali pakeisti PSG atliekant bruksizmo diagnostiką [44]. Apžvelgus esamus sprendimus galima kelti hipotezę, kad siekiant sukurti pranašesnį metodą nei esami ir galintį pakeisti PSG bruksizmo diagnostikoje, jis turėtų atitikti šias sąlygas:

- prietaisas turėtų turėti galimybę veikti tęstinai visą naktį;
- neturi būti uždengiamas okliuzinis paviršius;
- metodas turėtų būti tinkamas taikyti dėvimame prietaise, leidžiančiame pacientui atlikti bazines oralines funkcijas, įskaitant parafunkcijas;
- prietaisas turėtų būti atsparus drėgmei ir judesio artefaktams.

Saugu teigti, kad šiuo metu prieinami metodai neatitinka minėtų kriterijų, ir kad turėtų būti imamasi visiškai kitokio sprendimo. Ankstyvose šio tyrimo stadijose buvo teoriškai ir praktiškai ištirtos įvairių sprendimų galimybės. Teoriškai ir praktiškai įvertinti ultragarsiniai, inerciniai ir magnetiniai jutikliai. Iškelta hipotezė, jog nuolatinio magneto pozicijos sekimo sistema galėtų atitikti minėtus kriterijus, o inerciniai jutikliai galėtų suteikti papildomos informacijos. Tai yra vienintelis iš tirtų sprendimų, turintis perspektyvą nustatyti erdvinę žandikaulio padėtį be elektrinio kontakto tarp viršutinio ir apatinio žandikaulių.

2. NUOLATINIO MAGNETO LOKALIZACIJOS METODŲ KLINIKINIUOSE TAIKYMUOSE APŽVALGA

2.1. Nuolatinio magneto lokalizacijos principai

Magnetinė lokalizacija gali būti skirstoma į du esminius žingsnius. Pirmasis yra magnetinio lauko nustatymas dominančiame taške ar dominančiuose taškuose, kuris savo ruožtu susideda iš sekamo magnetinio objekto magnetinio lauko ir aplinkos magnetinio lauko. Biomedicininėse aplikacijose matavimai dažniausiai atliekami triašiais mikroelektromechaninių sistemų (MEMS) jutikliais, tačiau didesni, aukštesnių darbinių rėžių magnetometrai taip pat gali būti naudojami.

Nuolatinio magneto pozicijos sprendimas gali būti tiesinis [45], netiesinis [46], [47], arba kombinuotas. Trečiuoju atveju mažiau tikslus, bet patikimesnis metodas taikomas rasti preliminariai vietai; o tikslesnis, bet mažiau atsparus klaidoms metodas taikomas rasti galutiniam sprendiniui. Pavyzdžiui, tiesinis lygčių sprendimas gali būti taikomas rasti preliminariai pozicijai, kuri vėliau taikoma kaip pradinio spėjimo vertė mažiausiųjų kvadratų (MK) optimizavimo algoritmui [48]. Taip pat dalelių spiečiaus optimizacijos (DSO) algoritmas gali būti naudojamas rasti MK algoritmo pradinio spėjimo vertei [49]. Jutiklio pozicija irgigalėtų būti nustatyta panaudojant dirbtinius neuroninius tinklus (DNT), apmokytus baigtinių elementų modelyje (BEM) susimuliuotais duomenimis. Tačiau nėra aišku, kokiu tikslumu; ypač iš foniniu magnetiniu lauku (FML) užterštų duomenų.

2.2. Metodai, taikyti medicininėse aplikacijose

Magnetinė lokalizacija jau seniai taikoma medicininėms ir industrinėms pozicijos nustatymo problemoms spręsti. Vis dėlto, atsiradus tiksliems, mažų išmatavimų, Holo jutikliais paremtiems triašiams magnetometrams, šios srities galimybės gerokai išsiplėtė. Didėjant MEMS magnetometrų pajėgumui, auga ir naujų tyrimų bei publikacijų skaičius, susijęs su magnetine lokalizacija.

Ko gero, plačiausiai tyrinėjamas nuolatinio magneto lokalizacijos taikymas medicinoje yra medicininio instrumento pozicijos kūne sekimas. Pavyzdžiui, endoskopinė kapsulė yra labai patogus būdas virškinamojo trakto sistemai tirti, praryjant piliulėje integruotą kamerą. Tokiu atveju dažniausiai naudojama didelė magnetinių jutiklių matrica. Tyrėjų komanda iš Šendženo Kinijoje naujausiuose tyrimuose pademonstravo 1,8 mm tikslumą [49], [51], [52] su matrica, apsupančia tiriamojo instrumento korpusą. Kita komanda konceptą patvirtinančioje publikacijoje paskelbė pasiekę 2,65 mm vidutinę lokalizacijos paklaidą [53]. Jų sistemai reikalingi mažiausiai trys jutikliai, o pozicijai nustatyti taikoma trianguliacija. Daugiau informacijos šia tema, galima rasti išsamioje magnetinės endoskopinių kapsulių lokalizacijos sprendimų apžvalgoje; ji pateikta [54] publikacijoje. Šiuo atveju svarbu atkreipti dėmesį, kad nėra teisinga lyginti pozicijos nustatymo paklaidas dirbant su metodais, turinčiais skirtingo dydžio darbinę erdvę ir naudojant skirtingą skaičių jutiklių. Todėl svarbu gerai įvertinti ir pačius pozicijos

nustatymo algoritmus, iš kurių siekiant išrinkti geriausią gali tekti atlikti bandymus su vienodais duomenimis.

Šiuo metu aktyvi tyrėjų komanda iš Italijos kuria sistemą akies judesiams sekti [55] (2.1 pav.), kurią sudaro kontaktinis lęšis su integruotu nuolatiniu magnetu ir akinius primenantis rėmas aplink akį, su dviem paraleliais lygiais išdėstytais aštuoniais triašiais magnetometrais. Pozicijai nustatyti taikytas Levenbergo ir Marquardto optimizavimo algoritmas. Pasiektas tikslumas nėra prieinamas dėl tyrimo specifikos ir atraminio metodo nebuvimo, tačiau autoriai teigia pasiekę submilimetrinį akies sekimą, taip pat demonstruoja didelės skiriamosios gebos bandomųjų trajektorijų įrašus ir 100 Hz tikralaikį duomenų registravimo bei apdorojimo greitį.

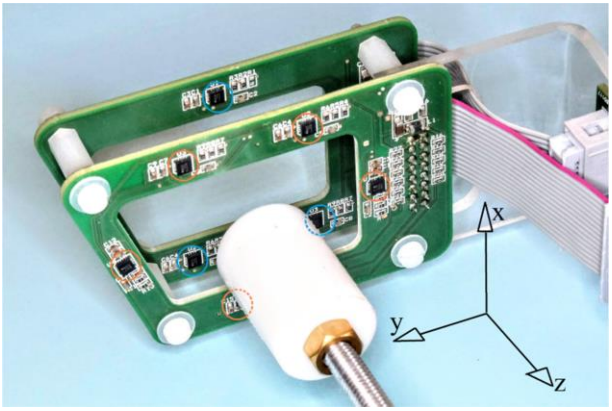

2.1 pav. Akies su magnetiniu kontaktiniu lęšiu judėjimo sekimo sistema [55]

Taip pat ganėtinai plačiai yra tyrinėjama galimybė sekti žmogaus rankos judesius. Piršto sekimo metodas, panaudojant nuolatinį magnetą ir 3–4 magnetometrus plaštakos viršuje buvo pasiūlytas [58] publikacijoje, siekiant įgyvendinti rodomojo valdiklio funkciją komunikacijai su elektroniniais įrenginiais. Lokalizacijai šiuo metodu naudojamas dalelių filtras su 500 dalelių. Pasiekta 4,8 mm pozicijos paklaida. Panašus metodas įgyvendintas rankinio rašymo registravimui su dviašiais magnetometrais [59], tačiau kiekybinis lokalizacijos įvertinimas nepateikiamas. „Finexus“ sistema [60] su aktyviais elektromagnetais trijų pirštų sekimui pasiekė 1,33 mm paklaidą. Esminis šio metodo trūkumas – elektrinis kontaktas tarp pirštų ir valdiklio – buvo išspręstas „AuraRing“ [61] sistemos atveju; šioje sistemoje yra baterija maitinama ritė, kuri nešiojama ant piršto kaip žiedas. Sistemos autoriai lokalizavimui išbandė du (MK ir DNT) metodus, ir MK pasiekė 4,4 mm pozicijos paklaidą.

2.3. Metodai lokalizacijai iš magnetinio lauko verčių

Šiame skyriuje aprašomi ir apžvelgiami algoritmai, kurie yra minimi literatūroje, kaip galimai tinkami magnetiniam pozicijos nustatymui.

Vienas žymiausių mokslininkų magnetinio lokalizavimo srityje Chao Hu 2007 m. pristatė veikiantį tiesinį algoritmą netiesinėms magnetinio lauko lygtims spręsti. Deja, siūlomam metodui reikalingi mažiausiai 6 magnetometrai, ir jis neprilygsta MK metodui tikslumu. Vis dėlto autorius rekomenduoja taikyti šį būdą tiek MK algoritmo pradinio spėjimo vertei rasti, tiek pagerinant MK algoritmo tikslumą ir atsparumą klaidoms.

Optimizavimo algoritmai sprendžia netiesines lygtis ar jų sistemas ieškodami minimumo jų paklaidos funkcijose. Yra padaromas pradinis spėjimas, įstatomas į lygtis (uždavinio funkciją) ir sprendinys palyginamas su žinomais teisingais sprendiniais (algoritmo įėjimais). Tada algoritmas keičia spėjimą paklaidos funkcijos gradiento mažėjimo kryptimi, ir iteratyviai kartoja procesą tol, kol sprendinio ir funkcijos įėjimo skirtumas (paklaida) yra minimalus. Rasta minimali reikšmė vadinama vietiniu minimumu. Ovalių, laipsniškai kintančių, tik vieną žemiausią tašką turinčių funkcijų atveju, vietinis minimumas sutampa su globaliu minimumu. Keleto lokalių minimumų problema yra kokybiško pradinio spėjimo svarbos priežastis.

Gradientas parodo greitį, kokiu kinta funkcija. Jis randamas skaičiuojant dalinę išvestinę. Gradientas yra funkcijos liestinė tiriamame funkcijos taške, kuri rodo didžiausio funkcijos augimo kryptį. Ieškant minimumo, einama prieš gradientą. Taškas, kuriame gradientas lygus 0, yra vietinio minimumo vieta. Kuo statesnė funkcija, tuo didesnis gradientas.

Svarbu paminėti Gauso ir Niutono metodą [63], kuris yra labai greitas. Jis gali būti apibūdinamas kaip iteratyvi paklaidos funkcijos šaknų aproksimacija. Kai mūsų tiriamas taškas x_k yra arti funkcijos minimumo x^*, metodas pasižymi kvadratiniu artėjimo greičiu. Deja, metodas nepasiekia minimumo, jei funkcijos gaubtumas yra neigiamas. Šios problemos galima išvengti taikant stačiausio nusileidimo algoritmą, tačiau jo greitis itin mažas.

Gradiento nusileidimo, arba stačiausio nusileidimo, algoritmas seka neigiamojo gradiento kryptį ir optimizuoja žengiamą žingsnį remdamasis gradiento statumu. Jam esant stačiam, tikimybė sutikti vietinį minimumą yra maža, todėl žingsniai gali būti didesni. Priešingu atveju žingsniai mažinami, nes tikimasi, kad algoritmas artėja prie sprendimo.

Kai funkcija turi keletą kintamųjų, ji turės ir keletą išvestinių. Dėl šios priežasties – ir keletą gradientų, po vieną kiekvienam kintamajam. MK metodu minimizuojama suma kvadratu pakeltų klaidų, taip sumažinant gradientų skaičių iki vieno. Du MK algoritmai, prieinami „Matlab Optimization Toolbox“ įrankyje, yra patikimo regiono (*Trust-Region*), tap pat Levenbergo ir Marquardto.

Patikimo regiono metodais pasirenkamas regionas aplink lokalioje imtyje geriausią tašką ir bandoma šį regioną aproksimuoti pagal kokį nors, dažniausiai kvadratinį, modelį. Tada algoritmas šoka į tariamai geriausią regiono lokaciją (remiantis aproksimuotu modeliu). Jei pastebimas žymus gradiento sumažėjimas, algoritmas laiko modelį gera realios funkcijos reprezentacija. Tokiu atveju

padidinamas kitos iteracijos regiono dydis. Neigiamo funkcijos gaubtumo atveju algoritmas paprasčiausiai atlieka didelį žingsnį į galimai geresnį regioną [65].

Levenbergo-Marquardto algoritmas adaptyviai keičia tai, kokiu metodu yra atnaujinami parametrai. Esant toli nuo minimumo, jis elgiasi panašiai lyg gradiento nusileidimo metodas ir panėšėja į Gauso ir Niutono metodą artėjant prie optimalių parametrų verčių [66]. Neigiamo funkcijos gaubtumo atveju Levenbergo ir Marquardto algoritmas yra lėtesnis nei patikimo regiono metodai.

Dalelių spiečiaus optimizacija (DSO) yra įdomus metodas, paremtas kolektyviniu didelių gyvūnų grupių elgesiu. Nors dalelių teorija ir anksčiau tyrinėjo žuvų tuntus bei paukščių pulkus, taip pat buvo mėginta jų elgesį simuliuoti matematiškai [67], dalelių spiečiaus metodologijos taikymas netiesinių funkcijų optimizavimui buvo pristatytas 1995 m. Kennedy ir Eberharto [68]. Šis algoritmas nepriklauso nuo funkcijos gradiento, ir tai jam leidžia spręsti nediferencijuojamus uždavinius. Antra vertus, DSO negarantuoja, jog optimalus sprendimas bus rastas. Algoritmas remiasi keletu paprastų lygčių bei bazinių matematinių operacijų ir naudoja mažai parametrų. Populiacijos, imituojančios gyvūnų grupę, nariai vadinami dalelėmis, o visa grupė – spiečiumi. Algoritmas inicializuojamas sukuriant grupę atsitiktinių dalelių, kurių kiekviena yra galimas uždavinio funkcijos sprendimas. Norint įvertinti, ar dalelės pozicija gera, sprendžiama tinkamumo funkcija, kuri iš esmės yra ta pati uždavinio funkcija kaip MK algoritmuose. Kiekviena dalelė pamena geriausią savo poziciją, geriausią visos grupės poziciją, savo poziciją ir greičio vektorių. Kiekvienos iteracijos metu kintamieji atnaujinami sprendžiant dvi paprastas greičio bei pozicijos lygtis ir tikrinant naujas pozicijas uždavinio funkcija. Lygtyse dar figūruoja inercijos koeficientas, atsitiktiniai skaičiai siekiant įnešti šiek tiek netvarkos (taip neleidžiant sistemai per greit nusistovėti) ir pagreičio koeficientai, nustatantys įnešamos netvarkos kiekį.

Dirbtiniai neuroniniai tinklai (DNT) yra kompiuterijos metodas, įkvėptas biologinių neuroninių tinklų smegenyse. Jie anotuotais duomenimis apmokomi atpažinti dėsningumus tuose duomenyse, apmokymo metu išvystant neuroninius takus programiškai sukurtame neuroninių ląstelių tinkle. Apmokytas DNT geba apdoroti ir kategorizuoti kitus, nematytus tokio paties tipo duomenis. Gali būti begalė įmanomų DNT konfigūracijų, tačiau esminės taisyklės ir dėsningumai tinka jiems visiems. Dirbtinius neuronus sujungiančios jungtys turi skaitinį daugiklį, vadinamą svoriu, kuris reprezentuoja to įėjimo svarbą. Dirbtiniai neuronai grupuojami sluoksniais. Įėjimo sluoksnis priima duomenis, ir jam reikia tiek neuronų, kiek duomenyse yra kintamųjų. Gali būti nuo 1 iki neriboto skaičiaus paslėptųjų sluoksnių, kuriuose vyksta duomenų apdorojimas formuojant aktyvinimo funkcijas neuronuose. Išėjimo sluoksnyje gaunamos tikimybės parodo, kuriai kategorijai ar vertei tikėtinai priklauso įvestieji duomenys.

Dalelių filtras (DF) [73], dar žinomas kaip nuoseklusis Monte Karlo metodas, yra tikimybinis metodas, skirtas spręsti deterministiniams uždaviniams. Jis naudingas, kai uždavinio funkcija netiesinė ar daugiakomponentė, tačiau esama galimybės patikrinti dalį jos parametrų. Labai tinka judantiems objektams

lokalizuoti. Dalelių filtro esmė – sugeneruoti daug galimų sprendimų (dalelių) galimų sprendimų erdvėje. Remiantis turimais sprendimų parametrais ir uždavinio funkcija, skaičiuojama tikimybė, kad dalelė yra sprendimas. Remiantis ta tikimybe, mažiausiai tikėtini sprendimai šalinami, o labiausiai tikėtini išsklaidomi erdvėje ir laike. Šie žingsniai kartojami, kol lokalizavimo objektui judant dėl kintančių parametrų atmetama vis daugiau dalelių. Dirbant šiuo metodu naudojamasi parametrų kitimu laike, todėl jis yra atsparesnis triukšmams ir tinkamas lokalizacijos uždaviniams su triukšmingais duomenimis spręsti.

Reziumuojant, kai dirbama apžvelgtais metodais, naudojami daugiau nei du magnetometrai magneto lokalizacijai; tačiau jų uždaviniai skiriasi nuo aprašomo šioje disertacijoje. Jiems reikalingas magneto orientacijos nustatymas ir tiriama daug didesnė darbinė erdvė. Atsisakant magneto orientacijos nustatymo, kai magnetas yra mechaniškai įtvirtintoje žmogaus žandikaulio sistemoje, metodas turėtų būti atsparesnis ir reikalauti mažiau jutiklių. Remiantis literatūros šaltiniais, MK metodai atrodo tinkamiausi magnetinio lauko lygčių sprendimui. Tiek patikimo regiono, tiek Levenbergo ir Marquardto metodai veiksmingi, tačiau patikimo regiono metodas yra greitesnis. Tiesinis metodas sudėtingas ir ne itin tikslus, tačiau gan patikimas; todėl gali būti taikomas pradiniam MK algoritmo spėjimui rasti. DSO ir DNT algoritmai taip pat turi potencialo ir turėtų būti praktiškai įvertinti.

3. METODŲ IR EKSPERIMENTŲ METODOLOGIJA

3.1. Vieno magnetometro lokalizacijos su akcelerometrine okliuzijos detekcija koncepto pagrindimas

3.1.1. Nuolatinio magneto baigtinių elementų modelis

Siekiant geriau pažinti magnetinio dipolio lauko fiziką, išbandyti metodą, įvertinti lokalizacijos algoritmus ir rasti optimalų magnetometrų išdėstymą bei nustatymus, naudotasis magnetas buvo sumodeliuotas BEM pritaikant „Comsol Multiphysics 5.1“ (*COMSOL Corporation*, Stokholmas, Švedija) programinę įrangą. Modelio ekrano vaizdas pateiktas 3.1 pav.

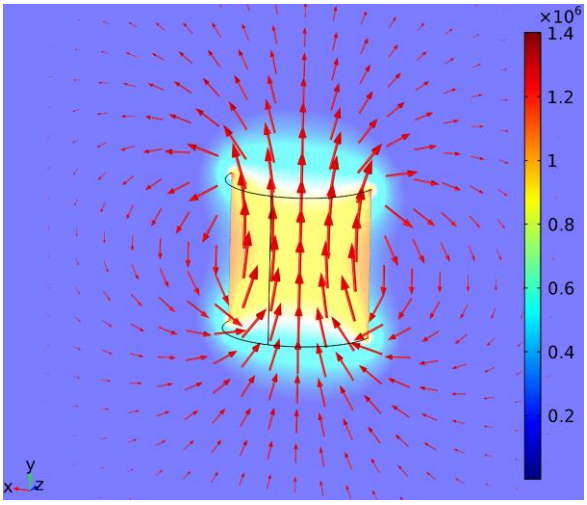

3.1 pav. Cilindrinio dipolio magnetinio lauko BEM. Spalva: magnetinio tankio norma (µT). Rodyklės (logaritminės): srauto tankis

Modeliui naudotas fizikinėmis priemonėmis valdomas itin smulkus tetraedrų tinklelis, kurio maksimalus elemento dydis – 0,401 mm, minimalus elemento dydis – 0,00401 mm, maksimalus elementų augimo spartumo koeficientas – 1,3, kreivumo faktorius – 0,2 ir siaurų regionų skiriamoji geba – 1. Visą tinklelį sudarė 2 168 866 plokštumos elementai, 36 288 ribiniai elementai ir 704 pakraščio elementai. Magnetinio lauko vertės buvo apskaičiuotos 0,1 mm žingsniu visoje (200 mm × 200 mm × 200 mm) erdvėje aplink magnetą. Prireikus imituoti FML, modeliuotieji duomenys buvo užteršti 65 µT vertikaliu magnetinio lauko vektoriumi, BMF = [0; 65; 0] µT.

3.1.2. Vieno magnetometro 3-LL lokalizacijos koncepto pagrindimas

Metodas. Nuolatinio magneto lokalizacijos konceptas paremtas magnetinio dipolio savybe, kad jo lauko vertės yra aiškiai apibrėžtos magnetinio lauko lygtimis

ir nei viename pusrutulyje, nei viename taške vertės nesikartoja [74]. Joms rasti reikalinga magneto orientacija ir jutiklio pozicija bei orientacija magneto atžvilgiu. Tai reiškia, kad įmanoma nustatyti jutiklio poziciją magneto atžvilgiu, žinant magnetinio lauko vertes. Koncepto iliustracija pavaizduota 3.2 pav. [8].

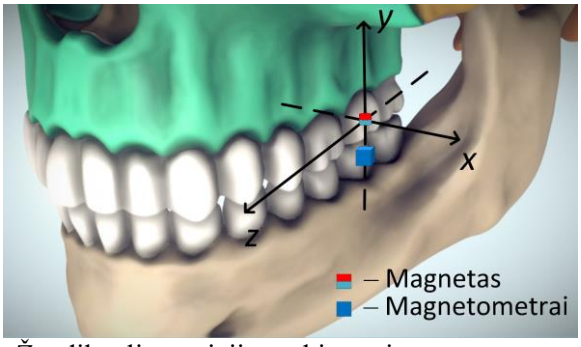

3.2 pav. Žandikaulio pozicijos sekimo vienu magnetometru konceptas ([75] publikacijos pagrindu)

Viso darbo metu naudotas cilindrinis 2 mm aukščio ir 1 mm spindulio neodimio (NdFeB) magnetas, kurio palei cilindro rotacinę ašį 1,4 T likutinis magnetizmas lėmė M_0 = 1 114 084 A/m magnetizacijos dydį.

Magnetinio (B) lauko vertė taške X randama pagal (3.1) formulę [45]:

$$B = B_T \left(\frac{3(\hat{m}_u \cdot X)X}{R^5} - \frac{\hat{m}_u}{R^3} \right) \quad (3.1);$$

$$B_T = \frac{\mu_r \mu_0 \pi r^2 L M_0}{4\pi} \quad (3.2);$$

$$X = \big((x-a),(y-b),(z-c)\big) \quad (3.3);$$

$$R = \sqrt{((x-a)^2 + (y-b)^2 + (z-c)^2)} \quad (3.4).$$

Čia $\hat{m}_u = (m; n; p)$ yra normalizuotas dipolio magnetinio momento vektorius, rodantis magneto magnetizmo orientaciją, kai (m; n; p) yra vektoriaus projekcijos, o (x; y; z) yra koordinačių ašis, atitinkamai. B_T yra konstanta, randama pagal (3.2) formulę, kurioje μ_r – santykinė terpės (oro) skvarba, $\mu_0 = 4\pi \times 10^{-7}$ (T·m/A) – magnetinė konstanta, L – magneto ilgis (m), r – magneto spindulys (m), ir M_0 – magneto magnetizacija (A/m). X yra magnetometro lokacija, randama pagal (3.3) formulę, atžvilgiu magneto lokacijos, kuri yra (a; b; c) = (0; 0; 0) ir atstoja pagrindinę koordinačių sistemą. R yra X vektoriaus tikrasis dydis, randamas pagal

(3.4) formulę [45]. Modelis gali būti išskleistas į tris atskiras lygtis kiekvienai magnetinio lauko dedamajai (3.5)–(3.7).

$$B_x = B_T\left(\frac{3[m(x-a)+n(y-b)+p(z-c)](x-a)}{R^5} - \frac{m}{R^3}\right) \quad (3.5);$$

$$B_y = B_T\left(\frac{3[m(x-a)+n(y-b)+p(z-c)](y-b)}{R^5} - \frac{n}{R^3}\right) \quad (3.6);$$

$$B_z = B_T\left(\frac{3[m(x-a)+n(y-b)+p(z-c)](z-c)}{R^5} - \frac{p}{R^3}\right) \quad (3.7).$$

Kadangi *B* verčių radimas iš šių formulių yra netiesinis uždavinys, nuspręsta taikyti MK optimizacijos patikimo regiono algoritmą. Kodas parašytas „Matlab“ (*Mathworks Inc.*, Natikas, Masačusetso valstija, JAV) aplinkoje. BEM, naudotas teoriškai patikrinti metodą, sukurtas „Comsol“ aplinkoje.

Eksperimentas. Siekiant patvirtinti magnetinės lokalizacijos konceptą, vieno magnetometro testas buvo įvykdytas tiek su teoriniais, tiek su praktiniais duomenimis. Matavimai atlikti naudojant „MPU-9250“ (*TDK InvenSense*, San Chosė, Kalifornijos valstija, JAV) inercinių matavimų sistemą (IMS). FML kompensuotas atimties metodu, matuojant atraminiu jutikliu už eksperimento ribų. Tyrimui natūrali kramtymo trajektorija buvo paimta iš [77] šaltinio. Jutiklio judėjimas valdytas „Elinta EMS-301“ (*Elintos matavimo sistemos*, Kaunas, Lietuva) trimačio (3D) pozicionavimo sistema, galinčia judėti 0,1 mm žingsniu. Eksperimento schema ir pozicionavimo sistema pavaizduotos 3.3 pav.

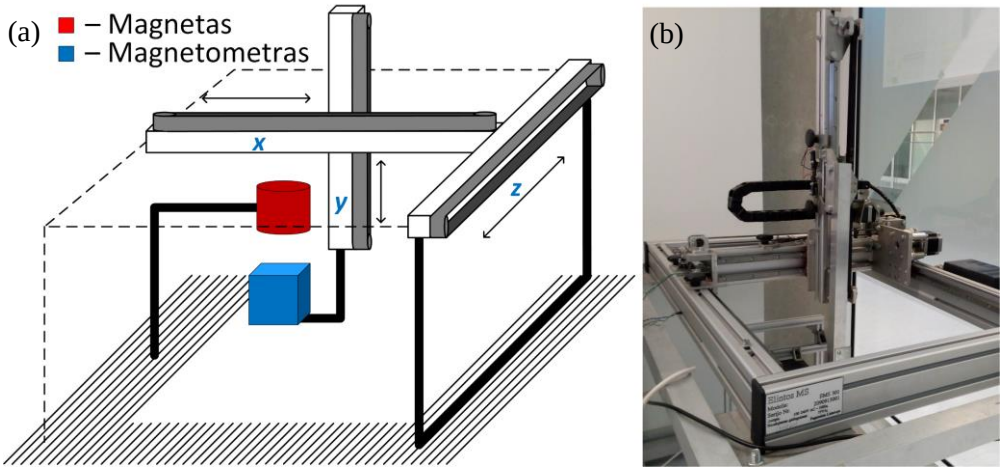

3.3 pav. Eksperimento schema (a), ir trimačio (3D) pozicionavimo sistema „EMS 301“ (b)

3.1.3. Dantų kontaktų atpažinimas akcelerometrija

Metodas. Dantų kontaktų atpažinimo iš pritvirtinto jutiklio pagreičio pokyčių metodas yra ganėtinai paprastas. Realiomis sąlygomis, ypač griežimo metu, dantys gali susitrenkti ne tik vertikaliai, bet ir protruziškai bei lateraliai. Tą įvertinus, pirmas žingsnis – apskaičiuoti pagreičio vektoriaus tikrąjį dydį. Tai daroma traukiant visų komponentų kvadratų sumos šaknį. Toliau gali būti reikalingas tolimesnis signalo apdorojimas, kaip filtravimas, kėlimas kvadratu ar diferenciacija, siekiant sustiprinti realius dantų smūgius ir slopinti kitus artefaktus. Vis dėlto šio eksperimento metu, laboratorinėmis sąlygomis, tai buvo nereikalinga, nes kiekvienas dantų kontaktas buvo aiškiai atpažįstamas. Antra vertus, buvo pastebima artikuliatoriaus variklių vibracija bei netolygus judesys, kurių klinikiniuose taikymuose neturėtų būti.

Eksperimentas. Savadarbis servo varikliu varomas vieno vyrio vertikalaus žandikaulio judesio artikuliatorius buvo pagamintas siekiant atkartoti vertikalų žandikaulio judesį su dantų kontakto (susitrenkimo) momentais. „MPU9250“ (*TDK InvenSense*, San Chosė, Kalifornijos valstija, JAV) 9-LL IMS plėtojimo plokštė buvo pritvirtinta prie judančios artikuliatoriaus dalies su cianoakrilato klijais siekiant gero mechaninio kontakto. Naudotoje IMS buvo integruotas akcelerometras, kuris panaudotas dantų kontakto atpažinimui, ir giroskopas, kuris panaudotas kaip atraminis matavimas artikuliatoriaus judesiui iliustruoti. Artikuliatorius ir eksperimento išdėstymas pateiktas 3.4 pav.

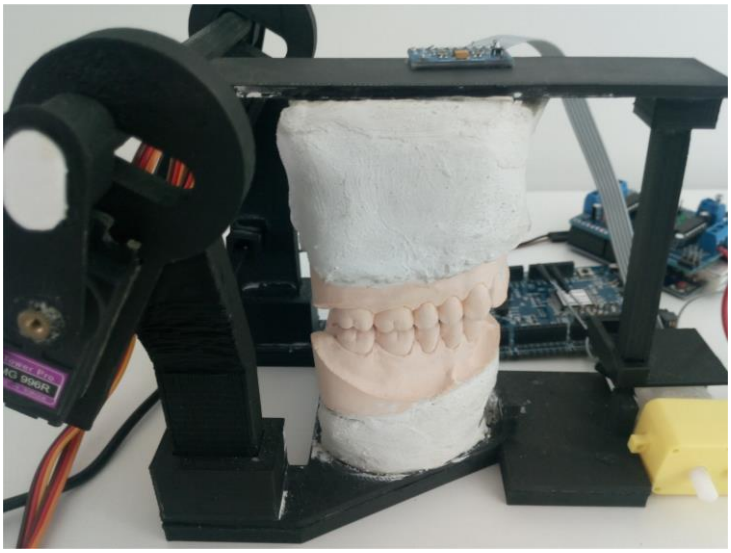

3.4 pav. Vertikalaus žandikaulio judesio artikuliatorius su pritvirtinta inercinių matavimų sistemos (IMS) plėtojimo plokšte

Eksperimento tikslas – atpažinti dantų kontaktus pakankamai gerai, kad būtų galima atskirti tarp panašių judesių su ir be kontakto. Todėl pusė judesių buvo

fiksuojama laikotarpiu, iki kol gipso dantų modeliai pasieks kontaktą, ir likusi pusė judesių nebuvo privesti iki kontakto. Judesio tipas buvo keičiamas kas tris ciklus.

3.1.4. Dinaminis 3-LL lokalizacijos tyrimas su akcelerometriniu dantų kontaktų atpažinimu

Eksperimentas. Robotinis žandikaulio judesių artikuliatorius (3.5 pav.) paremtas savadarbe Stiuarto platforma buvo pagamintas siekiant patvirtinti metodo galimybę kartu registruoti poziciją bei aptikti dantų įėjimą į okliuziją (susitrenkimą) panaudojant akcelerometriją. Dantų modelis buvo 3D atspausdintas iš poliaktido (PLA). Kaip atraminis lokalizacijos metodas buvo panaudota „3D Guidance TrakStar" (Ascension Technology Corporation, Šelburnas, VT, JAV) elektromagnetinė lokalizacijos sistema. Dėl naudojamo kintamo žemojo radijo dažnio elektromagnetinio lauko, sistema nedarė įtakos tiriamam metodui, bei tiriamas metodas neturėjo įtakos sistemos darbui.

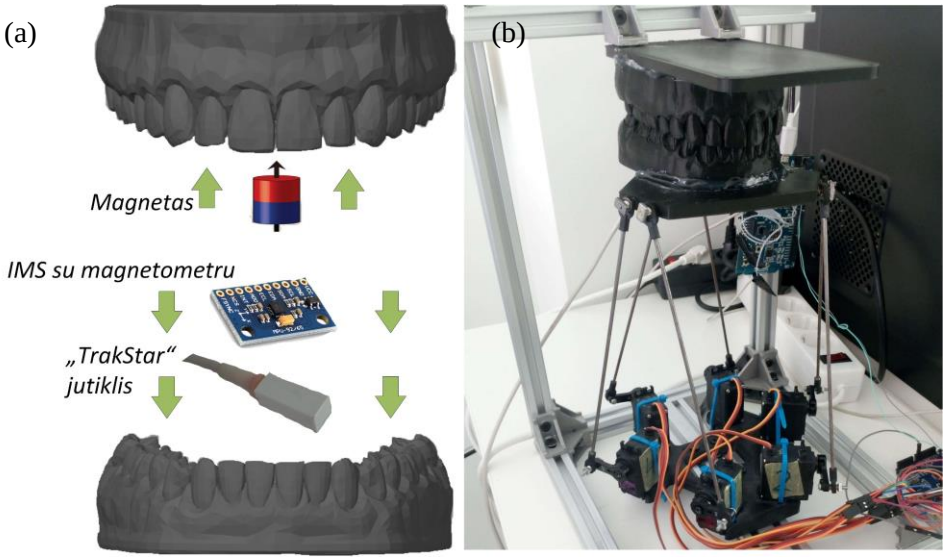

3.5 pav. Eksperimento schema dinaminiam lokalizacijos tyrimui su dinaminiu okliuzijos nustatymu (a), panaudojant Stiuarto platformą (b)

Duomenys registruoti 100 Hz dažniu. Siekiant sumažinti triukšmus ir išlyginti duomenis, panaudotas slenkamojo vidurkio filtras, kuriam eksperimentiškai buvo parinktas $N = 19$ lango dydis, siekiant pašalinti triukšmus ir suglotninti duomenis. Akcelerometrinio dantų susitrenkimo atpažinimo slenkstis pagreičiui taip pat buvo nustatytas eksperimentiškai.

3.2. Foninis magnetinis laukas

FML yra neišvengiamas visuose magnetiniuose matavimuose. Jo poveikis gali būti mažinamas pasyviai uždengiant visą eksperimento erdvę feromagnetinėmis medžiagomis, pasižyminčiomis didele magnetine skvarba [79]. Taip pat gali būti uždengiamas aktyviai, slopinant išmatuojamą lauką priešingu lauku [80] dėka magnetiniam laukui galiojančio superpozicijos principo. Paprasčiausias būdas kompensuoti FML yra atraminio matavimo metu užfiksuotos vertės atimtis. Taip pat šis laukas gali būti įvertinamas lokalizacijos optimizavimo algoritmuose, kai naudojamas daugiau nei vienas magnetometras ir yra aiškiai žinomos jų tarpusavio padėtys.

Eksperimentas. FML poveikis buvo įvertintas prieš pradedant lokalizacijos bandymus. Prie teorinių ir prie kompensuotų eksperimentinių duomenų įvairiomis kryptimis buvo pridėtas dirbtinis $B_{\mathrm{BMF}} = 65$ µT FML. Tada esant įvairiems atstumams tarp magneto ir jutiklio buvo įvertinti FML sąlygotų lokalizacijos paklaidų dydžiai. Tyrimą iliustruojanti schema pateikta 3.6 pav.

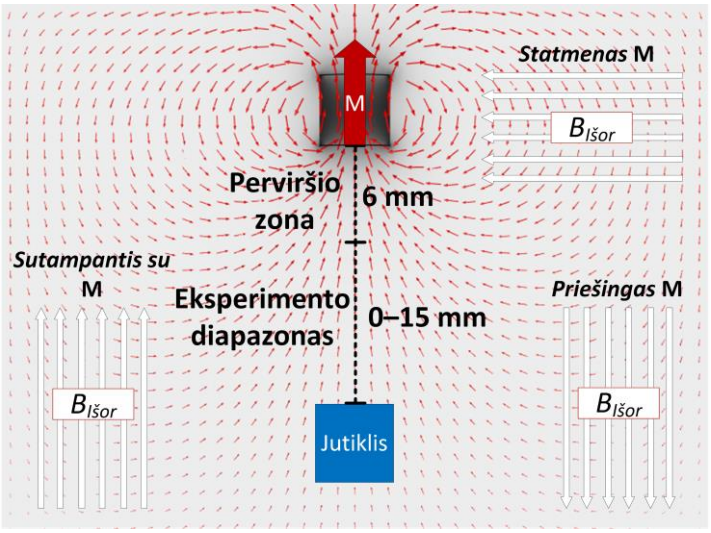

3.6 pav. Įvairiomis kryptimis simuliuoto FML esant įvairiems atstumams tarp magneto ir jutiklio sąlygotų paklaidų tyrimo schema. Tyrimas atliktas su teoriniais ir kompensuotais eksperimentiniais duomenimis

3.3. Dviejų magnetometrų metodas

3.3.1. Dviejų magnetometrų 3-LL lokalizacija su FML kompensavimu

Metodas. Žinant pastovią atraminio magneto poziciją pagrindinio magneto atžvilgiu (22 mm), galima atraminį magnetometrą laikyti magnetinio lauko viduje, įtraukti į pozicijos nustatymo lygtis ir tuo pačiu kompensuoti FML. Dviejų magnetometrų pozicijos jutiklio koncepcija iliustruojama 3.7 pav.

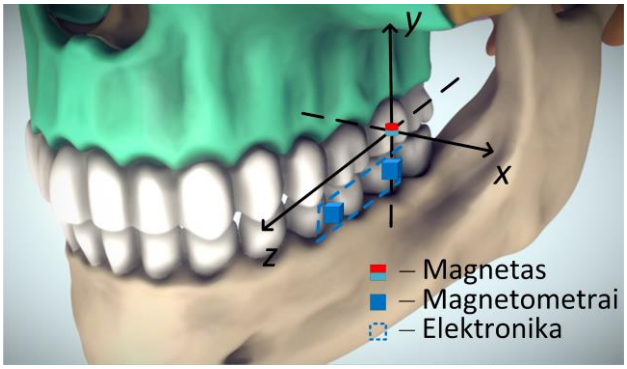

3.7 pav. Dviejų magnetometrų jutiklio koncepcijos iliustracija ([75] šaltinio pagrindu)

Pridėjus tris papildomas išmatuotas vertes (B_{refx}, B_{refy}, B_{refz}) su trimis jas apibrėžiančiomis lygtimis, gali būti nustatyti trys papildomi nežinomieji. Šiuo atveju galima spręsti tris FML komponentes (BMF_x, BMF_y, BMF_z), kartu jas kompensuojant. Lygčių sistema papildytam modeliui pateikiama toliau; joje (3.8)–(3.10) formulės yra pagrindiniam magnetometrui, (3.15)–(3.17) formulės – atraminiam, o (3.11)–(3.14) formulės apibrėžia ryšį tarp magnetometrų pozicijų.

$$B_x = B_T\left(\frac{3[m(x-a)+n(y-b)+p(z-c)](x-a)}{R^5} - \frac{m}{R^3}\right) + BMF_x \quad (3.8);$$

$$B_y = B_T\left(\frac{3[m(x_l-a)+n(y_l-b)+p(z_l-c)](y_l-b)}{R^5} - \frac{n}{R^3}\right) + BMF_y \quad (3.9);$$

$$B_z = B_T\left(\frac{3[m(x_l-a)+n(y_l-b)+p(z_l-c)](z_l-c)}{R^5} - \frac{p}{R^3}\right) + BMF_z \quad (3.10);$$

$$x_{ref} = x \quad (3.11);$$

$$y_{ref} = y \quad (3.12);$$

$$z_{ref} = z + \Delta z \quad (3.13);$$

$$R_{ref} = \sqrt{(x_{ref} - a)^2 + (y_{ref} - b)^2 + (z_{ref} - c)^2} \quad (3.14);$$

$$B_{refx} = B_T\left(\frac{3[m(x_{ref}-a)+n(y_{ref}-b)+p(z_{ref}-c)](x_{ref}-a)}{R_{ref}^5} - \frac{m}{R_{ref}^3}\right) + BMF_x \quad (3.15);$$

$$B_{refy} = B_T\left(\frac{3[m(x_{ref}-a)+n(y_{ref}-b)+p(z_{ref}-c)](y_{ref}-b)}{R_{ref}^5} - \frac{n}{R_{ref}^3}\right) + BMF_y \quad (3.16);$$

$$B_{refz} = B_T\left(\frac{3[m(x_{ref}-a)+n(y_{ref}-b)+p(z_{ref}-c)](z_{ref}-c)}{R_{ref}^5} - \frac{p}{R_{ref}^3}\right) + BMF_z \quad (3.17).$$

Čia Δz yra atstumas tarp magnetometrų (ant jutiklio plokštės) *z* ašyje. Kitose ašyse pagrindinio ir atraminio magnetometrų tarpusavio atstumai lygūs 0, tačiau prireikus gali būti pridėti.

Eksperimentas. Lokalizacijos tikslumo tyrimas, atliktas ant „Elinta“ trimačio (3D) pozicionavimo platformos ir aprašytas 3.1.2 poskyryje, buvo pakartotas dviejų magnetometrų 3-LL lokalizacijos metodui su FML kompensavimu įvertinti.

3.3.2. Žandikaulio pasisukimo kampų įvertinimas

Taikant aprašytą metoduą, pozicijos įvertinimas įmanomas tik žinant magneto ir magnetometro orientacijas erdvėje. Tai reikštų, jog dviejų magnetometrų metodu įmanoma nustatyti tik fiksuotos orientacijos objektų 3-LL tarpusavio pozicijos pokyčius. Antra vertus, jei tiriamos sistemos poslinkis ir sukimasis koreliuoja tarpusavyje, turėtų būti galima įvertinti sistemos pasisukimo kampus remiantis žinomais linijiniais poslinkiais.

Metodas. Vertikalaus sukimosi (aplink *x* ašį) kampas α_V gali būti susietas su vertikaliuoju poslinkiu Y_V pagal (3.18)–(3.20) formules, kurioms paaiškinamasis brėžinys pateiktas 3.8 pav. Tam reikalingi *L* (ilgis) ir *H* (aukštis) TMS ir jutiklio matmenys, o Y_V randamas iš jutiklio rodmenų.

$$TS_V = \sqrt{L^2 + H^2} \tag{3.18};$$

$$\beta_V = \arccos\left(\frac{L}{TS_V}\right) \tag{3.19};$$

$$\alpha_V = \arcsin\left(\frac{H+Y_V}{TS_V}\right) - \beta_V \tag{3.20}.$$

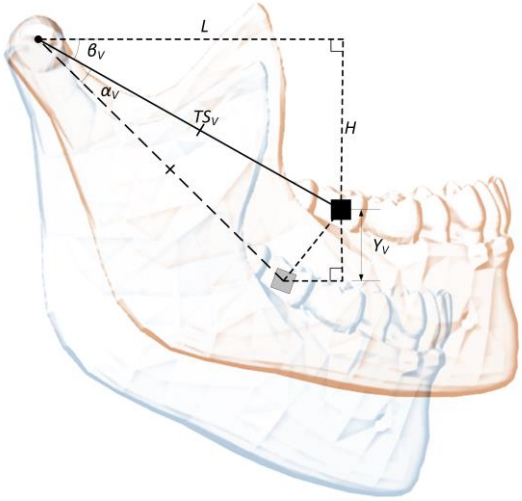

3.8 pav. Vertikalaus žandikaulio pasisukimo kampo santykis su vertikaliu linijiniu poslinkiu ([82] šaltinio pagrindu)

Susieti horizontalaus sukimosi (aplink *y* ašį) kampą α_H su horizontaliu šoniniu poslinkiu X_H yra šiek tiek sudėtingiau. Kadangi jutiklis tvirtinamas žandikaulio šone, abiem pusėms reikės skirtingų skaičiavimų, nors yra taikomos tos pačios (3.21)–(3.24) lygtys, kurioms aiškinamasis brėžinys pateiktas 3.9 pav. Tam reikalingi L (ilgis) ir W_H (plotis) TMS ir jutiklio matmenys, o X_H randamas iš jutiklio rodmenų.

$$TS_H = \sqrt{L^2 + W_H^2} \quad (3.21);$$

$$Y_H = W_H - X_H \quad (3.22);$$

$$\beta_H = \arccos\left(\frac{L}{TS_H}\right) \quad (3.23);$$

$$\alpha_H = \arcsin\left(\frac{Y_H}{TS_H}\right) - \beta_H \quad (3.24).$$

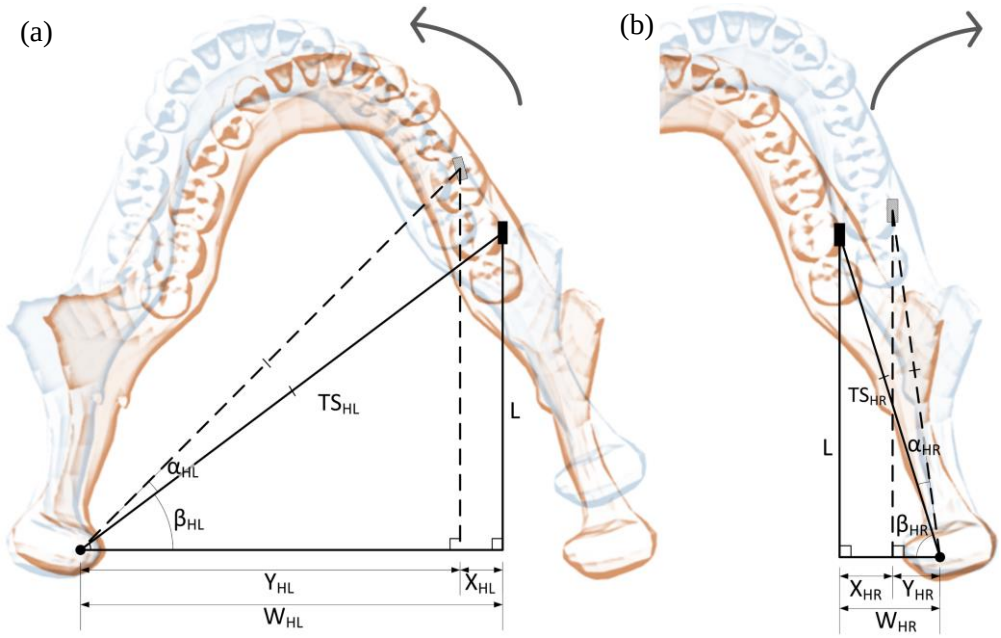

3.9 pav. Horizontalaus žandikaulio pasisukimo kampo santykis su kairiuoju (a) ir dešiniuoju (b) horizontaliu (šoniniu) linijiniu poslinkiu ([82] šaltinio pagrindu)

Esant aplink pagrindinį magnetometrą centruotos jutiklio koordinačių sistemos posūkiui, būtina iš naujo įvertinti atraminio magnetometro poziciją erdvėje. Jutikliui nesisukant, išliktų pastovus 22 mm atstumas *z* ašyje (kaip išdėstyta jutiklio plokštėje) ir 0 mm poslinkiai *x* bei *y* ašyse. Tačiau įvykus pasisukimui, tarpusavio atstumo projekcijos *z* ašyje trumpėja, o projekcijos *x* ir *y* ašyse ilgėja. Sukimasis aplink dvi ašis lemia linijinį poslinkį visose trijose ašyse. Šis ryšys yra apibrėžiamas

(3.25)–(3.28) lygtimis, įvertinant, jog žandikaulio posūkio kampai yra žymiai mažesni nei 90°:

$$y_{ref} = y + (\Delta z \cdot \sin(\alpha_V)) \quad (3.25);$$

$$\Delta z_y = \Delta z \cdot \cos(\alpha_V) \quad (3.26);$$

$$x_{ref} = x + (\Delta z_y \cdot \sin(\alpha_H)) \quad (3.27);$$

$$z_{ref} = \Delta z_y \cdot \cos(\alpha_H) \quad (3.28).$$

Vertėtų atkreipti dėmesį, jog remiantis kaukolės koordinačių sistema, pavaizduota 3.7 pav., vienintelis įmanomas vertikalus žandikaulio poslinkis yra neigiamasis. Todėl neigiamieji poslinkiai yra siejami su neigamaisiais posūkio kampais. Tas pats galioja visoms ašims.

Šis metodas buvo įgyvendintas praktiškai, poslinkio ir posūkio priklausomybės lygtis pridėjus į taikyto optimizavimo algoritmo užduoties lygčių sistemą. Kiekvienoje optimizavimo algoritmo iteracijoje algoritmo sprendiniai pasitelkus rotacines matricas buvo pasukti pagal šiame skyriuje aprašytas lygtis, ir užduoties funkcija sprendžiama su apskaičiuotais kampais. Tik tada buvo skaičiuojama paklaida, taip konverguojant į sprendimą su pasisukimu.

Eksperimentas. Įrodant pasiūlytų lygčių validumą, buvo panaudota „TrakStar“ trimatės (3D) lokalizacijos sistema. Jutiklis buvo pritvirtintas prie savanorio žandikaulio, kuris buvo judinamas siekiant padengti kuo daugiau galimų žandikaulio pozicijų. Galva buvo tvirtai imobilizuota ant medicininio gulto. Tyrimo metu užregistruotas debesis atsitiktinių 6-LL žandikaulio pozicijų, kurios pavaizduotos 3.10 pav. Šie duomenys atspindi poslinkio ir sukimosi priklausomybę per visą žandikaulio išsižiojimo amplitudę, visomis pasisukimo kryptimis. Pasisukimo kryptys pavaizduotos atitinkamomis rodyklių kryptimis.

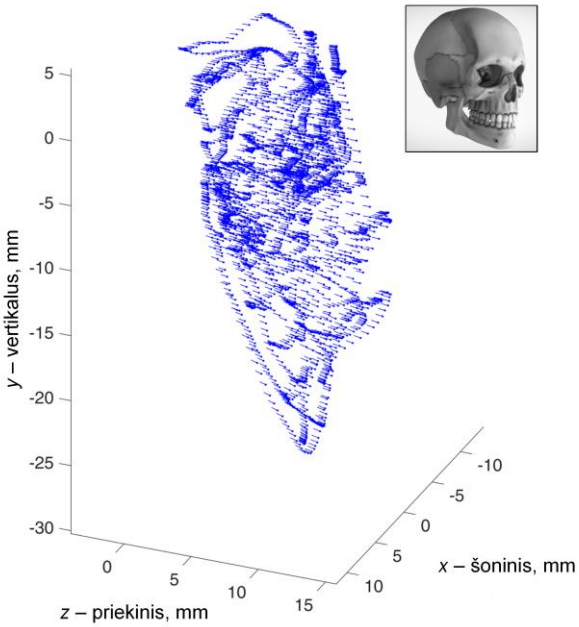

3.10 pav. Debesis atraminiu metodu užregistruotų 6-LL žandikaulio pozicijų su pasisukimo kampais, pavaizduotais juos atitinkančiomis rodyklių kryptimis. Kaukolės atvaizdas [11] pateiktas tiriamojo galvos orientacijai iliustruoti

Su šiais duomenimis buvo palygintos pasiūlytomis lygtimis apskaičiuotos poslinkio ir posūkio priklausomybės, taip įvertinant jų validumą.

3.4. Dviejų magnetometrų jutiklio prototipas

3.4.1. Laidinis jutiklio prototipas

Mažų matmenų (26,3 × 5,5 × 2) mm, mažų energijos sąnaudų jutiklio prototipas buvo sukurtas pasiūlytam metodui patvirtinti. Jo nuotrauka pateikta 3.11 pav.

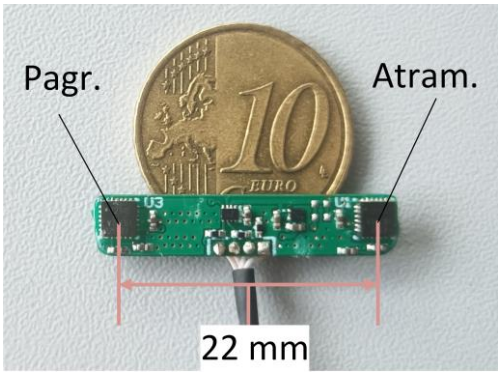

3.11 pav. Dviejų magnetometrų jutiklio laidinis prototipas

Jį sudaro dvi „ICM-20948“ (*TDK InvenSense*, San Chosė, Kalifornijos valstija, JAV) IMS, turinčios triašius magnetometrus, akcelerometrus ir giroskopus. Atstumas tarp IMS centrų buvo 22 mm. Taip pat buvo panaudotas „LDLN025“ (*STMicroelectronics*, Ženeva, Šveicarija) mažo triukšmo įtampos reguliatorius, „LSF0102“ (*Texas Instruments*, Dalasas, Teksaso valstija, JAV) dvikryptis loginės įtampos lygio keitiklis ir pasyvūs pagalbiniai komponentai. Komunikacijai su „nRF52832“ (*Nordic Semiconductor*, Oslas, Norvegija) mikrovaldikliu naudotas „I2C“ komunikacijos protokolas. Naudojant šį prototipą atlikta daugelis šioje disertacijoje aprašytų tyrimų. Jutiklio maksimalus duomenų registravimo greitis – 100 Hz.Belaidis jutiklio prototipas

Galutinė dviejų magnetometrų jutiklio prototipo versija buvo paremta „LSM303AGR“ (*STMicroelectronics*, Ženeva, Šveicarija) 6-LL IMS, turinčiomis triašius magnetometrus. Prototipo matmenys buvo (26 × 6.5 × 2) mm. Belaidis veikimas buvo įgalintas (8,5 × 3,25 × 0.85) mm „EYSHSN“ (*Tayo Yuden*, Tokijas, Japonija) valdymo ir komunikacijos modulio, turinčio integruotą „nRF52832“ mikrovaldiklį bei „Bluetooth“ anteną. Galutinio belaidžio prototipo nuotrauka pateikta 3.12 pav.

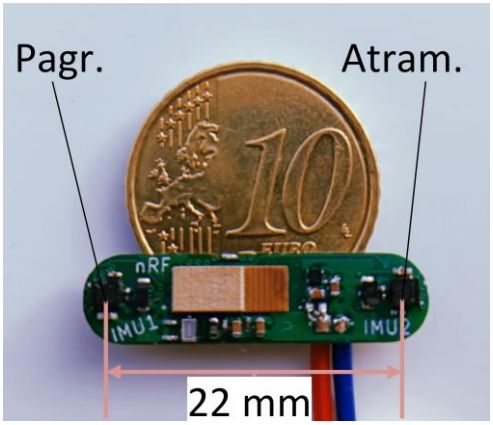

3.12 pav. Belaidžio dviejų magnetometrų jutiklio prototipas

Pagamintas jutiklio prototipo dydžio, 3,1 V, 64 mAh baterijų paketas iš keturių 1,55 V, 16 mAh sidabro oksido baterijų „379 SR521SW“ (*Renata SA*, Itingenas, Šveicarija). Su jutiklio 15 mAh vidutinėmis energijos sąnaudomis toks baterijų paketas galėtų maitinti jutiklį nuo 4 iki 5 h. Pagaminto baterijų paketo nuotrauka pateikta 3.13 pav.

3.13 pav. Pagamintas 3,1 V, 64 mAh baterijų paketas

3.4.2. Jutiklio tvirtinimo sprendimas

Esminė jutiklio, baterijos ir magneto tvirtinimo ant žandikaulio sąlyga buvo palikti atidengtą okliuzinį paviršių. Du galimi sprendimo variantai buvo tiesioginis komponentų klijavimas panaudojant „Panavia™V5“ (*Kuraray Noritake Dental Inc.*, Okajama, Japonija) plombą arba okliuzinio paviršiaus neuždengiančios kapos. Specialios dantų kapos savanorio viršutiniam ir apatiniam žandikauliams buvo sukurtos ir išfrezuotos privačioje laboratorijoje (*Dental 3D,* Vilnius, Lietuva) šio tyrimo partnerės (*Investigo*, Kaunas, Lietuva) užsakymu. Gamybai buvo pasirinkta „Zirilux Acetal“ (*Henry Schein Inc.*, Melvilis, Niujorko valstija, JAV) medžiaga, komponentų inkapsuliavimo dėžutes frezuojant kaip atskirus vienetus.

Nuolatinio magneto laikiklis buvo pritvirtintas prie viršutinio žandikaulio kapos (3.14(a) pav.), o inkapsuliuoti jutiklis ir baterija pritvirtinti prie apatinio žandikaulio kapos (3.14(b) pav.).

3.14 pav. Okliuzinio paviršiaus neuždengiančios kapos nuolatinio magneto tvirtinimui prie viršutinio žandikaulio (a) ir inkapsuliuotų jutiklio bei baterijos tvirtinimui prie apatinio žandikaulio (b)

Buvo nutarta, jog savanorio atveju nėra įmanoma pasiekti okliuziją su dvejomis okliuzinio paviršiaus neuždengiančiomis kapomis, todėl pasirinkta taikyti kombinuotą sprendimą – nuolatinį magnetą tvirtinti tiesiogiai prie danties panaudojant laikiną plombą, o jutiklį ir bateriją pritvirtinti prie okliuzinio paviršiaus neuždengiančios kapos. Intraoraliai įgyvendintos sistemos nuotrauka pateikta 3.5.4 poskyrio 3.21 pav.

3.4.3. Jutiklio kalibravimas

Ši procedūra turi būti atliekama prieš ir po eksperimentų siekiant didelio tikslumo matavimų dėl Holo jutikliuose stipriai pasireiškiančio nulinio lygio dreifo, ypač veikiant stipriam išoriniam magnetiniam laukui.

Eksperimentų metu jutiklis buvo kalibruojamas sukiojant jį įvairiomis kryptimis, taip iš kiekvieno magnetometro užregistruotų FML verčių sudarant sferą. Norint sukalibruoti jutiklį, prie duomenų pridedant kompensacines vertes sferos sucentruojamos ir taip tarpusavyje sulygiuojamos. FML verčių sferos prieš ir po kalibravimo pateiktos 3.15 pav.

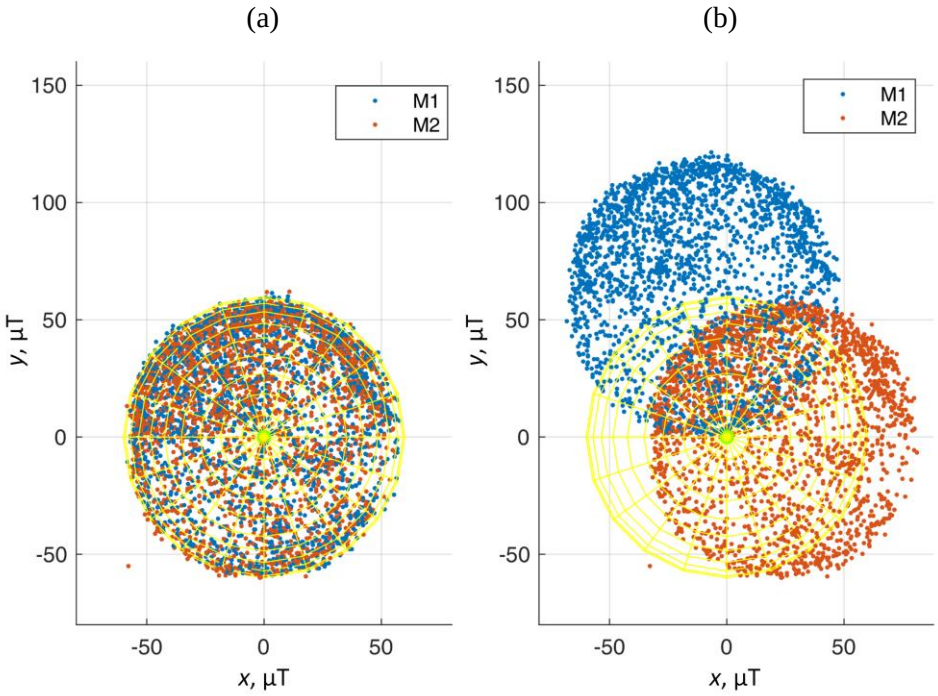

3.15 pav. FML verčių sferos prieš kalibravimą (a) ir po kalibravimo (b)

3.5. Galutinis sistemos patikrinimas

Siekiant preciziškai keisti jutiklio poziciją, naudota „IRB120-3/0.6“ (*ABB*, Ciurichas, Šveicarija) robotinė ranka. Roboto nuotrauka pateikta 3.16 pav.

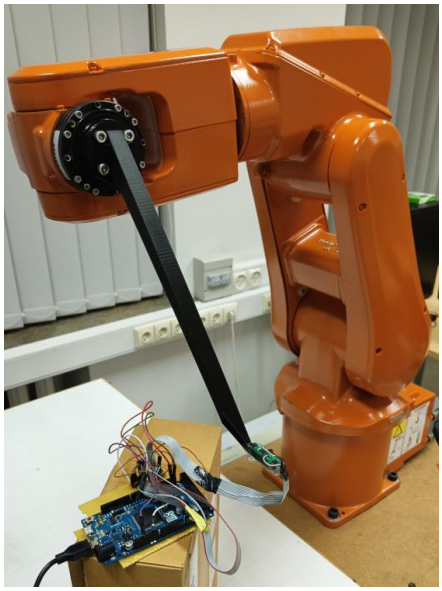

3.16 pav. Robotinė ranka su trimačiu (3D) spausdintu jutiklio tvirtinimo įrankiu ir jutikliu

Robotas programuotas „RobotStudio“ (*ABB*, Ciurichas, Šveicarija) programine įranga. Robotinės sistemos specifikacijoje nurodomas 0,01 mm linijinis ir 0,01° kampinis atsikartojamumas. Pagrindinis šio tyrimo iššūkis – nuolatiniai magnetai ir elektromagnetai roboto varikliuose, kurie gali daryti įtaką tiriamojo magnetinio metodo matavimams. Kadangi pasiūlytu metodu galima kompensuoti homogenišką natūralų FML, nuspręsta atitraukti jutiklį nuo roboto maksimaliu įmanomu atstumu panaudojant trimatį (3D) spausdintą tvirtinimo įrankį, taip sumažinant roboto magnetinio lauko skirtumus tarp greta esančių magnetometrų ir padarant jį homogeniškesnį. Tokiu būdu buvo sėkmingai kompensuojamas ir natūralus, ir roboto generuojamas išoriniai laukai, tačiau tai šiek tiek išaugino neapibrėžtis dėl minimalių įrankio vibracijų ir svyravimų. Galutinis 5-LL eksperimentas susidarė iš trijų etapų.

- Visos darbinės erdvės tyrimas su teoriniais ir eksperimentiškai užregistruotais duomenimis. Kiekvienas matavimas pakartotas 10 kartų.
- Statiškas diskretusis 5-LL lokalizacijos tyrimas, atliktas su visiškais sustojimais ir 20 matuotų verčių vidurkiu kiekviename trajektorijos taške. Kiekvienas matavimas pakartotas 10 kartų.

- Dinaminis 5-LL lokalizacijos tyrimas, atliktas tęstinai registruojant duomenis 100 Hz surinkimo dažniu, robotinei rankai maksimaliu greičiu judinant jutiklį bandomąja trajektorija.

3.5.1. Visos darbinės erdvės tyrimas

Eksperimentas. Jutiklio tikslumas yra labai priklausomas nuo atstumo iki magneto. Dėl kubiniu dėsniu kintančio magnetinio lauko FML dedamosios procentinė dalis signale sparčiai didėja jutikliui tolstant nuo magneto. Tai reiškia, jog matavimo tikslumas ir atsparumas priklauso nuo atstumo iki magneto. Tikslumo priklausomybei nuo magneto atstumo įvertinti atliktas nuoseklus visos darbinės erdvės matavimas, ją padalijant pagal atstumą (spindulį) nuo magneto. Kas 1 mm ištirta 15 skirtingų sričių ties skirtingais radialiniais atstumais (nuo $R = 6$ mm iki $R = 20$ mm) nuo magneto, kiekvieną matavimą atliekant atskirus 10 kartų. 1.17 pav. iliustruojama, kaip jutiklio darbinė erdvė buvo padalyta į skirtingo atstumo zonas.

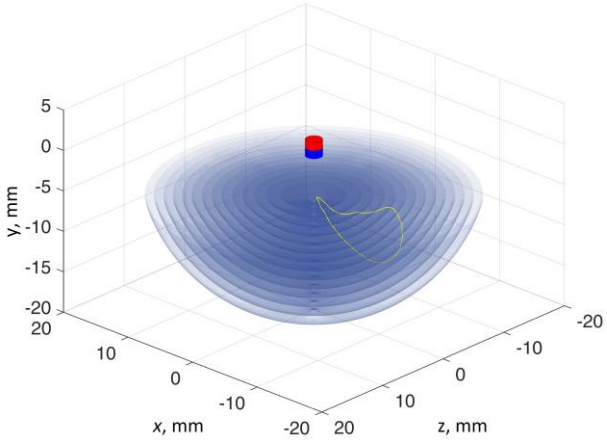

3.17 pav. Darbinė erdvė, padalyta į skirtingų atstumų (iki magneto) zonas. Kitiems bandymams taikyta bandomoji kramtymo kreivė pateikta dėl mastelio palyginimo

Eksperimentas atliktas su BEM susimuliuotais teoriniais duomenimis, užterštais 65 µT FML, ir su eksperimentiškai užregistruotais duomenimis su natūraliu FML. Eksperimentas parodė dešimties matavimų vidutinės kvadratinės paklaidos (VKP) vidurkį ir standartinį nuokrypį (std).

3.5.2. 5-LL lokalizacijos tyrimai

Eksperimentas. 3-LL bandomoji kramtymo trajektorija buvo išplėsta iki 5-LL panaudojant žandikaulio poslinkio ir posūkio priklausomybės lygtis (18)–(24), aprašytas 3.3.2 poskyryje. „RobotStudio“ programine įranga suprogramuota bandomoji kreivė pateikta 3.18 pav. Raudona, žalia ir mėlyna linijos atitinkamai parodo kiekvieno trajektorijos taško orientaciją kaip *x*, *y*, ir *z* projekcijas. Bandomoji

trajektorija atkartota iš [77] šaltinio. Duomenys registruoti 100 Hz surinkimo dažniu. Statiniam tyrimui matavimai buvo diskretieji, matavimo metu robotinei rankai sustojant kiekviename taške ir fiksuojant 20 matavimų vidurkį. Šio tyrimo tikslas – įvertinti algoritmo kokybę ir metodo veiksmingumą atliekant maksimaliai kokybišką matavimą. Dinaminiam tyrimui jutiklis buvo judinamas maksimaliu roboto greičiu, vienu kramtymo ciklu per 2 s, o duomenys išlyginti slenkamojo vidurkio filtru su $N = 4$ langu. Šio tyrimo tikslas – patikrinti, kiek prastėja metodo veiksmingumas jam veikiant realiomis dinaminėmis sąlygomis.

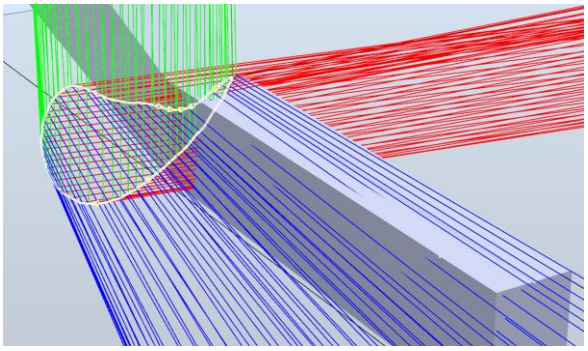

3.18 pav. „RobotStudio“ programine įranga suprogramuota bandomoji kramtymo kreivė.

3.5.3. Bandymas su automatiniu artikuliatoriumi

Buvo sukurta specializuota platforma tikroviškai atkartoti natūraliems žandikaulio judesiams, paremta aukštos kokybės „KaVo PROTAR evo 7“ (*KaVo Kerr*, *Brea*, Kalifornijos valstija, JAV) artikuliatoriumi, valdomu „Dobot Magician“ (*Shenzhen Yuejiang Technology Co., Ltd.*, Šendženas, Kinija) robotine ranka. Platformos nuotraukos su pažymėtais komponentais pateiktos 3.19 ir 3.20 pav.

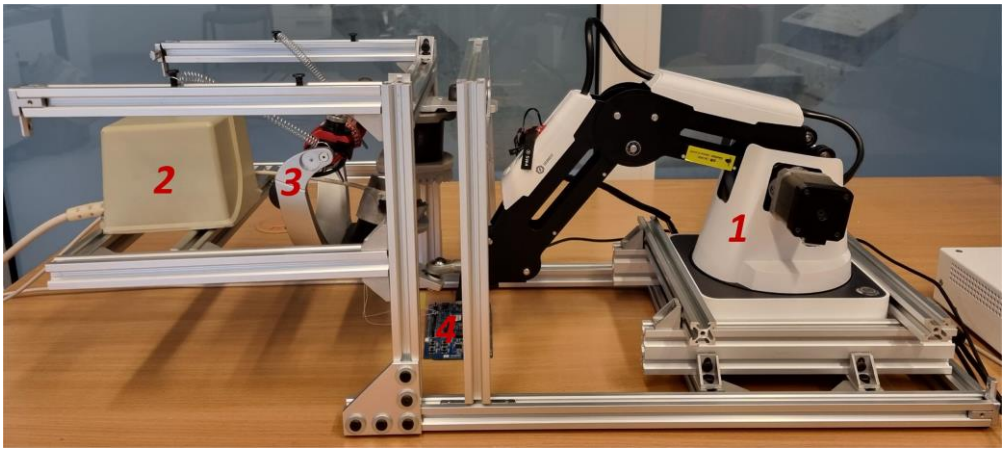

3.19 pav. Robotu valdomo artikuliatoriaus platforma (bendras vaizdas iš šono)

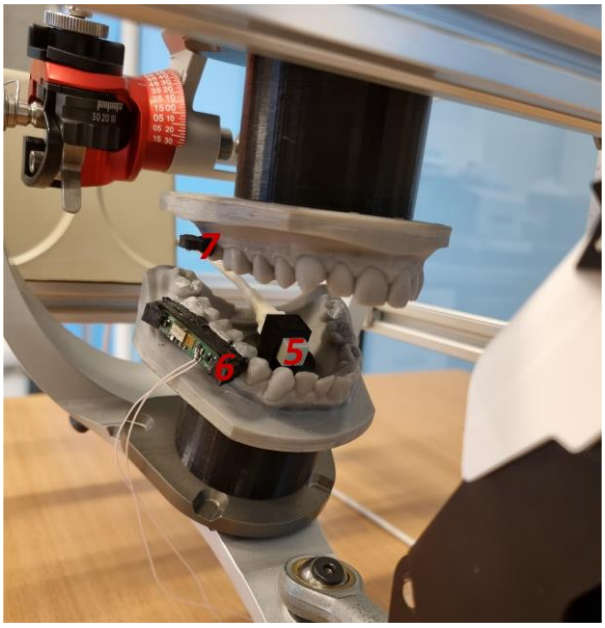

3.20 pav. Robotu valdomo artikuliatoriaus platforma (jutiklis, prototipas ir nuolatinis magnetas)

Platformos sudedamosios dalys:

1 – „Dobot Magician“ robotinė ranka;
2 – atraminės pozicijos nustatymo sistemos „TrakStar“ siųstuvas;
3 – puikios kokybės odontologinis artikuliatorius „KaVo PROTAR evo 7“;
4 – „nRF52832“ mikrovaldiklio tobulinimo plokštė;
5 – atraminės pozicijos nustatymo sistemos „TrakStar“ jutiklis;
6 – dviejų magnetometrų žandikaulio lokalizacijos jutiklio prototipas;
7 – nuolatinis magnetas.

Bandymo metu robotinė ranka valdė artikuliatorių, kuris leido dantų modeliui judėti tik tikroviškomis trajektorijomis ir pasisukimo kampais. Jutiklis buvo maitinamas iš „nRF52832“ mikrovaldiklio tobulinimo plokštės, kuri taip pat priėmė „Bluetooth“ ryšiu perduodamus jutiklio duomenis. „TrakStar“ sistema buvo naudojama kaip pagrindinė lokalizacijos priemonė.

3.5.4. Intraoralinis bandymas

Baigiamojo eksperimento metu jutiklis išbandytas intraoraliai. Nuolatinis magnetas pritvirtintas prie viršutinio žandikaulio panaudojant laikiną plombą, o jutiklis ir baterija inkapsuliuoti specializuotuose dėkluose ir pritvirtinti prie apatinio žandikaulio kapos, neuždengiančios okliuzinio paviršiaus. Intraoralinio bandymo nuotrauka pateikta 3.21 pav.

3.21 pav. Sistema, pritaikyta intraoraliam naudojimui. Inkapsuliuoti jutiklis ir baterija pritvirtinti prie okliuzinio paviršiaus neuždengiančių kapų, o nuolatinis magnetas pritvirtintas tiesiogiai prie viršutinio žandikaulio danties panaudojant laikiną plombą

Dantų kontaktai buvo atpažinti pritaikius slenkstį diferencijuotų pagreičio signalų sumai. Klaidingai teigiami sprendimai buvo atmesti remiantis jutiklio pozicijos duomenimis, įvertintais magnetinės lokalizacijos metodu.

3.6. Skyriaus išvados

Šiame skyriuje išsamiai aprašyti pasiūlytos sistemos veikimo metodai. Vieno magnetometro sistemos koncepto patvirtinimas parodė mažas paklaidas idealiomis sąlygomis, tačiau išorinių magnetinių laukų egzistavimas aplinkoje apriboja šito metodo pritaikomumą. Atraminio magnetometro verčių kompensavimo atimtimi metodas padidina sistemos matmenis ir paneigia vieno magnetometro metodo konceptą. Buvo pasiūlytas dviejų magnetometrų lokalizacijos metodas, galintis kompensuoti aplinkos magnetinį lauką netiesinės optimizacijos būdu išlaikant sąlygiškai mažus jutiklio matmenis. Kadangi pasiūlytas metodas yra 3-LL, pasiūlytos lygtys, susiejančios žandikaulio pasisukimo kampus su linijiniais poslinkiais. Šis žingsnis buvo esminis siekiant pritaikyti pasiūlytą magnetinės lokalizacijos metodą žandikaulio judesiams vertinti. 1 lentelėje pateikiamas kokybinis išplėtotų ir šiame skyriuje aprašytų žandikaulio lokalizacijos metodų palyginimas.

1 lentelė. Išplėtotų ir šiame skyriuje aprašytų magnetinės lokalizacijos metodų kiekybinių parametrų palyginimas

	Vieno magnetometro metodas	Dviejų magnetometrų metodas	Dviejų magnetometrų metodas su trigonometriniu žandikaulio kampo vertinimu
3-LL lokalizacija	✓	✓	✓
Foninio lauko kompensacija	×	✓	✓
3-LL žandikaulio lokalizacija	×	×	✓

Iš viso buvo sukurtos trys jutiklio prototipo iteracijos. Naujausia iš jų pritaikyta belaidžiam naudojimui ir perduoda duomenis „Bluetooth“ ryšiu. Išplėtotas metodas inkapsuliuoti ir pritvirtinti sistemos komponentus prie paciento žandikaulio. Pagamintas baterijų paketas, tinkamas 4–5 h tiekti energiją jutikliui (be programinio optimizavimo). Šie žingsniai įrodė sistemos praktinio pritaikymo galimybes.

Skyriuje taip pat aprašyta visų atliktų eksperimentų metodologija. Statinės ir dinaminės lokalizacijos eksperimentai buvo atlikti kiekviename kūrimo etape, pasitelkiant įvairias automatizuotas pozicionavimo platformas. Šie eksperimentai leido kiekybiškai įvertinti pasiūlytą sistemą. Galutiniais eksperimentais buvo siekiama pademonstruoti ir įvertinti sistemos veikimą realiomis sąlygomis. Natūralūs žandikaulio judesiai buvo atkartoti panaudojus sukurtą robotizuoto artikuliatoriaus platformą. Galiausiai, pasitelkus savanorį, buvo atliktas intraoralinis bandymas.

4. REZULTATAI

4.1. Vieno magnetometro lokalizacijos su akcelerometrine okliuzijos detekcija koncepcijos pagrindimas

4.1.1. Bazinis vieno magnetometro 3-LL lokalizacijos koncepcijos pagrindimas

Pozicijos nustatymo galimybių eksperimentai atlikti panaudojant „Elinta 3D“ pozicionavimo sistemą, pavaizduotą 3.3 pav., jutiklį judinant aiškiai išreikšta kubine ir natūralia kramtymo bandomosiomis trajektorijomis.

Kubinės bandomosios trajektorijos koordinatės buvo nustatytos 10 kartų atskirais matavimais. Gauta vidutinė lokalizacijos paklaida ir standartinis nuokrypis VKP = 0,328 ± 0,005 mm. FML kompensuotas atimties būdu panaudojant atraminį magnetometrą. Išmatuoti taškai sunumeruoti nuo 0 iki 90, ir visos 10 matavimo iteracijų pavaizduotos skaidriai raudonomis žymėmis 4.1 pav. Siekiant parodyti atsikartojamumą 10 matavimo iteracijų laikotarpiu, kiekvieno taško vidurkis ir standartinis nuokrypis pavaizduoti 4.2 pav., su taškais, žyminčiais kiekvieno matavimo paklaidą.

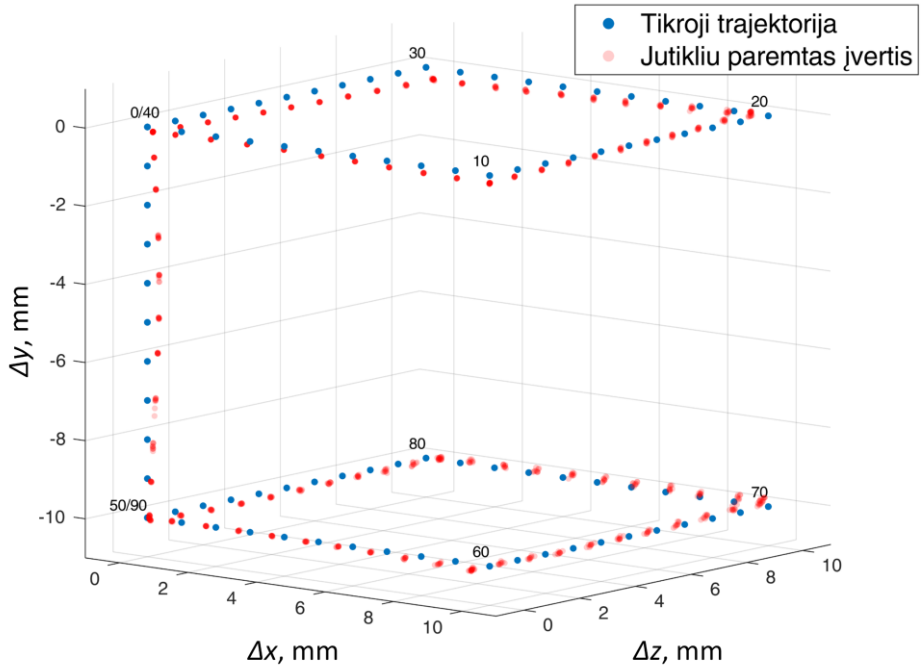

4.1 pav. Kubinės bandomosios trajektorijos pozicijos, apskaičiuotos iš magnetinio lauko verčių, užregistruotų vienu magnetometru. Išmatuotos koordinatės sunumeruotos nuo 0 iki 90, ir 10 matavimo iteracijų pavaizduotos skaidriomis raudonomis žymėmis

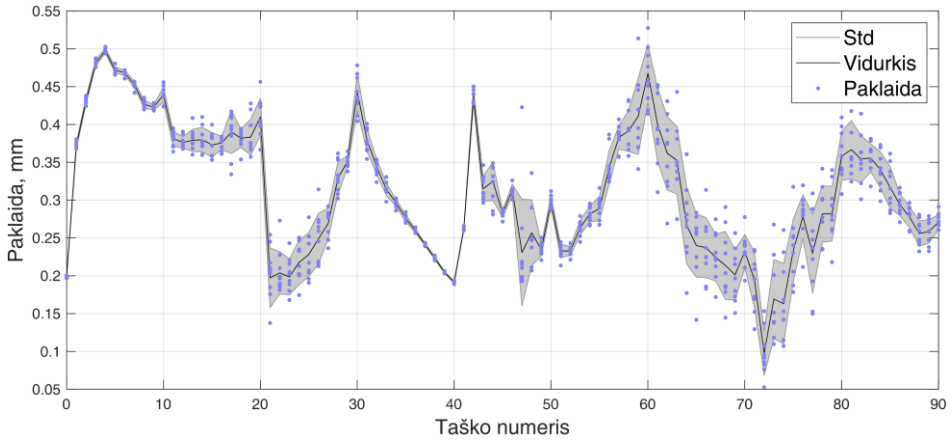

4.2 pav. Kiekvieno taško lokalizacijos paklaida per 10 kubinės bandomosios trajektorijos matavimo iteracijų su vidurkiu ir standartiniu nuokrypiu

Eksperimentas praktiškai patvirtino magnetinės lokalizacijos konceptą, leidžiant per kubinę bandomąją trajektoriją aiškiai suprasti ir įvertinti metodo darbą.

Bandomosios kramtymo trajektorijos koordinatės buvo nustatytos 10 kartų atskirais matavimais. Gauta vidutinė lokalizacijos klaida ir standartinis nuokrypis VKP = 0,260 ± 0,004 mm. FML buvo kompensuoti atimties būdu panaudojant atraminį magnetometrą. Išmatuoti taškai sunumeruoti nuo 0 iki 62, ir visos 10 matavimo iteracijų pavaizduotos skaidriai raudonomis žymėmis 4.3 pav. Siekiant parodyti atsikartojamumą 10 matavimo iteracijų laikotarpiu, kiekvieno taško vidurkis ir standartinis nuokrypis pavaizduoti 4.4 pav., su taškais, žyminčiais kiekvieno matavimo paklaidą.

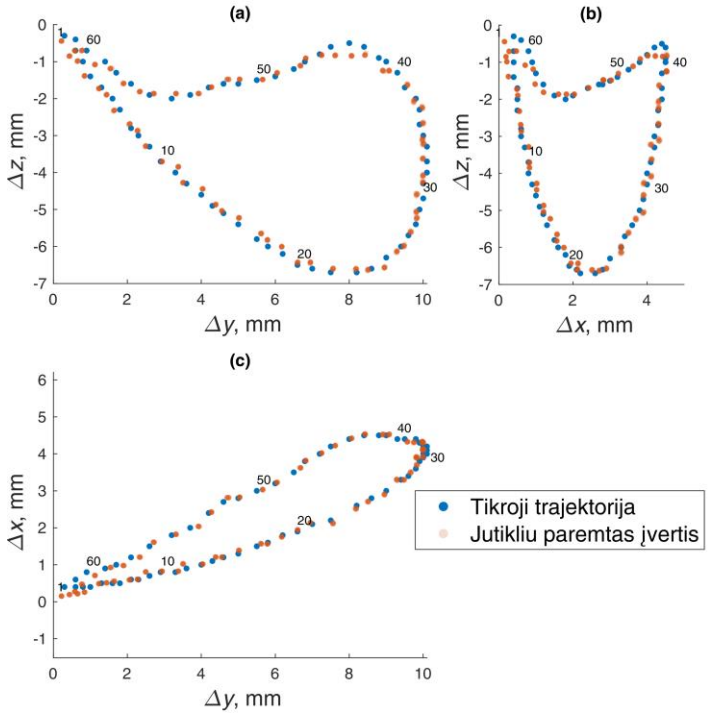

4.3 pav. Bandomosios kramtymo trajektorijos pozicijos, apskaičiuotos iš magnetinio lauko verčių, užregistruotų vienu magnetometru. Išmatuotos koordinatės sunumeruotos nuo 0 iki 62, ir 10 matavimo iteracijų pavaizduotos skaidriomis raudonomis žymėmis: (a) šoninis–vertikalus vaizdas (*y*–*z*); (b) priekinis–vertikalus vaizdas (*x*–*z*); (c) šoninis–priekinis vaizdas (*y*–*x*)

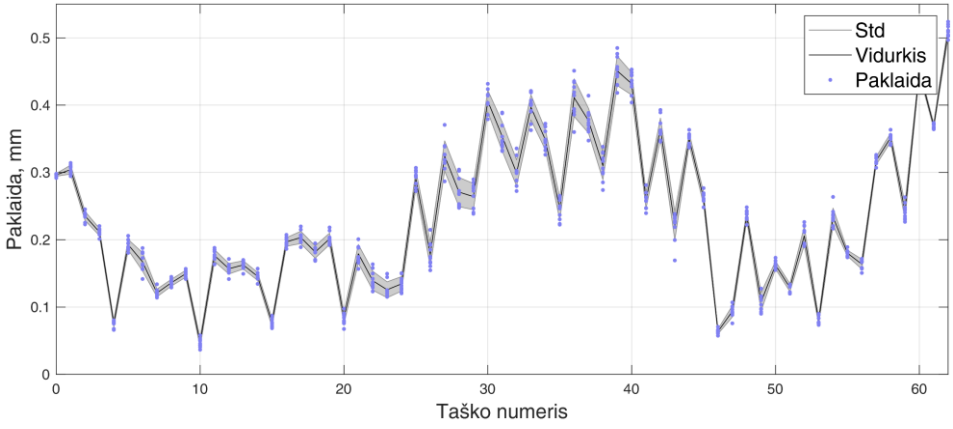

4.4 pav. Kiekvieno taško lokalizacijos paklaida per 10 bandomosios kramtymo trajektorijos matavimo iteracijų su vidurkiu ir standartiniu nuokrypiu

Natūralios kramtymo trajektorijos eksperimentas parodė, jog magnetinės lokalizacijos koncepcija yra tinkama žandikaulio veiklai vertinti ir verta tolimesnio plėtojimo.

4.1.2. Dantų kontaktų atpažinimas akcelerometrija

Šio eksperimento tikslas – patikrinti, ar įmanoma atpažinti dantų kontakto (susitrenkimo) momentą iš prie dantų pritvirtinto jutiklio pagreičio pokyčių. Vertikalus žandikaulio judėjimas buvo atkartotas savadarbiu automatiniu vertikalių judesių artikuliatoriumi, pavaizduotu 3.4 pav. Eksperimento metu matuotas jutiklio pagreitis ir kampinis greitis. Pagreičio vektoriaus tikrojo dydžio signalas su raudonai pažymėtais atpažintais dantų kontakto momentais pateiktas 4.5(a) pav. 5 m/s^2 atpažinimo slenkstis parinktas eksperimentiškai. Toje pačioje IMS integruotu giroskopu išmatuotas kampinis greitis buvo panaudotas kaip atraminis matavimas, iliustruojantis artikuliatoriaus judesius. Kampinio greičio signalas kartu su įvykusių smūgių anotacija pateikiamas 4.5(b) pav.

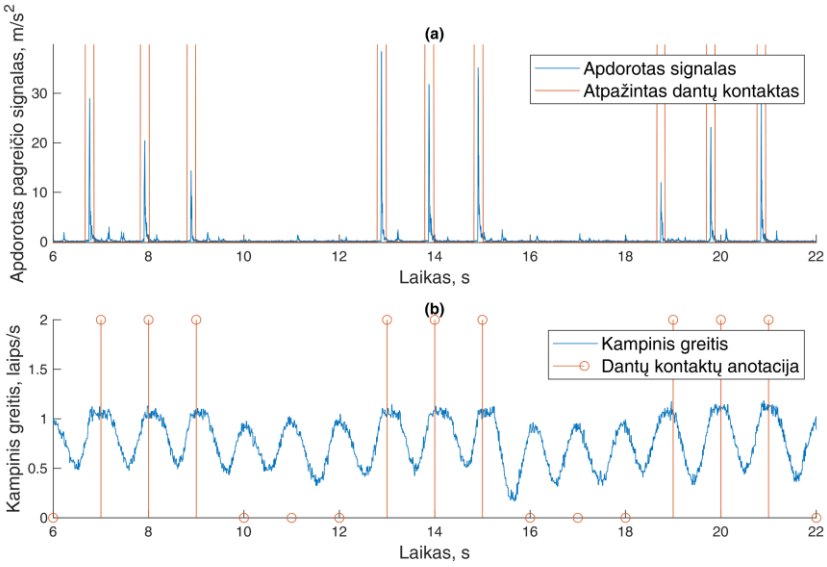

4.5 pav. Dantų kontaktų (susitrenkimų) atpažinimas vertikaliame judesyje: (a) pagreičio vektoriaus tikrojo dydžio signalas; (b) atraminis kampinio greičio signalas su dantų kontaktų anotacija

Eksperimentas parodo, jog įmanoma aptikti dantų kontaktus (susitrenkimus) panaudojant prie jų pritvirtintą MEMS akcelerometrą.

4.1.3. Dinaminis 3-LL lokalizacijos tyrimas su akcelerometriniu dantų okliuzijos atpažinimu

Dinaminiam lokalizacijos tyrimui su akcelerometriniu dantų kontaktų atpažinimu buvo panaudotas savadarbe 6-LL Stiuarto platforma paremtas žandikaulio judesių artikuliatorius, pavaizduotas 3.5 pav. 4.6(a) pav. pateiktas pagreičio tikrojo dydžio signalas su pažymėtais algoritmo atpažintais dantų kontakto momentais. 5 m/s^2 atpažinimo slenkstis pasirinktas eksperimentiškai. Matomos dvi signalo viršūnės – viena dėl judesio pradžios, o kita dėl dantų kontakto. 4.6(b–d) pav. vaizduojamos jutikliu ir atraminiu metodu užfiksuotos judėjimo kreivės. Taip pat pažymėtos pozicijos, ties kuriomis įvyko dantų kontaktai. Galima pastebėti, jog paryškintos koordinatės sutampa su trajektorijos dalimi, esančia okliuzinėje srityje.

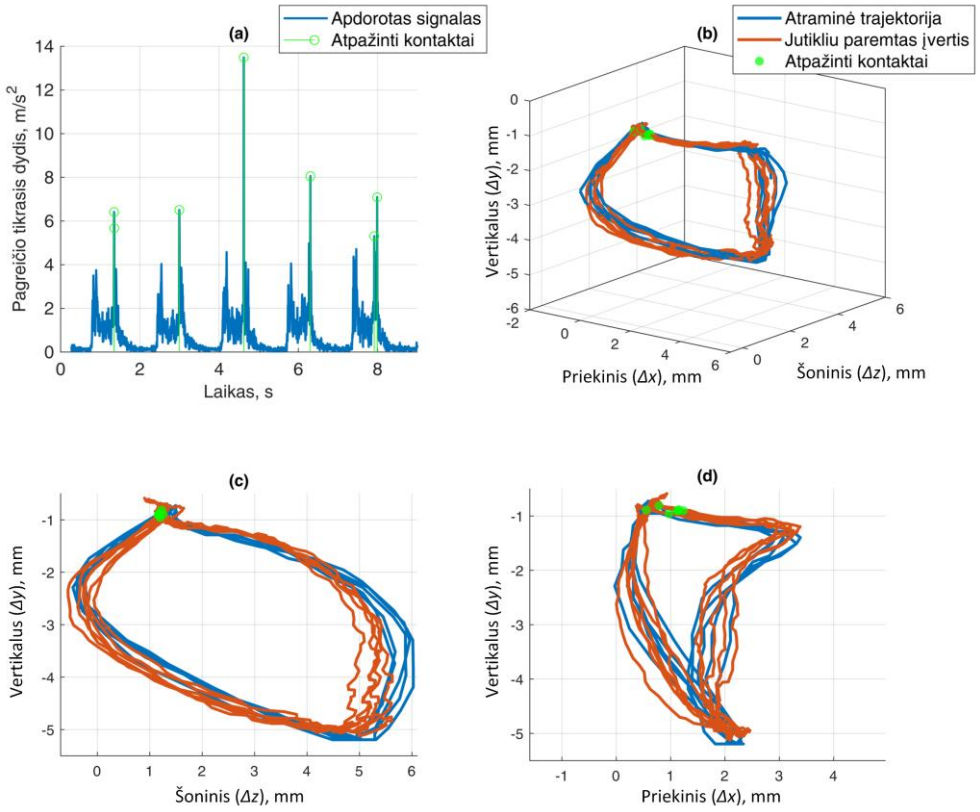

4.6 pav. (a) Dantų kontaktai, atpažinti pagreičio vektoriaus tikrojo dydžio signale su 5 m/s^2 aptikimo slenksčiu. (b) Bandomoji trajektorija, nustatyta atraminiu metodu ir magnetiniu lokalizacijos metodu, paryškintos pozicijos, ties kuriomis

aptikti dantų kontaktai. (c) Šoninis–vertikalus vaizdas (*z*–*y*). (d) Priekinis–vertikalus vaizdas (*x*–*y*)

Eksperimentu pademonstruota, jog yra logiška tikėtis, kad sukūrus solidų magnetinio žandikaulio judesių sekimo sprendimą, jis galėtų būti papildytas akcelerometriniu dantų kontaktų atpažinimu. Dėl šios priežasties kuriant prototipą magnetiniams matavimams turėtų būtų svarstomi MEMS su integruotais akcelerometrais.

4.2. Foninis magnetinis laukas

4.2.1. Foninio magnetinio lauko poveikis

Pozicijos nustatymo paklaidos įvairiais magneto ir jutiklio atstumais esant 65 µT FML buvo apskaičiuotos ir pateiktos 4.7 pav. Pridedant konkrečias FML vertes prie teorinių (BEM) ir kompensuotų eksperimentinių duomenų, FML buvo sumodeliuotas trimis skirtingomis kryptimis.

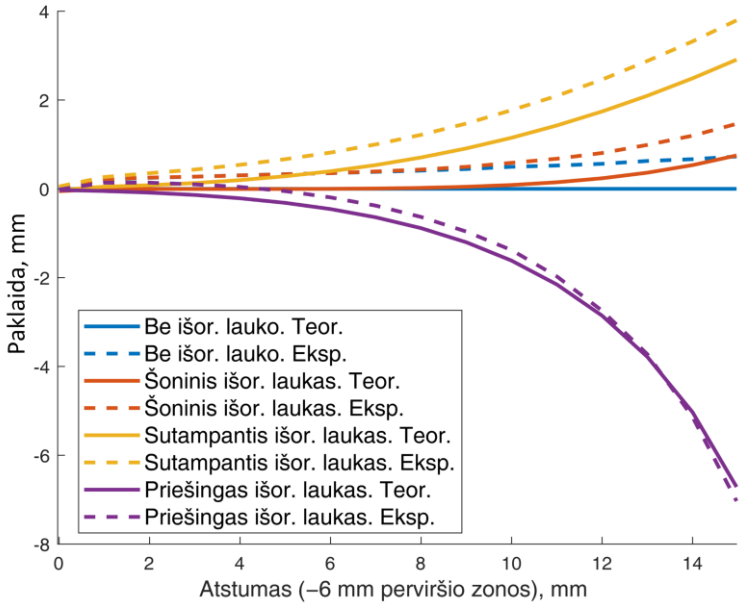

4.7 pav. Pozicijos nustatymo paklaidos (VKP), sukeltos įvairių krypčių dirbtinio 65 µT FML, pridėto prie teorinių ir eksperimentinių duomenų

Grafikas rodo, jog pradžioje matavimo erdvei FML beveik neturi įtakos, tačiau ši pastebimai auga jutikliui tolstant nuo magneto dėl kubiniu dėsniu silpnėjančio jo magnetinio lauko. Vertinant praktiškai, didžiausias tikslumas reikalingas dantims artėjant prie okliuzijos, todėl metodas gali būti taikomas žandikaulio stebėsenai. Vis dėlto reikia pripažinti, jog FML žymiai sumažina matavimo darbinę erdvę. Tai parodo FML kompensavimo būtinybę.

4.2.2. Dviejų magnetometrų lokalizacija su FML kompensavimu

Originali bandomoji kramtymo trajektorija pateikta 4.8 pav. kartu su dviejų magnetometrų metodu nustatytomis trajektorijomis iš teorinių (BEM) ir eksperimentinių duomenų. Teoriniu atveju lokalizacijos paklaida buvo VKP = 0,05 mm, o 65 µT FML vektorius nustatytas kaip BMF = [−0,13; 57,90; −0,05] µT. Palyginimui, tiriant vieno magnetometro metodu tame pačiame, tačiau FML neužterštame, baigtinių elementų modelyje gauta VKP = 0,1 mm. „Elinta“ trimačio (3D) pozicionavimo sistema atlikto eksperimentinio bandymo metu gauta VKP = 0,28 mm. Nustatytas natūralus FML = [−8,95; 57,19; −12,24] µT vektorius. Palyginimui, vieno magnetometro metodu ant tos pačios sistemos atliktas tyrimas parodė VKP = 0,26 mm.

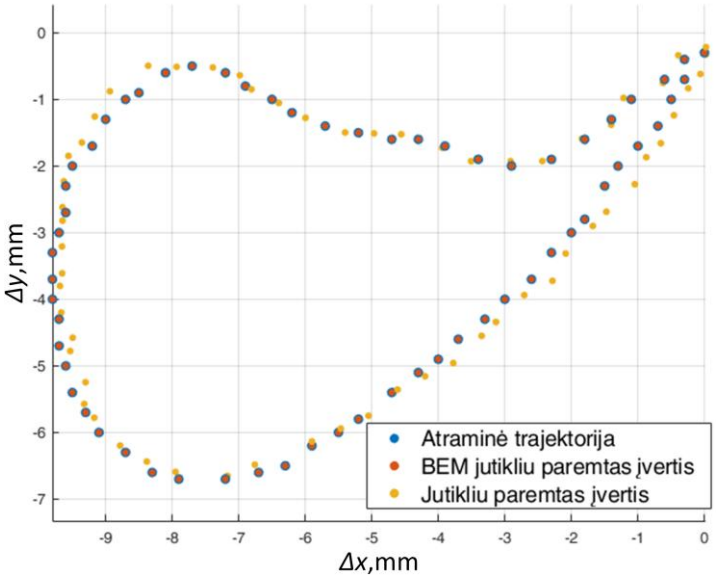

4.8 pav. Bandomoji trajektorija, nustatyta dvejų magnetometrų metodu su FML kompensavimu. Su teoriniais BEM duomenimis VKP = 0,05 mm (raudona), o su eksperimentiniais „Elinta“ trimačio (3D) pozicionavimo sistema užfiksuotais duomenimis VKP = 0,28 mm (geltona)

4.2.3. Lygčių žandikaulio posūkio kampo vertinimui validacija

Šis bandymas skirtas trigonometrinėms lygtims, parodančioms žandikaulio poslinkio ir pasisukimo priklausomybę, validuoti. Tai daroma palyginus 6-LL atraminės sistemos matavimais gautas realias priklausomybes su tam pačiam tiriamajam trigonometriškai apskaičiuotomis priklausomybėmis. Savanorio žandikaulio ir jutiklio atstumų matavimo rezultatai yra L = 45 mm, H = 33 mm, W_L = 64 mm ir W_R = 16 mm. Priklausomybės palygintos 4.9 ir 4.10 pav.

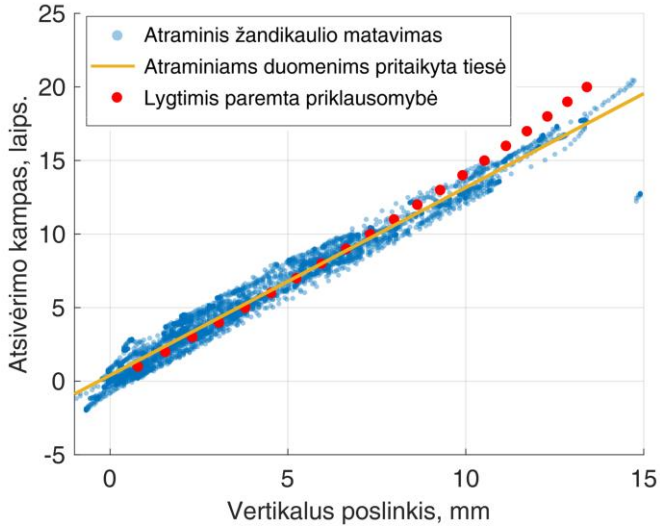

4.9 pav. Vertikalaus žandikaulio poslinkio ir atsivėrimo kampo priklausomybės. Išmatuota ir apskaičiuota pasiūlytomis lygtimis. Koreliacijos koeficientas tarp atraminiu metodu įvertintų ir lygtimis apskaičiuotų priklausomybių tiesių yra 0,9989

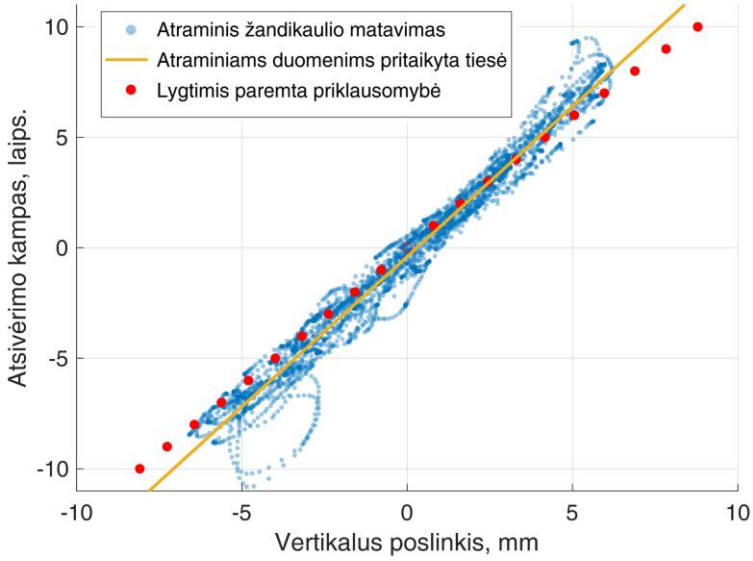

4.10 pav. Horizontalaus (šoninio) žandikaulio poslinkio ir šoninio pasisukimo kampo priklausomybės. Išmatuota ir apskaičiuota pasiūlytomis lygtimis. Koreliacijos koeficientas tarp atraminiu metodu įvertintų ir lygtimis apskaičiuotų priklausomybių tiesių yra 0,9996

Matome, jog poslinkio ir sukimosi priklausomybės yra tiesinės. Kiekybiškai vertinant apskaičiuotų ir atraminių duomenų atitikimą, koreliacijos koeficientas tarp atraminiu metodu įvertintų ir lygtimis apskaičiuotų priklausomybių tiesių vertikaliam judėjimui yra 0,9989, o šoniniam judesiui – 0,9996. Tiesiškumas prastėja žandikauliui artėjant prie ribinio atsivėrimo. Taigi, ir šiuo atveju vertinimo tikslumas gali minimaliai kristi plataus išsižiojimo atveju, tačiau priklausomybė lygtimis puikiai atspindima didžiojoje darbinio ruožo dalyje.

4.3. Galutinis sistemos patikrinimas

4.3.1. Visos darbinės erdvės tyrimas

Šio eksperimento metu buvo įvertintas metodo teorinės ir eksperimentinės lokalizacijos tikslumas, panaudojant BEM ir precizinę „ABB“ robotinę ranką. Teorinių duomenų atveju, erdvė buvo užteršta 65 µT FML, o eksperimentiniai duomenys turėjo natūralaus FML dedamąją. Abiem atvejais, 1 mm žingsniu, nuo R = 6 mm (minimalus metodo atstumas) iki R = 20 mm kintančiu radialiniu atstumu iki magneto, buvo apskaičiuotos vidutinės lokalizacijos paklaidos. Vizualizacijai 4.11 pav. pateikiamas maksimaliu R = 20 mm radialiniu atstumu atliktas teorinis BEM matavimas. Pavaizduotos tiek pagrindinio, tiek atraminio magnetometrų judėjimo trajektorijos. Šiuo atveju gauta teorinė lokalizacijos paklaida VKP = 0,088 mm.

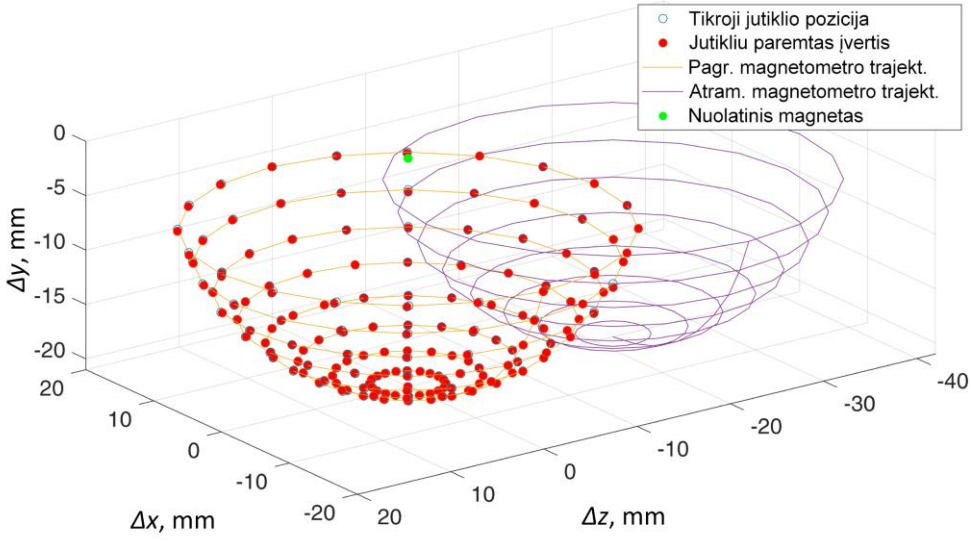

4.11 pav. Dviejų magnetometrų lokalizacijos su FML kompensavimu matavimas BEM aplinkoje, ties R = 20 mm radialiniu atstumu nuo magneto

Teorinis tyrimas. Teoriniame modelyje buvo nustatyta vidutinė kvadratinė paklaida (VKP) ir Euklidinis atstumas (EA) skirtingoms darbinės erdvės zonoms. Tyrimo rezultatai pateikti 4.12 pav.

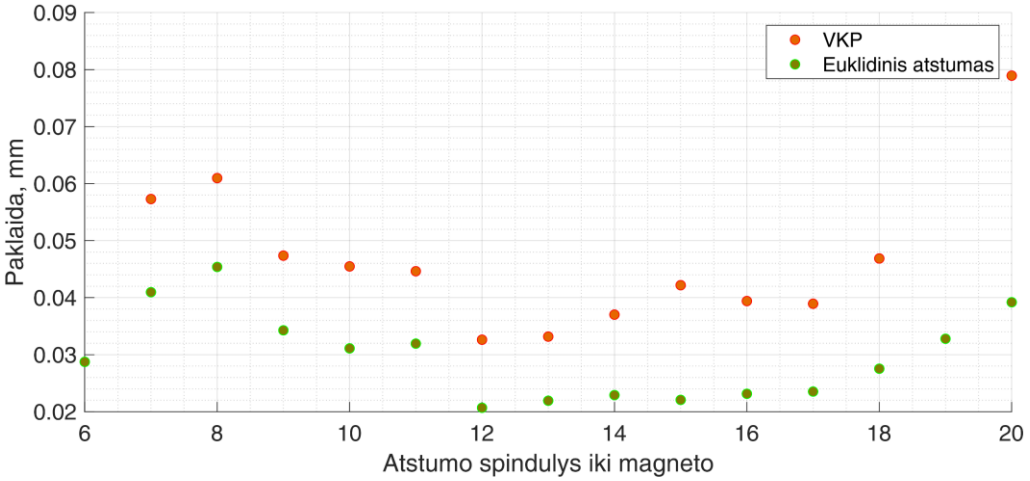

4.12 pav. Dviejų magnetometrų lokalizacijos su FML kompensavimu taikant MK optimizavimą BEM tyrimas. Vidutinės kvadratinės paklaidos (VKP) ir vidutinio Euklidinio atstumo (EA) iki tikrosios jutiklio trajektorijos priklausomybė nuo atstumo spindulio iki magneto

Eksperimentinis tyrimas. Dešimties matavimų mediana eksperimentiškai išmatuotos paklaidos ir atstumo priklausomybės vidutinei kvadratinei paklaidai (VKP) ir Euklidiniam atstumui (EA) pateiktos atitinkamai 4.13 ir 4.14 pav.

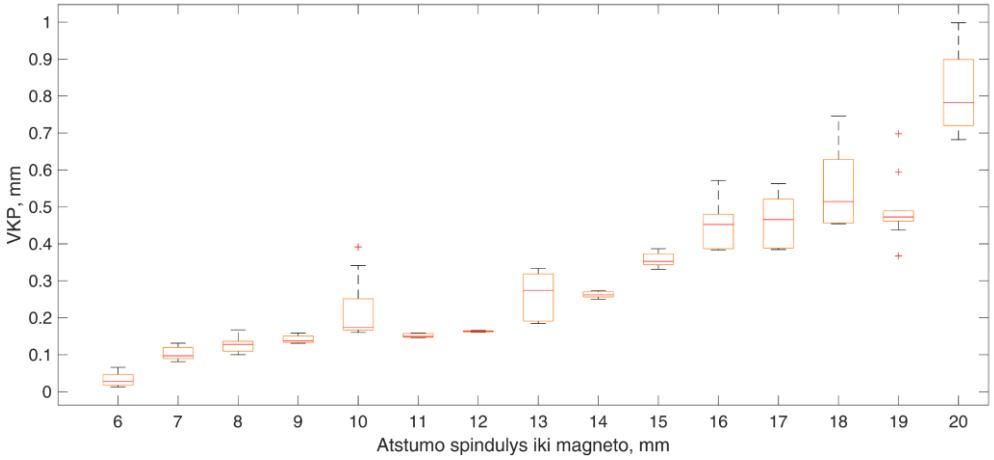

4.13 pav. 10 matavimų VKP mediana ir standartinis nuokrypis matavimams skirtingais atstumais nuo magneto

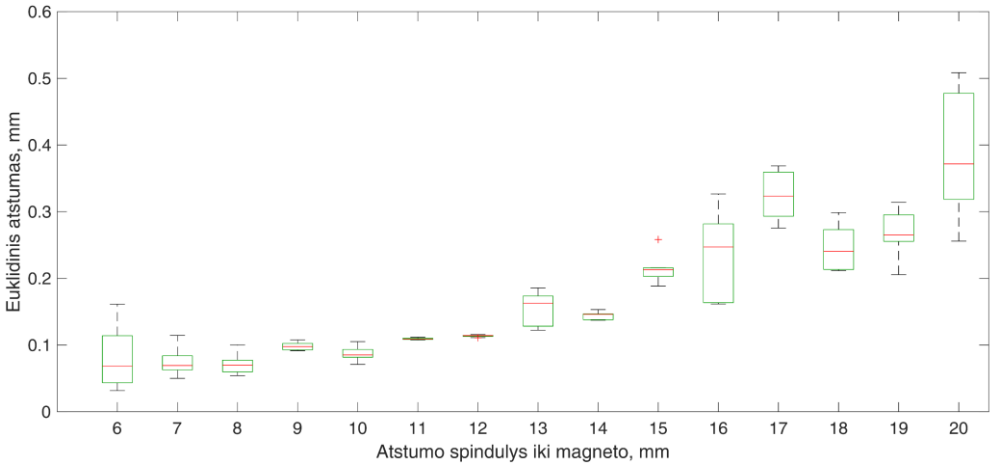

4.14 pav. 10 matavimų Euklidinio atstumo mediana ir standartinis nuokrypis matavimams skirtingais atstumais nuo magneto

Eksperimentas rodo, jog lokalizacijos paklaida neviršija VKP < 0,1 mm okliuzinėje zonoje ir VKP < 1 mm darbinio diapazono pabaigoje. Tokie rezultatai viršija lūkesčius, nes nėra tolimi nuo nurodomų klinikinių žandikaulio kinematikos vertinimo prietaisų specifikacijose. Tokio lygio veikimas yra pakankamas bruksizmo diagnostikai ir paciento elgsenos vertinimui su saugiu perviršiu galimam lokalizacijos paklaidos išaugimui dėl dekalibracijos.

Pastebėta, jog metodui itin būdingos paklaidos erdvėje tarp pagrindinio ir atraminio magnetometrų. Vis dėlto dėl žandikaulio mechanikos ir siūlomų magneto bei jutiklio tvirtinimo vietų žandikauliui judant magnetas galės tik tolti nuo atraminio magnetometro.

4.3.2. Statinis 5-LL žandikaulio lokalizacijos tyrimas

Statiniame 5-LL žandikaulio lokalizacijos tyrime bandomoji kramtymo trajektorija buvo atkartota 10 kartų „ABB“ robotine ranka. Matavimai buvo diskretieji, sustojant kiekviename matavimo taške. Nustatytos pozicijos pateiktos 4.15 pav., jų vidutinė lokalizacijos paklaida ir standartinis nuokrypis buvo VKP = 0,165 ± 0,020 mm. VKP paklaidų išsibarstymas kiekviename taške pateiktas 4.16 pav. Palyginimui su dinaminiu 5-LL lokalizacijos tyrimu, apskaičiuota ir vidutinė lokalizacijos paklaida, ir standartinis nuokrypis EA = 0,098 ± 0,014 mm. Matavimų išsibarstymas pavaizduotas 4.17 pav.

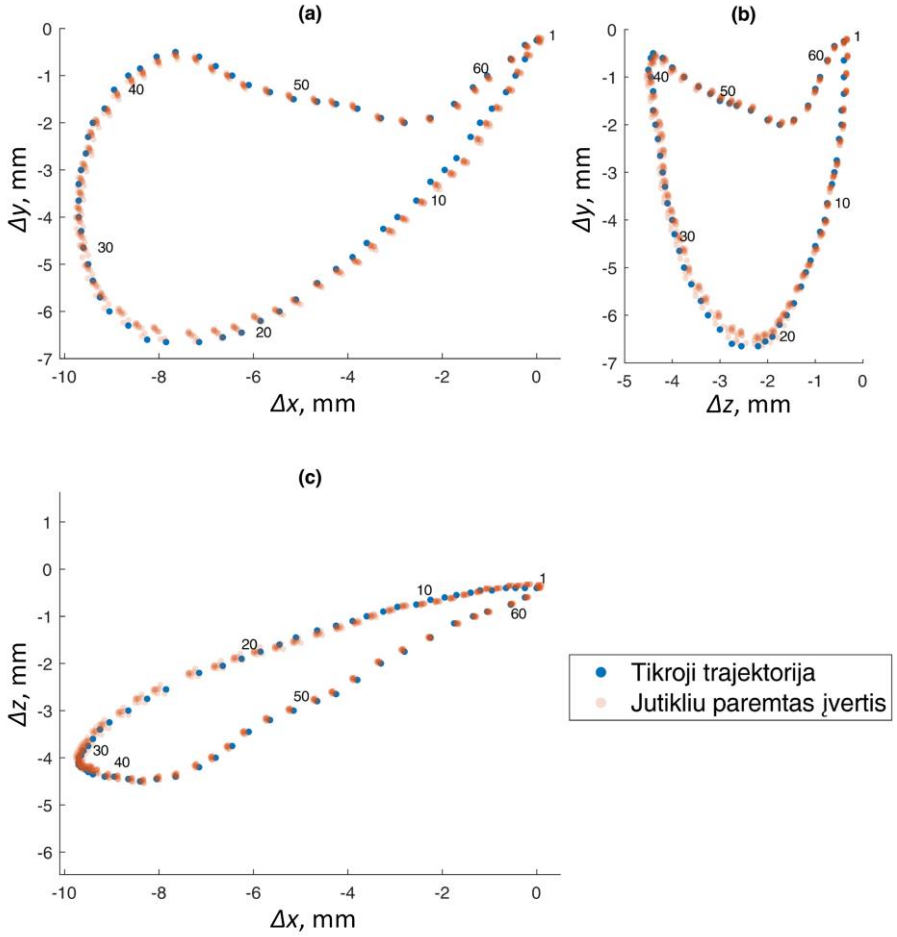

4.15 pav. Bandomosios kramtymo trajektorijos statinis 5-LL lokalizacijos su žandikaulio kampo ir FML kompensavimu tyrimas. Vidutinė lokalizacijos paklaida ir standartinis nuokrypis VKP = 0,165 ± 0,020 mm, *EA* = 0,098 ± 0,014 mm. Išmatuotos koordinatės sunumeruotos nuo 0 iki 62, ir 10 matavimo iteracijų pavaizduotos skaidriomis raudonomis žymėmis: (a) šoninis–vertikalus vaizdas (*x*–*y*); (b) priekinis–vertikalus vaizdas (*z*–*y*); (c) šoninis–priekinis vaizdas (*x*–*z*).

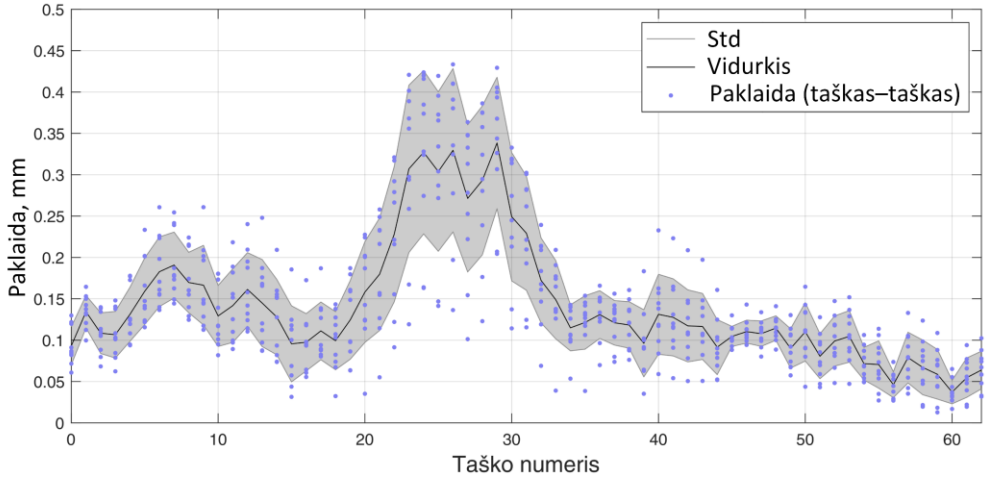

4.16 pav. Statinis 5-LL tyrimas. Lokalizacijos kiekvieno taško VKP (taškas–taškas) per 10 kreivės matavimo iteracijų su vidurkiu ir standartiniu nuokrypiu

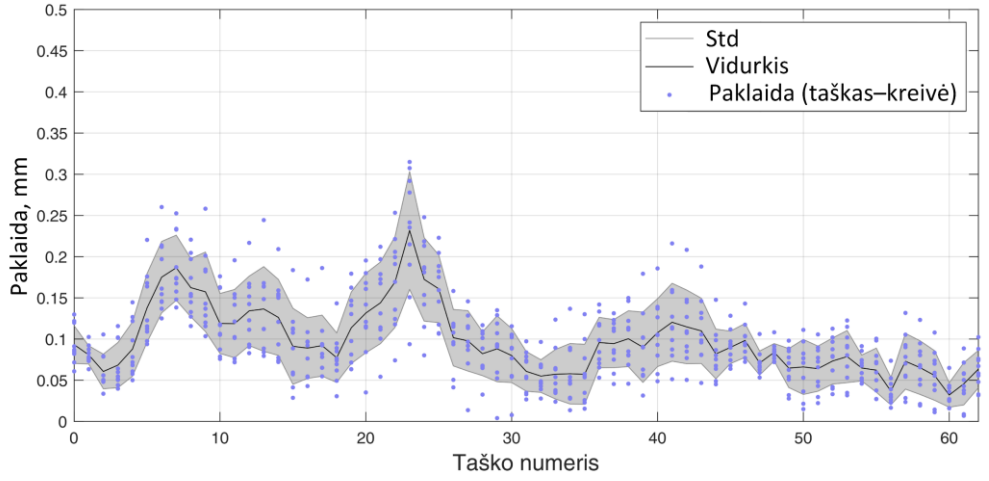

4.17 pav. Statinis 5-LL tyrimas. Lokalizacijos kiekvieno taško paklaidos ir Euklidinis atstumas (taškas–kreivė) per 10 kreivės matavimo iteracijų su vidurkiu ir standartiniu nuokrypiu

Nors statinės sąlygos nėra tikroviškos klinikiniam taikymui, šis eksperimentas parodo tikrąsias metodo galimybes su minimalia mechaninių vibracijų ir magnetometrų techninių ribotumų įtaka. Akivaizdu, jog taikant šį metodą galima pakankamai tiksliai įvertinti realias žandikaulio judėjimo trajektorijas.

4.3.3. Dinaminis 5-LL žandikaulio lokalizacijos tyrimas

Dinaminio 5-LL lokalizacijos tyrimo metu bandomoji kramtymo trajektorija taip pat buvo atkartota 10 kartų „ABB“ robotine ranka, maksimaliu prietaiso greičiu,

trunkant ~2 s vienai trajektorijos iteracijai. Dėl atsitiktinių triukšmų magnetometro rodmenyse slenkamojo vidurkio (N = 4) filtras žymiai padidino dinaminių matavimų tikslumą. Duomenys registruoti 100 Hz surinkimo dažniu. Užregistruotos trajektorijos pateiktos 4.18 pav. Užregistruotų trajektorijų vidutinė lokalizacijos paklaida iki tikrosios trajektorijos ir standartinis nuokrypis buvo EA = 0,175 ± 0,003 mm. Paklaidų išsibarstymas kiekvienam taškui pateiktas 4.19 pav. Pažymėtina, jog nemaža dalis trajektorijos neatitikimų buvo sukelta ilgo jutiklio tvirtinimo įrankio amortizavimo, robotui keičiant judėjimo kryptį.

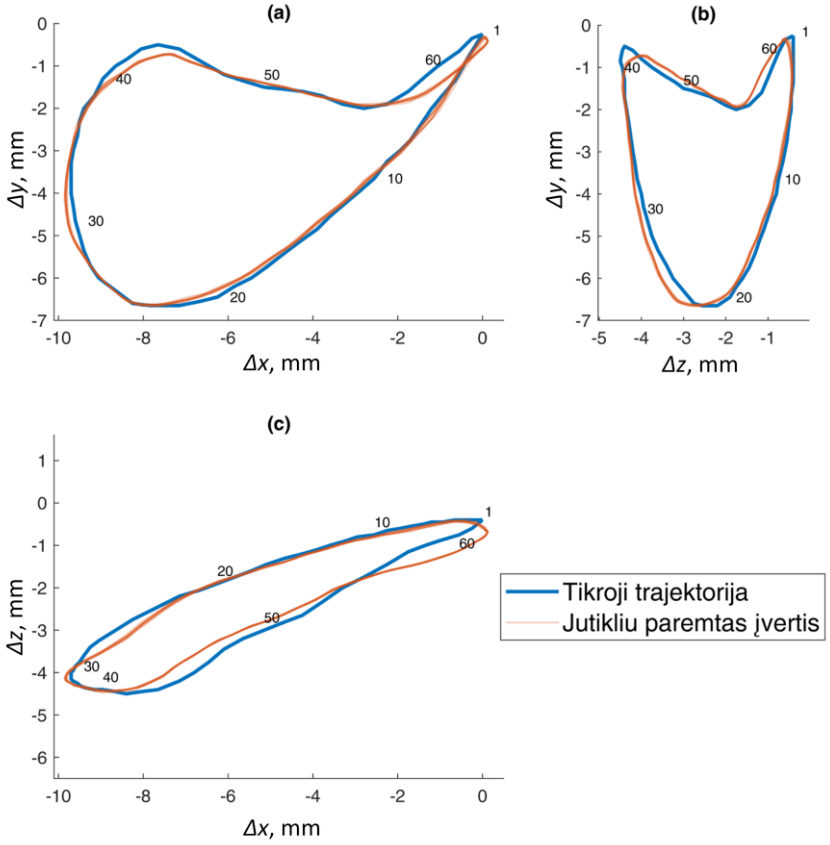

4.18 pav. Bandomosios kramtymo trajektorijos dinaminis 5-LL lokalizacijos su žandikaulio kampo ir FML kompensavimu tyrimas. Vidutinė lokalizacijos paklaida iki tikrosios kreivės ir standartinis nuokrypis EA = 0,175 ± 0,003 mm. 10 matavimo iteracijų pavaizduotos skaidriomis raudonomis žymėmis: (a) šoninis–vertikalus vaizdas (x–y); (b) priekinis–vertikalus vaizdas (z–y); (c) šoninis–priekinis vaizdas (x–z)

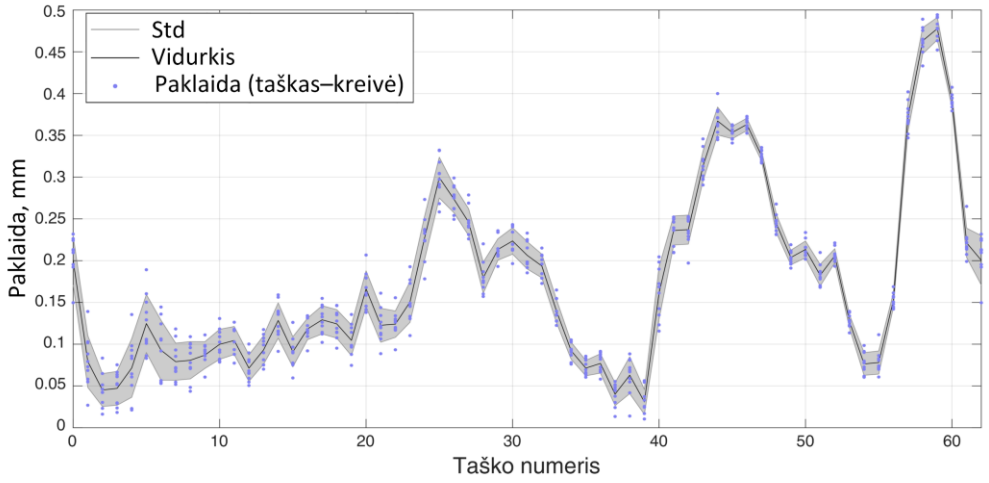

4.19 pav. Dinaminis 5-LL tyrimas. Kiekvieno taško lokalizacijos paklaidos ir Euklidinis atstumas (taškas–kreivė) per 10 kreivės matavimo iteracijų su vidurkiu ir standartiniu nuokrypiu

Dinaminis eksperimentas parodo, jog šiuo metodu galima vertinti žandikaulio judėjimo trajektorijas realiomis sąlygomis, su esamais techniniais apribojimais. Nepaisant mažos lokalizacijos paklaidos, matomi sisteminiai jutikliu įvertintos trajektorijos formos ir tikrosios trajektorijos neatitikimai. Tikėtina, jog tai buvo sukelta mechaninių ir elastinių ilgo jutiklio tvirtinimo įrankių, kurie būtini siekiant padidinti jutiklio atstumą iki roboto variklių. Deja, ~28 cm ilgio tvirtinimo detalei tam tikras lankstumas ir vibravimas buvo neišvengiamas, taip pat buvo matoma amortizacija ir minimalus vėlavimas robotui keičiant jutiklio judėjimo kryptį. Faktas, jog nepavyko idealiai įgyvendinti užsibrėžtos trajektorijos, yra tyrimo apribojimas. Tai gali reikšti, jog pakėlus tyrimo kokybę būtų įmanoma pasiekti dar mažesnę lokalizacijos paklaidą.

4.3.4. Bandymas su automatiniu artikuliatoriumi

Roboto valdomu artikuliatoriumi susimuliuotų kramtymo trajektorijų įvertis, paremtas magnetinio jutiklio duomenimis, pateiktas 4.20 pav. kartu su atramine trajektorija, užregistruota sistema „TrakStar“. Kramtymo trajektorija buvo pakartota keletą kartų.

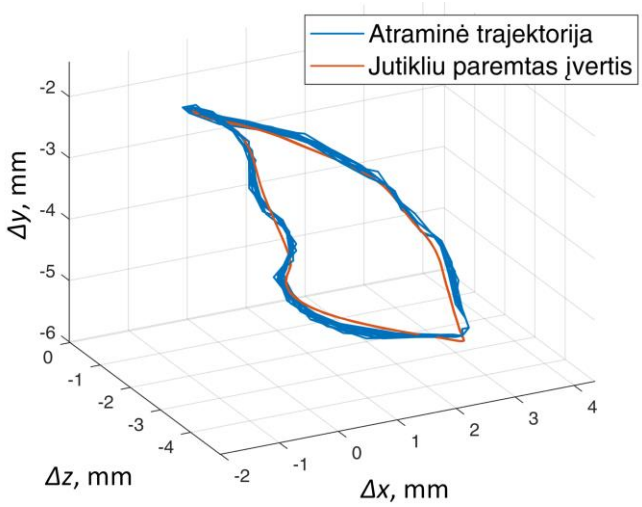

4.20 pav. Magnetiniu jutikliu paremtas kramtymo kreivės įvertis, užregistruotas robotizuoto artikuliatoriaus bandymo metu. Atraminė trajektorija užregistruota sistema „TrakStar“

Nustatyta EA = 0,240 mm lokalizacijos paklaida. Jutikliu nustatyta trajektorija per 10 iteracijų parodė didelį atsikartojamumą, priešingai nei atraminis metodas. Todėl atliekant tolimesnius tyrimus vertėtų apsvarstyti geresnės kokybės atraminės sistemos naudojimą.

4.3.5. Intraoralinis bandymas

Sistemos veikimas pademonstruotas intraoralinio bandymo metu, užregistruojant vertikalaus kalenimo ir natūralaus kramtymo trajektorijas, kurios atitinkamai pavaizduotos 4.21 ir 4.22 pav.

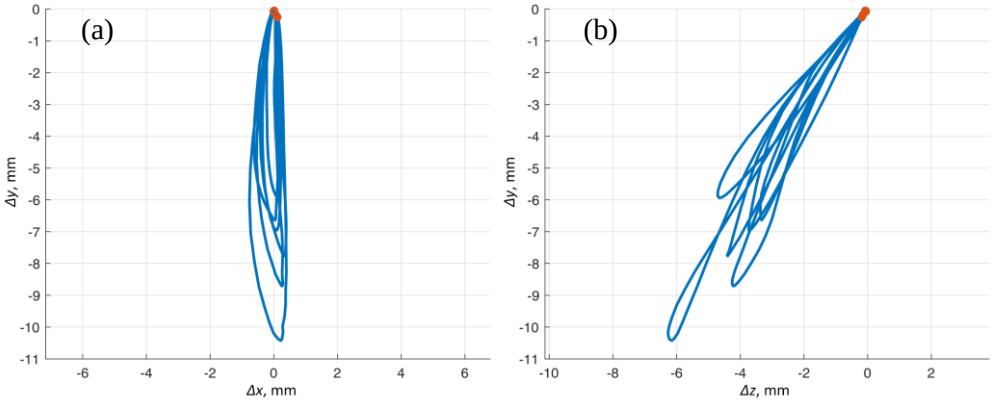

4.21 pav. Intraoraliai jutikliu užregistruotos vertikalaus kalenimo trajektorijos įvertis su raudonai pažymėtais dantų kontaktais. Priekinė (a) ir šoninė (b) projekcijos

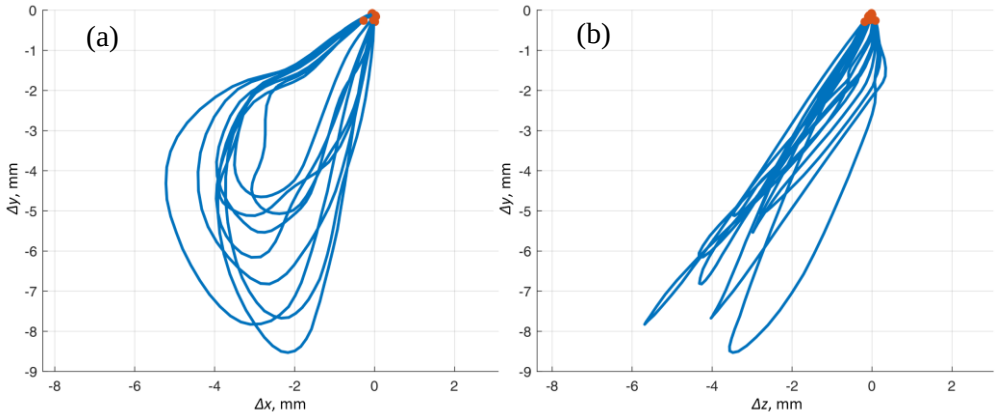

4.22 pav. Intraoraliai jutikliu užregistruotos natūralios kramtymo trajektorijos įvertis su raudonai pažymėtais dantų kontaktais. Priekinė (a) ir šoninė (b) projekcijos

Praktinis intraoralinis eksperimentas padėjo geriau suprasti sistemos stipriąsias ir silpnąsias puses. Magnetinė lokalizacija parodė stabilumą ir praktiškumą. Metodas leido užregistruoti aiškiai išreikštas žandikaulio judėjimo trajektorijas net be magnetometrų kalibracijos. Vis dėlto iš pagreičio signalų atpažinti dantų kontaktus pasirodė sudėtingiau, nei tikėtasi, ir kontaktų atpažinimui prireikė atlikti kombinuotą pozicijos ir pagreičio duomenų analizę.

4.3.6. Skyriaus išvados ir diskusija

Tyrimo ribotumai. „Elinta“ trimačio (3D) pozicionavimo sistemos minimalus žingsnis yra 0,1 mm. Tokia pozicionavimo skiriamoji geba yra kiek per maža tirtoms kreivėms. Tai gali būti priežastis nepagerėjusio dviejų magnetometrų metodo atliekant 3-LL lokalizacijos tyrimą (VKP = 0,28 mm), palyginus su vieno magnetometro tyrimu (VKP = 0,26 mm). „ABB“ robotinės rankos minimalus žingsnis yra 0,01 mm, ir su ja atliktame 5-LL tyrime gauta vidutinė lokalizacijos paklaida bei standartinis nuokrypis VKP = 0,175 ± 0,003 mm, nepaisant dviejų papildomų laisvės laipsnių.

Visose naudotose elektromechaninėse sistemose buvo elektriniai motorai, kurie generuoja magnetinius laukus. Tai buvo ypač pastebima su „ABB“ robotine ranka. Šio tipo užteršimas buvo sprendžiamas ilgu tvirtinimo įrankiu padidinant atstumą tarp jutiklio ir roboto. Didesniu atstumu variklių magnetinis laukas jutiklio prototipo plote buvo beveik homogeniškas, todėl jį buvo galima sėkmingai kompensuoti kartu su natūraliu FML. Juolab, tokių BMF šaltinių klinikinėje aplinkoje neturėtų pasitaikyti.

Ilga jutiklio tvirtinimo detalė, skirta atitraukti jutiklį nuo „ABB“ roboto variklių, dėl savo lankstumo įvedė netikslumų į dinaminės 5-LL lokalizacijos eksperimentą. Numatyta tikroji trajektorija nebuvo idealiai atkartota. Tai sąlygojo prastesnį lokalizacijos paklaidos įvertį.

Tiek savadarbių artikuliatorių, tiek naudotų pozicionavimo sistemų judėjimo greitis (~2 s kramtymo kreivės ciklui) buvo kiek per mažas idealiai atkartoti natūraliems žandikaulio judesiams. Dėl šios priežasties reikia pripažinti dalinį dinaminių eksperimentų ribotumą atkartojant tikroviškus judesius.

Robotizuoto artikuliatoriaus eksperimento metu atraminė sistema „TrakStar“ parodė akivaizdžiai mažesnį atsikartojamumą nei tiriama magnetinė sistema. Galima daryti išvadą, jog šiam darbui reikalingas geresnės kokybės atraminis lokalizacijos metodas.

Metodo ribotumai. Dviejų magnetometrų metodu galima kompensuoti FML, kurie yra homogeniški 22 mm plote tarp dviejų prototipo magnetometrų. Esant nehomogeniškam FML, šiuo metodu nepavyks jo kompensuoti.

Magnetometrų surinkimo netikslumai ir magnetometrų bei nuolatinio magneto gamyklinės tolerancijos gali padidinti lokalizavimo paklaidą iki 0,1 mm ir 0,4 mm, atitinkamai. Nepaisant to, tokios klaidos būtų sisteminės ir jas galima kompensuoti derinant programinėje įrangoje.

Pasiūlytos sistemos mastelį keisti būtų sudėtinga dėl magnetizmo fizikos – norint padidinti sistemos darbinį diapazoną keliais milimetrais, reikalingas magnetometras 10 kartų didesniu darbiniu diapazonu ir 10 kartų stipresnis magnetas.

Lokalizacijos algoritmas nestabiliausias, kai magnetas yra zonoje tarp pagrindinio ir atraminio magnetometrų. Visgi magneto ir magnetometrų išdėstymas ant žandikaulio pasirinktas taip, kad žandikaulio anatomija leistų magnetui judėti tik tolyn nuo atraminio magnetometro.

Vertėtų paminėti lokalizacijos paklaidos priklausomybę nuo atstumo iki magneto, reiškiančią, jog metodo lokalizacijos paklaida darbiniame diapazone kinta. Vis dėlto teigiamas aspektas yra tai, jog klaida yra maža ten, kur svarbiausia stebėti – pradžioje darbinio diapazono, aplink okliuzinę zoną.

Rimčiausias metodo trūkumas yra magnetometrų nulio dedamosios pokytis. Juolab, kad šį reiškinį sustiprina magnetometro aplinkoje veikiantys stiprūs magnetiniai laukai. Tai reiškia, jog sistemoje su nuolatiniu magnetu šis efektas yra neišvengiamas. Atlikus eksperimentus nustatyta, jog magnetometrų nulio vertė gali pasislinkti per ±40 μT. Be magnetometro kalibracijos, tokio dydžio nulio dedamosios pokytis gali sukelti iki 4 mm lokalizacijos paklaidos išaugimą sistemos darbinio diapazono pakraštyje. Visgi diapazono pradžioje, okliuzinėje zonoje, tokia vertė yra nereikšminga. Nepaisant to, magnetometrų nulio vertės kalibracija yra būtina.

Rezultatų santrauka. Šių eksperimentų metu buvo sukurta ir ištirta dviejų magnetometrų, 5-LL žandikaulio lokalizacijos koncepcija. Metodas patvirtintas su BEM duomenimis. Sukurtas jutiklio prototipas siekiant patikrinti metodo veikimą praktiškai. Pasiūlytas metodas aprašytas kartu su sprendimais dviem pagrindiniams kylančiams iššūkiams – FML kompensavimui ir žandikaulio pasisukimo kampo įvertinimui. Šie sprendimai iliustruojami 4.23 pav. pateiktomis kreivėmis, vizualizuojančiomis algoritmų įtaką.

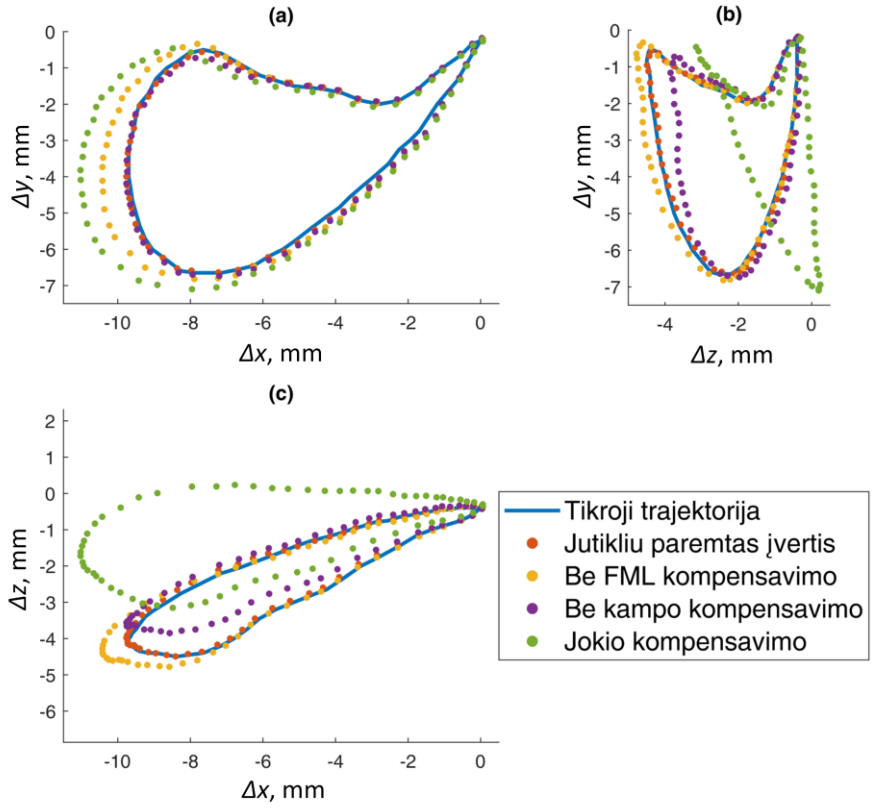

4.23 pav. 5-LL bandomoji kramtymo kreivė, įvertinta be FML kompensavimo bei žandikaulio pasisukimo kampo vertinimo algoritmų ir su jais. Magnetinio lauko vertės kiekviename taške užrašytos jutikliui nejudant: (a) šoninis–vertikalus vaizdas (*x*–*y*); (b) priekinis–vertikalus vaizdas (*z*–*y*); (c) šoninis-priekinis vaizdas (*x*–*z*)

Pasiūlytos trigonometrinės lygtys, atspindinčios sukimosi ir šoninio poslinkio priklausomybę, leido padidinti metodo LL skaičių nuo 3 iki 5. Taip atveriama galimybė pritaikyti metodą realiomis sąlygomis, nes neįvertinti žandikaulio pasisukimai sąlygotų dideles lokalizacijos paklaidas. Lygtys sėkmingai patikrintos lyginant jomis suskaičiuotus savanorio žandikaulio pasisukimo kampus su atraminiu metodu užregistruota to paties savanorio 6-LL žandikaulio pozicijų informacija.

3-LL tyrimuose vieno magnetometro metodo be FML kompensavimo koncepcijos patvirtinimo metu gauta vidutinė lokalizacijos paklaida ir standartinis nuokrypis VKP = 0,260 ± 0,004 mm. Dviejų magnetometrų su FML kompensavimu koncepto patvirtinimo metu gauta VKP = 0,28 mm lokalizacijos paklaida. Teoriniu FML atveju gautos lokalizacijos paklaidos VKP = 0,1 mm ir VKP = 0,05 mm, atitinkamai. Statinio 5-LL tyrimo metu gauta vidutinė lokalizacijos paklaida ir standartinis nuokrypis VKP = 0,165 ± 0,020 mm (EA = 0,098 ± 0,014 mm).

Dinaminio 5-LL tyrimo metu gauta vidutinė lokalizacijos paklaida ir standartinis nuokrypis EA = 0,175 ± 0,003 mm.

4.1 ir 4.2 lentelėse palyginimui pateikta praktinių 3-LL ir 5-LL eksperimentų su bandomąja kramtymo trajektorija lokalizacijos paklaida, išreikšta VKP ir EA.

2 lentelė. Vieno magnetometro 3-LL metodo statinio eksperimento ir dviejų magnetometrų 5-LL metodo statinio bei dinaminio eksperimentų rezultatai palyginimui. Dešimties matavimų VKP vidurkis bei standartinis nuokrypis ir jų projekcijos į skirtingas ašis

Metodas, tyrimas	**VKP, mm**	**VKP, *x* projekcijoje, mm**	**VKP, *y* projekcijoje, mm**	**VKP, *z* projekcijoje, mm**
1 magneto, statinis	0,260 ± 0,004	0,174 ± 0,003	0,107 ± 0,001	0,064 ± 0,001
2 magnetų, statinis	0,165 ± 0,011	0,114 ± 0,008	0,043 ± 0,009	0,036 ± 0,005
2 magnetų, dinaminis	–	–	–	–

3 lentelė. Vieno magnetometro 3-LL metodo statinio eksperimento ir dviejų magnetometrų 5-LL metodo statinio bei dinaminio eksperimentų rezultatai palyginimui. Dešimties matavimų *EA* vidurkis bei standartinis nuokrypis ir jų projekcijos į skirtingas ašis.

Metodas, tyrimas	**EA, mm**	**EA, *x* projekcijoje, mm**	**EA, *y* projekcijoje, mm**	**EA, *z* projekcijoje, mm**
1 magneto, statinis	0,127 ± 0,002	0,071 ± 0,001	0,059 ± 0,002	0,060 ± 0,001
2 magnetų, statinis	0,098 ± 0,014	0,049 ± 0,014	0,056 ± 0,010	0,042 ± 0,009
2 magnetų, dinaminis	0,175 ± 0,003	0,080 ± 0,001	0,103 ± 0,002	0,076 ± 0,001

Tikroviški žandikaulio judesiai simuliuoti panaudojant sukurtą robotu valdomo artikuliatoriaus platformą ir gauta EA = 0,240 mm lokalizacijos paklaida. Sukurtas belaidis jutiklio prototipas ir maitinimo bei tvirtinimo sprendimai, tinkami intraoraliam naudojimui. Sistemos veikimas pademonstruotas intraoraliniu bandymu.

Lyginant su klinikinėmis žandikaulio kinematikos vertinimo sistemomis, siūlomo metodo (R = 15 mm) darbinis diapazonas yra pakankamas, nes daugelio klinikinių sistemų specifikacijose nurodomi panašūs efektyviausio darbinio diapazono rėžiai. Tai nereiškia, jog metodas lygintinas su preciziniais klinikiniais sprendimais – dažnos nulinio lygio kalibracijos poreikis stato šį metodą į žemesnę lentyną. Taip pat temporomandibuliarinė kinematika negali būti tinkamai įvertinta, nenustačius žandikaulio sąnarių galvų pozicijų kaukolės atžvilgiu. Nepaisant to,

metodas, kaip ir buvo planuota, yra labiau tinkamas paciento elgsenos stebėsenai nei preciziniam žandikaulio kinematikos vertinimui. Apibendrinant, 5-LL eksperimentais patvirtintas žandikaulio lokalizacijos metodas su FML kompensavimu ir žandikaulio pasisukimo kampo vertinimu, taip pat pagrįsta metodo tolimesnio plėtojimo perspektyva. Ateityje reikėtų, kiek įmanoma, sumažinti jutiklio dydį, ištobulinti belaidę komunikaciją, rasti saugų maitinimo sprendimą. Taip pat vertėtų sekti technologinę pažangą magnetinių jutiklių srityje, nes pasiūlytas metodas yra ribojamas dabartinių MEMS magnetometrų veikimo charakteristikų.

5. IŠVADOS

1. Išplėtotas metodas dinaminiam žandikaulio pozicijos nustatymui su žandikaulio pasisukimo įvertinimu ir foninio magnetinio lauko kompensavimu. Metodo koncepcija patvirtinta panaudojant BEM sukurtą nuolatinio magneto magnetinio lauko žemėlapį. Bandomosios kramtymo trajektorijos teoriniu atveju gauta paklaida buvo lygi VKP = 0,05 m. Koncepcijos patvirtinimo vienu magnetometru metu (be FML kompensavimo) gauta teorinė vidutinė lokalizacijos paklaida ir standartinis nuokrypis VKP = 0,260 ± 0,004 mm. Prototipu dviejų magnetometrų metodui (su FML kompensavimu) gauta teorinė lokalizavimo paklaida VKP = 0,282 mm. Taip pat patvirtinta galimybė papildyti metodą akcelerometriniu dantų kontaktų atpažinimu.
2. Atliktas palyginamasis vertinimas metodams, tinkamiems iš magnetinio lauko verčių įvertinti jutiklio poziciją magneto atžvilgiu. Mažiausių kvadratų optimizavimas parodė žymiai geresnius rezultatus nei dalelių spiečiaus optimizavimas. MK metodas su FML kompensavimu ir žandikaulio pasisukimo vertinimu, taip pat papildytas adaptyviomis FML ribomis, buvo sėkmingai patikrintas su teoriškai modeliuotais ir eksperimentiniais duomenimis. Visame darbiniame diapazone teorinės lokalizavimo paklaidos vidurkiai ties įvairiais radialiniais atstumais (nuo R = 6 mm iki R = 20 mm) neviršijo 0,1 mm VKP.
3. Sukurtas jutiklio prototipas dviejų magnetometrų metodui su FML kompensavimu ir žandikaulio pasisukimo įvertinimu. Prietaisas išbandytas robotine ranka imituojant 5-LL žandikaulio judesius statinio ir dinaminio eksperimentų metu. Optimalus magnetometrų tarpusavio atstumas jutiklyje nustatytas panaudojant BEM. Statinio eksperimento metu gauta vidutinė lokalizacijos paklaida ir standartinis nuokrypis VKP = 0,165 ± 0,020 mm (EA = 0,098 ± 0,014 mm), o dinaminio eksperimento metu gauta vidutinė lokalizavimo paklaida ir standartinis nuokrypis EA = 0,175 ± 0,003 mm. Taip pat visos darbinės erdvės tyrimo metu parodyta, jog paklaida labai priklauso nuo magneto ir jutiklio atstumo. Nuo R = 6 mm iki R = 20 mm (radialinis atstumas iki magneto) darbiniame diapazone eksperimentinės lokalizacijos vidutinės paklaidos kito nuo VKP < 0,1 mm diapazono pradžioje iki VKP < 1 mm diapazono pabaigoje. Tikroviški žandikaulio judesiai simuliuoti panaudojant sukurtą robotu valdomo artikuliatoriaus platformą. Lyginant su atraminiu metodu, gauta EA = 0,240 mm lokalizacijos paklaida. Buvo sukurtas belaidis jutiklio prototipas ir maitinimo bei tvirtinimo sprendimai, tinkami intraoraliam naudojimui. Sistemos veikimas pademonstruotas intraoraliniu bandymu.

6. ATEITIES TYRIMŲ KRYPTYS

Pasiūlytas metodas yra galingas įrankis reikšmingų diagnostinių duomenų surinkimui. Vis dėlto nebuvo pasiūlytas metodas parafunkcijų atpažinimui iš surinktų žandikaulio judėjimo duomenų. Taip pat prietaiso prototipas gali būti patobulintas veikimo bei ergonomikos požiūriu. Atsižvelgiant į tai, ateities tyrimų kryptys yra tokios:

1. Metodo, skirto žandikaulio parafunkcijų atpažinimui iš žandikaulio judesio trajektorijų, tobulinimas.
2. Klinikiniai tyrimai su bruksizmo problemą turinčiais pacientais ir kontroline grupe.
3. Sistemos naudojimo ergonomikos pacientui bei gydytojui tobulinimas.
4. Tolimesnis jutiklio minimizavimas ir maitinimo sprendimo tobulinimas.
5. Algoritmų optimizavimas greičiui arba geresnio ir greitesnio algoritmo magnetinių duomenų apdorojimui paieška.

REFERENCES

[1] D. Manfredini, E. Winocur, L. Guarda-Nardini, D. Paesani, and F. Lobbezoo, "Epidemiology of Bruxism in Adults: A Systematic Review of the Literature," *Journal of Orofacial Pain*, vol. 27, no. 2, pp. 99–110, 2013.

[2] O. Leissner, M. Maulén-Yáñez, W. Meeder-Bella, C. León-Morales, E. Vergara-Bruna, and W. A. González-Arriagada, "Assessment of mandibular kinematics values and its relevance for the diagnosis of temporomandibular joint disorders," *Journal of Dental Sciences*, vol. 16, no. 1, pp. 241–248, 2021.

[3] T. Castroflorio, A. Deregibus, A. Bargellini, C. Debernardi, and D. Manfredini, "Detection of sleep bruxism: Comparison between an electromyographic and electrocardiographic portable holter and polysomnography," *Journal of Oral Rehabilitation*, vol. 41, no. 3, pp. 163–169, 2014.

[4] F. Lobbezoo *et al.*, "International consensus on the assessment of bruxism: Report of a work in progress," *Journal of Oral Rehabilitation*, vol. 45, no. 11, pp. 837–844, 2018.

[5] A. Claude, O. Robin, C. Gehin, and B. Massot, "Design and evaluation of a novel technology for ambulatory monitoring of bruxism events," *Sensors and Actuators, A: Physical*, vol. 295, pp. 532–540, 2019.

[6] S. Hiyama, T. Ono, Y. Ishiwata, Y. Kato, and T. Kuroda, "First night effect of an interocclusal appliance on nocturnal masticatory muscle activity," *Journal of Oral Rehabilitation*, vol. 30, no. 2, pp. 139–145, 2003.

[7] W. D. McCall and E. J. Rohan, "A Linear Position Transducer Using a Magnet and Hall Effect Devices," *IEEE Transactions on Instrumentation and Measurement*, vol. 26, no. 2, pp. 133–136, 1977.

[8] M. Jucevičius, R. Ožiūnas, M. Mažeika, V. Marozas, and D. Jegelevičius, "Accelerometry-enhanced magnetic sensor for intra-oral continuous jaw motion tracking," *Sensors*, vol. 21, no. 4, pp. 1–15, 2021.

[9] M. Jucevičius, R. Ožiūnas, G. Narvydas, and D. Jegelevičius, "Permanent Magnet Tracking Method Resistant to Background Magnetic Field for Assessing Jaw Movement in Wearable Devices," *Sensors*, vol. 22, no. 3, pp. 1–17, 2022.

[10] A. G. Glaros and S. M. Rao, "Bruxism: A Critical Review," *Psychological Bulletin*, vol. 84, no. 4, pp. 767–781, 1977.

[11] M. I. Fluerașu, I. C. Bocșan, I. A. Țig, S. M. Iacob, D. Popa, and S. Buduru, "The Epidemiology of Bruxism in Relation to Psychological Factors," *International Journal of Environmental Research and Public Health*, vol. 19, no. 2, 2022.

[12] M. K. Wruble, M. A. Lumley, and F. D. McGlynn, "Sleep-related bruxism and sleep variables: a critical review," *Journal of Craniomandibular Disorders*, vol. 3, no. 3, pp. 152–8, 1989.

[13] M. Wieckiewicz, A. Paradowska-Stolarz, and W. Wieckiewicz, "Psychosocial aspects of bruxism: The most paramount factor influencing teeth grinding," *BioMed Research International*, vol. 2014, 2014.
[14] R. A. Pizolato, M. B. D. Gavião, G. Berretin-Felix, A. C. M. Sampaio, and A. S. Trindade Junior, "Maximal bite force in young adults with temporomandibular disorders and bruxism," *Brazilian Oral Research*, vol. 21, no. 3, pp. 278–283, 2007.
[15] A. M. El Marakby, F. A. Al Sabri, S. A. Alharbi, and S. M. Halawani, "Noncarious Cervical Lesions as Abfraction: Etiology, Diagnosis, and Treatment Modalities of Lesions: A Review Article," *Dentistry*, vol. 07, no. 06, 2017.
[16] B. R. Chrcanovic, J. Kisch, T. Albrektsson, and A. Wennerberg, "Bruxism and dental implant treatment complications: a retrospective comparative study of 98 bruxer patients and a matched group," *Clinical Oral Implants Research*, vol. 28, no. 7, pp. e1–e9, 2017.
[17] D. Manfredini, M. B. Bucci, F. Montagna, and L. Guarda-Nardini, "Temporomandibular disorders assessment: Medicolegal considerations in the evidence-based era," *Journal of Oral Rehabilitation*, vol. 38, no. 2, pp. 101–119, 2011.
[18] H. Martynowicz *et al.*, "Evaluation of relationship between sleep bruxism and headache impact test-6 (HIT-6) scores: A polysomnographic study," *Frontiers in Neurology*, vol. 10, no. MAY, pp. 1–8, 2019.
[19] J. Tao, W. Liu, J. Wu, X. Zhang, and Y. Zhang, "The study of grinding patterns and factors influencing the grinding areas during sleep bruxism," *Archives of Oral Biology*, vol. 60, no. 10, pp. 1595–1600, 2015.
[20] M. M. Helland, "Anatomy and Function of the Temporomandibular Joint," *The journal of orthopaedic and sports physical therapy*, vol. 1, no. 3, pp. 145–152, 1980.
[21] K. Hwang, J. Y. Kim, and J. H. Lim, "Anatomy of the Platysma Muscle," *Journal of Craniofacial Surgery*, vol. 28, no. 2, pp. 539–542, 2017.
[22] N. R. Mehta, S. J. Scrivani, and E. L. H. Spierings, *Dental and facial pain*, Fifth Edit. Elsevier Inc., 2013.
[23] S. Choudhary, H. M. Rao, A. K. Rohilla, and C. Jayam, "The Occlusal Splint Therapy: A Literature Review," *Indian Journal of Dental Sciences.*, vol. 7, no. 1, pp. 101–108, 2015.
[24] B. Sagl *et al.*, "A novel quantitative method for tooth grinding surface assessment using 3d scanning," *Diagnostics*, vol. 11, no. 8, 2021.
[25] Bruxane. [Accessed on 11 November 2022]. Available online: https://bruxane.com/en.
[26] P. F. Nascimento *et al.*, "Characterization of the occlusal splints using optical fiber sensors," *SBMO/IEEE MTT-S International Microwave and Optoelectronics Conference, IMOC 2017*, vol. 2017-Janua, pp. 1–4, 2017.
[27] A. Bergmann, D. Edelhoff, O. Schubert, K. J. Erdelt, and J. M. Pho Duc,

"Effect of treatment with a full-occlusion biofeedback splint on sleep bruxism and TMD pain: a randomized controlled clinical trial," *Clinical Oral Investigations*, vol. 24, no. 11, pp. 4005–4018, 2020.

[28] Y. L. Cheng, Y. C. Chen, W. J. Chen, P. Huang, and H. H. Chu, "Sensor-embedded teeth for oral activity recognition," *ISWC 2013 - Proceedings of the 2013 ACM International Symposium on Wearable Computers*, pp. 41–44, 2013.

[29] A. C. Saueressig *et al.*, "Analysis of the influence of a mandibular advancement device on sleep and sleep bruxism scores by means of the BiteStrip and the Sleep Assessment Questionnaire.," *The International journal of prosthodontics*, vol. 23, no. 3, pp. 204–13, 2014.

[30] S. Lundqvist and T. Haraldson, "Occlusal perception of thickness in patients with bridges on osseointegrated oral implants," *Scandinavian Journal of Dental Research*, vol. 92, no. 1, pp. 88–92, 1984.

[31] M. Thymi *et al.*, "Signal acquisition and analysis of ambulatory electromyographic recordings for the assessment of sleep bruxism: A scoping review," *Journal of Oral Rehabilitation*, vol. 48, no. 7, pp. 846–871, 2021.

[32] T. Yamaguchi *et al.*, "Portable and wearable electromyographic devices for the assessment of sleep bruxism and awake bruxism: A literature review," *Cranio - Journal of Craniomandibular Practice*, pp. 1–9, 2020.

[33] T. Shochat *et al.*, "Validation of the BiteStrip screener for sleep bruxism," *Oral Surgery, Oral Medicine, Oral Pathology, Oral Radiology and Endodontology*, vol. 104, no. 3, 2007.

[34] V. C. Mainieri, A. C. Saueressig, Marcos Pascoal Pattussi, S. C. Fagondes, and M. L. Grossi, "Validation of the Bitestrip versus polysomnography in the diagnosis of patients with a clinical history of sleep bruxism," *Oral Surgery, Oral Medicine, Oral Pathology and Oral Radiology*, vol. 113, no. 5, pp. 612–617, 2012.

[35] BruxOff Diagnosis Device. [Accessed on 11 November 2022]. Available online: http://www.bruxoff.com/en/.

[36] G. J. Lavigne *et al.*, "Genesis of sleep bruxism: Motor and autonomic-cardiac interactions," *Archives of Oral Biology*, vol. 52, no. 4, pp. 381–384, 2007.

[37] T. Castroflorio, L. Mesin, G. M. Tartaglia, C. Sforza, and D. Farina, "Use of electromyographic and electrocardiographic signals to detect sleep bruxism episodes in a natural environment," *IEEE Journal of Biomedical and Health Informatics*, vol. 17, no. 6, pp. 994–1001, 2013.

[38] R. Needham and S. J. Davies, "Use of the Grindcare ® device in the management of nocturnal bruxism: A pilot study," *British Dental Journal*, vol. 215, no. 1, pp. 1–4, 2013.

[39] KaVo Arcus Digma. [Accessed on 11 November 2022]. Available online: https://www.kavo.com/dental-lab-equipment/arcusdigma-3-articulation." .

[40] "ModJaw. [Accessed on 11 November 2022]. Available online: https://www.modjaw.com/en.

[41] JT-3D. [Accessed on 11 November 2022]. Available online: https://www.bioresearchinc.com/products/jt3d.
[42] K7x. [Accessed on 11 November 2022]. Available online: https://www.myotronics.com/k7x.
[43] Planmeca 4D Jaw Motion. [Accessed on 11 November 2022]. Available online: https://www.planmeca.com/imaging/3d-imaging/planmeca-4d-jaw-motion/.
[44] D. Manfredini, J. Ahlberg, T. Castroflorio, C. E. Poggio, L. Guarda-Nardini, and F. Lobbezoo, "Diagnostic accuracy of portable instrumental devices to measure sleep bruxism: A systematic literature review of polysomnographic studies," *Journal of Oral Rehabilitation*, vol. 41, no. 11, pp. 836–842, 2014.
[45] C. Hu, M. Q. H. Meng, and M. Mandal, "A linear algorithm for tracing magnet position and orientation by using three-axis magnetic sensors," *IEEE Transactions on Magnetics*, vol. 43, no. 12, pp. 4096–4101, 2007.
[46] W. Weitschies, J. Wedemeyer, R. Stehr, and L. Trahms, "Magnetic Markers as a Noninvasive Tool to Monitor Gastrointestinal Transit," *IEEE Transactions on Biomedical Engineering*, vol. 41, no. 2, pp. 192–195, 1994.
[47] V. Schlageter, P. A. Besse, R. S. Popovic, and P. Kucera, "Tracking system with five degrees of freedom using a 2D-array of Hall sensors and a permanent magnet," *Sensors and Actuators, A: Physical*, vol. 92, no. 1–3, pp. 37–42, 2001.
[48] C. Hu, W. Yang, D. Chen, M. Q. H. Meng, and H. Dai, "An improved magnetic localization and orientation algorithm for wireless capsule endoscope," *Proceedings of the 30th Annual International Conference of the IEEE Engineering in Medicine and Biology Society, EMBS'08 - "Personalized Healthcare through Technology,"* vol. 1, pp. 2055–2058, 2008.
[49] W. Yang, C. Hu, M. Li, M. Q. H. Meng, and S. Song, "A new tracking system for three magnetic objectives," *IEEE Transactions on Magnetics*, vol. 46, no. 12, pp. 4023–4029, 2010.
[50] W. Wang, "A study on RF based wireless capsule endoscope," *2006 IEEE International Conference on Mechatronics and Automation, ICMA 2006*, vol. 2006, pp. 1663–1667, 2006.
[51] M. Li, S. Song, C. Hu, W. Yang, L. Wang, and M. Q. H. Meng, "A new calibration method for magnetic sensor array for tracking capsule endoscope," *2009 IEEE International Conference on Robotics and Biomimetics, ROBIO 2009*, no. January, pp. 1561–1566, 2009.
[52] C. Hu, M. Li, S. Song, W. Yang, R. Zhang, and M. Q. H. Meng, "A Cubic 3-Axis Magnetic Sensor Array for Wirelessly Tracking Magnet Position and Orientation," *IEEE Sensors Journal*, vol. 10, no. 5, pp. 903–913, 2010.
[53] M. Odeh, E. D. Nichols, F. L. Fenoglietto, and J. Stubbs, "Real-Time, Non-Contact Position Tracking of Medical Devices and Surgical Tools through the Analysis of Magnetic Field Vectors," *Proceedings of the 2018 Design of*

Medical Devices Conference, pp. 1–5, 2018.
[54] T. D. Than, G. Alici, H. Zhou, and W. Li, "A review of localization systems for robotic endoscopic capsules," *IEEE Transactions on Biomedical Engineering*, vol. 59, no. 9, pp. 2387–2399, 2012.
[55] V. Biancalana *et al.*, "Validation of a fast and accurate magnetic tracker operating in the environmental field," *Instruments*, vol. 5, no.1, pp.1–15, 2021.
[56] V. Biancalana, R. Cecchi, P. Chessa, G. Bevilacqua, Y. Dancheva, and A. Vigilante, "Fast, cheap, and scalable magnetic tracker with an array of magnetoresistors," *Instruments*, vol. 5, no. 1, pp. 1–18, 2021.
[57] L. Bellizzi *et al.*, "An innovative eye-tracker: Main features and demonstrative tests," *Review of Scientific Instruments*, vol. 93, no. 3, 2022.
[58] K. Lyons, "Wearable magnetic field sensing for finger tracking," *Proceedings - International Symposium on Wearable Computers, ISWC*, pp. 63–67, 2020.
[59] H. Xinying, H. Seki, Y. Kamiya, and M. Hikizu, "Wearable handwriting input device using magnetic field," *Proceedings of the SICE Annual Conference*, pp. 365–368, 2007.
[60] K.-Y. Chen, S. N. Patel, and S. Keller, "Finexus," pp. 1504–1514, 2016.
[61] F. S. Parizi, E. Whitmire, and S. Patel, "AuraRing: Precise electromagnetic finger tracking," *Proceedings of the ACM on Interactive, Mobile, Wearable and Ubiquitous Technologies*, vol. 3, no. 4, pp. 1–28, 2019.
[62] E. M. Rozhin, A. V. Rozhina, V. D. Panteleev, I. A. Kudryavcev, and I. V. Savin, RU patent RU2628064C2. [Accessed on 11 November 2022]. Available online: https://patentimages.storage.googleapis.com/63/e1/01/\432ad6d4c0ffd6/RU2628064C2.pdf, 2015.
[63] Y. Wang, "Gauss-Newton method," *Wiley Interdisciplinary Reviews: Computational Statistics*, vol. 4, no. 4, pp. 415–420, 2012.
[64] F. Vanden Berghen, "Levenberg-Marquardt algorithms vs Trust Region algorithms," *Methods*, no. 1, pp. 3–6, 2004.
[65] R. H. Byrd, R. B. Schnabel, and G. A. Shultz, "A Trust Region Algorithm for Nonlinearly Constrained Optimization," *SIAM Journal on Numerical Analysis*, vol. 24, no. 5, pp. 1152–1170, 1987.
[66] H. P. Gavin, "The Levenberg-Marquardt Algorithm For Nonlinear Least Squares Curve-Fitting Problems," *Duke University*, pp. 1–19, 2019.
[67] F. H. Heppner and U. Grenander, "A Stochastic NonLinear Model for Coordinated Bird Flocks," *The Ubiquity of Chaos*, no. July, pp. 233–238, 1990.
[68] J. Kennedy and R. Eberhart, "Particle Swarm Optimization," *The Industrial Electronics Handbook - Five Volume Set*, pp. 1942–1948, 1995.
[69] W. S. McCulloch and W. Pitts, "A Logical Calculus of the Ideas Immanent in Nervous Activity," *Bulletin of Mathematical Biophysics*, vol. 5, pp. 115–133, 1943.

[70] P. Werbos, “New Tools for Prediction and Analysis in the Behavioral Sciences,” *Ph. D. dissertation, Harvard University*, 1974.
[71] D. Wang, “Unsupervised learning: Foundations of neural computation,” *AI Magazine*, vol. 22, no. 2, p. 256, 2001.
[72] A. I. Sasaki, “Effectiveness of Artificial Neural Networks for Solving Inverse Problems in Magnetic Field-Based Localization,” *Sensors*, vol. 22, no. 6, 2022.
[73] B. Liu, S. Cheng, and Y. Shi, “Particle filter optimization: A brief introduction,” *Lecture Notes in Computer Science*, vol. 9712 LNCS, no. June, pp. 95–104, 2016.
[74] D. K. Cheng, *Field and Wave Electromagnetics. Chapter 6: Static magnetic fields*. Reading: Addison - Wesley, 1989.
[75] H. Moran, Skull For Reference - 3D model. [Accessed on 11 November 2022]. Available online: https://skfb.ly/Lqtz.
[76] A. J. Petruska and J. J. Abbott, “Optimal permanent-magnet geometries for dipole field approximation,” *IEEE Transactions on Magnetics*, vol. 49, no. 2, pp. 811–819, 2013.
[77] D. Raabe, A. Harrison, K. Alemzadeh, A. Ireland, and J. Sandy, “Capturing motions and forces of the human masticatory system to replicate chewing and to perform dental wear experiments,” *Proceedings - IEEE Symposium on Computer-Based Medical Systems*, pp. 1–6, 2011.
[78] G. Hulot, C. C. Finlay, C. G. Constable, N. Olsen, and M. Mandea, “The magnetic field of planet earth,” *Space Science Reviews*, vol. 152, no. 1–4, pp. 159–222, 2010.
[79] P. Arpaia, P. N. Burrows, M. Buzio, C. Gohil, M. Pentella, and D. Schulte, “Magnetic characterization of Mumetal® for passive shielding of stray fields down to the nano-Tesla level,” *Nuclear Instruments and Methods in Physics Research, Section A: Accelerators, Spectrometers, Detectors and Associated Equipment*, vol. 988, no. December 2020, p. 164904, 2021.
[80] K. Kato, K. Yamazaki, H. Matsuba, C. Sumi, and S. Sato, “Active magnetic shield for biomagnetic measurements,” *Proc. of the 12th Int. Conf. on Biomagnetism*, no. December 2001, pp. 965–967, 2000.
[81] Z. Ahmed, “Clinical measurements of the dimensions of the dental arches and its application on construction of dental prosthesis,” *Al-Rafidain Dental Journal*, vol. 6, no. 1, pp. 88–97, 2006.
[82] University of Dundee, School of Dentistry. 3D Skull Model. [Accessed on 11 November 2022]. Available online: https://skfb.ly/KQsq. .
[83] A. Mapelli, D. Galante, N. Lovecchio, C. Sforza, and V. F. Ferrario, “Translation and rotation movements of the mandible during mouth opening and closing,” *Clinical Anatomy*, vol. 22, no. 3, pp. 311–318, 2009.
[84] S. Su, H. Dai, S. Cheng, P. Lin, C. Hu, and B. Lv, “A Robust Magnetic Tracking Approach Based on Graph Optimization,” *IEEE Transactions on Instrumentation and Measurement*, vol. 69, no. 10, pp. 7933–7940, 2020.

[85] S. C. Woodford, D. L. Robinson, A. Mehl, P. V. S. Lee, and D. C. Ackland, “Measurement of normal and pathological mandibular and temporomandibular joint kinematics: A systematic review,” *Journal of Biomechanics*, vol. 111, 2020.

LIST OF PUBLICATIONS RELATED TO THE DISSERTATION

Publications indexed in the Web of Science with impact factor

1. **Jucevičius M.**, Ožiūnas R., Mažeika M., Marozas V., Jegelevičius D. Accelerometry-Enhanced Magnetic Sensor for Intra-Oral Continuous Jaw Motion Tracking. *Sensors MDPI*. 2021; 21(4):1409. (*IF: 3.576).*
2. **Jucevičius M.**, Ožiūnas R., Narvydas G., Jegelevičius D. Permanent Magnet Tracking Method Resistant to Background Magnetic Field for Assessing Jaw Movement in Wearable Devices. *Sensors MDPI*. 2022; 22(3):971. (*IF: 3.576).*

Scientific conferences where the research results were presented

1. **Jucevičius M.**, Ožiūnas R. Perteklinio kramtymo funkcijos stebėsenos techniniai aspektai. *Bioateitis: gamtos ir gyvybės mokslų perspektyvos.* Programa ir pranešimų santraukos. 18p. 2019, Kaunas, Lithuania.
2. **Jucevičius M.**, Ožiūnas R., Mažeika M., Jegelevičius D., Marozas V. Investigation of Magnetic Sensor for Intra-oral Continuous Jaw Tracking. *8th European Medical and Biological Engineering Conference EMBEC 2020*, IFMBE Proceedings, vol 80. Springer, Cham.
3. **Jucevičius M.** Magnetic method for 5 Degree-of-freedom jaw position estimation. Oral presentation. *Biomechanics, Medical Diagnostics, Locomotion and Rehabilitation international conference BIOMDLORE*, 2021, Vilnius, Lithuania.

ACKNOWLEDGEMENTS

I would like to express great gratitude and appreciation to my supervisor Dr. Darius Jegelevičius for his invaluable guidance and advice reaching well beyond academia. I would also like to thank Dr. Vaidotas Marozas for his continuous interest in my work and well-being. My special gratitude is dedicated to my fiancée Gabija Babrauskaitė as well as my parents Valdas and Elytė for their understanding and support.

UDK 611.716+616-073+621.317.4](043.3)

SL 344. 2023-xx-xx, xx leidyb. apsk. l. Tiražas xx egz. Užsakymas xxx.
Išleido Kauno technologijos universitetas, K. Donelaičio g. 73, 44249 Kaunas
Spausdino leidyklos „Technologija“ spaustuvė, Studentų g. 54, 51424 Kaunas